Macrophages in cardiac development, repair and regeneration

A thesis submitted for the degree of Doctor of Philosophy

at the

University of Oxford

Dr Thomas J Cahill MA MBBS MRCP

Merton College

Supervised by

Professor Paul R Riley & Professor Robin P Choudhury



Abstract

Background & Aims

Macrophages are highly plastic cells of the innate immune system with a functional repertoire spanning homeostasis, inflammation, repair and remodelling. Originally described as immune cells responsible for phagocytosis and cytokine production, in recent years a plethora of non-classical, tissue-specific, and subspecialised roles for macrophages have emerged. Macrophages have been implicated in organogenesis during embryonic development, and tissue regeneration after injury, often viewed as a recapitulation of development. Understanding the mechanisms underlying these 'trophic' functions has translational potential to improve healing in the human heart after myocardial infarction (MI). The principal aim of the work contained in this thesis was to investigate the non-classical roles of macrophages in the heart in the setting of development and following injury, during regenerative and scar-based repair.

Methods

Macrophage functions were initially investigated during mouse cardiac development. First, the identity, timing, and localisation of macrophages in the embryonic mouse heart was investigated. To gain insight into the functional roles of macrophages in development, heart formation was analysed in a genetic mouse model of macrophage deficiency, the *Pu.1*$^{-/-}$ mouse. To understand the roles of macrophages in cardiac regeneration, the recently described neonatal mouse model of MI, which heals without scar formation, was compared with the adult mouse which undergoes scarring following injury. Unbiased analysis of the macrophage transcriptome was then conducted by RNA sequencing on isolated macrophages from both regenerative and scar-forming hearts. Putative novel functions for macrophages in injury and repair were then validated.

Results

Macrophages were found to be present in the embryonic mouse heart from E12.5, and a subset colocalised closely with the developing coronary and lymphatic vasculature. Macrophages did not act as progenitor cells giving rise to the lymphatic vasculature, as has been proposed, although a $CSF1R^{+}$ myeloid-like progenitor was shown to incorporate into the cardiac lymphatic endothelium. The absence of macrophages in the *Pu.1*$^{-/-}$ mouse was associated with defects in vessel branching, length and calibre, suggesting that a key role of macrophages in the developing heart is to pattern the coronary and lymphatic vasculature.

Following cardiac injury, RNA sequencing demonstrated that macrophages activate distinct transcriptional programmes during tissue healing by regeneration and scar formation. Macrophages were dynamically regulated through the time course of injury and were found to upregulate numerous regenerative and pro-fibrotic soluble factors which modulate tissue repair. Furthermore, in the context of scar formation macrophages expressed extracellular matrix components including collagens, suggesting a direct role in formation of scar. The macrophage response was found to be a key determinant of tissue repair, and adoptive transfer of adult splenic monocytes to the neonatal environment was sufficient to block regeneration, at least in part by direct deposition of collagen.

Conclusions

Macrophages have previously unrecognised functions in the context of heart development, regeneration and repair. Further analysis of molecular mechanisms, heterogeneity and the intrinsic and environmental factors which regulate macrophage

responses is required in order to translate these insights toward therapies for improved repair following human MI.

.

Acknowledgments

Firstly, thank you to Paul and Robin as my supervisors. It has been a privilege to work with you and I have learnt a lot – about science, research, writing, publishing and myself – in the process. Thank you to the Wellcome Trust for funding me, and the cost of this research, over the last three years.

It has been a pleasure working with the members of the Riley and Choudhury groups. In particular, to Cristina and Damien – it is what it is, and it was what it was – thank you for your support, advice and friendship. To Xin and Joey – thank you for supporting a wayward clinician through the intricacies of developmental biology. Thank you to Megan and Mala for teaching me the mouse surgery, and to Denise and Katie, for everything you do to facilitate work away from the bench. Outside the department, I am grateful to the staff of the BMS (in particular Angela, Richard, Nina, and Richard) for animal support. I would like to acknowledge help from Kevin Clark for FACS, Alan Wainman for confocal microscopy, Neil Ashley, Ruth Williams and Tatjana Sauka-Spengler for RNA sequencing, and Madeleine Lemieux for bioinformatic analyses.

Outside the lab I am grateful to friends and family for their support and for helping me keep a sense of perspective. To my friends Mark and Dave, thank you for your feigned interest in mice over the years and for listening to tales of woe from the lab! To my family – thank you for being a constant support, anchoring me, and providing a welcome periodic escape from Oxford. Finally, but above all – my most heartfelt thanks to my wife Charlotte –for your love, support, advice, patience and encouragement – I could not have done it without you.

Table of contents

Abstract **2**

Background & Aims 2

Methods 2

Results 3

Conclusions 3

Table of contents **6**

List of figures & tables **12**

Abbreviations **15**

Chapter 1: Introduction **16**

1.1 Cardiac injury and repair **17**

1.1.1 Heart failure following MI: a paradigm for failed repair 17

1.1.2 Heart regeneration: from models to man 20

1.2 Macrophages: classification & ontogeny **26**

1.2.1 Macrophage classification and function 26

1.2.2 Macrophage ontogeny 30

1.3 Macrophage markers & models **33**

1.3.1 F4/80 33

1.3.2 CD68 33

1.3.3 CX3CR1 34

1.3.4 CSF1R 34

1.3.5 PU.1 35

1.4 Macrophages in cardiac development, injury and repair **36**

1.4.1 Cardiac development 36

1.4.2 Cardiac injury & scar formation 37

1.4.3 Cardiac regeneration 39

1.5 Hypotheses **42**

1.6 Aims of the Thesis **43**

Chapter 2: Materials & Methods 44

2.1 Mice 45

2.1.1 Mouse strains 45

Table 2.1 Genetic mouse lines 46

2.1.2 Timed matings 47

2.1.3 Tamoxifen activation of Cre recombinase 47

2.1.4 Embryo dissection 47

2.1.5 Adult heart dissection 47

2.2 Myocardial infarction models 49

2.2.1 Adult myocardial infarction model 49

2.2.2 Neonatal myocardial infarction model 50

2.3 Molecular methods 53

2.3.1 DNA extraction for genotyping 53

2.3.2 Genotyping PCRs 53

Table 2.2 – PCR primers for genotyping 54

Table 2.3 – PCR programs 55

2.3.3 Agarose gel electrophoresis 56

2.3.4 RNA extraction from tissue 56

2.3.5 cDNA synthesis 57

2.3.6 Quantitative real-time PCR 57

Table 2.4 – Primers for qRT-PCR 58

2.3.7 RNA sequencing 58

2.4 Staining 59

2.4.1 Wax embedding for histology 59

2.4.2 Masson's Trichrome staining 59

2.4.3 Immunofluorescence – cryosections 60

2.4.4 Immunofluorescence – whole mount embryo hearts 61

Table 2.5: Primary antibodies for immunofluorescence 62

Table 2.6: Secondary antibodies for immunofluorescence 62

Table 2.7 Solutions 62

Table 2.8 Kits and reagents 63

2.5 Flow cytometry 64

2.5.1 Digestion 64
2.5.2 Antibody staining 64
Table 2.9 Antibodies for flow cytometry 65
2.6 Adoptive transfer studies 66
2.7 Statistical analysis 67
Chapter 3: Macrophages in cardiac development 68
3.1 Background 69
3.1.1 Development of the heart & coronary vasculature 69
Table 3.1: Comparative time course of heart development in mouse and human 70
3.1.2 Development of the cardiac lymphatic vasculature 70
3.1.3 Macrophages in the embryonic heart 71
3.1.4 Aims 72
3.2 Results 73
3.2.1 Macrophages infiltrate the embryonic heart 73
3.2.2 Macrophages colocalise with coronary vessels and lymphatics 75
3.2.3 A LYVE1-positive macrophage subset localises to the epicardium 79
3.2.4 LYVE1+ lymphatic-associated macrophages are derived from the yolk sac 81
3.2.5 CSF1R+ progenitors contribute to the cardiac lymphatics 84
3.2.6 Macrophages do not contribute directly to the cardiac lymphatic endothelial lineage 88
3.2.7 The progeny of FLT3+ definitive haematopoiesis do not contribute to the cardiac lymphatic endothelial lineage 92
3.2.8 CSF1R and CX3CR1 identify overlapping but distinct myeloid populations in the embryonic heart 94
3.3 Discussion 96
3.3.1 Macrophages in the embryonic heart 96
3.3.2 Ontogeny of macrophages in the embryonic heart 97
3.3.3 Myeloid cells as lymphatic endothelial progenitor cells 97
3.3.4. Heterogeneity of myeloid cells in the embryonic heart 99
3.4 Conclusions 101
Chapter 4: Cardiac development in a mouse model of macrophage deficiency 102
4.1 Background 103

4.1.1 Mouse models for targeting macrophages 103
4.1.2 Macrophage roles in development and growth 107
4.1.3 Aims 109

4.2 Results 110

4.2.1 *Pu.1*$^{-/-}$ mice lack macrophages in the embryonic heart 110
4.2.2 *Pu.1*$^{-/-}$ mice have abnormal lymphatic vessel patterning 112
4.2.3 *Pu.1*$^{-/-}$ mice have abnormal coronary blood vessel patterning 117
4.2.4 Lymphatic endothelial cell proliferation is not affected in the *Pu.1*$^{-/-}$ mouse 122
4.2.5 Macrophages are not a source of VEGFc in the developing heart 124

4.3 Discussion 126

4.3.1 Macrophages in lymphatic development 126
4.3.2 Macrophages in vascular development 129

4.4 Conclusions 133

Chapter 5: Macrophages in repair and regeneration after MI 134

5.1 Background 135

5.1.1 Tissue repair by scar formation and regeneration 135
5.1.2 Macrophages in tissue repair 136
5.1.3 Macrophages in tissue regeneration 137
5.1.4 Macrophages as determinants of wound healing 138
5.1.5 Aims 139

5.2 Results 141

5.2.1 The P1 neonatal mouse heart regenerates after myocardial infarction 141
5.2.2 Analysis of the immune response to MI in the neonatal and adult heart 144
5.2.3 Macrophages infiltrate the infarct zone in the neonatal and adult heart following MI 150
5.2.4 RNA sequencing of cardiac macrophages 152
5.2.5 Macrophages in the P1, P7 and adult heart are transcriptionally distinct at baseline and following MI 155
5.2.6 Myocardial repair by regeneration and scar formation is associated with differential macrophage gene expression 158
5.2.7 Macrophage gene expression is dynamically regulated after MI 162
5.2.8 Macrophages in the scar-forming heart upregulate extracellular matrix pathways 167

5.3 Discussion 169

5.3.1 The neonatal and adult immune response to injury 169
5.3.2 Macrophages roles in regenerative versus scar-based healing 170
5.3.3 Dynamics of macrophage function after myocardial infarction 171

Chapter 6: Macrophages in scar formation following myocardial infarction...174

6.1 Background 175

6.1.1 Mechanisms of scar formation following MI 175
6.1.2 Linking inflammation to scar formation 176
6.1.3 Aims 177

6.2 Results 178

6.2.1 Scar formation in the late neonatal mouse MI model 178
6.2.2 Macrophages differentially express pro-fibrotic mediators in the regenerating and scar-forming heart 180
6.2.3 Macrophages express collagen proteins 182
6.2.4 Adult splenic monocytes are sufficient to impede regeneration in the P1 neonatal mouse model 184
6.2.5 Adult splenic monocyte-derived macrophages produce collagen in the neonatal environment 186

6.3 Discussion 188

6.3.1 Macrophage expression of pro-fibrotic mediators 188
6.3.2 Macrophages as collagen-producing cells 188
6.3.3 Monocytes as a determinant of wound healing 190

6.4 Conclusions 193

Chapter 7: General discussion 194

7.1 Discussion of findings 195

7.1.1 Spatiotemporal infiltration of macrophages in cardiac development 196
7.1.2 Embryonic macrophages as lymphatic progenitor cells 198
7.1.3 Functional roles for macrophages in remodelling of coronary or lymphatic vessels in cardiac development 200
7.1.4 Comparison of macrophage pathways during healing by regeneration compared to scar formation 203
7.1.5 Functional roles for macrophages during regenerative and scar-forming healing 204

7.2 Conclusions 207

7.3 Future work 208

7.3.1 Confirmation of the *Pu.1*$^{-/-}$ coronary vascular and lymphatic phenotype in an inducible model of macrophage ablation 209
7.3.2 Mechanisms of macrophage patterning of the developing coronary and lymphatic vessels 209
7.3.3 Intrinsic factors controlling the macrophage response to injury 210
7.3.4 Functional effects of macrophage-derived soluble factors 211
7.3.5 Macrophage heterogeneity in development, injury and repair 212

7.4 Appendices 213

7.4.1 Timing & venue of research 213
7.4.2 Funding 213
7.4.3 Publications 213
7.4.4 Presentations at scientific meetings 214

References 215

List of figures & tables

Chapter 1

Figure 1.1: Heart failure pipeline: from conventional to regenerative therapies

Figure 1.2: Key studies of cell therapy for acute myocardial infarction & heart failure

Table 1.1: Macrophage polarisation states

Figure 1.3: Macrophage ontogeny

Figure 1.4: Classical and non-classical roles of macrophages

Chapter 2

Table 2.1: Genetic mouse lines

Figure 2.1: Mouse models of myocardial infarction

Table 2.2: PCR primers for genotyping

Table 2.3: PCR programs

Table 2.4: Primers for qRT-PCR

Table 2.5: Primary antibodies for immunofluorescence

Table 2.6: Secondary antibodies for immunofluorescence

Table 2.7: Solutions

Table 2.8: Kits and reagents

Table 2.9: Antibodies for flow cytometry

Chapter 3

Table 3.1: Comparative time course of heart development in mouse and human

Figure 3.1: Macrophages infiltrate the developing heart

Figure 3.2: Macrophages colocalise with coronary vessels and lymphatics

Figure 3.3: A LYVE1-positive macrophage subset localises to the epicardium

Figure 3.4: Lymphatic-associated macrophages are derived from the yolk sac

Figure 3.5: CSF1R+ progenitors contribute to the cardiac lymphatics

Figure 3.6: Macrophages do not contribute directly to the cardiac lymphatic endothelial lineage

Figure 3.7: The progeny of FLT3+ definitive haematopoiesis do not contribute to the cardiac lymphatic endothelial lineage

Figure 3.8: CSF1R and CX3CR1 label overlapping and distinct population in the embryonic heart

Chapter 4

Figure 4.1: Signalling pathways involved in specification of macrophage fate

Figure 4.2: *Pu.1*$^{-/-}$ mice lack macrophages in the embryonic heart

Figure 4.3: *Pu.1*$^{-/-}$ mice have abnormal lymphatic vessel patterning

Figure 4.4: *Pu.1*$^{-/-}$ mice have abnormal coronary blood vessel patterning

Figure 4.5: Lymphatic endothelial cell proliferation is not affected in the *Pu.1*$^{-/-}$ mouse

Figure 4.6: Macrophages are not a source of VEGFC in the developing heart

Chapter 5

Figure 5.1: The P1 neonatal mouse regenerates after myocardial infarction

Figure 5.2: Analysis of the immune response to MI in the neonatal and adult heart

Figure 5.3: Macrophages infiltrate the infarct zone in the neonatal and adult heart following MI

Figure 5.4: RNA sequencing of cardiac macrophages

Figure 5.5: Macrophages in the P1, P7 and adult heart are transcriptionally distinct at baseline and following MI

Figure 5.6: Myocardial repair by regeneration and scar formation is associated with differential macrophage gene expression

Figure 5.7: Macrophage gene expression is dynamically regulated after MI

Figure 5.8: Macrophages in the scar-forming heart upregulate extracellular matrix pathways

Chapter 6

Figure 6.1: Scar formation in the late neonatal mouse MI model

Figure 6.2: Macrophages differentially express pro-fibrotic mediators in the regenerating and scar-forming heart

Figure 6.3: Macrophages produce collagen following MI

Figure 6.4: Adult splenic monocytes are sufficient to impede regeneration in the P1 neonatal mouse model

Figure 6.5: Adult splenic monocyte-derived macrophages produce collagen in the neonatal environment

Abbreviations

AGM	aorta-gonad-mesonephros
CCR2	C-C chemokine receptor type 2
DC	dendritic cell
E	embryonic day
ECM	extracellular matrix
EMT	epithelial to mesenchymal transition
HA	hyaluronic acid
HSC	haematopoietic stem cell
IFN-γ	interferon gamma
LA	left atrium
LAD	left anterior descending (coronary artery)
LEC	lymphatic endothelial cell
LV	left ventricle
MHC	major histocompatibility complex
MI	myocardial infarction
MRI	magnetic resonance imaging
OFT	outflow tract
P1	postnatal day 1
P7	postnatal day 7
PPCI	primary percutaneous coronary intervention
RA	right atrium
RV	right ventricle
TNF	tumour necrosis factor
YS	yolk sac

Chapter 1: Introduction

1.1 Cardiac injury and repair

1.1.1 Heart failure following MI: a paradigm for failed repair

Heart failure is a clinical syndrome defined by insufficient cardiac output to meet the metabolic demands of the body.(1) It develops due to cardiomyocyte death or dysfunction and has a diverse aetiology including ischaemic heart disease, hypertension, chemotherapy, infection, infiltration or genetic cardiomyopathy.(2, 3) 38 million people worldwide suffer from heart failure, which is associated with adverse quality of life, recurrent hospitalisation, and premature mortality.(4) Whilst current therapeutic options can alleviate symptoms and slow disease progression, heart failure remains incurable.

Coronary artery disease is the commonest cause of heart failure worldwide.(2) Acute myocardial infarction (MI) causes ischaemic necrosis of cardiomyocytes within minutes to hours, and the subsequent development of heart failure is a paradigm for failure of effective tissue repair following injury. In mammals, MI activates a patterned, spatiotemporally regulated biphasic immune response. The first phase is defined by activation of sterile inflammation, including release of pro-inflammatory cytokines and mobilisation of neutrophils and monocytes.(5) The second phase is characterised by resolution of inflammation, activation of fibroblasts to myofibroblasts and deposition of a collagen-based scar. Critically, lost cardiomyocytes are not replaced and scar tissue becomes a substrate for downstream complications including intracardiac thrombus formation, arrhythmia and heart failure.

Following the initial injury, further progression of ventricular dysfunction is driven by the body's adaptive physiological response.(6) Reduced cardiac output triggers activation of the sympathetic nervous system and neurohormonal systems, leading to angiotensin II and aldosterone release, sodium retention and peripheral

vasoconstriction, which attempt to maintain systemic perfusion. Whilst these are initially compensatory, chronic activation is maladaptive, driving ventricular dilatation, scar thinning, interstitial fibrosis and ongoing cardiomyocyte death.(7, 8)

In the last three decades the development of reperfusion therapy by pharmacological thrombolysis or primary percutaneous coronary intervention (PPCI) has significantly improved survival from MI.(9, 10) However, downstream heart failure remains common and furthermore, may be increasing in incidence as early survival from MI improves.(11) Whilst current therapeutic approaches to heart failure successfully target maladaptive physiology (Figure 1.1), they fail to address the underlying loss of functional myocardium. Novel therapeutic approaches to preserve or regenerate cardiomyocytes following cardiac injury are urgently required to tackle the pandemic of heart failure.

Figure 1.1

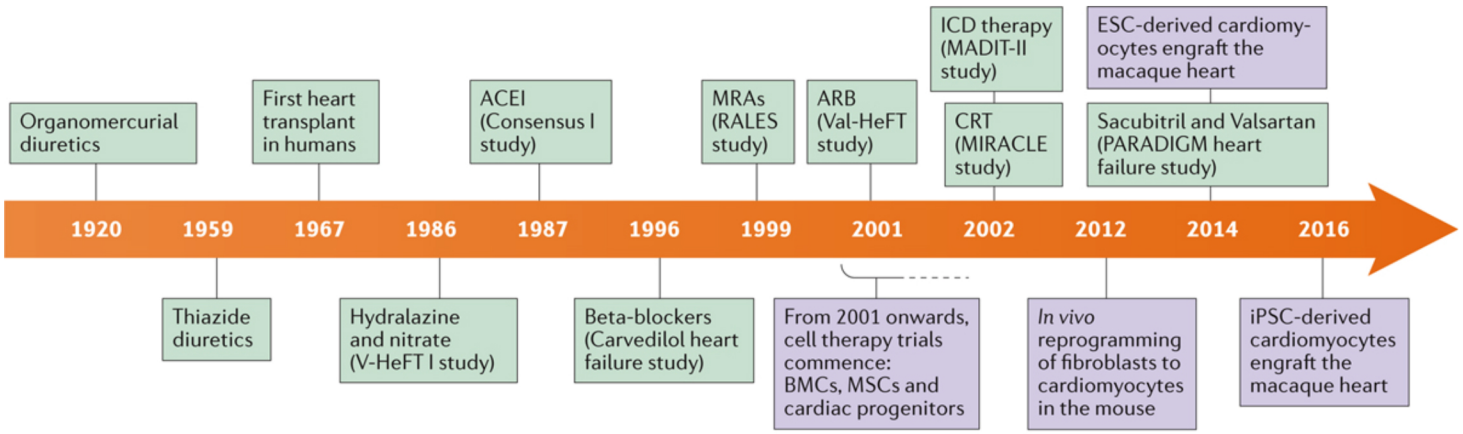


Figure 1.1 Heart failure therapeutic pipeline: from conventional to regenerative therapies
Land-mark breakthroughs in heart failure therapy are indicated in green, and progress in regenerative therapies for heart failure are shown in purple. Key trials in heart failure are shown in brackets. ACEI, angiotensin-converting enzyme inhibitors; ARB angiotensin receptor blockers; BMCs bone-marrow derived cells; ESC embryonic stem cell; CRT cardiac resynchronisation therapy; ICD implantable cardioverter defibrillator; iPSC induced pluripotent stem cell; MRAs mineralocorticoid receptor antagonists; MSCs mesenchymal stem cells. Reproduced from Cahill *et al*[12] with permission.

1.1.2 Heart regeneration: from models to man

Healing by regeneration, defined as anatomical and functional restoration of the injured tissue, is seen widely across the animal kingdom. It is recounted in antiquity: Zeus punished Prometheus for stealing fire by sending an eagle to feed daily on his liver, but 'whatever this long-winged bird ate during the day grew during the night again to perfection.'(13) Regeneration of the lizard tail was first reported in 1686, and crustaceans, newts and the polyp *Hydra* became the first model organisms for scientific study of regeneration from the mid-18th century onwards.(13) Three types of regeneration have been described: epimorphic regeneration, in which a dedifferentiated 'blastema' of cells undergo re-specification and differentiation; morphallaxis, in which regeneration occurs by repatterning of existing tissues without new growth; and compensatory regeneration, in which differentiated cells undergo division.

Although proliferation of cardiomyocytes following injury had been reported in the newt in the 1970s, the first definitive description of heart regeneration was in the zebrafish (*Danio rerio)* in 2001.(14, 15) A teleost fish with a two-chambered heart, the zebrafish is capable of cardiac regeneration after diverse insults including resection of the apex, cryoinjury, genetic ablation, or hypoxia.(15-18) Following resection of the apex, a fibrin clot and transient scar is progressively replaced by new cardiomyocytes, leading to full restoration of structure and function without residual fibrosis. Urodele amphibians, including the salamander, axolotl and newt, are also capable of heart regeneration.(19) After apical resection, cryoinjury or isoproterenol-induced cardiac injury, a transient scar is replaced with functional cardiomyocytes over a time period of 60 – 90 days.(20)

Heart regeneration in mammals was first reported in a landmark study in 2011, when Porrello *et al* reported that cardiac injury caused by apical resection or ligation of the left anterior descending (LAD) coronary artery in the neonatal mouse at postnatal day 1 (P1) healed by regeneration.(21, 22) This capacity for regenerative repair was restricted to a limited time period of the first few days of life, and by postnatal day 7 (P7), the 'regenerative window' was closed, with healing occurring by scar formation, similar to the adult mouse.

Replacement of lost cardiomyocytes to restore myocardial structure and function is the sine qua non of heart regeneration. Significant research focus has been directed at the sources of new cardiomyocytes in endogenous regeneration. Studies in both the zebrafish and mouse using genetic lineage tracing have now determined that new cardiomyocytes are almost exclusively (if not entirely) derived from the pre-existing cardiomyocyte pool, which proliferates in response to injury.(23-25) In parallel, the concept of a bone-marrow derived progenitor, which dominated the field for over a decade (Figure 1.2), has been largely discredited, and the small effects of bone marrow-derived cells seen in some clinical trials have been ascribed to paracrine effects.(26, 27) In turn, this has directed research away from the hunt for cardiomyocyte progenitors towards understanding the mechanisms of endogenous regeneration in model organisms. In this regard, the role of the immune system, and specifically macrophages, in mediating repair by regeneration is poorly understood.

The intrinsic mechanisms which regulate cardiomyocyte proliferation may hold the key to understanding heart regeneration. In mammals, cardiomyocytes have traditionally been thought to proliferate only in utero and during early postnatal life.(28) In fact, elegant studies relying on integration of carbon-14 into DNA during Cold War nuclear testing suggests that low-level cardiomyocyte proliferation does occur in adult humans, providing hope that reactivation of the cell cycle in adult

cardiomyocytes, as occurs in regenerative models, may be possible to achieve improved cardiac repair.(29)

Several signalling pathways that regulate cardiomyocyte proliferation in regenerative model organisms have known roles in development. Neuregulin 1 (NRG1), an agonist for the ERBB2 and ERBB4 receptor tyrosine kinases of the epidermal growth factor (EGF) receptor family, is a key example. NRG1 is reactivated during zebrafish heart regeneration and its overexpression enhances cardiomyocyte proliferation.(30) In addition, the transcription factor heart and neural crest derivatives-expressed protein 2 (HAND2), which controls cardiomyocyte proliferation in the second heart field, is upregulated in the injured zebrafish ventricle, and its overexpression is sufficient to drive cardiomyocyte proliferation.(31) The Hippo pathway, which regulates the transcription factor YES-associated protein 1 (YAP1) and its co-activator TAZ, controls growth and heart size in embryonic development.(32) In a recapitulation of development, in the regenerating neonatal mouse heart YAP1 also promotes cardiomyocyte proliferation, acting via insulin-like growth factor and WNT signalling pathways.(33)

It is unclear whether the concept of a regenerative window for healing extends to neonatal humans. Intriguingly, there are some data to support this; in 2015 a case of a neonate with a large anterior MI caused by LAD thrombus was reported, who was thrombolysed only after 24 hours of coronary occlusion.(34) Although cardiac biomarkers suggested that there had been significant myocardial necrosis, over time there was complete recovery of ventricular function. Furthermore, despite evidence of impairment of cardiac function and myocardial scarring in infants undergoing surgical correction of anomalous left coronary artery from the pulmonary artery, at long-term follow-up the residual scar burden as assessed by cardiac magnetic resonance imaging (MRI) is extremely low.(35)

Endogenous cardiac regeneration has been viewed as a recapitulation of embryonic development.(20) There are parallels in the overall process, which requires controlled proliferation of cardiomyocytes and involves the interaction of multiple cell types in order to achieve precise organ morphogenesis.(36) Mechanistically, regeneration commonly reactivates developmental pathways or paradigms, for example the program of coronary vasculogenesis directed by the epicardium, or transcriptional mediators of cardiomyocyte proliferation.(12) As such, the study of developmental biology and endogenous regeneration have become intricately linked, and lessons from embryology may be applied to yield mechanistic insights and therapeutic strategies in the setting of injury and regeneration.

Figure 1.2

Name	Design	Patient group and number of patients	Cell type, dose and delivery route	Primary end point	Outcome	Comment
Menasche *et al.* (2001)	Case report	• Ischaemic heart failure undergoing CABG • $n=1$	• Skeletal myoblasts • 800×10^6 cells • Intramyocardial injection during CABG	NA	NA	• First-in-man report of skeletal myoblast injection • Improved wall motion and perfusion on PET
Strauer *et al.* (2002)	• Non-randomized • Open-label	• Acute myocardial infarction • $n=20$	• Autologous bone marrow-derived cells‡ • 2.8×10^7 cells • Intracoronary delivery	Not specified	Reduced infarct size in cell therapy arm	First study of bone marrow cells in acute myocardial infarction
Perin *et al.* (2003)	• Non-randomized • Open-label	• Ischaemic heart failure • $n=21$	• Autologous bone marrow-derived cells‡ • 25.5×10^6 cells • Transendocardial injection	Safety	• Improved left ventricular function • Reduced reversible perfusion defect	First study of bone marrow cells in heart failure
BOOST (2004)	• Randomized • Non-placebo controlled	• Acute myocardial infarction • $n=60$	• Autologous bone marrow-derived cells‡ • 24.6×10^8 nucleated cells • Intracoronary delivery	Change in LVEF	Improved global left ventricular function	First randomized study of bone marrow cells
ASTAMI (2006)	• Randomized • Non-placebo controlled	• Acute myocardial infarction • $n=100$	• Autologous bone marrow-derived cells‡ • 68×10^6 cells • Intracoronary delivery	Change in LVEF	No change in left ventricular function, end-diastolic volume or infarct size at 6 months	Negative trial concurrent with REPAIR-AMI
REPAIR-AMI (2006)	• Randomized • Double-blind • Placebo controlled	• Acute myocardial infarction • $n=204$	• Autologous bone marrow-derived cells‡ • 236×10^6 cells • Intracoronary delivery	Change in LVEF	Significant improvement in global left ventricular function at 4 months	Largest trial of bone marrow cells. Showed reduction in clinical end point of death, recurrent myocardial infarction and revascularization
Janssens *et al.* (2006)	• Randomized • Double-blind • Placebo controlled	• Acute myocardial infarction • $n=67$	• Autologous bone marrow-derived cells‡ • 304×10^6 nucleated cells • Intracoronary delivery	Change in LVEF	Negative for primary end point	Reduction in infarct volume
MAGIC (2008)	• Randomized • Double-blind • Placebo controlled	• Heart failure and previous myocardial infarction undergoing CABG • $n=97$	• Skeletal myoblasts • 400×10^6 cells (low dose) – 800×10^6 cells (high dose) • Surgical injection during CABG	Change in regional and global left ventricular function	Negative for primary efficacy end points	• High-cell-dose arm had reduced left ventricular remodelling with decreased left ventricular volumes • Increased arrhythmias in the cell therapy arms
SCIPIO* (2011)	• Randomized • Open-label • Non-placebo controlled	• Ischaemic heart failure • $n=23$	• Autologous KIT$^+$ cardiac stem cells • 1×10^6 cells • Intracoronary delivery	Safety	No adverse events reported	Increase in LVEF and decrease in infarct size reported in cell therapy recipients (secondary end points)
CADUCEUS (2012)	• Randomized • Non-placebo controlled	• Acute myocardial infarction • $n=25$	• Cardiosphere-derived cells • $12.5–25\times10^6$ cells • Intracoronary delivery	Safety: unexpected or arrhythmia-related death, myocardial infarction, tumour formation or MACE	Met safety end point	Reduction in scar size and mass in cell therapy arm

Figure 1.2

FOCUS-CCTRN (2012)	• Randomized • Double-blind • Placebo controlled	• Ischaemic heart failure • $n = 92$	• Autologous bone marrow-derived cells‡ • 100×10^6 cells • Transendocardial injection	• Change in left ventricular end-systolic volume • Maximal O_2 consumption, • Reversibility on SPECT	Negative for primary end points	–
SWISS-AMI (2013)	• Randomized • Open-label • Non-placebo controlled	• Acute myocardial infarction (either early (5–7 days) or late (3–4 weeks)) • $n = 200$	• Autologous bone marrow-derived cells‡ • $140–160 \times 10^6$ nucleated cells • Intracoronary delivery	Change in LVEF	Negative for primary end point	–
PROMETHEUS (2014)	• Non-randomized • Non-placebo controlled	• Ischaemic heart failure undergoing CABG • $n = 6$	• Mesenchymal stem cells • 2×10^7 cells (low dose) – 2×10^8 cells (high dose) • Intramyocardial injection during CABG	NA	NA	• Increased ejection fraction • Decreased scar mass
Menasche *et al.* (2015)	Case report	• Ischaemic heart failure undergoing CABG • $n = 1$	• Human ESC-derived cardiac progenitor cells on a fibrin scaffold • Surgical patch implantation	NA	NA	• First-in-man study • New-onset contractility observed in the patched region
REGENERATE-AMI (2016)	• Randomized • Double-blind • Placebo controlled	• Acute myocardial infarction • $n = 100$	• Autologous bone marrow-derived cells‡ • 59.8×10^6 cells • Intracoronary delivery	Change in LVEF	Negative for primary end point	Large, double-blinded study that failed to meet primary efficacy end point

Figure 1.2 Key studies of cell therapy for acute myocardial infarction and heart failure
Abbreviations: CABG, coronary artery bypass grafting; ESC, embryonic stem cell; LVEF, left ventricular ejection fraction; MACE, major adverse cardiovascular events; NA, not applicable; PET, positron emission tomography, SPECT, single-photon emission-computed tomography. *Subject to expression of concern. ‡See individual studies for precise characteristics of bone marrow-derived cells used. Reproduced from Cahill *et al.*[12] with permission.

1.2 Macrophages: classification & ontogeny

1.2.1 Macrophage classification and function

The macrophage was first described by the Russian zoologist Élie Metchnikoff, who observed migration of cells toward the site of injury after inserting rose thorns into starfish larvae in 1883.(37) Having previously observed cellular uptake of a nutrient dye, he realised that migrating 'phagocytes' (from Greek *phago*, to devour, *cytos*, cell) could employ this mechanism as a strategy for host defence.(37) He subsequently distinguished macrophages from neutrophils ('microphages') on the basis of nuclear morphology and alongside Paul Ehrlich, who made the first steps to identifying adaptive immunity mediated by antibodies, was awarded the Nobel Prize for Medicine in 1908.

Macrophages are highly plastic cells with a broad functional repertoire spanning homeostasis, injury, and infection.(38) They are resident in most organs of the body and undertake tissue-specialised roles including thermoregulation in brown adipose tissue(39), iron recycling in the splenic red pulp(40) and direction of spermatogonial stem cell differentiation in the testis.(40) Whilst originally described as professional phagocytes, following tissue injury they have a dynamic response and are involved in both inflammation and repair. Macrophage infiltration is a critical component of the response to bacterial and parasitic infection, including recognition of foreign material via toll-like receptors, phagocytosis and intracellular killing of pathogens. They constitutively express major histocompatibility complex (MHC) class II and are capable of presenting antigen to stimulate T and B cell responses.(41, 42)

Macrophages have also been implicated in the pathophysiology or progression of disease. In solid organ cancers, infiltration of tumour-associated macrophages is

associated with tumour proliferation, neoangiogenesis and adverse prognosis.(43) In atherosclerosis, macrophages are a major scavenger of low-density lipoprotein, and form fat-laden 'foam cells' within arterial wall plaque, contributing to the disease pathogenesis.(44) In obesity, secretion of pro-inflammatory cytokines by adipose tissue macrophages contributes insulin resistance and development of the metabolic syndrome.(45) Pro-inflammatory macrophage recruitment is key to the pathogenesis of autoimmune diseases such as Crohn's disease, rheumatoid arthritis, multiple sclerosis and autoimmune hepatitis.(46)

In the last two decades major insights into macrophage function have been made through categorising discrete activation states. This paradigm emerged following the recognition that different cytokines drive divergent gene expression profiles in macrophages, with interferon gamma (IFN-γ) capable of directing a pro-inflammatory state, and IL-4 an alternate activation state defined by upregulation of the mannose receptor.(47, 48) Adopting the nomenclature of T-helper cell polarisation (T_h1 and T_h2 cells), the concept of macrophage 'polarisation' developed and pro-inflammatory and alternate macrophages were labelled M1 and M2 respectively.(49)

Over time the features of macrophage polarisation have expanded to encompass upstream stimuli, transcriptional regulators, surface markers, metabolic profiles and secreted cytokines (Table 1.3).(50) M1 polarisation is classically stimulated by IFN-γ or lipopolysaccharide and leads to upregulation of inducible nitric oxide synthase and secretion of pro-inflammatory cytokines (e.g. TNF-α and IL-1β) via activation of STAT1 and IRF5. In contrast, M2 macrophage polarisation is stimulated by CSF1, IL-4 and IL-10, leads to the upregulation of arginase-1, and is mediated by STAT6, PPARγ and IRF4. These states have been mapped back to a range of *in vivo* functions: for example, the M1 macrophage is largely responsible for inflammation

and antimicrobial defense, while M2 macrophages are activated in parasitic infection and wound repair.(46)

Although the concept of macrophage polarisation has been useful for dissection of macrophage pathways and functions *in vitro*, it has important limitations. As a blunt dichotomy it is likely to be an oversimplification of the spectrum of macrophage function, and despite additional polarisation states being described, fails to adequately take account of the probable heterogeneity, plasticity and stimuli *in vivo*. Furthermore, M1/M2 categorisation relies on several markers without known cellular functions, and in cardiovascular biology there have been recent calls to abandon the concept of polarisation entirely.(51)

Table 1.1

	M1 polarisation	**M2 polarisation**
Stimuli	IFN-γ / LPS	Il-4, IL-13
Gene expression	*Nos2*	*Fizz1, Ym1, Arg1*
Surface markers	CD86, MARCO	CD206, CD163
Transcription factors	STAT1, STAT2, IRF5	IRF4, PPARγ
Metabolism	Glycolysis	Oxidative phosphorylation Fatty acid oxidation
Cytokines	IL-1β, IL-6, IL-12, IL-23	IGF-1, IL-10, TGF-β

Table 1.1 Macrophage polarisation in mouse

Macrophage functions have historically been categorised according to discrete polarisation states. Macrophage polarization *in vitro* can be driven by specific stimuli, for example IFN-γ / LPS for M1, and IL-4 or IL-13 for M2. Polarisation is associated with classical gene expression and surface marker profiles, transcription factors, metabolism and cytokines.

1.2.2 Macrophage ontogeny

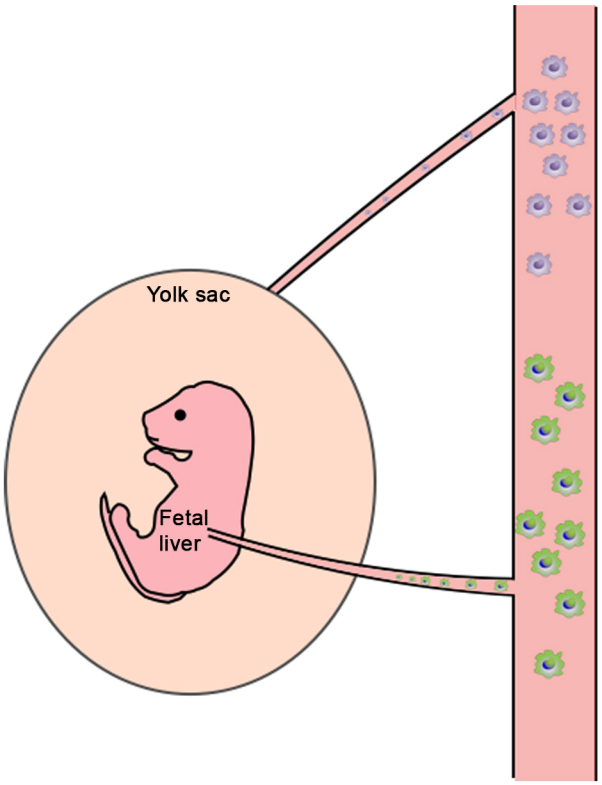
Understanding the ontogeny of myeloid cells has undergone a fundamental shift in recent years. Since the 1970s the dogma has been that macrophages are derived from blood-borne monocytes descended from progenitors in the bone marrow.(52) Established by Van Furth, this hierarchical model placed monocytes as the circulating precursors of tissue-resident macrophages, with monocytes providing the pool for renewal of macrophages when required.(52) The discovery that tissue-resident macrophages do not always derive from circulating monocytes, but can be seeded directly to organs during embryonic development, has been a paradigm shift in the field.(53) Organ-specific tissue-resident macrophages such as microglia are able to renew *in situ* entirely independently of adult haematopoiesis. In other organs, such as the gut, macrophages are replaced by circulating monocytes, from a common macrophage dendritic progenitor which resides in the bone marrow.(54)

Identifying the primitive precursors which give rise to tissue-resident macrophages in embryonic development has been the focus of extensive research. Embryonic haematopoiesis is complex and occurs in distinct temporal waves from both intra- and extra-embryonic sites.(55) In mice, primitive haematopoiesis (occurring prior to the emergence of the haematopoietic stem cell, HSC) begins in the yolk sac (YS) from approximately embryonic day 7.0 (E7.0).(53) A wave of 'erythromyeloid progenitors' (EMPs) emerge from the haemogenic endothelium of the YS and are the precursors to both embryonic macrophages and fetal liver monocytes.(56) An early wave of EMPs at approximately E7.5, which is independent of the transcription factor c-Myb, generates primitive macrophages.(57) A later wave (at ~ E8.25), which is c-Myb+, seeds the fetal liver to produce multiple lineages including monocytes.(58) Following the YS stage, haematopoiesis shifts to the para-aortic splanchnopleura

and aorta-gonads-mesonephros (AGM) region, where the first HSCs emerge at approximately E8.5-10.5. At E9.5-10.5, progenitors from the YS and AGM, including both EMPs and HSCs, migrate to and colonize the fetal liver, which becomes the principal site of haematopoiesis from E12.5 until progenitors seed the bone marrow.

In the heart, at least three resident macrophage populations have been described, which can be distinguished on the basis of variable cell surface expression of MHC class II and the C-C chemokine receptor type 2 (CCR2), the major receptor for monocyte chemoattractant protein 1 (MCP1).(59) A population of CCR2- macrophages, derived from the embryonic YS, seeds the heart as early as E12.5. In addition, CCR2+ monocyte-derived macrophages derived from the fetal liver seed the heart in development and persist in the adult heart, including MHCII hi and low subsets.(59) Using parabiosis in adult mice, at steady-state cardiac tissue resident macrophages have been show to undergo self-renewal by proliferation, with minimal replenishment from monocytes.(60) This remains contentious, however, with another study showing significant replacement of YS-derived macrophages from the monocyte pool with age.(61) When the resident macrophage pool is ablated, for example by diphtheria-induced macrophage depletion (using the CD11b-DTR model) or MI, macrophages are replenished from circulating monocytes.(60) The functional differences between cardiac macrophage subsets is still emerging and is discussed further below.

Figure 1.3



Primitive YS-derived macrophages

- Derived from blood islands & haemogenic endothelium of the YS
- Erythromyeloid progenitors (EMPs) emerge between E7.5-E8.25
- First wave of early EMPs at E7.5 express CSF1R (but not MYB)
- Second wave of late EMPs at E8.25 express MYB
- Macrophages seed organs to become tissue-resident

Definitive HSC-derived macrophages

- Derived from the haematopoietic stem cell (HSC)
- HSCs first emerge from the AGM from E10.5 onwards
- Definitive haematopoiesis occurs in the mouse fetal liver from E12.0, until the bone marrow takes over around the time of birth
- HSCs give rise to blood-borne circulating monocytes
- Dependent on MYB
- Monocytes can seed organs to give rise to tissue-resident macrophages, or remain circulating/in pools in the spleen & bone marrow marrow around the time of birth (in the mouse)

Figure 1.3 Macrophage ontogeny
Macrophages are derived from two sources in the embryo, the yolk sac (YS) and the haematopoietic stem cell (HSC). Primitive macrophages emerge in waves from blood islands and the haemogenic endothelium of the yolk sac via erythromyeloid progenitor (EMP) precursors. Definitive macrophages arise from monocytes in the bloodstream after the initiation of the circulation, which are in turn derived from the HSC. Both primitive and definitive macrophages may inhabit tissue-resident niches, and primitive macrophages are capable of self-renewal in situ. These distinct lineages of macrophages have differing and emerging roles in homeostasis and disease.

1.3 Macrophage markers & models

Since Metchnikoff's description of the macrophage as a phagocytic, migratory cell, a repertoire of molecular markers for macrophage identity has been described. Some markers have also been used to make transgenic mouse models which are used in this thesis, and these are discussed in turn.

1.3.1 F4/80

F4/80 is the canonical macrophage marker in mice and was first identified and characterised by Professor Siamon Gordon in Oxford.(62, 63) F4/80 was a hybridoma secreting a rat IgG_{2b} subclass monoclonal antibody which specifically recognised the EGF-like module-containing mucin-like hormone receptor-like 1 (EMR1) protein on macrophages. F4/80 is expressed on macrophages, Kupffer cells, splenic red pulp macrophages, Langerhans cells, microglia and at lower levels on blood monocytes and eosinophils. EMR1 is an adhesion-type heterotrimeric guanine nucleotide-binding protein (G protein)-coupled receptor (adhesion-GPCR), a seven-transmembrane spanning receptor comprised of extracellular and intracellular domains. EMR1 was the first adhesion-GPCR studied, but at least 33 receptors in humans have now been identified.(64) Adhesion GPCRs have common functions in adhesion, migration, recognition of other cells, interaction with extracellular matrix components and pathogens through their N-terminal fragment. Specifically, EMR1 has been demonstrated to play a role in induction of T-regulatory cells.(65)

1.3.2 CD68

CD68 is a type I transmembrane protein in mice and humans belonging to the lysosomal/endosomal-associated membrane protein family. It may play a role in

antigen processing or as a scavenger receptor, but its function is not fully defined.(66) In mice, CD68 (macrosialin) expression is restricted to monocytes, macrophages and dendritic cells, and in human samples it is routinely used as a macrophage marker for immunohistochemistry.(67) A transgenic mouse model expressing EGFP under control of the human CD68 promoter sequence has been generated and validated in the Greaves laboratory in Oxford, with bright GFP expression in myeloid cells including monocytes, macrophages, neutrophils and eosinophils.(68)

1.3.3 CX3CR1

Chemokine CX3C motif receptor 1 (CX3CR1) is a seven-transmembrane domain G-protein-coupled receptor which functions as the receptor for the chemokine fractalkine and as an adhesion molecule for monocyte migration.(69) The endogenous *Cx3cr1* locus in mice has been targeted with *EGP* to make CX3CR1-GFP reporter mice, with expression in monocytes, natural killer (NK) cells, dendritic cells and some tissue resident macrophages (e.g. microglia, but not Kupffer cells or splenic macrophages), but not neutrophils or eosinophils.(70) This line has become widely used as a macrophage reporter. Parkhurst *et al* produced CreERT2 line in order to have temporal control over macrophage labelling.(71)

1.3.4 CSF1R

Colony-stimulating factor 1 (CSF-1; also known as macrophage colony stimulating factor, M-CSF) is the key haematopoietic growth factor directing differentiation of macrophages from bone marrow progenitor cells. CSF-1 directs myeloid differentiation in bone marrow HSCs, and mutation or knock-out of the *Csf1* gene in mice ($Csf1^{op/op}$) leads to significant reduction in the numbers of macrophages and

development of osteopetrosis.(72, 73) The receptor for CSF1, CSF1-R, is a receptor tyrosine kinase encoded by the *c-fms* proto-oncogene.(74) CSF1-R expression is a key regulator of macrophage fate and is expressed in immature and differentiated cells of the mononuclear phagocytic system, but has also been reported to be expressed on cells of the trophoblast, neural progenitors and kidney tubular epithelium.(75-77) A transgenic mouse reporter in which GFP is expressed under the control of the CSF1-R promoter (MacGreen), demonstrated fluorescence throughout the mononuclear phagocyte system and in cells of the trophoblast.(78) Lineage tracing of CSF1-R positive cells in the embryo using both constitutive (*Csf1r*^{iCre}) and inducible (*Csf1r*^{MeriCreMer}) mouse reporter lines has been important in demonstrating that YS EMPs give rise to embryonic macrophages.(56)

1.3.5 PU.1

The transcription factor PU.1 has been identified as a master regulator of myeloid cell lineage commitment in haematopoietic progenitors.(79) In mice, targeted knock-out of the *Spi1* locus, encoding PU.1, leads to early postnatal lethality with either a complete lack of, or aberrant, development of granulocytes, macrophages, B and T cells.(80, 81) CSF-1 directly activates the *Spi1* promoter, and CSF1R is a downstream target of PU.1, providing positive feedback loop for myeloid differentiation.(73, 82) The requirement for PU.1 in early myeloid progenitors is not fully defined, but may be dispensable for generation of EMPs in the early embryo.(83)

1.4 Macrophages in cardiac development, injury and repair

1.4.1 Cardiac development

Primitive macrophages appear in the developing heart from approximately E12.5.(84) Although the precise mechanisms by which macrophages are recruited to the developing heart, prior to the onset of the circulation, are largely unknown, activation of the epicardium, a developmental cell niche which functions as a master regulator of coronary and heart formation, is a necessary step for cardiac seeding of YS-derived macrophages.(85) Using the inducible $Wt1^{CreERT2}$ mouse line to drive epicardial expression of the diphtheria toxin at E11-11.5, the epicardium was selectively ablated, which resulted in failure of recruitment or retention of embryonic macrophages.(85)

The roles of macrophages in the embryonic heart are starting to emerge. In 2016, Leid *et al* reported that a CCR2- YS-derived macrophage population closely associated with the nascent developing coronary vasculature.(84) Loss of macrophages in two knock-out mouse models, the genetic $Csf1^{op/op}$ model and knockdown using *LysM*-Cre;R26-DTA, led to hyperbranching of coronary vessels and dysregulation of vessel calibre at E17.5.(84) The authors identified increased expression of IGF1 in the YS-derived macrophage population, compared to fetal liver-derived monocytes, and suggested this may underlie the mechanism of remodelling observed. Recently, a novel role for tissue resident macrophages was described in facilitating cardiac conduction.(86) Hulsmans *et al* reported presence and coupling of macrophages to conduction system via connexin43 in the mouse and human atrioventricular node. Constitutive or induced ablation of macrophages led to development of atrioventricular block.

1.4.2 Cardiac injury & scar formation

Macrophages are resident in the normal adult heart and make up approximately 10% of the cells present.(60) These cardiac-resident macrophages have a sentinel role and are suggested to sample the local antigen milieu and respond to cardiac stress or injury. Cellular damage or necrosis leads to release of 'alarmins', a diverse group of signalling mediators including heat shock proteins, HMGB1, extracellular RNAs, ATP, extracellular matrix components, complement and reactive oxygen species, which activate pro-inflammatory pathways in macrophages via toll-like receptor activation.(5, 87, 88) Activation of alarmin-induced signalling leads to a cascade resulting in macrophage release of TNF, IL-1β and IL-6, activation of endothelial integrins and adhesion molecules, and release of chemokines and cytokines which drive recruitment of neutrophils and monocytes.

Release of inflammatory mediators, exosomes and chemokines such as MCP 1 leads to mobilisation, activation and recruitment of innate immune cells to the injury site from reservoirs in the bone marrow and spleen.(89-91) Two subsets of monocytes ($Ly6C^{hi}$ and $Ly6C^{lo}$) have been identified and suggested to drive the inflammatory and resolution phases post-MI.(91) Whilst these had been thought to reflect different populations, knockout of Nr4a1, which is required for the production (but not differentiation) of $Ly6C^{lo}$ monocytes, does not abolish the biphasic inflammatory response, suggesting that $Ly6C^{lo}$ monocytes are derived by differentiation from $Ly6C^{hi}$ monocytes.(92) $Ly6C^{hi}$ monocytes are thus the major source of both $Ly6C^{hi}$ pro-inflammatory macrophages and as the infarct heals, $Ly6C^{lo}$ pro-reparative macrophages.

Functionally, macrophages have multiple roles within injury and repair. In the early injury phase, they function to amplify and sustain pro-inflammatory cytokine

signalling. As phagocytes they have a central role in ingestion and degradation (efferocytosis) of neutrophils, apoptotic cardiomyocytes and matrix debris, a process which requires activation of the tyrosine kinase Mer.(93) The process of macrophage efferocytosis is intrinsic to the switch from inflammation to repair – knockout of Mer leads to delayed resolution of inflammation, impaired macrophage transition to an 'M2' state and reduced cardiac function.(93) In the resolution phase, macrophages secrete a number of factors, such as TGF-β, which promote recruitment and activation of fibroblasts to matrix-producing myofibroblasts. Additionally, macrophages are a source of growth factors which promote angiogenesis and lymphangiogenesis. Recently, Korf-Kilngebiel identified production of 'myeloid derived growth factor' (C19orf10) as a novel mediator of cardiomyocyte survival and angiogenesis in the injured mouse heart.(94) Knockdown of macrophages, by injection of clodronate or splenectomy, leads to impaired formation of myocardial scar and increased risk of rupture.(95, 96)

While macrophages are required for activation of inflammation, scar formation and stabilisation, the number of macrophages and the precise timing of their influx and departure are highly regulated and influence tissue repair.(97) In humans, the level of peripheral blood monocytosis after MI is an independent predictor of heart failure events and adverse clinical outcome downstream.(98) Mechanistically, this may be due to macrophage-induced ventricular remodelling, where the LV dilates and becomes globular in shape, promoting mitral regurgitation and further functional impairment. In preclinical models, macrophages have been shown to drive ventricular remodelling through production of matrix metalloproteinases, and targeting the monocyte CCR2 receptor protects against remodelling due to lack of monocyte infiltration.(99) A failure to clear macrophages post-MI, which occurs predominantly via the cardiac lymphatic system, leads to a failure to resolve inflammation and enlarged scar size.(97) These findings support the concept that

macrophages have both beneficial and potentially detrimental roles in the healing heart.

1.4.3 Cardiac regeneration

Macrophages have also been directly implicated in tissue repair by regeneration. Inflammation stimulates cardiomyocyte proliferation in the injured neonatal heart, and blockade of IL6 or cardiomyocyte STAT3, its downstream effector, blocks heart regeneration after apical resection.(100) In the neonatal MI model, macrophages are actively recruited to the neonatal heart and ablation of macrophages using clodronate liposomes blocks regenerative repair through inhibition of angiogenesis.(101)

Divergent roles from different macrophage subsets are emerging. In particular, there is a recognition that the origins of macrophages – either from monocyte or the embryonic yolk sac – influence the cellular response to inflammation. Using a cardiomyocyte-ablation model, Lavine *et al* found that depletion of resident macrophages in the neonatal heart led to reduced cardiomyocyte and endothelial cell proliferation, interstitial fibrosis and chamber dilatation.(102) In contrast, inhibition of CCR2+ macrophages, derived from monocytes, led to dominance of embryonic subsets and improved myocardial repair.(102)

The finding that macrophages are implicated in tissue regeneration are inconsistent alongside their known roles in the injured adult mammalian heart, where they mediate scar formation. There is therefore a need to dissect regenerative macrophage functions from those implicated in scar formation, remodelling and heart failure. Identification of regenerative functions could serve as potential therapeutic targets, as incremental gains to improve healing following injury would reduce the

incidence or severity of downstream heart failure.

Figure 1.4

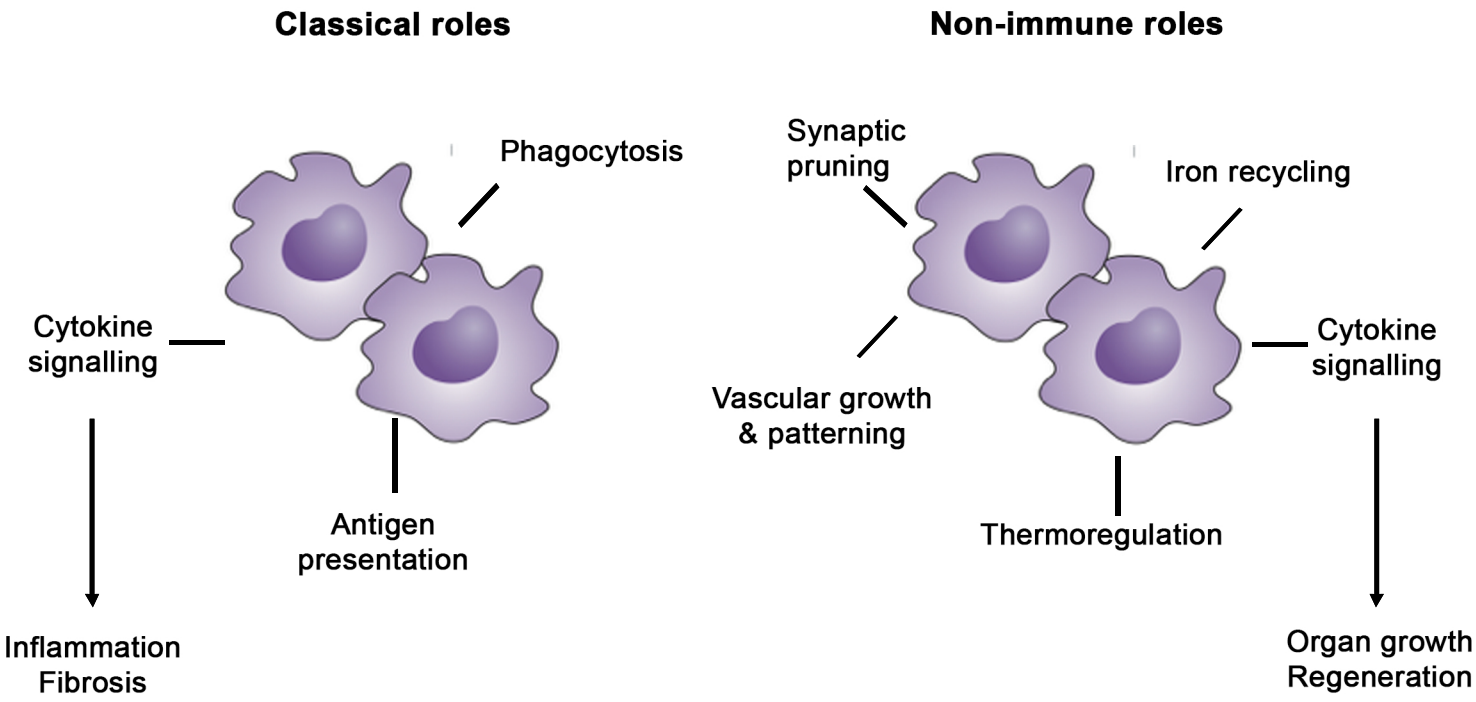


Figure 1.4 Classical and non-classical roles of macrophages in the heart
While originally described as professional phagocytes and regulators of inflammation through cytokine production and antigen presentation (left),a number of emerging 'non-immune' roles for macrophages have been described (right). These are frequently tissue specific and include regulation of iron recycling in the spleen, synaptic pruning in the developing brain, thermoregulation in adipose tisue, and vascular patterning.

1.5 Hypotheses

The primary aim of this thesis was to investigate the non-immune roles of macrophages during cardiac development, repair and regeneration. I hypothesised that macrophages play tissue-specific, trophic roles during the context of cardiac development and regeneration, to support growth and repair of the heart. By direct comparison of regeneration and scar formation, I hypothesised that the beneficial functions of macrophages might be dissected apart from the known inflammatory and pro-fibrotic roles of macrophages in mammalian wound healing.

1.6 Aims of the Thesis

1) To characterise the spatiotemporal infiltration of macrophages in cardiac development

2) To determine whether embryonic macrophages function as lymphatic progenitor cells within the embryonic heart

3) To investigate potential roles for macrophages in remodelling of coronary or lymphatic vessels in cardiac development

4) To compare macrophage pathways during cardiac repair by regeneration compared to scar formation

5) To validate functional roles for macrophages in directing repair by regeneration or scar formation

Chapter 2: Materials & Methods

2.1 Mice

2.1.1 Mouse strains

Genetically modified mouse lines used in experiments for this thesis are shown in Table 2.1. All lines were on a pure C57BL/6 background backcrossed for at least eight generations unless otherwise specified. In experiments where wild type mice were used, the CD1 strain was used as indicated (Charles River Laboratories). Mice were housed in the University of Oxford Biomedical Services Building and the Department of Pharmacology Biomedical Services Building. All animal experiments were carried out in accordance with the UK Animals (Scientific Procedures) Act 1986 under project licences PPL 30/2987 and PPL30/3155.

Table 2.1 Genetic mouse lines

(a) Reporter mouse lines

Name	Promoter	Locus	Construct	Reported expression	Reference
Cx3Cr1-GFP	*Cx3Cr1*	Endogenous *Cx3cr1* locus	*GFP*	Monocytes, macrophages, natural killer cells, dendritic cells	(70)
Cd68-GFP	*Human Cd68*	Unknown	*GFP*	Monocytes, macrophages, neutrophils	(68)
R26R-tdTom	*R26*	*Gt(ROSA)26Sor*	*LoxP-STOP-LoxP tdTomato*	Driven by Cre expression	(103)
R26R-EYFP	*R26*	*Gt(ROSA)26Sor*	*LoxP-STOP-LoxP EYFP*	Driven by Cre expression	(104)

(b) Cre recombinase & knock-out mouse lines

Name	Promoter	Locus	Construct	Reported expression	Reference
Cx3cr1-CreERT2	*Cx3cr1*	Endogenous *Cx3cr1* locus	*EYFP* & *CreERT2* recombinase	Monocytes, macrophages	(71)
Csf1R-MeriCreMer	*Csf1R*	Unknown	*MeriCreMer* recombinase	Monocytes, macrophages	(105)
Pu.1$^{-/-}$	Not applicable	*Pu.1*	Mutation in exon 5	Myeloid cells, B cells	(80)
Flt3-CreERT2	*Flt3*	Endogenous *Flt3* locus	*CreERT* recombinase	HSC derivatives	(106)
Col1a2-CreERT2	*Col1a2*	Unknown	*CreERT* recombinase	Cells expressing COL1A2	(107)

Table 2.1 Genetic mouse lines Genetic mouse lines used in this thesis can be divided into reporter mouse lines (a), and Cre recombinase and knock-out mouse lines (b). Details of the transgene promoter, locus, construct and reported expression for each genetic mouse line are indicated, where applicable. Abbreviations: HSC – haematopoietic stem cell.

2.1.2 Timed matings

For timed mating experiments, females were paired with male studs and were checked for the presence of a vaginal plug each morning. The morning of plugging was designated as embryonic day 0.5 (E0.5).

2.1.3 Tamoxifen activation of Cre recombinase

For studies in embryos, 4-hydroxytamoxifen and progesterone (both from Sigma) were dissolved in peanut oil (Sigma) to a final concentration of 10 mg/ml and stored in aliquots at -20°C. Pregnant females received 1.5 mg 4-hydroxytamoxifen and 1 mg of progesterone by intraperitoneal injection at the indicated embryonic stage. For studies in neonatal pups, tamoxifen (Sigma) was dissolved in peanut oil (Sigma) to a final concentration of 10 mg/ml and stored in aliquots at -20°C. Pups received 0.5 mg tamoxifen by subcutaneous injection at day 5 post-MI.

2.1.4 Embryo dissection

Embryos were harvested from pregnant females at the required embryonic stage. The mother was euthanised by cervical dislocation and the uterine horns were dissected from the abdominal cavity. Embryos were extracted from the uterine horns, placed in ice-cold PBS (Sigma) and the amniotic sac was removed. The heart was micro-dissected from the embryo for experiments using fine forceps, and a 1 mm piece of tail was retained for genotyping.

2.1.5 Adult heart dissection

Adult mice were euthanized by cervical dislocation and the heart was blunt dissected from the thorax through a median sternotomy. After rinsing away blood in ice-cold

PBS, and trimming away adherent connective tissue or lung, hearts were fixed, digested or snap-frozen in liquid nitrogen for subsequent experiments.

2.2 Myocardial infarction models

2.2.1 Adult myocardial infarction model

All adult MI surgery was performed in CD1 mice at age 8-12 weeks. General anaesthesia was induced by inhalation of 4% isoflurane in oxygen at 1.5L/minute delivered to an anaesthetic chamber. After approximately 2 minutes, mice were transferred to a heated pad and taped in the supine position with 4% isoflurane delivered to a nose cone to maintain anaesthesia. Under microscopic visualisation an endotracheal tube was inserted and placement confirmed by watching for symmetrical lung expansion with mechanical ventilation. Isoflurane then reduced to 2%, and positive pressure ventilation was set to 200 per minute with a stroke volume of 200 µl. A core temperature probe was inserted per rectum for perioperative monitoring. All mice received a dose of buprenorphine (0.3 mg/kg) prior to surgery. After shaving the left side of the chest and cleaning with Hibiscrub, the surgical site was draped

The surgical procedure was conducted in the following sequence: first, the skin was incised for a left lateral thoracotomy and the subcutaneous fascia and pectoral muscles were retracted. Using sharp forceps, the intercostal space was punctured and widened to insert a rib retractor. The pericardium was then opened with iridectomy scissors and a 8-0 prolene suture tied in the anterior left ventricular wall, encircling the expected position of the left anterior descending coronary artery. Immediate blanching of the myocardium is seen when coronary ligation is successfully achieved. The ribs and skin are then closed in layers with interrupted sutures (7-0 prolene).

Following completion of surgery, isoflurane was progressively weaned and after recovery of consciousness and normal spontaneous respiration, the mouse was extubated and transferred to a heated chamber at 30°C. 100 µl of normal saline was given to each mouse by subcutaneous injection to replace perioperative losses. Once active, mice were transferred back to a cage, kept warm overnight at 33°C in an incubator, and given a moist diet. The following morning mice were returned to normal temperature. All mice were closely observed for 48 hours post-procedure and given additional buprenorphine analgesia if required.

2.2.2 Neonatal myocardial infarction model

Surgical induction of MI in the neonatal mouse has recently been described and has been adapted in the Riley group to comply with U.K. regulation.(108) CD1 mothers were used for all experiments due to reduced rates of maternal cannibalization. At postnatal day 1 (early within the regenerative window), or postnatal day 7 (outside this window), the litter was removed from the mother and placed in an incubator at 33°C. General anaesthesia was induced with 4% isoflurane inhalation (for 1-2 minutes). Once unconscious, cardiorespiratory arrest was induced by immersion in ice for 2-4 minutes, depending on size. The pup was then taped onto an ice block in the supine position, the incision site was cleaned with Hibiscrub and a sterile field constructed with drapes.

Once draped, the skin was cut in a horizontal incision across the left mid-thorax. Sharp dissecting forceps were used to puncture between the ribs, close to the chondrocostal junction, in approximately the 9-10th rib space (Figure 1B). The space was then widened using blunt forceps (Figure 1C). The heart was manipulated out of the thoracic cavity by gentle pressure on the abdomen and the contralateral chest wall. Once exposed, a prolene 7-0 suture was passed through the anterior wall of the

left ventricle (1D), to encompass the left anterior descending artery, and tied. The ribs and skin were then closed in layers with prolene 7-0 (1F).

The pup was then gently warmed under a heat lamp, leading to gradual return of circulation and breathing. Low concentration (0.5%) isoflurane was then supplied by tube to minimise (potential) pain associated with systemic reperfusion. Once fully alert the pup was returned to its littermates. After surgery was completed on all pups, the animals were covered with faeces from their cage (which reduces cannibalization) and returned as a group to the mother.

Figure 2.1

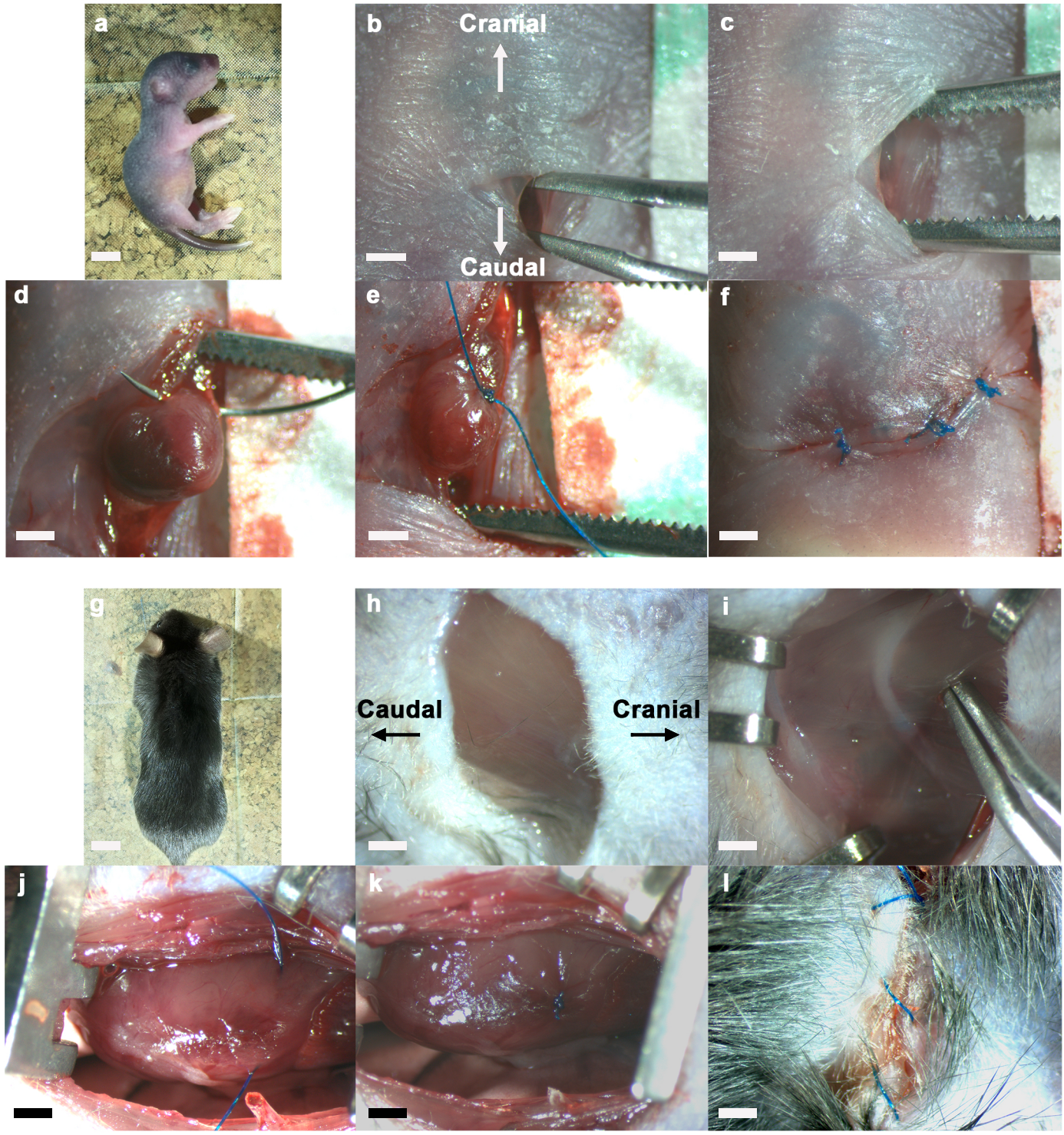


Figure 2.1 Mouse models of myocardial infarction (a) Neonatal mouse, postnatal day 3 (b) After induction of cardiorespiratory arrest, the mouse was positioned supine, the skin was incised and the chest wall was punctured in the 5th intercostal space near the midline (c) The rib space was opened using blunt forceps (d-e) The heart was manipulated out of the thorax by gentle pressure on the contralateral chest and the abdomen. A 7-0 prolene suture was then tied through the anterior left ventricular wall to interrupt coronary flow (f) The heart was pushed back into the chest, and the chest wall and skin were closed in layers (g) Adult mouse (h) After induction of general anaesthesia and intubation, the mouse was positioned supine, the chest was shaved, the skin incised and the muscle layer exposed by blunt dissection (i) The pectoralis muscles were then retracted, the intercostal muscles punctured, and the ribs separated using a retractor to access the heart. (j-k) A 7-0 prolene suture was then passed through the anterior left ventricular wall, to encompass the left anterior descending coronary artery, and tied (l) The chest wall and skin were closed in layers using interrupted prolene 7-0 sutures. Scale bars in (a) and (g) are 1cm, all others are 1mm.

2.3 Molecular methods

2.3.1 DNA extraction for genotyping

DNA was extracted from ear punch biopsies (adult mice) or tail samples (embryos). Protein was first removed by overnight digestion in proteinase K (1 µl/ml) (at 55°C in 500 µl tail lysis buffer). DNA was then precipitated by addition of 500 µl of isopropanol. Samples were centrifuged at 13,000 rpm for 15 minutes, the supernatant removed, and the remaining DNA pellet washed in 1ml of 70% ethanol. The pellet was re-centrifuged at 13,000 rpm for 5 minutes, 70% ethanol removed and the remaining DNA re-suspended in 200 µl TE Buffer prior to genotyping.

2.3.2 Genotyping PCRs

Primers for genotyping PCRs are shown in Table 2.3. The following reagents were used per reaction: illustra PuReTaq Ready-To-Go PCR Beads (GE Healthcare), 1 µl of each primer (at a concentration of 0.05 pmol/ml), 2 µl DNA and 21 µl sterile H_2O, giving a total reaction volume of 25 µl. The PCR reaction was performed on a 96 well Veriti thermal cycler (Applied Biosystems) using the specific program shown in Table 2.4. For each genotyping reaction a positive control sample of known genotype and a 'no-DNA' water control were included.

Table 2.2 – PCR primers for genotyping

Gene	Primers	PCR program
Cre (*Cx3cr1*-CreERT2; *Col1a2*-CreERT2)	FWD: GTTCGCAAGAACCTGATGGACA REV: CTAGAGCCTGTTTTGCACGTTC	Taqgenom2
iCre (*Csf1R*-MeriCreMer)	FWD: AGATGCCAGGACATCAGGAAC CTG REV: ATCAGCCACACCAGACACAGAG ATC	iCre
Pu.1	WT allele detection PUKO: GCCCCGGATGTGCTTCCCTTATCAAAC 920: TGCCTCGGCCCTGGGAATGTC PU.1$^{-/-}$ allele detection PUKO: GCCCCGGATGTGCTTCCCTTATCAAAC NEO: CGCACGGGTGTTGGGTCGTTTGTTCGG	Pu1
Gfp *(Cd68-GFP)*	FWD: CAGCCCTCTCTTGGAAAGGAGG REV: TTCTCGGCTCTGTGAATGACA	CD68

Table 2.3 – PCR programs

Taqgenom2

Temperature (°C)	Duration (mins.secs)	Cycles
94	2.00	1
94 60 72	0.30 0.30 0.45	35
72	5.00	1
4	∞	1

iCre

Temperature (°C)	Duration (mins.secs)	Cycles
94	1.30	1
94 64 72	0.30 0.45 0.45	35
72	2.00	1
4	∞	1

PU.1

Temperature (°C)	Duration (mins.secs)	Cycles
95	15	1
94 63 72	0.45 0.45 1.30	36
72	10	1
4	∞	1

CD68

Temperature (°C)	Duration (mins.secs)	Cycles
94	2.00	1
94 55 72	0.30 0.45 1.00	35
72	3.00	1
4	∞	1

2.3.3 Agarose gel electrophoresis

PCR amplification products were separated by agarose gel electrophoresis. To prepare an agarose gel (1.5%), 1.5 g of agarose (Sigma Aldrich, UK) was added to 100 ml of TBE buffer and heated in a microwave until fully dissolved (approximately 30 seconds). 5 µl of GelRed (VWR) was added to the agarose gel after heating to allow UV visualisation of DNA. The gel was then poured into a mould to set. PCR products were mixed with 5 µl DNA Gel Loading Dye (6X), loaded into the gel and run at 110 V for 45 minutes. PCR products were visualised on the gel using a UV light box.

2.3.4 RNA extraction from tissue

Following harvest, cardiac tissue was snap frozen in liquid nitrogen. To extract RNA, samples were homogenised in 1 ml of TRIzol reagent (Thermo Fisher Scientific) by grinding with a manual tissue homogeniser and passing through a 21G sterile needle into a 1ml syringe (BD Biosciences). 200 µl of chloroform was added, samples were vigorously shaken and incubated for 2 minutes at room temperature. To separate RNA, samples were centrifuged at 12,000 x *g* for 15 minutes at 4°C, and the (upper) aqueous layer was aspirated off and transferred to a new Eppendorf tube. RNA was then precipitated by addition of isopropanol, and samples were incubated on ice for 20 minutes. RNA was pelleted by centrifugation (11,000 rpm for 15 minutes at 4°C), washed in 75% ethanol, air-dried and re-suspended in DEPC-treated water. RNA concentration and purity was assessed using a Nanodrop 2000 (Thermo Fisher Scientific).

2.3.5 cDNA synthesis

Complementary DNA (cDNA) was synthesised by reverse transcription. For each sample, the volume required for 1µg of RNA was calculated (based on known concentration) and was made up to 8.5µl with DEPC water. A master mix containing the following reagents was then prepared (volumes per sample shown): 0.5µl of random primers (20µg/ml; Promega); 1µl dNTPs (10mM; GE Healthcare); 2µl $MgCl_2$ (25mM; Thermo Scientific); 2µl Dithiothreitol (DTT; 0.1M, Life Technologies); 1µl RNasin Plus RNase inhibitor (Promega); 4µl 5X FS Buffer (Life Technologies) and 1µl of SuperScript III Reverse Transcriptase (Life Technologies). 11.5µl of master mix was added to each sample. The reverse transcription reaction was run on a Veriti thermal cycler (Applied Biosystems) according to the following cycling program: 25°C for 10 minutes, 42°C for 50 minutes, 70°C for 15 minutes, then held at 4°C. cDNA was diluted to 4ng/µl in DEPC water and stored at -20°C until use.

2.3.6 Quantitative real-time PCR

The relative expression of mRNA of selected genes was assessed by quantitative real time PCR (qPCR). Each reaction contained 8ng of cDNA with 13 µl Fast SYBR Green Master Mix (Thermo Fisher Scientific), 6.5 µl DEPC H_2O, and 0.5 µl (concentration 0.05 pmol/ml) of each primer. Reactions were run in triplicate on a MicroAmp Fast Optical 96-well plate (Thermo Fisher Scientific). A no-template (no cDNA) control was run for each gene. qPCR reactions were run using a ViiA 7 Real-Time PCR System (Thermo Fisher Scientific). Cycle threshold (Ct) values for each reaction were exported to Microsoft Excel and analysed according to the comparative cycle threshold method. To calculate mRNA expression relative to a housekeeping gene (e.g. *gapdh*), the difference in cycle thresholds (ΔCt) between the gene of interest (mean ΔCt of three replicates) and housekeeping gene was calculated. This

value was compared across experimental groups ($\Delta\Delta$Ct) and transformed to estimate fold change ($2^{-\Delta\Delta CT}$).

Table 2.4 – Primers for qRT-PCR

Gene	Forward primer	Reverse primer
Col1a1	GCAAGAGGCGAGAGAGGTTT	GACCACGGGCACCATCTTTA
Col1a2	CTGGAACAAATGGGCTCACTG	CAGGCTCACCAACAAGTCCTC
Col3a1	ACGTAGATGAATTGGGATGCAG	GGGTTGGGGCAGTCTAG

2.3.7 RNA sequencing

Described in Chapter 5

2.4 Staining

2.4.1 Wax embedding for histology

Following dissection hearts were fixed in 4% paraformaldehyde (PFA)/PBS at 4°C overnight. After washing 3 times in PBS samples were dehydrated by passage through a rising concentration of ethanol: initially 50% ethanol (in PBS) followed by 70%, 80% 90%, 96%, 100%, 100%, for 2 hours each. Samples were then transferred to butanol overnight before being placed in a solution of 50% molten Histoplast paraffin wax/butanol (Fisher) at 56°C for 1 hour. After three changes of 100% paraffin wax to remove residual butanol, the samples were oriented and embedded onto a mould pre-loaded with paraffin, then left to cool at room temperature. Short axis cardiac sections of 10 μm thickness were cut using a Microtome and transferred onto Superfrost Plus slides (VWR). Slides were dried overnight at 37°C before staining.

2.4.2 Masson's Trichrome staining

Sections were first deparaffinised in Histoclear solution (two passages of 5 minutes each), followed by rehydration through a rising concentration of MQ water in ethanol (50% MQ water, then 70%, 80%, 90% and 100% for 5 minutes each). Staining was performed using a Masson's Trichrome kit (Sigma Aldrich, UK) according to the manufacturer's instructions. Following rehydration samples were mordanted in Bouin's solution for 15 minutes at 56°C. Samples were then stained by immersion in a) Weigert's Iron Haematoxylin solution (5 minutes) b) Biebrich Scarlet-Acid Fuchsin (5 minutes) c) Aniline Blue (5 minutes) d) Phosphotungstic/ Phosphomolybdic acid solution (5 minutes) and e) 1% Acetic acid solution (2 minutes). Samples were rinsed in MQ water and dehydrated by passage through a rising ethanol gradient (as above, in reverse), before clearing in Xylene (1 minute) and mounting using DPX media.

2.4.3 Immunofluorescence – cryosections

For immunofluorescence imaging hearts were initially fixed in PFA (adult hearts – 4% PFA/PBS, overnight at 4°C; embryonic hearts – 2% PFA/PBS for 6 hours at room temperature). Samples were then washed in PBS and incubated overnight in 30% sucrose/PBS at 4°C. Samples were transferred to 50/50 30% sucrose/optimal cutting temperature compound (OCT, VWR chemicals) for 1 hour, then into 100% OCT in an embedding mould. Once oriented correctly hearts were transferred to the -80°C freezer and left overnight. Sections (8-10 μm slices) were cut using a cryostat and were transferred onto Superfrost Plus slides and stored at -80°C prior to staining.

For staining, slides were dried at room temperature for 10 minutes, rinsed in PBS, permeabilised in 0.5% Triton X-100/PBS for 10 minutes, and re-rinsed in PBS. Individual sections were encircled using an ImmEdge hydrophobic barrier pen (Vector Laboratories) to allow different antibody staining combinations on the same slide. Sections were blocked with 10% donkey serum/1% bovine serum albumin/0.1% Triton X-100 in PBS for 1 hour at room temperature. After blocking, slides were transferred to a humidified chamber, primary antibodies (diluted in block) were added and incubated on sections at 4°C overnight. The next day all sections were rinsed three times in 0.1% Triton X-100/PBS, then washed three times in 0.1% Triton X-100/PBS (for 10 minutes each wash). Secondary antibodies (diluted in PBS) were then added and incubated on sections for 1 hour at room temperature. Sections were washed three times in PBS (10 minutes each), incubated for 5 minutes in 4',6-Diamidino-2-Phenylindole, Dihydrochloride (DAPI; concentration 0.1 μg/ml) diluted in PBS and mounted using 50% glycerol/PBS. Slides were coverslipped and sealed with nail varnish. Primary and secondary antibodies used are shown in Table 2.5 and Table 2.6. All experiments included a ‘secondary only’ control to test for non-specific

binding of secondary antibody. Imaging was performed using a Olympus FV 1000 confocal microscope. Image analysis was carried out using Image J.

2.4.4 Immunofluorescence – whole mount embryo hearts

Dissected hearts were fixed for 6 hours in 2% PFA/PBS at room temperature, permeabilised in 0.3% Triton X-100/PBS (2 x 10 minutes) and then blocked in 1% BSA, 0.3% Triton X-100 in PBS for at least 2 hours. Samples from fluorescent reporter lines were protected from light throughout. Samples were incubated with primary antibodies (diluted in block) overnight at 4°C, then washed three times for at least 1 hour each in 0.3% Triton X-100/PBS. Samples were incubated with secondary antibodies (diluted in PBS) overnight at 4°C, protected from light, then rinsed three times for at least 10 minutes each with PBS. The hearts were then oriented and mounted in 50% glycerol/PBS in glass-bottomed dishes (Mattek). Imaging was performed using an Olympus FV 1000 confocal microscope. Image analysis was carried out using Image J.

Table 2.5: Primary antibodies for immunofluorescence

Antibody target (species raised in)	Supplier Cat no	Reactivity	Dilution
COL1 (rabbit)	Abcam Ab34710	Collagen I	1:50
CD68 (rat)	Bio-Rad MCA1957	Macrophages	1:200
CTGF (mouse)	SC Biotechnology SC-365970	CTGF	1:50
ENDOMUCIN (rat)	SC Biotechnology SC-53941	Vascular endothelium	1:50
GFP (chicken)	Abcam ab13970	GFP	1:2000
LYVE-1 (rabbit)	Angiobio 11-034	Lymphatic endothelium	1:200
LYVE-1 (rat)	Novus Biologicals NBP1-43411	Lymphatic endothelium	1:500
PROX1 (rabbit)	Angiobio 11-002	Lymphatic endothelium	1:200
PROX1 (goat)	R&D Systems AF2727	Lymphatic endothelium	1:200
VEGFC (rabbit)	Abcam ab9546	VEGFC	1:200
VEGFR-3 (goat)	R&D Systems AF743	Lymphatic endothelium	1:50

Table 2.6: Secondary antibodies for immunofluorescence

Antibody	Supplier	Dilution
AF goat α-chicken 488	Invitrogen	1 in 200
AF donkey α-goat 488	Invitrogen	1 in 200
AF donkey α-goat 594	Invitrogen	1 in 200
AF donkey α-goat 647	Invitrogen	1 in 200
AF goat α-mouse 488	Invitrogen	1 in 200
AF donkey α-rabbit 488	Invitrogen	1 in 200
AF donkey α-rabbit 594	Invitrogen	1 in 200
AF donkey α-rabbit 647	Invitrogen	1 in 200
AF donkey α-rat 488	Invitrogen	1 in 200
AF goat α-rat 594	Invitrogen	1 in 200
AF chicken α-rat 647	Invitrogen	1 in 200

Table 2.7 Solutions

Solution	Constituents
Tail lysis buffer (TLB)	100mM Tris pH 8.5, 5mM EDTA, 0.2% SDS, 200mM NaCl, 0.05mg/ml Proteinase K
Tris-borate-EDTA buffer (TBE)	40mM Tris pH 8.0, 20mM Boric acid, 1mM EDTA

Tris-EDTA buffer (TE)	10mM Tris pH 8.0, 1mM EDTA

Table 2.8 Kits and reagents

Kit	Supplier	Catalogue no
SMART-Seq v4 Ultra Low Input RNA Kit for Sequencing	Takara Clontech	634891
Nextera XT DNA Sample Preparation Kit (96 Samples)	Illumina	FC-131-1096
NextSeq 500/550 high output v2 kit 150 cycles; High output	Illumina	FC-404-2002

2.5 Flow cytometry

2.5.1 Digestion

Single cell suspensions from the mouse heart were prepared according to a published protocol.(109) For each mouse, the heart was dissected out and transferred into ice-cold PBS. Blood was rinsed out and adherent lung and fat were removed. The atria were left intact. The heart was then briefly dried before transfer to a Petri dish, where it was finely minced using a scalpel. Hearts were then transferred to a Falcon tube containing collagenase II (Worthington, 500 units per ml) in HBSS (adult – 10mls, neonatal and embryonic hearts 5 mls). All tubes were then placed in a shaking incubator at 37°C and 180 rpm for 1 hour (embryonic hearts 30 minutes), with pipetting every 10 minutes to help break up tissue chunks. Dissociated samples were then passed into a 50ml Falcon tube through a 70 μm cell strainer, then rinsed with 3 mls ice cold HBSS and transferred back to a 15 ml Falcon. Samples were spun for 7 minutes at 350g at 4 degC, and the HBSS/collagenase supernatant carefully removed by pipette. Cell pellets were resuspended in 5 mls of red cell lysis buffer (BioLegend) and incubated at room temperature for 10 minutes, followed by a repeat spin at 350*g* at 4°C for 7 minutes. Red cell lysis buffer was removed and cells were resuspended in 2% FBS/PBS (adult 500 μl, P7+7 200 μl, other neonatal and embryonic heart samples 100 μl).

2.5.2 Antibody staining

Prior to antibody staining, samples were incubated with 1% mouse Fc receptor block (Miltenyi Biotec) for 5 minutes on ice. Antibodies were then added (Table 2.9) and the samples incubated for 20 minutes at room temperature protected from light. Samples were then rinsed with 1ml of 2% FBS/PBS and spun down at 350g for 7 minutes. Cells were resuspended in 200 μl 2% FBS/PBS. 5 minutes before FACS, 7-

AAD viability stain (eBioscience) was added to a final concentration of 1%. For analysis, samples were run on a FACSAria III (BD Biosciences). When sorted by FACS, cells were collected into 20 µl of 2% FBS/PBS on a FACSAria Fusion (BD Biosciences) sorter.

Table 2.9 Antibodies for flow cytometry

Target	Clone	Isotype	Supplier; Cat #	Fluorophore	Dilution
CD45	30-F11	Rat IgG2b, κ	Biolegend 103124	AF647	1:200
CD11b	M1/70	Rat IgG2b, κ	Biolegend 101206	FITC	1:100
Ly6G	1A8	Rat IgG2a, κ	Biolegend 127636	BV421	1:200
F4/80	BM8	Rat IgG2a, κ	Biolegend 123110	PE	1:100
Ly6C	HK1.4	Rat IgG2c, κ	Biolegend 128026	APC-Cy7	1:800
CD206	C068C2	Rat IgG2a, κ	Biolegend 141721	BV605	1:100

2.6 Adoptive transfer studies

Monocytes were isolated from the spleen of CD68-GFP+ adult mice. Following Schedule 1 killing, the spleen was removed by dissection and the tissue disrupted with the blunt end of a sterile syringe. The disrupted spleen tissue was washed through a 70 μm cell filter into red cell lysis buffer and incubated at room temperature for 10 minutes. Cells were then spun down (400*g* for 5 minutes) and red cell lysis buffer removed by aspiration. Monocytes were then purified from the cell pellet using the EasySep^{TM} Mouse Monocyte Enrichment Kit according to the manufacturer's instructions. Prior to surgery, cells were counted and resuspended in PBS to give a final concentration of 50 x 10^3 per 5 μl for injection. Each recipient received 1 x 5 μl injection of cells by intracardiac injection (using a 30G insulin syringe) at the time of MI surgery.

2.7 Statistical analysis

Statistical analyses were performed in GraphPad Prism 7 software. Comparisons between two groups were made using an unpaired student T test (two tailed). A one-way ANOVA was used to make multiple comparisons between three experimental groups. A p-value of less than or equal to 0.05 was considered statistically significant.

Chapter 3: Macrophages in cardiac development

The heart of animals is the foundation of their life, the sovereign of everything within them, the sun of their microcosm, that upon which all growth depends, from which all power proceeds

William Harvey

1628

3.1 Background

3.1.1 Development of the heart & coronary vasculature

The heart is the first organ to form in the vertebrate embryo.(110) In the mouse, cardiac development begins at embryonic day 7.5 (E7.5) with formation of the cardiac crescent, comprised of cardiac progenitors in the anterior mesoderm (Table 3.1).(111) The cardiac crescent converges along the midline to form the linear heart tube by E8.0, which undergoes rightward looping at E8.5 to position the prospective chambers of the primitive four-chambered heart.(112) In addition to the cells of the linear heart tube, there is a contribution to the forming heart from progenitor cells of the second heart field, the neural crest and the proepicardium. Cardiac morphogenesis is completed by septation of the ventricles, atria and outflow tract.

The cardiac vasculature, made up of the coronary circulation and lymphatic vessels, develops from approximately E11.5 (Table 3.1).(113) A primitive coronary endothelial network first emerges along the dorsal aspect of the heart, originating from the sinus venosus, the embryological precursor of the right atrium.(114) On the ventral aspect of the heart, endothelial cells appear in the interventricular groove and spread laterally. At least three embryological origins of coronary endothelial cells have been identified, including the sinus venosus, which contributes the majority of coronary endothelium, the epicardium, and the endocardium, which gives rise to the vessels within the interventricular septum.(114-116)

The primitive coronary vascular plexus is connected to the aortic root at E13.5, after which there is coronary blood flow.(117, 118) The initiation of coronary flow is an important driver of arterial and venous specification, and between E14.5 and E16.5, smooth muscle cells derived from the epicardium associate with the arterial

endothelium in a process mediated by pericytes, Angiopoietin-1 and PDGF-A.(119, 120)

Table 3.1: Comparative time course of heart development in mouse and human

Process	Mouse	Human
Cardiac crescent formation	E7.5	Day 15
Linear heart tube formation	E8.0	Day 20
Cardiac looping	E8.5	Day 28
Chamber formation	E10.0	Day 32
Coronary vessel formation begins	E11.5	Day 33-36
Lymphatic vessel formation begins	E12.0	Day 40-60(121)
Coronary vessels connect to the aortic root	E13.5	Day 44-46
Myocardial maturation	E15.5 onwards	Day 56 onwards

Abbreviations: E – embryonic day

3.1.2 Development of the cardiac lymphatic vasculature

The lymphatic vasculature is a unidirectional transport pathway from the extracellular space to the venous system. Functionally, it is required for tissue fluid homeostasis, immune cell trafficking, and transport of lipids.(122) In the developing heart, lymphatic vessels first develop along the dorsal aspect of the heart at approximately E12.0.(123) Lymphatic endothelial cells (LECs) can be identified by expression of prospero homeobox 1 transcription factor (PROX1), a transcription factor directing LEC fate, and vascular endothelial growth factor receptor (VEGFR)-3.(123, 124) Lymphatic vessels migrate from the base of the heart towards the apex, and by E18.5, a dense, interconnected network has formed over the surface of the heart, which continues to develop and remodel into early post-natal life.(125)

The embryological origins of cardiac LECs have been the focus of a recent paradigm shift. Historically it was believed that LECs are exclusively derived from the venous

endothelium, a view first postulated by Florence Sabin in 1902.(126) This dogma has recently been overturned, however, with the finding that a small proportion of LECs in the heart, as well as in the mesenteric and dermal lymphatics, have a non-venous, mesenchymal lineage origin.(123, 127, 128) The precise identity and origin of these non-venous 'lymphangioblast' precursors is uncertain, with recent lineage tracing studies by Klotz *et al* and Stanczuk *et al* implicating a CSF1R+ PDGFB+ KIT+ VAV+ precursor.(123, 127)

3.1.3 Macrophages in the embryonic heart

Phagocytic cells were first identified in the embryonic heart by Manasek in 1969,(129) and were described further by Pexieder in 1972.(130, 131) Using light- and electron- microscopy to study the embryonic chick and rat heart, these studies reported the presence of macrophages localised to sites of physiological cell death in the bulbus cordis. Sorokin *et al* subsequently observed macrophages in the rat heart from embryonic day 12, primarily distributed along the bulbus cordis and the aortic arch.(132) Macrophages were confirmed to be phagocytically active *in vitro* and it was hypothesised that their role was to clear debris following apoptotic cell death.

Few studies to date have focused on characterising the identity, ontogeny and functional roles of macrophages during organogenesis. In the heart, the reported timescale of macrophage infiltration corresponds to the development of the coronary and lymphatic vasculature, the cardiac conduction system, the valves, and cardiac growth, maturation and remodelling (Table 3.1). In principle, macrophages might contribute to any of these processes through phagocytosis, release of soluble signalling mediators, interaction or recruitment of progenitor cells, or transdifferentiation. Based on recent data suggesting that macrophages in the developing mouse hindbrain are required for normal development and patterning of

the cerebral vasculature, I hypothesised that macrophages play a similar role in development of the vasculature of the heart, and more specifically in the formation of coronary lymphatic vessels.(133)

3.1.4 Aims

This chapter addresses four experimental aims:

1. To quantify the number of macrophages in the embryonic heart, and analyse the timing of macrophage infiltration.
2. To investigate the spatial localisation of macrophages in the embryonic heart, to gain insights into possible functional roles.
3. To investigate the ontogeny of macrophages in the embryonic heart, specifically to identify the localisation of macrophage populations derived from the yolk sac and from definitive haematopoiesis.
4. To undertake lineage tracing of macrophages to determine whether they may contribute as progenitors to developing lymphatic vessels.

3.2 Results

3.2.1 Macrophages infiltrate the embryonic heart

Macrophages were identified and quantified by flow cytometric analysis of CX3CR1-GFP embryonic mouse hearts. CX3CR1-GFP has previously been described as a highly specific marker of macrophages and is not expressed on other cell types.(86) To provide a further level of confirmation that cells expressing CX3CR1-GFP+ were macrophages, they were also stained for the canonical macrophage marker F4/80.(62) Timed matings were established using the CX3CR1-GFP mice, and based on the previous literature,(130, 132) embryos were harvested at E12.5, E14.5 and E16.5 for analysis. Hearts were microdissected, digested in collagenase, stained and analysed by multicolour flow cytometry.

At E12.5, E14.5 and E16.5, macrophages were identified in the embryonic heart as a distinct population of live singlet cells expressing both CX3CR1-GFP and F4/80 (Figure 3.1a, gate indicated). The absolute number of macrophages per heart increased significantly from E12.5 to E14.5: from a mean (± S.E.M.) of 297 ± 60 cells at E12.5 (n=6) to 1018 ± 154 cells at E14.5 (n=8), $p=0.0023$. There was a further significant increase in macrophage numbers from E14.5 to E16.5: from 1018 ± 154 cells at E14.5 (n=8) to 1569 ± 175 cells at E16.5 (n=6), $p=0.0365$ (Figure 3.1b). These findings confirm the presence of macrophages within the embryonic heart in significant numbers, and suggest active recruitment or proliferation of macrophages throughout the time course of development.

Figure 3.1

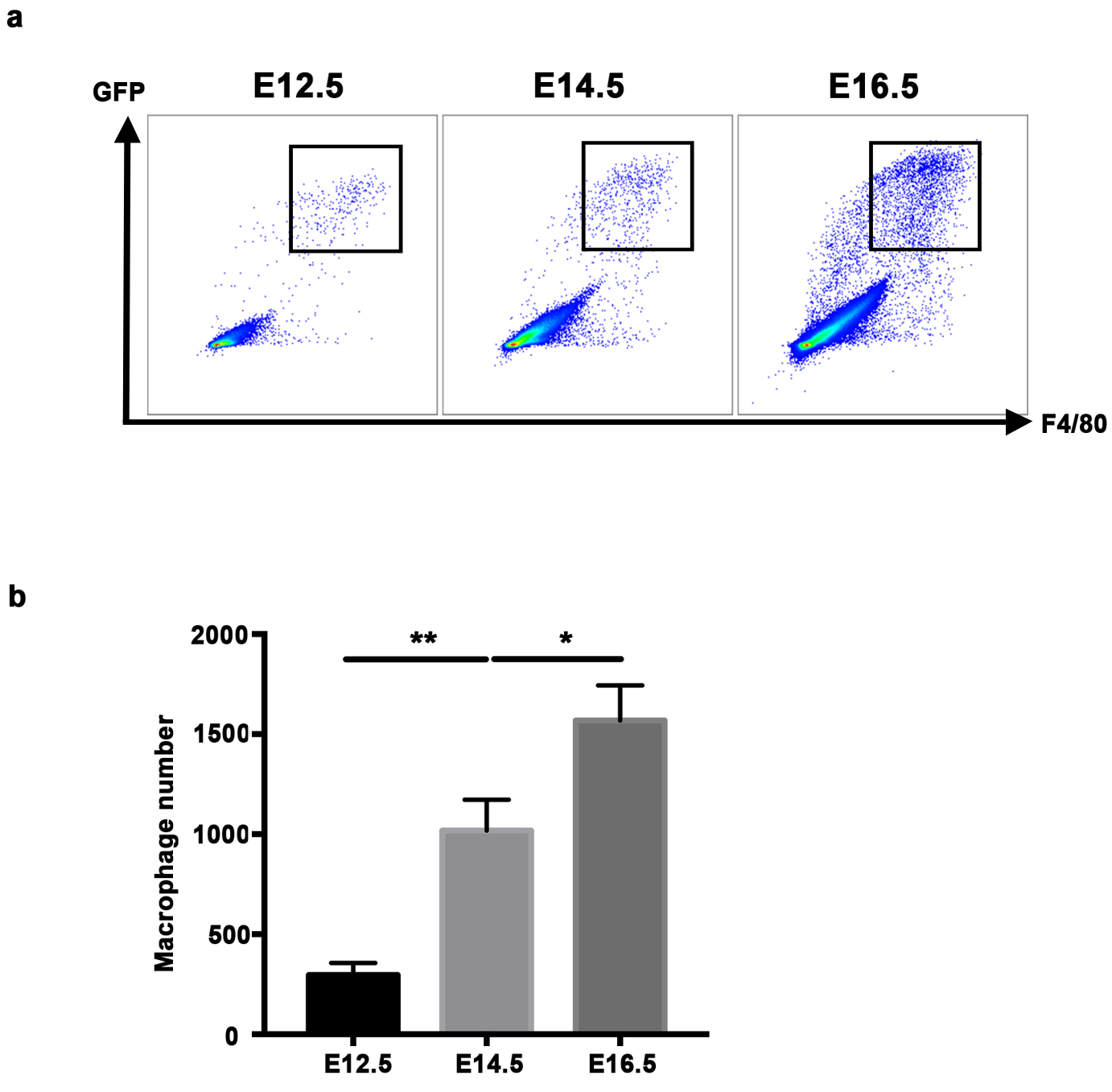


Figure 3.1 Macrophages infiltrate the developing heart
(a) Representative flow cytometry plots showing all live singlet cells from the hearts of CX-3CR1-GFP+ mice at embryonic day (E) 12.5, 14.5 and 16.5. Macrophages were identified as cells positive for both CX3CR1-GFP and F4/80 (gate shown) (b) Quantification of the mean (+/- SEM) number of macrophages in the heart at E12.5, E14.5 and E16.5. * $p < 0.05$, ** $p < 0.01$, n = 6-8 per experimental group.

3.2.2 Macrophages colocalise with coronary vessels and lymphatics

The localisation of cardiac macrophages in the embryonic heart was further investigated by whole mount immunofluorescence staining. Timed matings were established using CX3CR1-GFP mice and embryos were harvested at E12.5, E14.5 and E16.5. Embryos were also harvested from the CD68-GFP reporter line at E16.5 Hearts were isolated by microdissection and fixed. Hearts were stained (as indicated) with antibodies to the vascular endothelial marker Endomucin (EMCN) or the LEC markers LYVE1 and VEGFR3. EMCN is initially expressed widely throughout the coronary endothelium and is restricted to veins and capillaries from approximately E15.5 onwards.(134, 135) Imaging was performed by confocal microscopy with Z-stack reconstruction.

At E12.5, CX3CR1-GFP+ macrophages were concentrated around the outflow tract (ventral aspect), the sinus venosus (dorsal aspect) and the epicardium (Figure 3.2a, b). Although a primitive EMCN+ capillary network had developed by E12.5, there was no evidence of LYVE1+ lymphatic vessel formation. Furthermore, the majority of CX3CR1-GFP+ macrophages were negative for the marker LYVE1. At E14.5, CX3CR1-GFP+ macrophages had spread across both the ventral and dorsal aspects of the heart and increasingly co-expressed LYVE1 (Figure 3.2a). At high power, macrophages were visualised to lie in close proximity to, or in direct contact with, vessels of the nascent EMCN+ coronary vascular network. The first LYVE1+ lymphatic vessels were seen on the dorsal aspect of the heart at E14.5 (Figure 3.2b). At E16.5, CX3CR1-GFP+ LYVE1+ macrophages were commonly visualised in close proximity to coronary vascular and lymphatic vessels, in particular at branch points, leading edges or in contact with the adventitial surface of the vessel wall. By E16.5

both coronary and lymphatic vasculature had developed, although had not yet expanded to cover the entire epicardial surface.

Direct association between macrophages and lymphatic endothelium was confirmed utilising E16.5 hearts from the CD68-GFP reporter mouse line, stained for VEGFR3 to visualise LECs (Figure 3.2c). Direct contact between the macrophage cell body or filopodia was clearly visualised (Figure 3.2c, arrowheads), suggesting that macrophages physically associate with the developing lymphatic network in the embryonic heart.

Figure 3.2

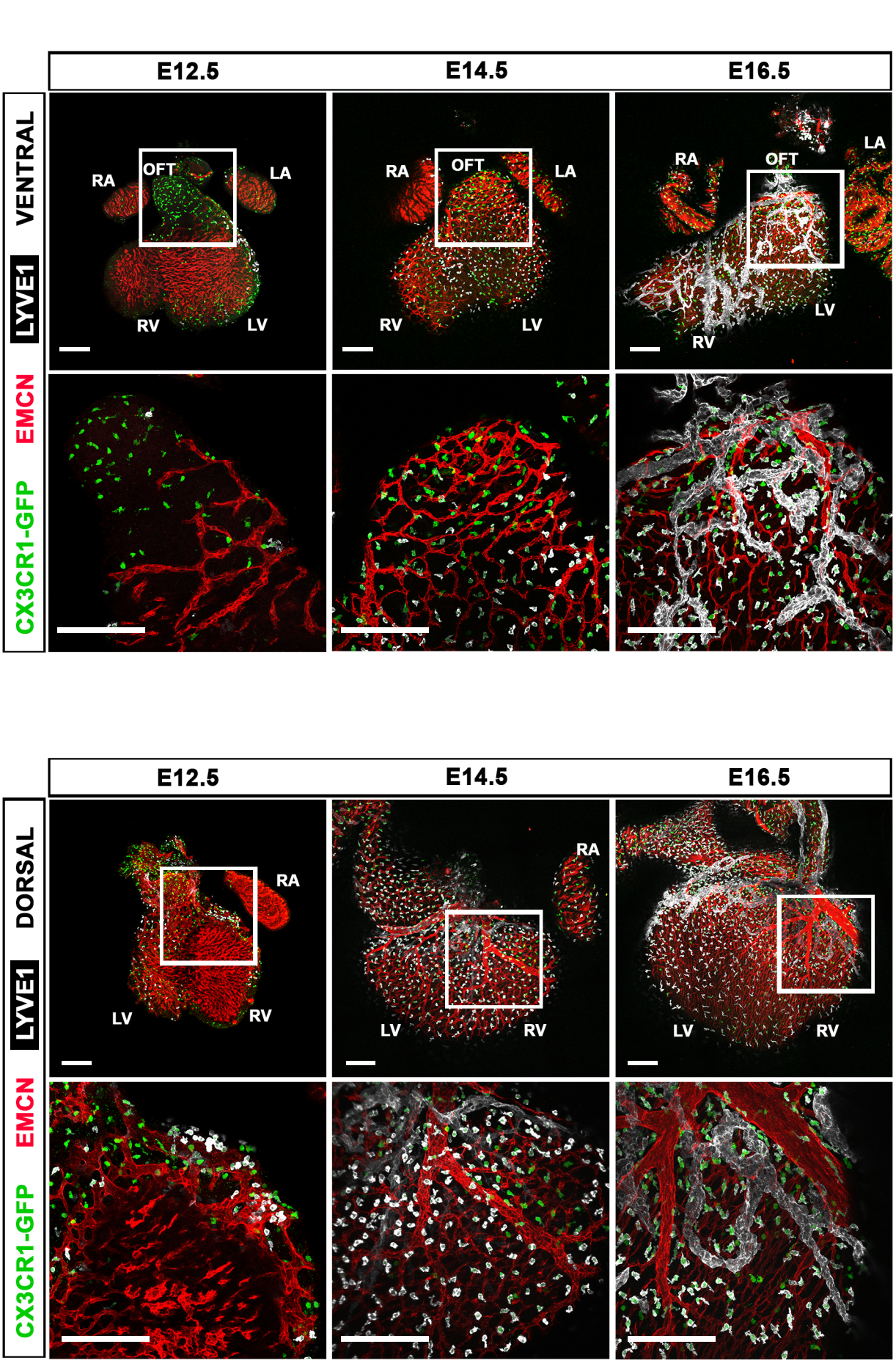

a
E12.5
E14.5
E16.5
VENTRAL
LYVE1
EMCN
CX3CR1-GFP
RA
OFT
LA
RV
LV
b
DORSAL

Figure 3.2

c

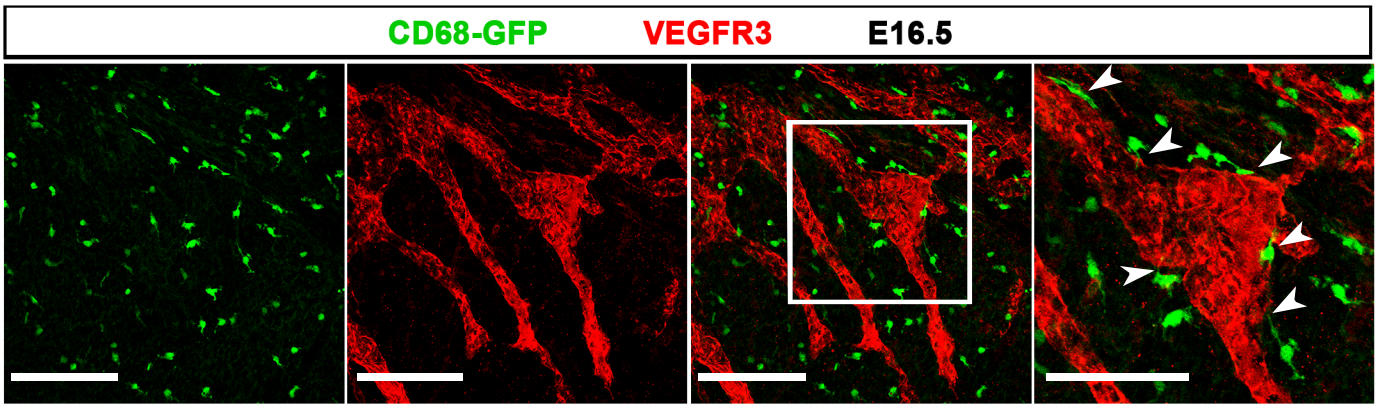


Figure 3.2 Macrophages colocalise with coronary vessels and lymphatics
(a) Confocal imaging of the dorsal aspect of whole mount hearts immunofluorescence stained for macrophages (CX3CR1-GFP), coronary vessels (EMCN) and lymphatics (LYVE1) at E12.5-E16.5, demonstrating colocalisation of macrophages with the developing coronary and lymphatic vasculature at E14.5 and E16.5. Scale bar 200 μm. Respective white inset boxes are shown beneath at higher magnification (Scale bar 200 μm). (b) Confocal imaging of the ventral aspect of whole mount hearts immunofluorescence stained for macrophages (CX3CR1-GFP), coronary vessels (EMCN) and lymphatics (LYVE1) at E12.5-E16.5, demonstrating colocalisation of macrophages with the developing coronary and lymphatic vasculature at E14.5 and E16.5. Scale bar 200 μm. Respective white inset boxes are shown beneath at higher magnification (Scale bar 200 μm). All images representative of n=4 per group. (c) Confocal imaging of whole mount hearts immunofluorescence stained for macrophages (CD68-GFP) and lymphatic vessels (VEGFR3) at E16.5, demonstrating direct physical contact between macrophages and lymphatic endothelium (arrowheads). Scale bar 200 μm; Inset scale bar 100 μm. Images representative of n=3. Abbreviations: LA left atrium, LV left ventricle, OFT outflow tract, RA right atrium, RV right ventricle.

3.2.3 A LYVE1-positive macrophage subset localises to the epicardium

The spatial localisation of macrophages in the embryonic heart was first investigated by immunofluorescence staining of cryosections. Timed matings were established using CX3CR1-GFP mice and embryos were harvested at E16.5. Hearts were isolated by microdissection, fixed, embedded and sectioned in a long axis orientation. Hearts were stained using antibodies raised to GFP, the macrophage marker CD68(68), lymphatic vessel endothelial hyaluronan receptor 1 (LYVE1) a marker of LECs and tissue-resident macrophages(136), and the nuclear stain 4',6-diamidino-2-phenylindole (DAPI). Imaging was performed by confocal microscopy.

In the E16.5 embryonic heart, macrophages were identified as cells coexpressing the markers CX3CR1-GFP+ and CD68+, which showed complete overlap (Figure 3.3). Macrophages were distributed throughout the heart and could be visualised in the epicardium, the myocardium, and in the trabeculae of the left ventricle (Figure 3.3). A subset of CX3CR1-GFP+ CD68+ macrophages also expressed the marker LYVE1+. LYVE1+ macrophages were observed to localise exclusively to the epicardium (see merged panel, Figure 3.3), and were not seen within the myocardium or trabeculae (inset high-magnification panel, Figure 3.3).

Figure 3.3

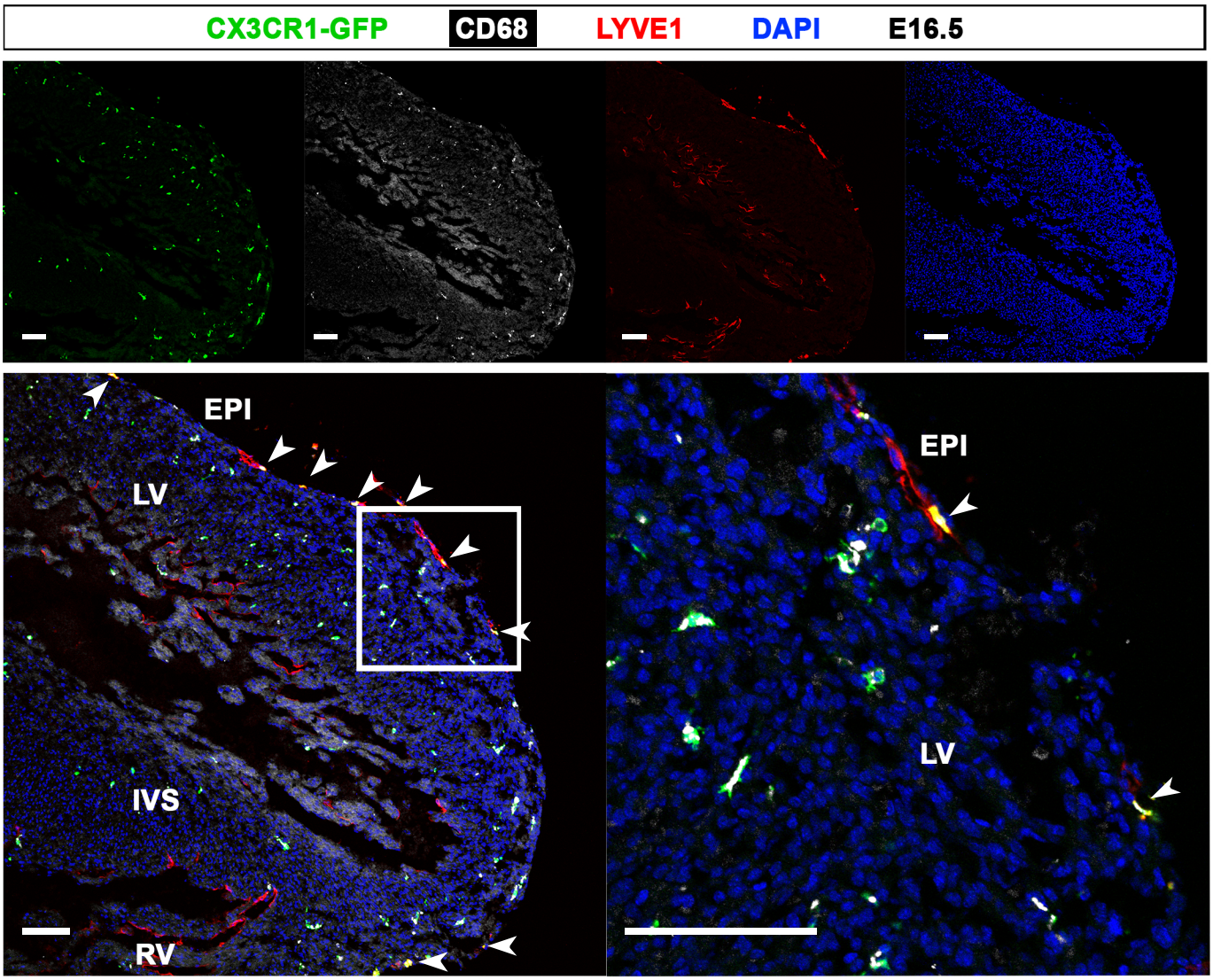


Figure 3.3 A LYVE1-positive macrophage subset localises to the epicardium
Confocal imaging of immunofluorescence-stained heart cryosections from CX3CR1-GFP mice at E16.5 demonstrating macrophages (CX3CR1-GFP+ CD68+ cells) disributed within the epicardium, myocardium and trabeculae of the embryonic heart. A subset of macrophages staining positive for LYVE1 localised exclusively to the epicardium (arrowheads). Inset, high-magnification image. Scale bar 100 µm. Images representative of n=3. Abbreviations: EPI epicardium, IVS interventricular septum, LV left ventricle (free wall), RV right ventricle (free wall).

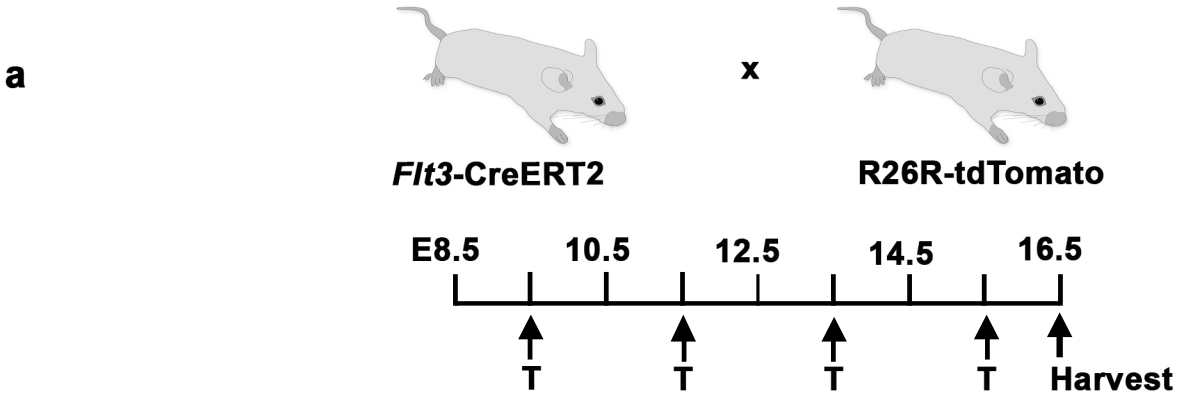
3.2.4 LYVE1+ lymphatic-associated macrophages are derived from the yolk sac

During embryonic development, macrophages arise from either the yolk sac (YS) or from haematopoietic stem cells (HSCs).(53) YS-derived macrophages seed tissue-resident niches where they have distinct roles and responses compared to macrophages which arise from HSCs via a blood-borne circulating monocyte intermediate.(102) The ontogeny of macrophages can be identified by using a lineage tracing approach. Upregulation of *Flk2* (*Flt3*) is a critical stage in loss of self-renewal of definitive HSCs, and Cre recombinase driven by the *Flt3* promoter has been demonstrated to label all progeny arising from HSCs.(137)

The ontogeny of macrophages in the embryonic heart was investigated using embryonic hearts obtained from *Flt3*-CreERT2;tdTomato mice, obtained in collaboration with Professor Sten-Eirik Jacobsen at the Karolinska Institute. After establishing timed matings between *Flt3*-CreERT2 males and R26RtdTomato females, pregnant dams were dosed with 1mg tamoxifen and 0.5mg progesterone by oral gavage at E9.5, E11.5, E13.5, and E15.5 (Figure 3.4a; total dose 4mg tamoxifen and 2mg progesterone). This labelling strategy resulted in almost 100% of the Flt3+ lymphoid-primed multipotent progenitor population being labelled as tdTomato+, confirming highly efficient recombination (data not shown). Embryos were harvested at E16.5, hearts were isolated by microdissection and fixed, and tail samples were used to genotype for *Cre* and *TdTomato*. Hearts were then stained (as indicated) to visualise macrophages (CD68 and LYVE1) and LECs (LYVE1), with HSC progeny indicated by positivity for tdTomato. Imaging was performed by confocal microscopy with Z-stack reconstruction.

At E16.5, punctate CD68+ LYVE1+ macrophages were clearly visualised in close association with LYVE1+ lymphatic vessels (Figure 3.4b). No overlap between CD68+ LYVE1+ macrophages and TdTomato signal was observed (Figure 3.4b). Furthermore, unlike the CD68+ LYVE1+ macrophage population, most TdTomato+ cells in the heart did not make direct contact with LYVE1+ lymphatic vessels (Figure 3.4b high magnification insets, arrowheads). Taken together, these data indicate that the lymphatic vessel-associated CD68+ LYVE1+ macrophage subset is not derived from the HSC, but arises from primitive haematopoiesis from the YS.

Figure 3.4



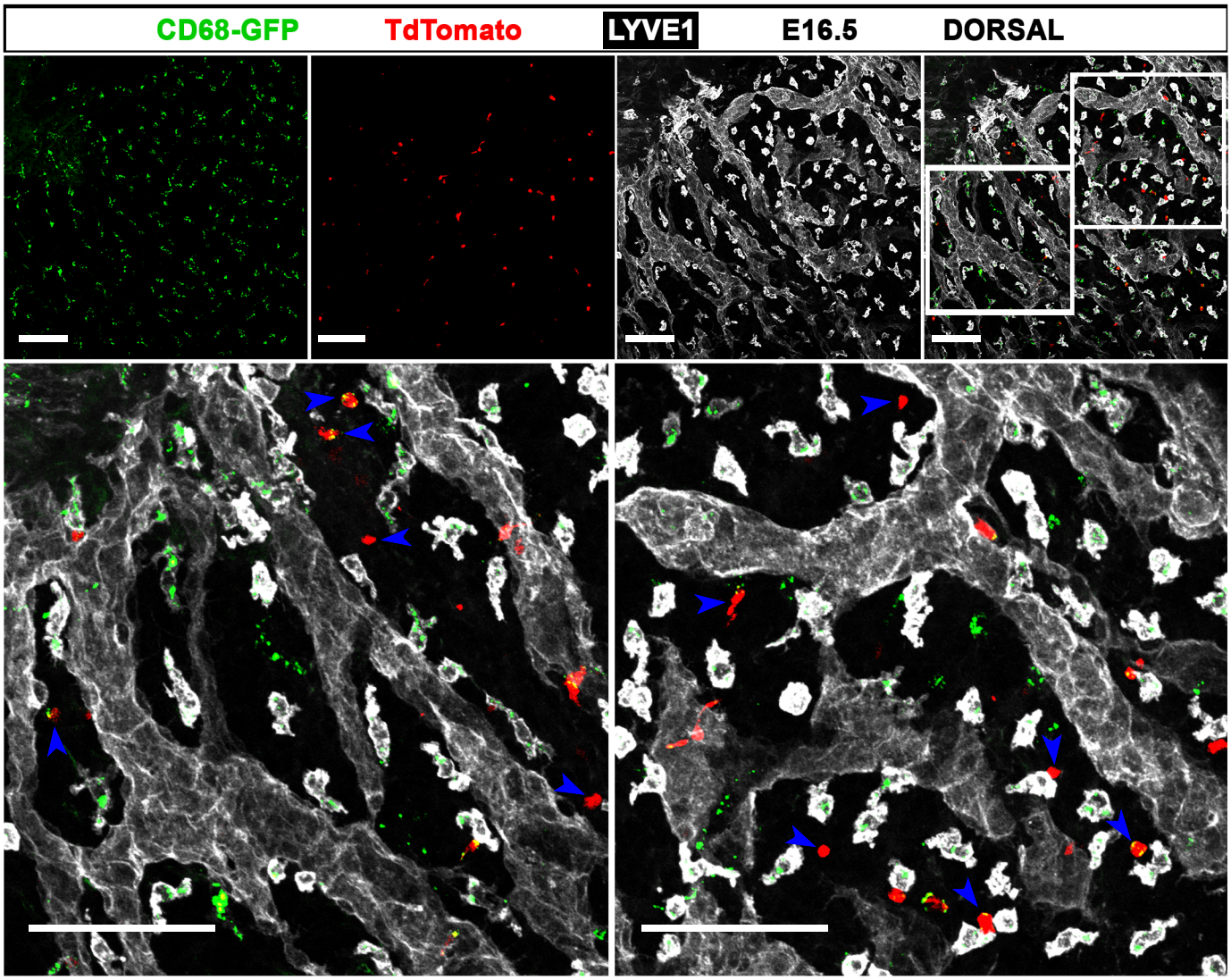


Figure 3.4 LYVE1+ lymphatic-associated macrophages are derived from the yolk sac
(a) Experimental strategy. Timed matings between *Flt3*-CreERT2 males and R26R-TdTomato females were established. Pregnant dams were dosed with tamoxifen (T) 1mg and progesterone (0.5mg) at E9.5, E11.5, E13.5 and E15.5 (total dose tamoxifen 4mg, progesterone 2mg). Embryos were harvested for analysis at E16.5. (b) Confocal imaging of whole mount *Flt3*-CreERT2;R26R-TdTomato embryonic hearts immunofluorescence stained to visualise macrophages (CD68, LYVE1) and lymphatic vessels (LYVE1), demonstrating no overlap between CD68+ LYVE1+ macrophages and TdTomato signal, suggesting that this macrophage subset arises from the yolk sac rather than from the haematopoietic stem cell. Unlike CD68+ LYVE1+ macrophages, TdTomato+ cells are not commonly in contact with LYVE1+ lymphatic endothelium. Scale bar 100 μm. Images representative of n=3.

3.2.5 CSF1R+ progenitors contribute to the cardiac lymphatics

Recent work in the Riley laboratory has demonstrated that the cardiac lymphatic endothelium arises from at least two progenitor cell origins.(123) The majority (~ 80%) of LECs are derived from the coronary endothelium and are labelled by a *Tie2*-Cre-driven lineage trace, which labels all venous endothelial cells.(138) However, a further 20% were found not to be labelled by *Tie2*-Cre; R26R-EYFP, suggesting a non-venous origin. Although the precise origin and identity of the non-venous progenitors is unclear, they have been shown to be labelled (at low level) by lineage tracing for the haematopoetic marker VAV1, the myeloid marker CSF1R, the mesenchymal marker PDGFB, and the stem cell marker KIT.(123, 127)

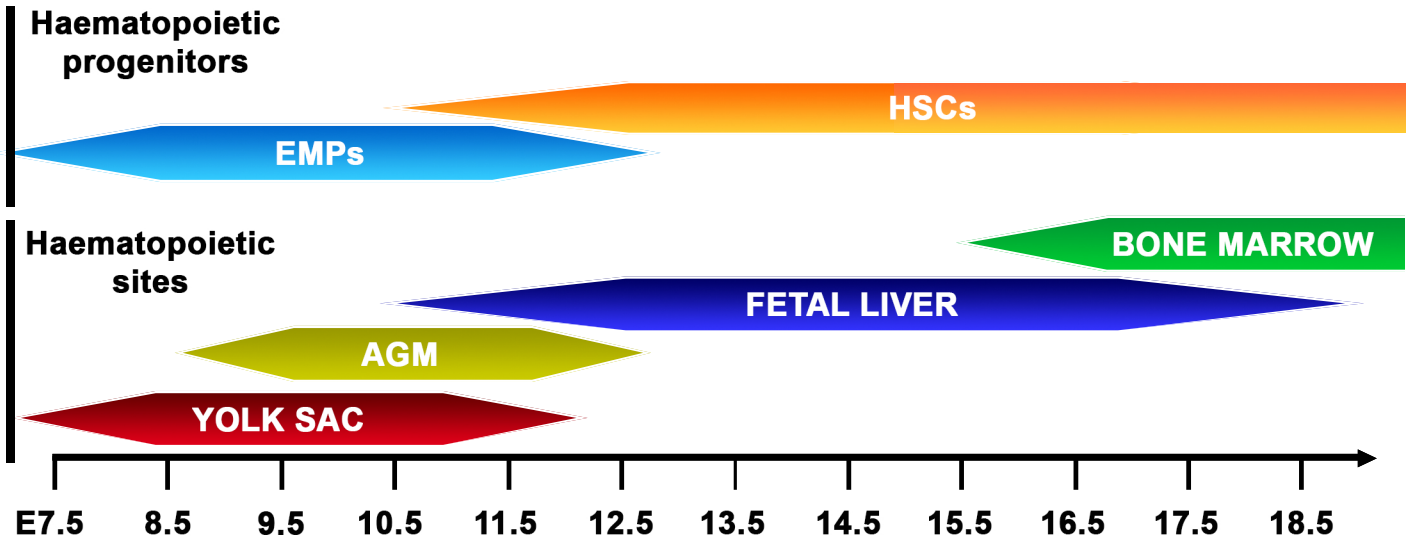
Haematopoiesis occurs at distinct sites through the time course of fetal development, from different progenitor cell types (Figure 3.5a). Prior to the emergence of the definitive HSC (from E8.5-10.5 onwards), which produces all blood lineages, erythrocytes and myeloid cells are derived from a YS-derived population of primitive myeloid progenitors, called erythromyeloid progenitors (EMPs). EMPs are a transient population, defined on the basis of CSF1R expression, which emerge in waves from the YS and give rise to tissue-resident macrophages.(56) An early wave of EMPs arises from the YS at approximately E7.5, which is independent of the transcription factor c-Myb, and generates primitive macrophages.(57, 123) A later c-Myb+ wave at ~ E8.25 seeds the fetal liver to produce multiple lineages including monocytes.(58) Between E9.5-10.5, EMPs and early HSCs migrate to, and colonize, the fetal liver, which becomes the principal site of haematopoiesis from until the bone marow takes over prior to birth.

To further investigate the nature and origin of the CSF1R+ progenitor contribution to LECs, timed matings were established between *Csf1r*-Mer-iCre-Mer male mice and R26R-tdTomato females. Activation of Cre recombinase was induced by a single intraperitoneal injection of tamoxifen (1.5mg, alongside progesterone 1mg to prevent abortion) at one of three time points: E8.5, E10.5, E12.5, mapping approximately to haematopoietic precursors originating from the YS, AGM and fetal liver respectively (Figure 3.5b). Embryos were harvested at E16.5 and hearts were isolated by microdissection and fixed. *Csf1r*-Mer-iCre-Mer;R26R-TdTomato hearts were then stained (as indicated) for PROX1 and LYVE1 to visualise LECs. Whole mount imaging was performed by confocal microscopy with Z-stack reconstruction.

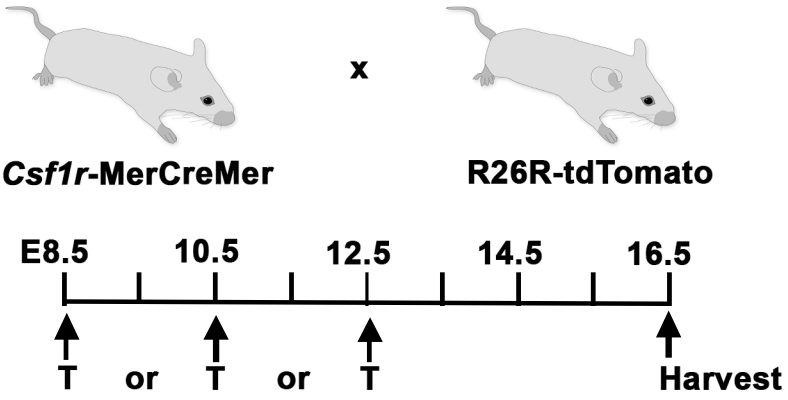
After activation of Cre recombinase at E8.5, minor incorporation of TdTomato labelled cells into the PROX1+ LEC lineage was observed (Figure 3.5c, left-hand panel, arrowheads), as previously reported by Klotz *et al*.(123) Similarly, a low level of TdTomato+ PROX1+ labelling was seen after activation of Cre at E10.5, corresponding to haematopoiesis arising from the AGM region (Figure 3.5c, middle panel, arrowheads). However, following activation of Cre at E12.5, corresponding to haematopoiesis arising at the fetal liver, a greater proportion of TdTomato+ PROX1+ labelled cells were observed (Figure 3.5c, right-hand panel, arrowheads). After induction of Cre at E12.5, TdTomato+ PROX1+ LECs could be observed ahead of the leading edge of advancing LYVE1+ lymphatic vessels (Figure 3.5d), suggesting that a migrating CSF1R+ progenitor may ‘pathfind’ ahead of the existing lymphatic vascular tree, and subsequently become incorporated. Taken together, these data indicate that a CSF1R+ progenitor, although not a classical EMP, contributes to the cardiac lymphatic endothelial lineage.

Figure 3.5

a



b



c

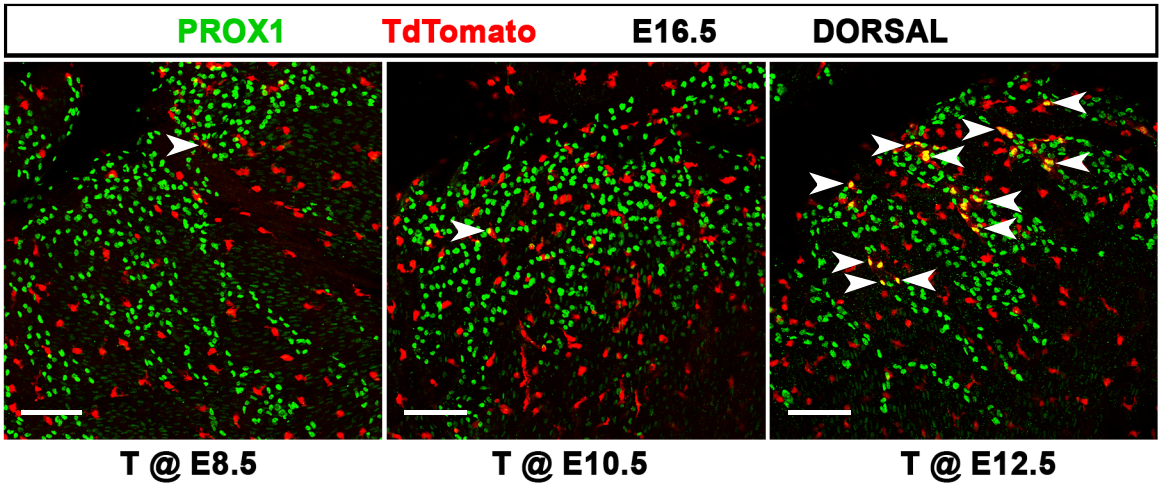


Figure 3.5

d

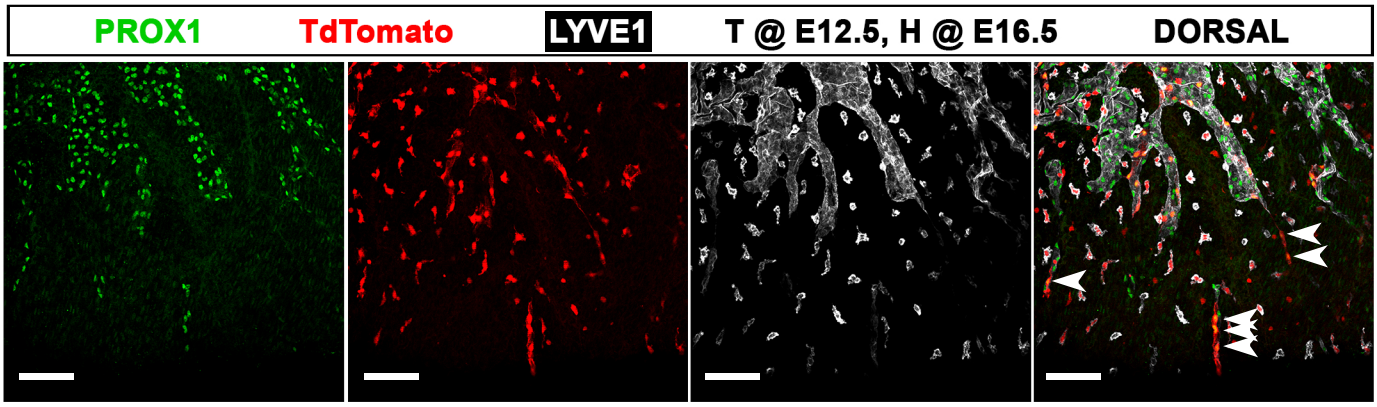


Figure 3.5 CSF1R+ progenitors contribute to the cardiac lymphatics (a) Timeline showing haematopoietic progenitor cell types and haematopoietic sites through fetal development in the mouse. From approximately E7.5 onwards, CSF1R+ erythromyeloid progenitors (EMPs) emerge from the yolk sac, to give rise to erythrocytes and macrophages. The first haematopoietic stem cells emerge from the aorta-gonad-mesonephros (AGM) region at approximately E10.5. EMPs and HSCs migrate to seed the fetal liver between E10.5 and E12.5, which becomes the main site of haematopoiesis until the bone marrow takes over close to birth. (b) Experimental approach: Timed matings were established between *Csf1r*-MerCreMer males and R26R-tdTomato females. Pregnant dams received a single dose of tamoxifen (T) by intraperitoneal injection at either E8.5, E10.5, or E12.5. Embryos were harvested for analysis at E16.5 (c) Confocal imaging of the dorsal aspect of whole mount *Csf1r*-MerCreMer; R26R-TdTomato E16.5 hearts immunofluorescence stained for the LEC transcription factor PROX1. Activation of Cre recombinase at E8.5 or E10.5 results in minimal labelling of PROX1 LECs by TdTomato, suggesting minor contribution from a CSF1R+ progenitor during this time period. Significantly greater TdTomato labelling of PROX1 LECs (arrowheads) is seen after Cre is activated at E12.5. Representative of n=3 per time point. Scale bar 100 μm. (d) Confocal imaging of the dorsal aspect of whole mount *Csf1r*-MerCreMer; R26R-TdTomato E16.5 hearts immunofluorescence stained for the LEC transcription factor PROX1 and LEC marker LYVE1. After activation of Cre recombinase at E12.5, TdTomato+ PROX1+ cells (arrowheads) are identified preceding the leading edge of advancing LYVE1+ lymphatic vessels. Images representative of n=3 per time point. Scale bar 100 μm. Abbreviations: AGM aorta-gonad-mesonephros, EMP erythromyeloid progenitor, HSC haematopoietic stem cell

3.2.6 Macrophages do not contribute directly to the cardiac lymphatic endothelial lineage

Several experimental studies have suggested that myeloid immune cells can transdifferentiate to form lymphatic endothelium both *in vitro* and *in vivo*.(139-143) In adult mice, CSF1R has been described as a specific marker of phagocytes.(78) Given the finding that CSF1R+ progenitors contribute to cardiac LECs (Figure 3.5), it was hypothesised that macrophages in the embryonic heart may act as a LEC progenitor.

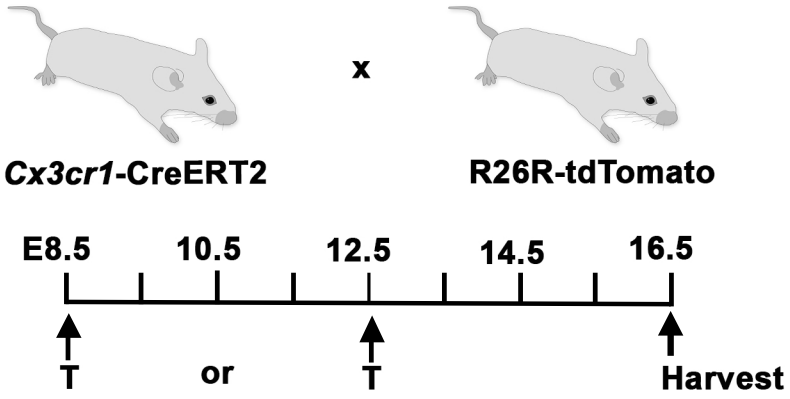
To investigate this hypothesis, lineage tracing of macrophages was performed using the *Cx3cr1*-CreERT2 mouse line, which has previously been demonstrated to label YS-derived macrophages at high-efficiency in studies of microglia.(144) In addition to Cre recombinase, this knock-in transgenic line also carries a GFP reporter cassette which reports *Cx3cr1* expression.

Timed matings were established between male *Cx3cr1*-CreERT2 mice and female R26R-tdTomato females. Activation of Cre recombinase was induced by a single intraperitoneal injection of tamoxifen (1.5mg, alongside progesterone 1mg to prevent abortion) at either E8.5 or E12.5, mapping approximately to either YS stage haematopoiesis or fetal liver haematopoiesis (Figure 3.6a). At E16.5, embryos were harvested and hearts were isolated by microdissection and fixed. *Cx3cr1*-CreERT2;R26R-tdTomato hearts were then stained (as indicated) for PROX1 to visualise LECs. Whole-mount hearts were imaged by confocal microscopy with Z-stack reconstruction.

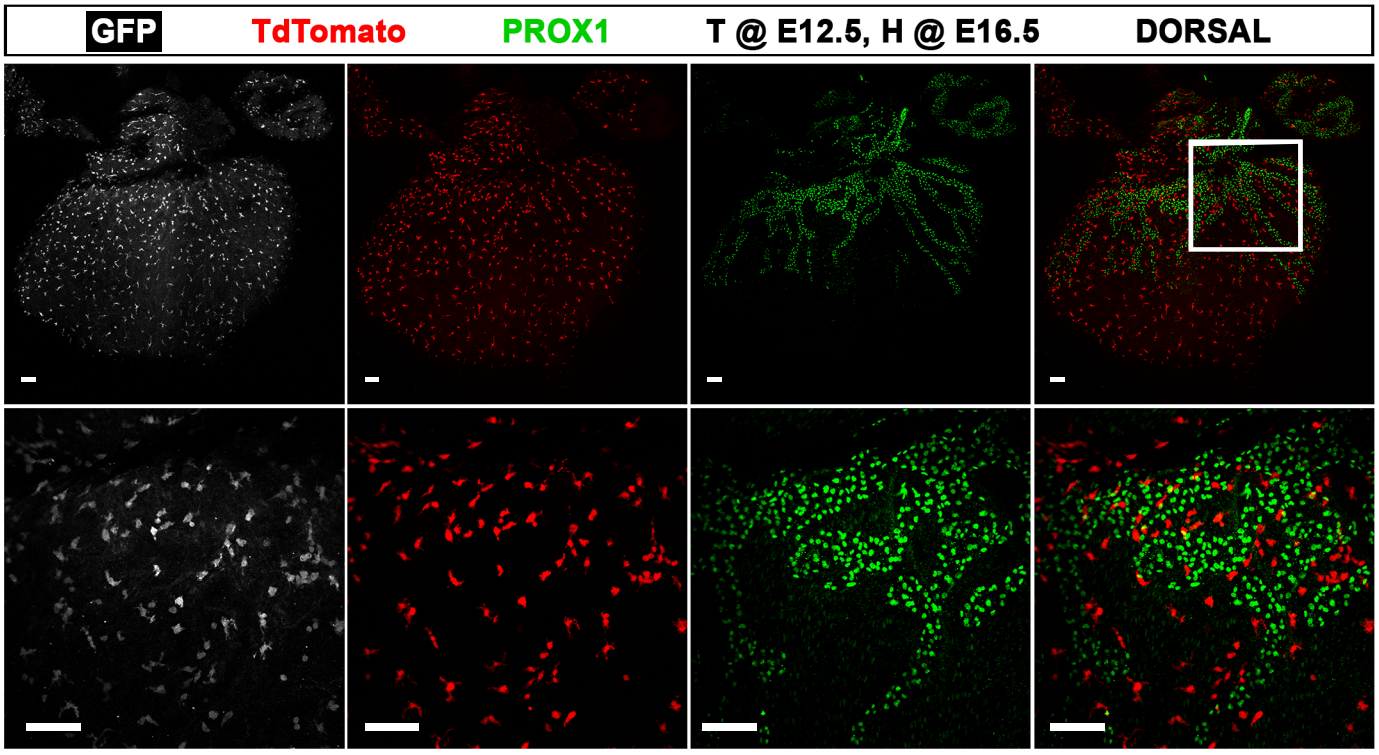
After activation of Cre recombinase at E12.5, successful recombination was observed with TdTomato signal mapping closely onto the GFP reporter signal (Figure 3.6b). However, no significant overlap between TdTomato+ cells and PROX1+ LECs was observed, suggesting that there is no direct contribution to the cardiac LEC lineage from E12.5 CX3CR1+ macrophages (Figure 3.6b). After activation of Cre recombinase at E8.5, targeting early CX3CR1+ macrophages from the YS, no overlap between TdTomato+ cells and PROX1+ LECs was observed, again suggesting that there is no contribution from macrophages to cardiac LECs. Taken together, these data exclude a lineage contribution from differentiated CX3CR1+ macrophages to cardiac LECs.

Figure 3.6

a



b



c

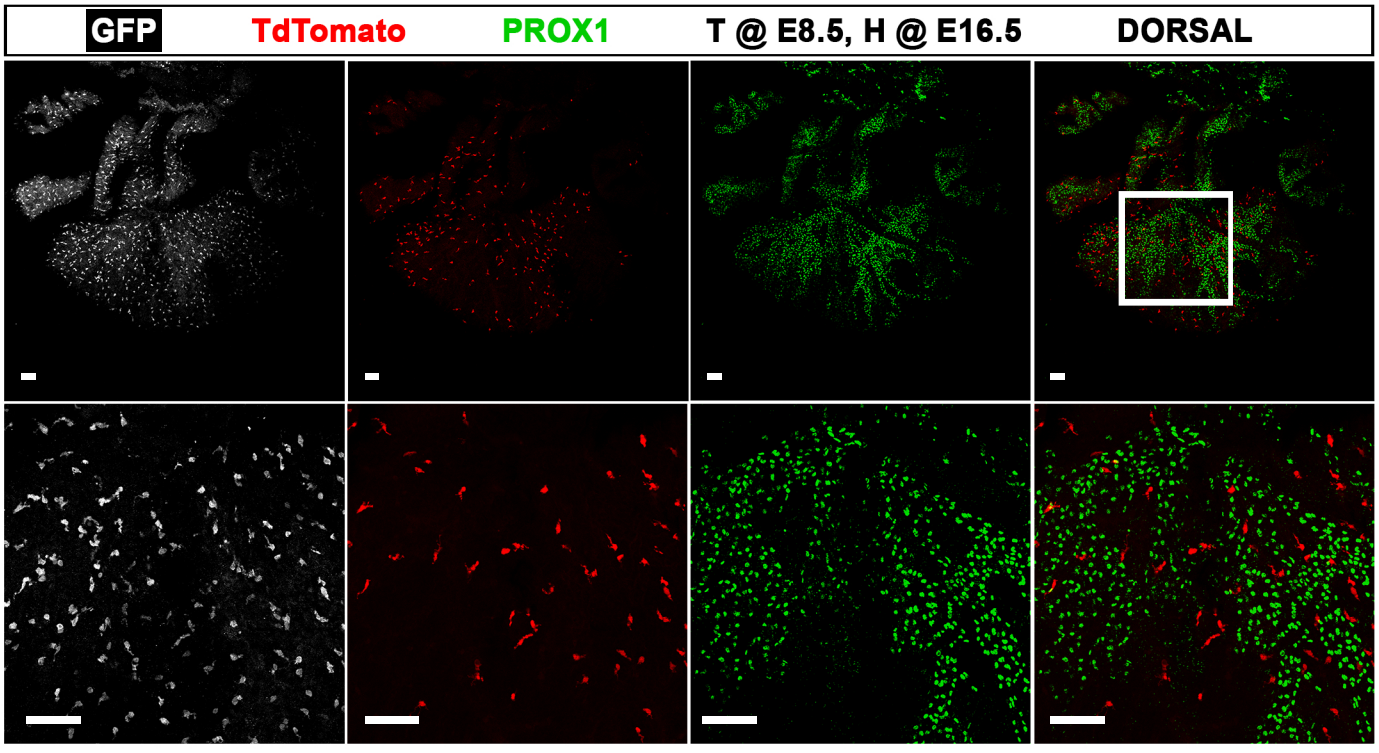


Figure 3.6 CX3CR1+ macrophages do not contribute directly to the cardiac lymphatic endothelial lineage (a) Experimental approach: Timed matings were established between *Cx3cr1*-CreERT2 males and R26R-tdTomato females. Pregnant dams received a single dose of tamoxifen (T) by intraperitoneal injection at either E8.5, or E12.5. Embryos were harvested for analysis at E16.5 (b) Confocal imaging of the dorsal aspect of whole mount *Cx3cr1*-CreERT2; R26R-TdTomato E16.5 hearts immunofluorescence stained for the LEC transcription factor PROX1, demonstrating that after activation of Cre recombinase at E12.5, there is no significant labelling of PROX1+ LECs by TdTomato, suggesting no contribution from a CX3CR1+ progenitor. Representative of n=3. Scale bar 100 μm.(c) Confocal imaging of the dorsal aspect of whole mount *Cx3cr1*-CreERT2; R26R-TdTomato E16.5 hearts immunofluorescence stained for the LEC transcription factor PROX1, demonstrating that after activation of Cre recombinase at E8.5, there is no significant labelling of PROX1+ LECs by TdTomato, suggesting no contribution from a CX3CR1+ progenitor. Representative of n=3. Scale bar 100 μm.

3.2.7 The progeny of FLT3+ definitive haematopoiesis do not contribute to the cardiac lymphatic endothelial lineage

The finding that E12.5 CSF1R+ progenitors contribute to the cardiac lymphatic lineage in greater numbers than CSF1R+ progenitors at E8.5 or E10.5 (Figure 3.5) implicates a late progenitor population, subsequent to the YS and AGM stages. At approximately E12.5, definitive haematopoiesis becomes established in the fetal liver, with all blood lineages produced from FLT3+ HSCs. As the shift to definitive haematopoiesis coincides with the timepoint at which CSF1R+ incorporation is seen to the cardiac LEC lineage, it was hypothesised that the cardiac LEC progenitor might lie downstream of FLT3+ HSCs. To test this, the *Flt3*-CreERT2 mouse line was used to label all progeny arising from HSCs.(137)

Timed matings were established between *Flt3*-CreERT2 males and R26RtdTomato females, and pregnant dams were dosed with 1mg tamoxifen and 0.5mg progesterone by oral gavage at E9.5, E11.5, E13.5, and E15.5 (Figure 3.7a; total dose 4mg tamoxifen and 2mg progesterone). Embryos were harvested at E16.5, hearts were isolated by microdissection and fixed, and tail samples were used to genotype for *Cre* and *TdTomato*. Hearts were then stained by immunofluorescence to visualise LECs (PROX1), with the progeny of FLT3+ definitive haematopoiesis indicated by positivity for tdTomato. Imaging was performed by confocal microscopy with Z-stack reconstruction.

At E16.5, successful recombination was observed, with punctate TdTomato signal observed in the heart. However, no significant overlap between PROX1+ LECs and TdTomato signal was observed, suggesting that there is no direct contribution to the cardiac LEC lineage from FLT3+ HSCs (Figure 3.7b). This experiment refutes the hypothesis that the cardiac LEC progenitor lies downstream of the HSC.

Figure 3.7

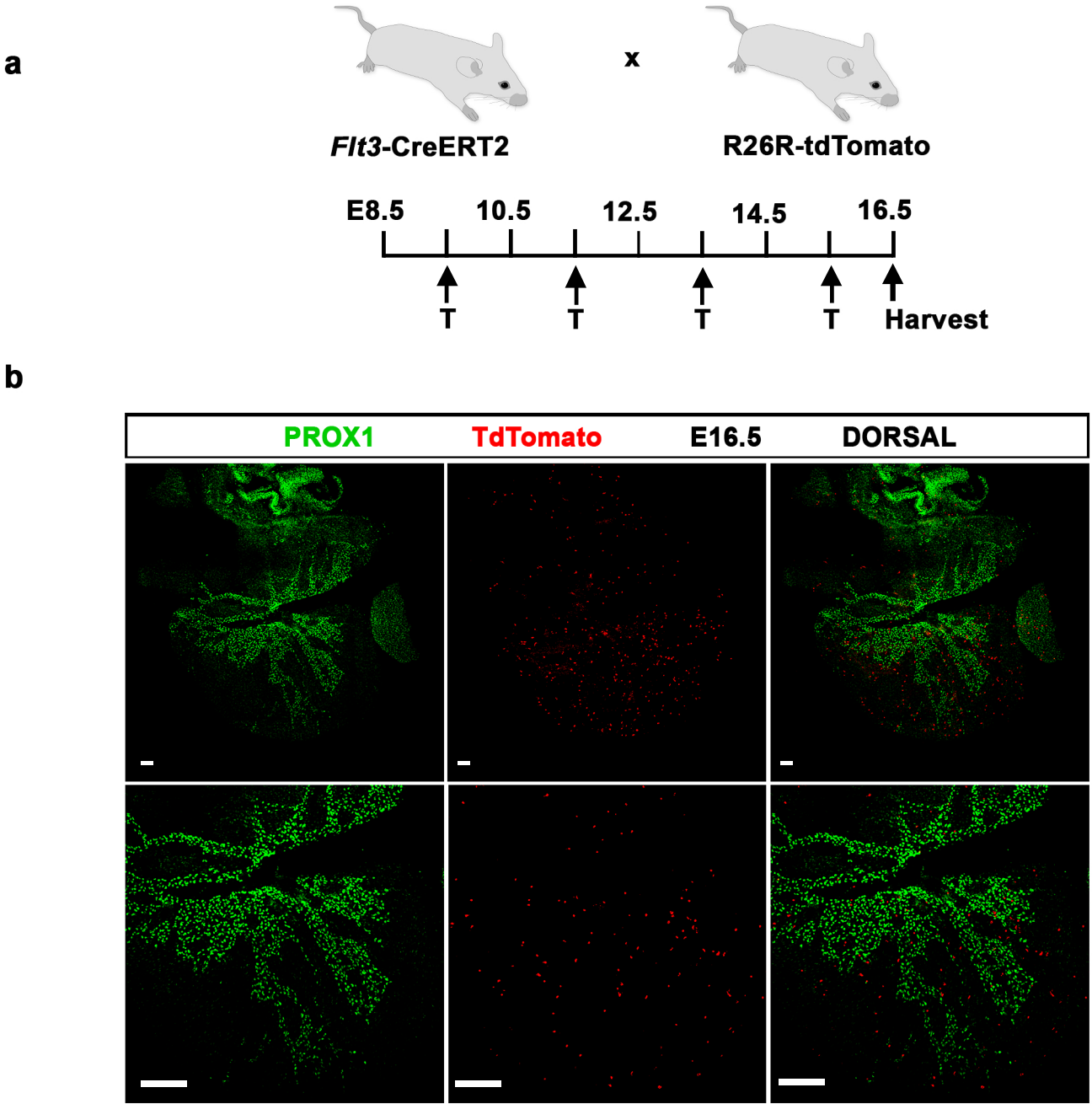


Figure 3.7 The progeny of FLT3+ definitive haematopoiesis do not do not contribute to the cardiac lymphatic endothelial lineage (a) Experimental strategy. Timed matings between *Flt3*-CreERT2 males and R26R-TdTomato females were established. Pregnant dams were dosed with tamoxifen (T) 1mg and progesterone (0.5mg) at E9.5, E11.5, E13.5 and E15.5 (total dose tamoxifen 4mg, progesterone 2mg). Embryos were harvested for analysis at E16.5. (b) Confocal imaging of whole mount *Flt3*-CreERT2;R26R-TdTomato embryonic hearts immunofluorescence stained to visualise lymphatic vessels (PROX1). No overlap between PROX1+ lymphatic endothelial cells and TdTomato signal was seen, suggesting that the progeny of FLT3+ definitive haematopoiesis do not contribute to the cardiac lymphatic endothelial cell lineage. Scale bar 100 μm. Images representative of n=3.

3.2.8 CSF1R and CX3CR1 identify overlapping but distinct myeloid populations in the embryonic heart

To understand the divergent results from *Csf1r*-Mer-iCre-Mer and *Cx3cr1*-CreERT2 myeloid cell lineage tracing, the expression of CSF1R and CX3CR1 by cells in the embryonic heart was analysed. Timed matings were established between male CX3CR1-GFP males and wild-type females. At E14.5, selected as a key time point during which lymphatic vessels are developing, embryos were harvested, hearts were isolated by microdissection and digested. Samples were stained for CSF1R, F4/80 and the endothelial progenitor cell marker KIT, previously reported to label LEC progenitors(127), and analysed by multicolour flow cytometry. Hearts from *Cx3cr1*-GFP at E14.5 were also fixed and stained (as indicated) with antibodies to CSF1R and CD68. Whole-mount hearts were imaged by confocal microscopy with Z-stack reconstruction.

By flow cytometry, CX3CR1-GFP and CSF1R were found to label overlapping but also distinct populations of myeloid or myeloid-like cells in the E14.5 embryonic heart (Figure 3.8a). CX3CR1-GFP+ cells were strongly positive for F4/80 (Figure 3.8b) compared to the CSF1R population (mean fluorescence index 9143 ± 869 vs 1463 ± 82.6, n=7 per group, $p<0.0001$), suggesting that they are classical macrophages. In contrast, CSF1R+ CX3CR1-GFP- cells expressed higher levels of the stem cell marker KIT (Figure 3.8c) compared to the CX3CR1-GFP+ population (mean fluorescence index 13843 ± 1310 vs 1709 ± 117.9, n=7 per group, $p<0.0001$). By confocal microscopy of whole mount CX3CR1-GFP E14.5 hearts stained for CSF1R and CD68, it was confirmed that CX3CR1-GFP and CSF1R label a partially overlapping myeloid cell population, but that each marker also identifies a distinct subset of cells. CX3CR1-GFP and CD68 were observed to completely colocalise, confirming that this population is comprised of classical macrophages.

Figure 3.8

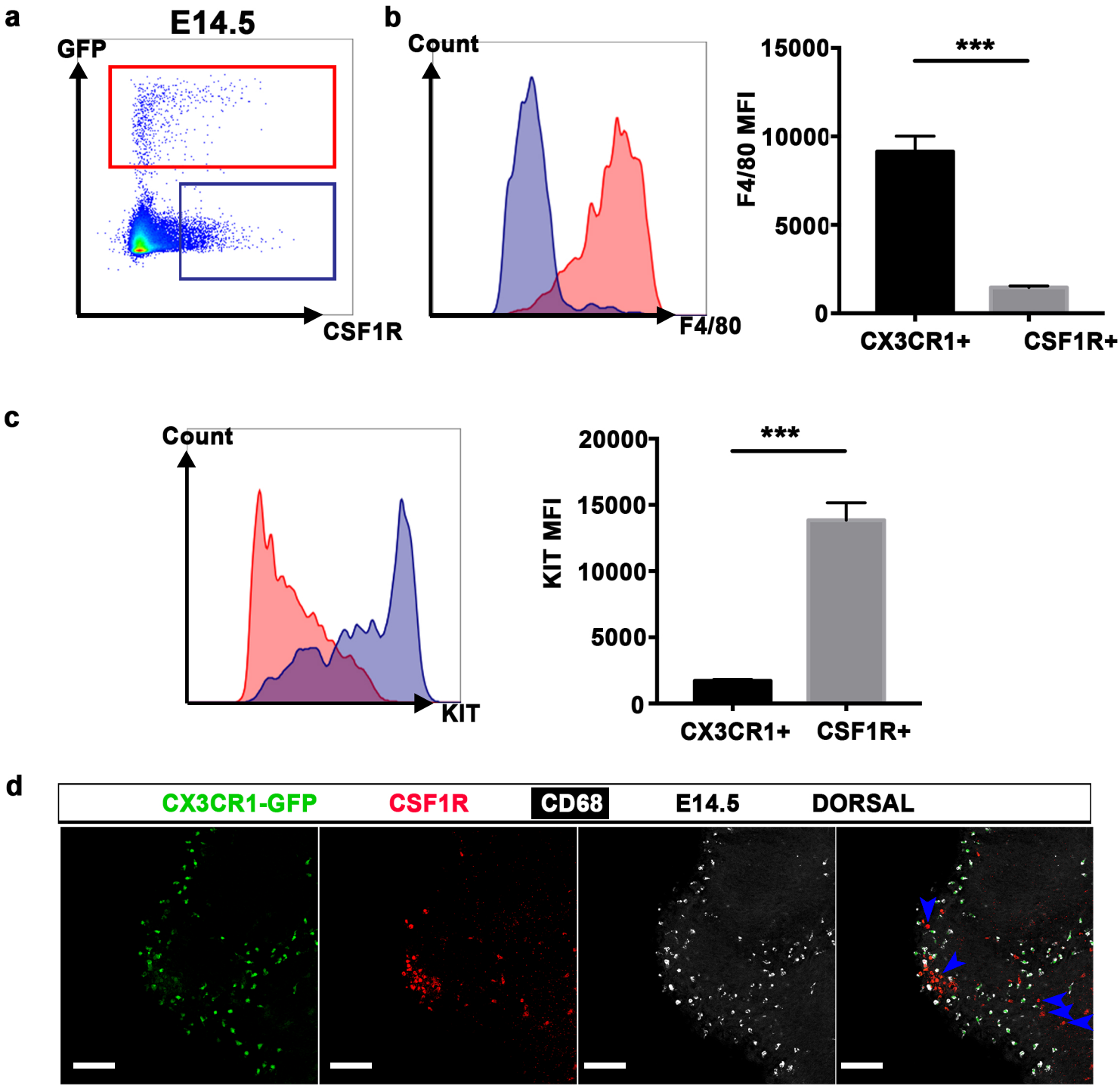


Figure 3.8 CSF1R and CX3CR1 identify overlapping but distinct myeloid populations in the embryonic heart

(a) Representative flow cytometry plot showing all live singlet cells from the hearts of CX3CR1-GFP+ mice at E14.5. CX3CR1-GFP+ cells are shown in the red gate, CSF1R+ CX3CR1-GFP- cells in the blue gate. (b) Representative histogram (left) and graph of mean fluorescence intensity (MFI; right) demonstrating significantly higher expression of F4/80 in the CX3CR1-GFP+ population (red) compared to the CSF1R+ CX3CR1-GFP- population (blue). n=7 per group, *** $p<0.0001$. (c) Representative histogram (left) and graph of MFI (right) demonstrating significantly higher expression of KIT in the CSF1R+ CX3CR1-GFP- population (blue) compared to the CX3CR1-GFP+ population (red). n=7 per group, *** $p<0.0001$. (d) Confocal imaging of the dorsal aspect of whole mount CX3CR1-GFP E14.5 hearts immunofluorescence stained for CSF1R, demonstrating partial overlap of these two markers, but also distinct subsets of cells (CSF1R+ CX3CR1-GFP- cells shown by arrowheads). Images representative of n=3. Scale bar 100 μm

3.3 Discussion

3.3.1 Macrophages in the embryonic heart

Previous studies have reported the presence of macrophages in the embryonic heart but their spatiotemporal organisation, ontogeny and functional roles remain largely uncharacterised. The data presented in this chapter demonstrate that macrophage recruitment to the embryonic heart begins by E12.5, and that macrophages expand significantly in number by E16.5. At E12.5 macrophages are initially concentrated in the outflow tract, sinus venosus and epicardium, before distributing across and penetrating the myocardium at later stages. A subpopulation of YS-derived (*Flt3*-CreERT2;R26R-TdTomato negative) LYVE1+ CX3CR1-GFP+ macrophages remain localised to the epicardium and closely associated with the leading edge and branch points of developing coronary and lymphatic vessels. This strongly suggests that macrophages play a functional role in developmental organisation or patterning of the cardiac lymphatics, and this hypothesis forms the focus of the next chapter of this thesis. Finally, data are presented which confirm a CSF1R+ lineage contribution to the cardiac LECs, but exclude CX3CR1+ macrophages as the progenitor cell type. This divergent finding may be explained in part by previously unrecognised heterogeneity in myeloid-like cells in the embryonic heart.

Two recently published studies have also analysed macrophages in the embryonic heart. First, Leid *et al* (2016) described macrophages in both the compact myocardium and trabecular myocardium of the heart from E10.5 onwards. The authors showed that two distinct populations of macrophages were present: CCR2+ macrophages, derived from monocytes, and CCR2- macrophages, which consist of both YS-derived and monocyte-derived macrophages.(84) These subpopulations had differing localisation within the heart, with the CCR2+ population primarily found

in the trabecular myocardium and the CCR2- population infiltrating the compact myocardium. Using a genetic mouse model of macrophage deficiency (*Csf1*$^{op/op}$), it was demonstrated that CCR2- macrophages play a role in remodelling of the coronary vascular network, discussed in detail in Chapter 4 of this thesis. In addition, Stevens *et al* (2016) reported the presence of macrophages from E12.5 onwards.(85) They identified that a population of LYVE1+ macrophages accumulate within and below the epicardium.(85) Targeted ablation of epicardial cells at E11.5 (using Wt1CreERT2; R26-DTA mice) led to a failure to recruit (or retain) epicardial macrophages as measured at E13.5.(85)

3.3.2 Ontogeny of macrophages in the embryonic heart

Identification of a lineage of macrophages which arise independently of the HSC, from the embryonic YS has been a major breakthrough in the field.(57) YS-derived macrophages, which in turn originate from EMPs, seed multiple tissues where they adopt specific tissue-resident fates and renew *in situ*.(58) Whether YS-derived macrophages and HSC-derived macrophages have different roles, and how these might be specified and achieved, remains largely unknown. In this chapter data are presented to show that the embryonic heart is seeded by both YS-derived and HSC-derived macrophages in development. Importantly, a LYVE1+ CX3CR1-GFP+ macrophage population in the epicardium, which co-localises with coronary and lymphatic vessels was shown to be derived exclusively from the YS, on the basis that this population was not labelled in a *Flt3*-CreERT2;R26R-TdTomato lineage trace.

3.3.3 Myeloid cells as lymphatic endothelial progenitor cells

A body of literature suggests that macrophages may be capable of transdifferentiation to adopt a LEC fate, thus acting as a LEC progenitor cell.(139-

143) The evidence for this theory comes from *in vitro*, mouse and human studies, although none have used a formal lineage tracing system (e.g. Cre-LoxP) to track cells over time.(145) First, stimulation of macrophages *in vitro* with lipopolysaccharide leads to upregulation of LEC-specific genes including VEGFR3 and Podoplanin, leading to the proposal that inflammation might prime macrophages to transdifferentiate into LECs.(143) In mice, CD11b+ macrophages have been reported to express the LEC master transcription factor PROX1 in the context of corneal inflammation, again suggesting they may be capable of adopting an LEC fate.(139) In the same study, macrophages were shown to form tube-like structures *in vitro* which stained positive for lymphatic markers.(139) In other mouse models of tumour or inflammation-induced lymphangiogenesis, non-host derived cells have been identified in newly formed lymphatic vessels, in keeping with the concept of a bone-marrow progenitor cell capable of differentiating into an LEC.(140-142) As discussed above, recent work from the Riley laboratory also supports the concept of a VAV1+ CSF1R+ haematopoietic cell, a marker profile consistent with a macrophage, which contributes to LECs in mouse cardiac development.(123) Finally, in humans, myeloid cells have been proposed to contribute to *de novo* lymphangiogenesis in renal allografts after transplantation, on the basis of the finding of XY chromosomal LECs (i.e. recipient-derived) in XX donor transplanted kidneys.(146) A population of VEGFR3+ (i.e. LEC-like) monocytes were isolated from human blood, leading the authors to propose that monocytes could transdifferentiate into LECs.(146)

The hypothesis that macrophages are capable of transdifferentiation into LECs in heart development was experimentally tested in this chapter. It was confirmed that CSF1R+ progenitors contribute to LECs in the embryonic heart, but demonstrated that these progenitors are unlikely to be derived from classical EMPs which emerge from the yolk sac at E7.5-E8.5. Instead, given the significant increase in contribution

to LECs seen after labelling at E12.5, this population may be derived from the fetal liver. Next, by demonstrating that *Cx3cr1*-CreERT2;R26R-TdTomato embryos have no incorporation of TdTomato signal within PROX1+ LECs, the hypothesis that macrophages can transdifferentiate into LECs in heart development was refuted. Finally, by examining *Flt3*-CreERT2;R26R-TdTomato embryos, cardiac LECs were shown not to be derived from a HSC source.

3.3.4. Heterogeneity of myeloid cells in the embryonic heart

Expression of either CSF1R or CX3CR1 is used throughout the literature to identify macrophages in the adult mouse. CSF1 regulates the proliferation and survival of macrophages, and mice which lack either CSF1 or CSF1R are deficient in macrophage populations.(147, 148) In the developing brain, macrophages are the only cell type to express CSF1R and it has become widely used as a specific marker of microglia.(148) Similarly, the CX3CR1 promoter has been widely used both in the heart and other organs to identify monocytes and macrophages and is accepted as both sensitive and specific.(60, 61) As such, it might be assumed that CSF1R and CX3CR1 are interchangeable markers of classical macrophages.

The final experiments presented in this chapter attempt to reconcile the divergent lineage tracing results obtained using the *Csf1r*-Mer-iCre-Mer and *Cx3cr1*-CreERT2 mouse lines. By flow cytometry of embryonic hearts at E14.5, it was shown that CX3CR1-GFP labels a ‘classical’ macrophage population expressing high levels of F4/80. However, while CSF1R is also expressed on some CX3CR1-GFP+ macrophages, it also labels a CX3CR1-GFP- KIT+ F4/80- population. Based on expression of CSF1R alone, this population might be described as ‘myeloid-like’, but cannot be called a macrophage. Lineage tracing of KIT+ cells has previously been reported to label non-venous progenitor cells giving rise to mesenteric LECs(127),

and it is possible that the CSF1R+ CX3CR1-GFP- KIT+ population in the embryonic heart at E14.5 represents the LEC progenitor. This might further be analysed by FAC-sorting these different populations for transcriptional analysis.

3.4 Conclusions

The experiments presented in this chapter characterise the infiltration and spatial organisation of macrophages within the developing heart. The data demonstrate that macrophages colocalise with developing coronary and lymphatic vessels, suggesting a functional interaction between macrophages and endothelial cells. The findings presented here exclude a direct lineage contribution from macrophages to the developing lymphatic system. Heterogeneity of surface marker expression within subpopulations of myeloid-like cells in the developing heart may underlie the divergent results of lineage tracing from the *Csf1r*- and *Cx3cr1*-promoter driven Cre recombinase.

Chapter 4: Cardiac development in a mouse model of macrophage deficiency

Our real teacher has been and still is the embryo, who is, incidentally, the only teacher who is always right

Viktor Hamburger, 1900-2001

4.1 Background

4.1.1 Mouse models for targeting macrophages

Insights into the functional roles of macrophages in embryonic development have been gained through the use of mouse models of constitutive or acquired macrophage deficiency. The experimental approaches used and phenotypes identified are outlined in turn.

Colony simulating factor 1 (CSF1, also known as macrophage colony stimulating factor; M-CSF) is the canonical signalling ligand required for specification of macrophage differentiation, proliferation and survival (Figure 4.1).(149) The CSF1 receptor, CSF1R (also known as CD115, encoded by the proto-oncogene *c-fms*), is a transmembrane tyrosine kinase receptor which is expressed ubiquitously on macrophages, as well as at low levels in the trophoblast, on neural stem cells and the renal tubular epithelium.(76-78, 150) A naturally occurring null mutation in the *Csf1* locus in mice, $Csf1^{op}$ ('osteopetrotic') leads to widespread depletion of tissue-resident macrophages in homozygous animals.(151) Similarly, knockout of CSF1R by gene targeting leads to loss of macrophages and recapitulates the features of the $Csf1^{op/op}$ mouse.(152) Interestingly, the phenotype of the $Csf1r^{-/-}$ mouse is more severe than that of $Csf1^{op/op}$ mouse, a finding which led to the identification of IL34 as a second ligand for CSF1R.(152, 153)

Genetic loss of macrophages has also been achieved by targeting of the transcription factor PU.1, a 272-amino acid master regulator of myeloid lineage differentiation (Figure 4.1).(154) PU.1 regulates expression of multiple gene targets required for myeloid specification including *Csf1r* and *Itgam* (encoding the myeloid marker CD11b).(82) Two mouse models targeting the PU.1 locus (*Pu.1*, also known as *Sfpi1*) have been reported. Scott *et al* undertook mutational targeting of *Pu.1*

within exon 5, producing *Pu.1*$^{-/-}$ embryos which died at approximately E18.5.(81) McKercher *et al* subsequently disrupted the Ets (DNA binding) domain of *Pu.1*, also in exon 5, reporting that homozygotes were born alive and at expected Mendelian ratios, but died within 48 hours of septicaemia.(80) In both models, loss of PU.1 was associated with an absence of CD11b+ F4/80+ macrophages (including YS-derived embryonic macrophages) and these mice have been widely used to study the roles of macrophages in development.(57, 80, 81) However, PU.1 has been found to have complex effects on early immune cell lineage specification and *Pu.1*$^{-/-}$ mice show evidence of reduced numbers of neutrophils, B cells, mature T cells, mast cells and a mild defect in erythropoiesis, in addition to loss of macrophages.(80, 81, 155, 156)

Several inducible strategies for ablation of macrophages have been developed to gain insights into macrophage function.(157) Liposomes containing the bisphosphonate drug clodronate are taken up by phagocytically active cells including monocytes, macrophages and dendritic cells. Once ingested, clodronate induces apoptosis and cell death, although the efficiency of ablation is incomplete and is variable between different tissues and models.(158) Alternatively, neutralising antibodies to CSF1R have been utilised effectively to deplete macrophages *in vivo*.(159)

Conditional ablation of macrophages can also be achieved using a transgenic mouse model approach, in which targeted expression of the diphtheria toxin fragment A (DTA) leads to cell death by inhibition of protein synthesis. To achieve this, Ivanova *et al* generated a mouse model carrying a cassette encoding the DTA sequence with an upstream LoxP-flanked STOP sequence knocked into the *Rosa26* locus.(160) When crossed with a mouse line carrying Cre recombinase under a macrophage or myeloid-specific promoter, DTA is expressed specifically in myeloid cells which are then ablated. This approach has been used successfully to knock down dendritic

cells using CD11c-Cre.(161) Alternatively, DTA-mediated knockdown can be achieved by myeloid-restricted expression of the human diphtheria toxin receptor *DTR* gene, using the CD11b myeloid promoter.(162) Myeloid cells then express DTR and can be specifically ablated by dosing animals with diphtheria toxin. Using the myeloid CD11b-DTR model, inducible knockdown was achieved selectively and at high efficiency in a recent study demonstrating a role for macrophages in cardiac conduction.(86)

Figure 4.1

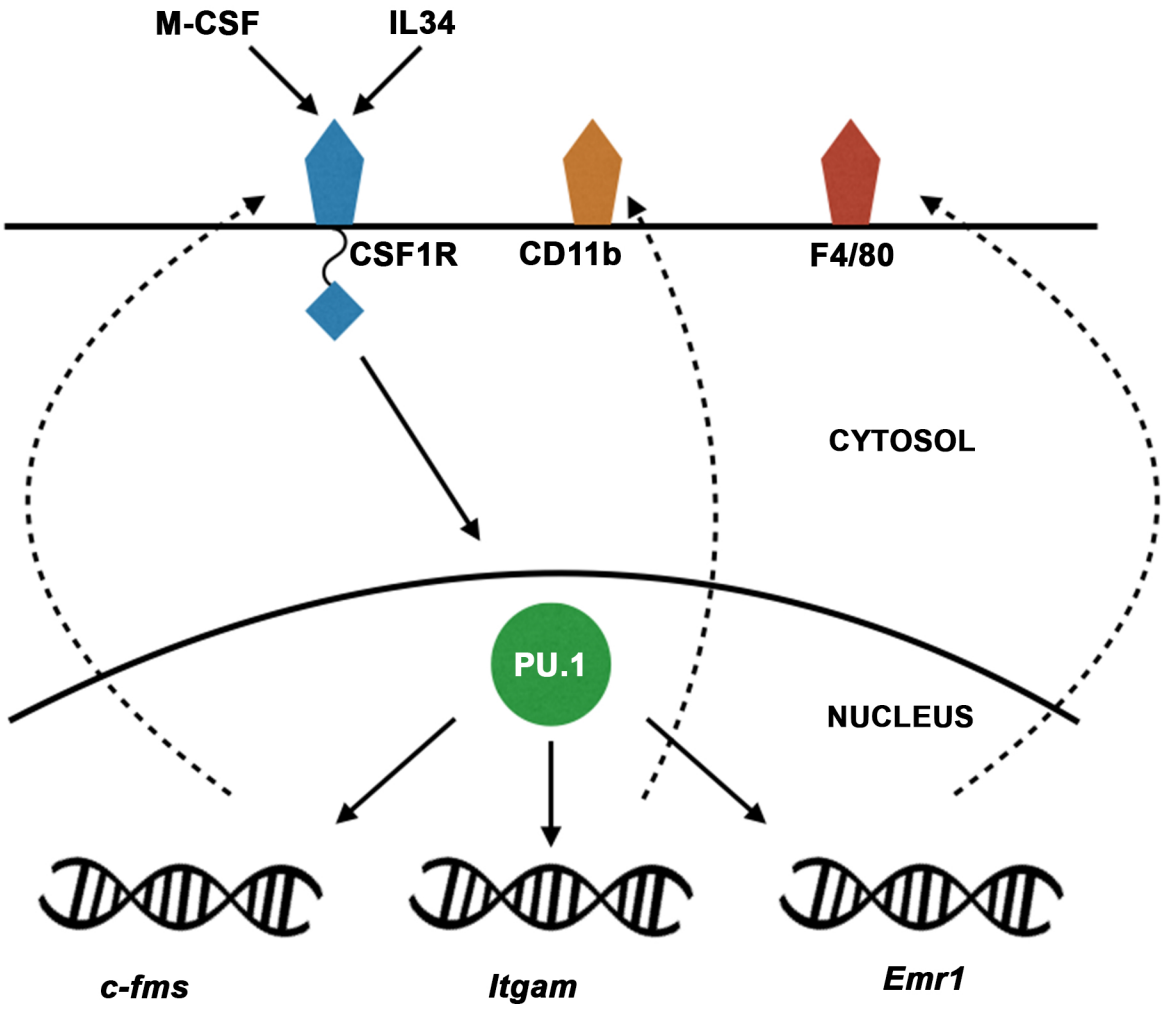


Figure 4.1 Signalling pathways involved in specification of macrophage fate The glycoprotein M-CSF is the canonical signalling ligand required for specification of macrophage differentiation and survival. It binds to the CSF1 receptor (CSF1R), a tyrosine kinase receptor which is a member of the platelet-derived growth factor family. CSF1R activates multiple downstream targets to promote myeloid specification, including PU.1, the master transcription factor directing myeloid fate. PU.1 directs transcription of myeloid-specific genes including *c-fms*, encoding CSF1R (thus providing a positive feedback loop) in addition to *Itgam* and *Emr1*, encoding CD11b and F4/80 respectively.

4.1.2 Macrophage roles in development and growth

The experimental models outlined above have facilitated the identification of a number of 'non-immune' roles for macrophages in embryonic development and growth.(150)

Mice that are homozygous for spontaneous *osteopetrotic* (*Csf1*^{op}) mutation develop osteopetrosis, a sclerotic bone disease characterised by increased bone density and the loss of the bone marrow cavity.(151) Osteopetrosis is not a macrophage-dependent phenotype, however, and develops due to loss of osteoclasts, specialised multinucleated bone-resorbing cells. Osteoclasts are absent, alongside macrophages, in *Csf1*$^{op/op}$ mice, *Pu.1*$^{-/-}$ mice and in the rat model *toothless*, which carries a spontaneous *Csf1* mutation.(163-165) These models provided the first evidence that osteoclasts differentiate from a common monocyte-osteoclast bone marrow progenitor in a PU.1-dependent manner.(166)

A range of trophic roles for macrophages have been identified in the developing brain. Microglia are specialised, tissue-resident, YS-derived macrophages which seed the brain early in embryonic development.(167) A loss of microglia (in the *Csf1*$^{op/op}$ or *Csf1r*$^{-/-}$ models) is associated with abnormal brain function as evidenced by abnormal visual, auditory and olfactory processing.(148, 168) Diverse mechanisms have been implicated: microglia have been show to modulate recruitment and proliferation of neural progenitor cells, neuron viability, and activity.(169) Microglia have been shown to undertake synaptic pruning, required for learning, and phagocytose neurons in the hippocampus.(170, 171) The role of microglia in brain development appears to be conserved: in humans, a mutation in

the *CSF1R* gene has been identified as a cause of hereditary diffuse leuokoencephalopathy with spheroids.(172)

Multiple studies have implicated macrophages in vascular patterning. In the eye, programmed regression of the fetal (hyaloid) vasculature occurs after birth as the retinal vasculature matures.(173),(174) In the zebrafish hindbrain, macrophages assist in patterning the cerebral vasculature by promoting sprouting angiogenesis.(133) Recently, macrophages have been shown to prune branches of the developing coronary vasculature in the mouse heart, with ablation of macrophages resulting in increased vascular branching and dysregulated calibre.(84) Macrophages have also been implicated in regulation of lymphatic vessel calibre in the skin.(175) In the *Pu.1*$^{-/-}$ mouse, Gordon *et al* identified increased calibre, hyperproliferative lymphatic vessels and suggested that macrophages act to restrain LEC proliferation to maintain normal vessel calibre.

Macrophages also modulate tissue growth and remodelling. In muscle, macrophages stimulate growth of muscle progenitor cells, satellite cells, and provide soluble growth signals which rescue progenitors from apoptosis.(176) In the developing breast, macrophages are required for remodelling of the extracellular matrix, a process which is required for duct outgrowth and branching.(177) In the pancreas, macrophages are involved in formation of normal islets: the *Csf1*$^{op/op}$ mouse has been shown to have a reduced mass of functional beta-cells.(178) Finally, macrophages have been identified as a source of catecholamines which directs the development of beige fat for thermogenesis.(179)

4.1.3 Aims

This chapter addresses the following aims:

1. To confirm the absence of cardiac macrophages in the embryonic heart in the *Pu.1*$^{-/-}$ mouse model.
2. To assess the functional effects of macrophage deficiency on the development and patterning of the cardiac lymphatic system.
3. To assess the functional effects of macrophage deficiency on the development and patterning of the coronary vasculature.
4. To investigate the potential mechanisms by which macrophages may modulate lymphatic or vascular development.

4.2 Results

4.2.1 *Pu.1*$^{-/-}$ mice lack macrophages in the embryonic heart

The *Pu.1*$^{-/-}$ transgenic mouse developed by McKercher *et al*(80) was used as a model of macrophage deficiency. To confirm that *Pu.1*$^{-/-}$ results in loss of macrophages in the developing heart, timed matings were established between heterozygous mice (*Pu.1*$^{+/-}$), generating homozygous, heterozygote and wild type (WT) littermate embryos. Embryos were harvested at E14.5, hearts were isolated by microdissection, and tail clips were harvested for genotyping. Hearts were digested in collagenase, stained and analysed by multicolour flow cytometry.

Myeloid cells were identified in the embryonic heart at E14.5 based on co-expression of the pan-leucocyte marker CD45 and the myeloid marker CD11b (Figure 4.2a). In the WT embryonic heart at E14.5, CD45+ CD11b+ myeloid cells accounted for 1.35 ± 0.25% of all live cells, compared to 0.02 ± 0.008% in the *Pu.1*$^{-/-}$ embryonic heart (*p=0.0019*; Figure 4.2b). Myeloid cells in the WT heart comprised 85.4 ± 2.77% CD11b+ F4/80+ macrophages (Figure 4.1c). A small number of CD45+ CD11b- non-myeloid leucocytes were present in the WT heart but absent in the *Pu.1*$^{-/-}$ heart (WT 0.15 ± 0.02% vs *Pu.1*$^{-/-}$ 0002 ± 0.00%, *p=0.0003*). This population may consist of lymphocytes but cannot be definitively identified without further surface marker profiling.

Figure 4.2

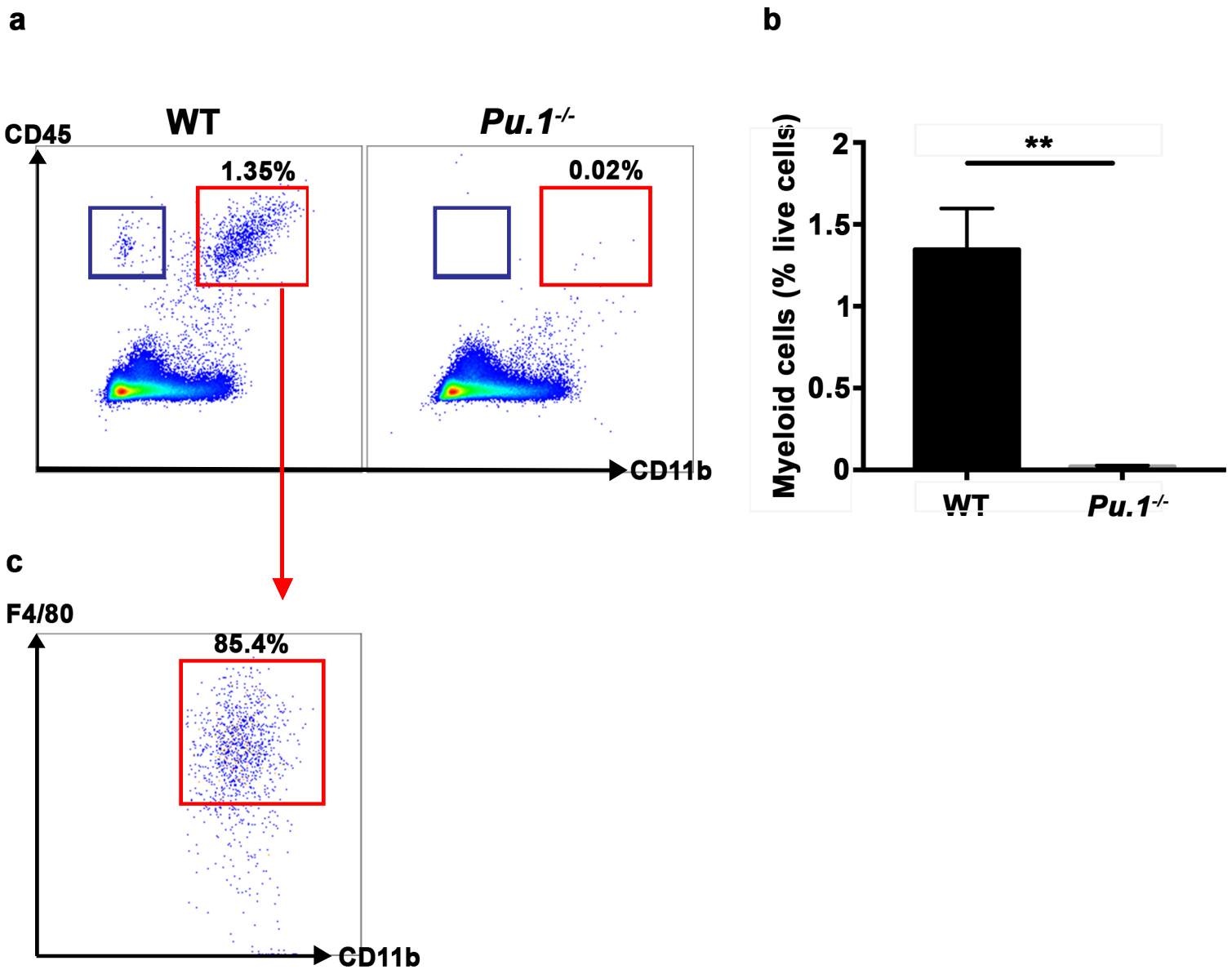


Figure 4.2 *Pu.1*$^{-/-}$ mice lack macrophages in the embryonic heart
(a) Representative flow cytometry plots showing all live singlet cells from the hearts of *Pu.1*$^{-/-}$ mice and wild-type (WT) littermate controls at embryonic day (E) 14.5. Gates are shown to indicate CD45+ CD11b+ myeloid leucocytes (red), and CD45+ CD11b- non-myeloid leucocytes (blue). (b) Graph quantifying CD45+ CD11b+ myeloid leuocytes in the hearts of *Pu.1*$^{-/-}$ mice and wild-type (WT) mice at E14.5. ** $p < 0.01$, n=4 per group. (c) Representative flow cytometry plot demonstrating expression of the macrophage marker F4/80 by myeloid leucocytes in the heart at E14.5. CD11b+ F4/80+ macrophages are indicated by the red gate.

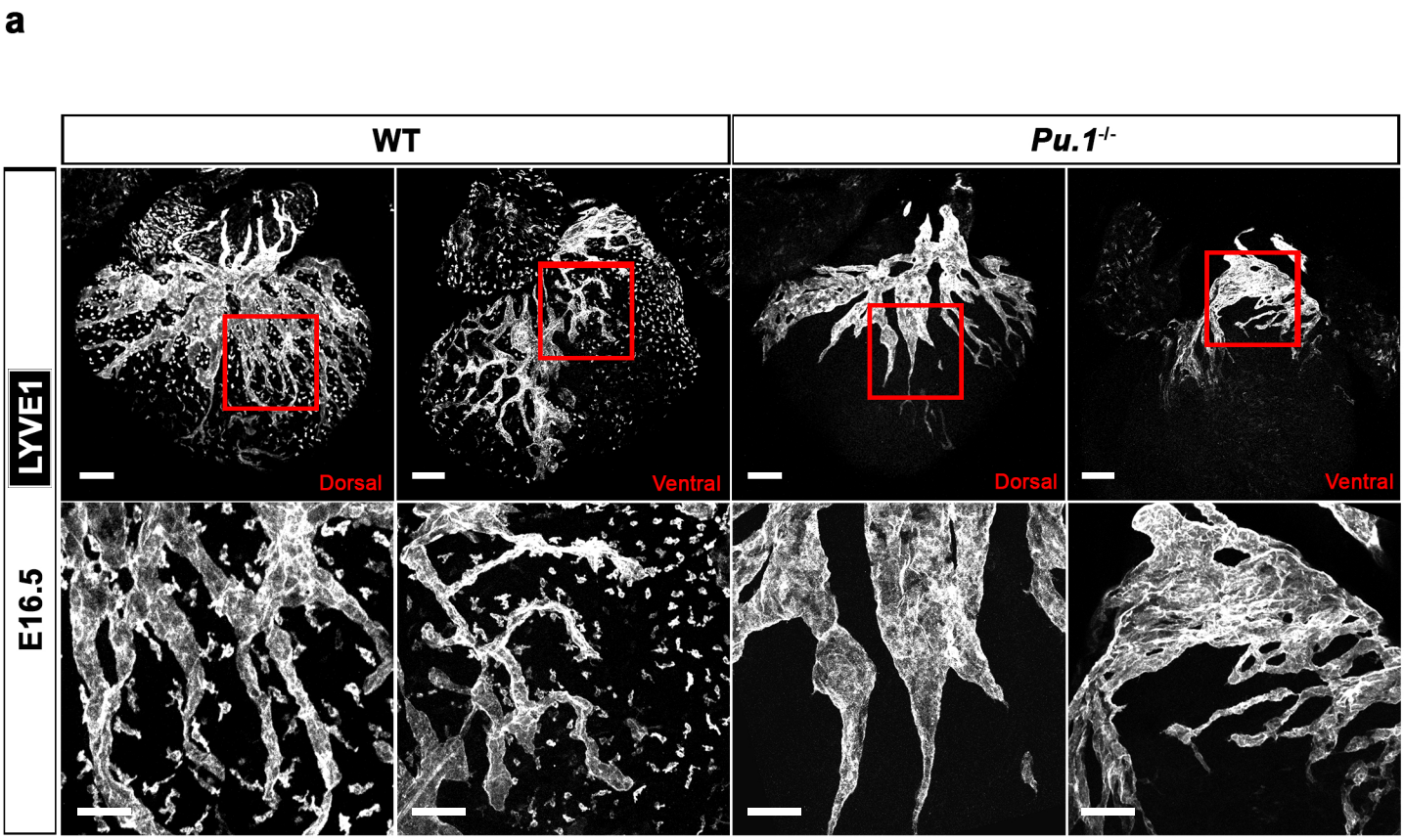
4.2.2 *Pu.1*$^{-/-}$ mice have abnormal lymphatic vessel patterning

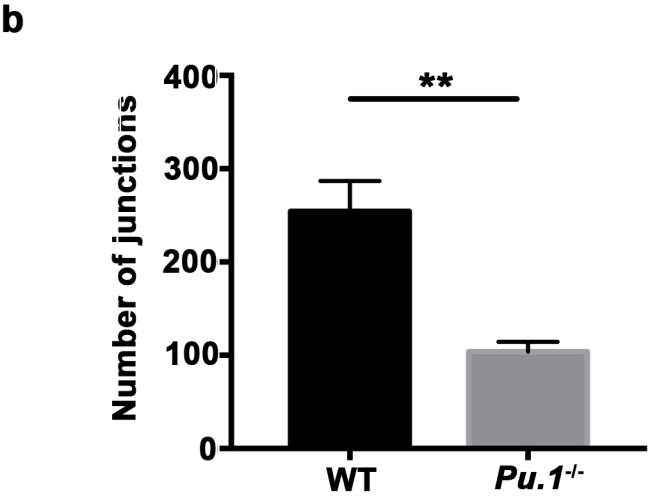
Macrophages have previously been described to play a role in patterning of the developing lymphatic vasculature. In the skin of *Pu.1*$^{-/-}$ mice, Gordon *et al* observed hyperplastic, enlarged lymphatic vessels with evidence of hyperproliferation in LECs.(175) I hypothesised that embryonic macrophages in the heart may play a similar role to pattern the cardiac lymphatic vasculature. After establishing timed matings, embryos were harvested at E16.5 or E19.5, hearts were isolated by microdissection, and tail clips were harvested to identify *Pu.1*$^{-/-}$ embryos and WT littermate controls . Hearts were fixed and stained for the LEC marker LYVE1. Whole-mount hearts were then imaged by confocal microscopy with Z-stack reconstruction. Lymphatic vascular morphology and branching were quantified using the AngioTool™ plugin for ImageJ.(180)

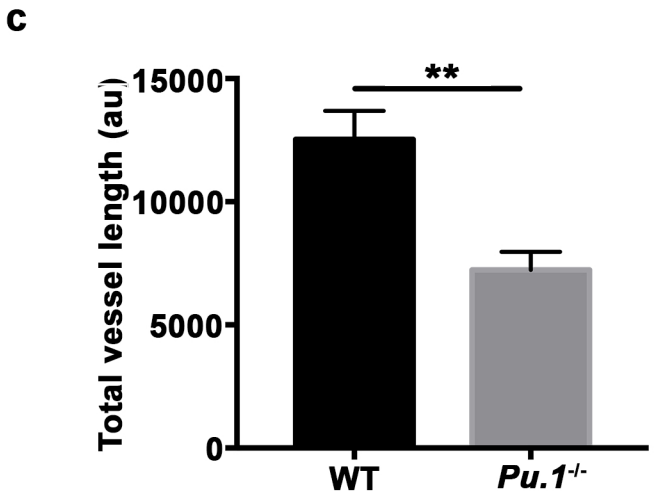
At E16.5, lymphatic vessel morphology was abnormal on both the dorsal and ventral aspect of the *Pu.1*$^{-/-}$ heart (Figure 4.3a). The vessels were enlarged in calibre, with evidence of reduced branching, and reduced distal migration towards the apex of the heart compared to WT (Figure 4.3a). The lymphatic vascular phenotype was quantified on the dorsal surface, where compared with WT, *Pu.1*$^{-/-}$ mice had evidence of a reduced number of lymphatic vessel junctions (104 ± 11 vs 254 ± 33, n=6 per group, *p=0.0014*, Figure 4.3b). *Pu.1*$^{-/-}$ mice had a significant reduction in total vessel length (7231 ± 735 vs 12536 ± 1155, n=6 per group, *p=0.0031*; Figure 4.3c). Furthermore, *Pu.1*$^{-/-}$ mice showed a trend (not statistically significant) towards reduced average vessel length (201 ± 43 vs 1005 ± 504, n=6 per group*, p=0.1425*; Figure 4.3d). Finally, compared with WT, lymphatic vessels in the hearts of E16.5 *Pu.1*$^{-/-}$ mice had significantly fewer endpoints (132 ± 12.5 vs 404 ± 125, n=6 per group, *p=0.0261*), suggesting reduced lymphatic network complexity.

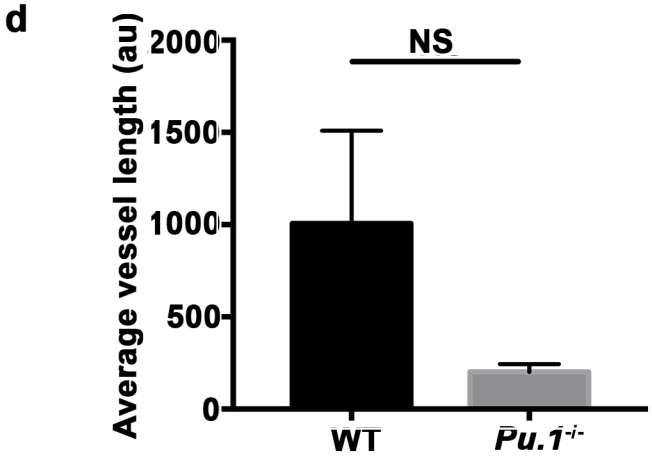
At E19.5, lymphatic vessel morphology remained abnormal on both the dorsal and ventral surfaces of the *Pu.1*$^{-/-}$ heart (Figure 4.3f). While lymphatic vessel migration across the heart was similar to WT, vessel calibre and branching again remained abnormal (Figure 4.3f). The lymphatic vascular phenotype was quantified on the dorsal surface of the heart and revealed that compared with WT, *Pu.1*$^{-/-}$ mice had persistently reduced lymphatic vessel junctions (127 ± 27 vs 382 ± 45, n=5-6 per group, *p=0.0007*, Figure 4.3g), compared with WT. *Pu.1*$^{-/-}$ mice also showed a (non-statistically significant) trend towards reduced total vessel length (13641 ± 1435 vs 26058 ± 6910, n=5-6 per group, *p=0.0858*, Figure 4.3h) and reduced average vessel length (296 ± 46 vs 427 ± 132, n=5-6 per group, *p=0.3341*, Figure 4.3i). Finally, compared with WT, lymphatic vessels in the hearts of E19.5 *Pu.1*$^{-/-}$ mice again had significantly fewer endpoints (500 ± 123 vs 169 ± 17, n=5-6 per group, *p=0.0162*, Figure 4.3j) at this later stage of development.

Figure 4.3


a
WT
Pu.1-/-
LYVE1
E16.5
Dorsal
Ventral
Dorsal
Ventral


b
Number of junctions
400
300
200
100
0
**
WT
Pu.1-/-


c
Total vessel length (au)
15000
10000
5000
0
**
WT
Pu.1-/-


d
Average vessel length (au)
2000
1500
1000
500
0
NS
WT
Pu.1-/-

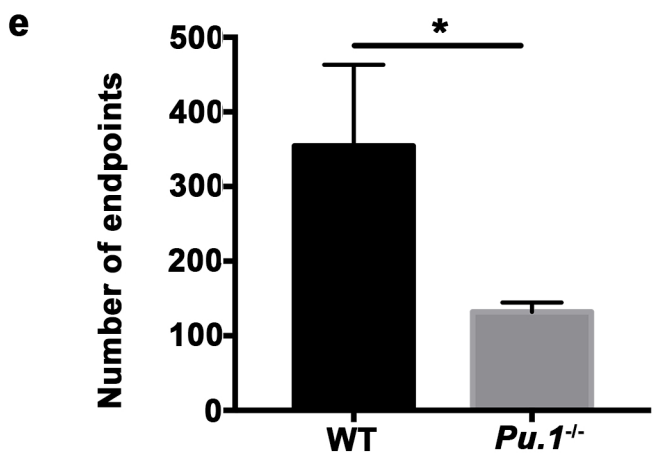
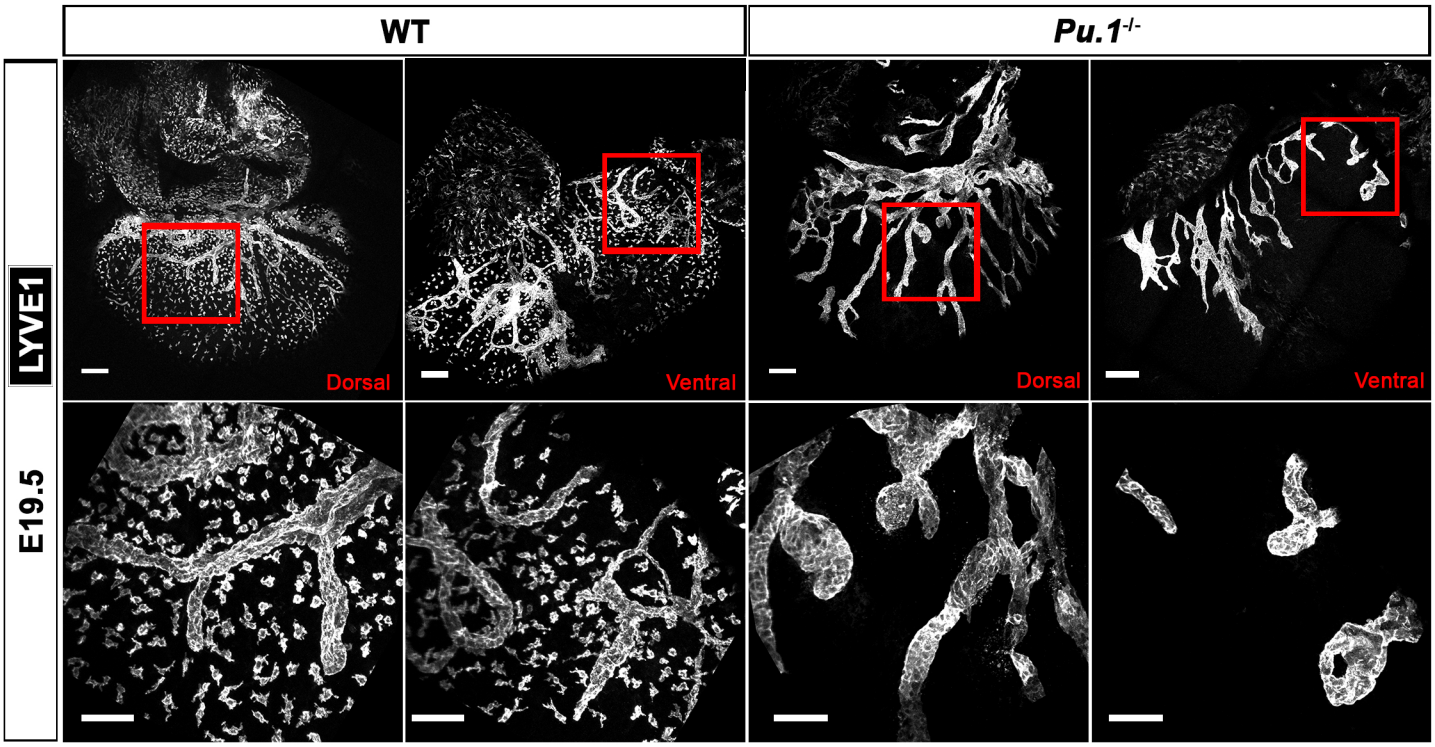
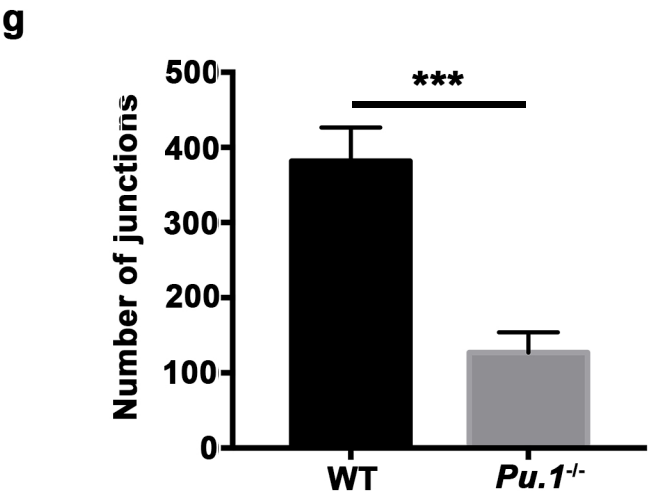
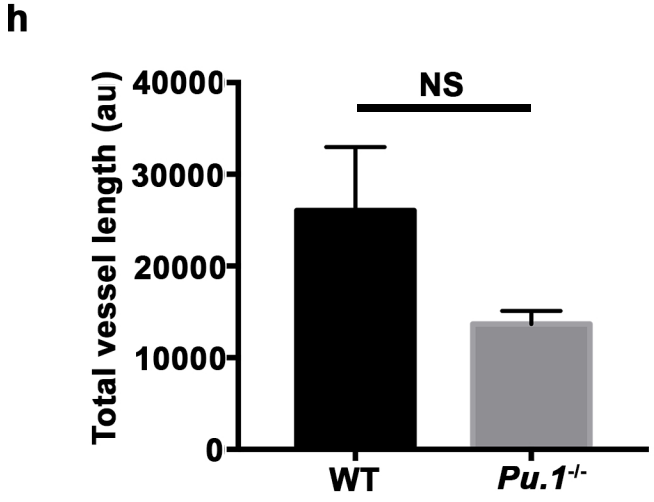
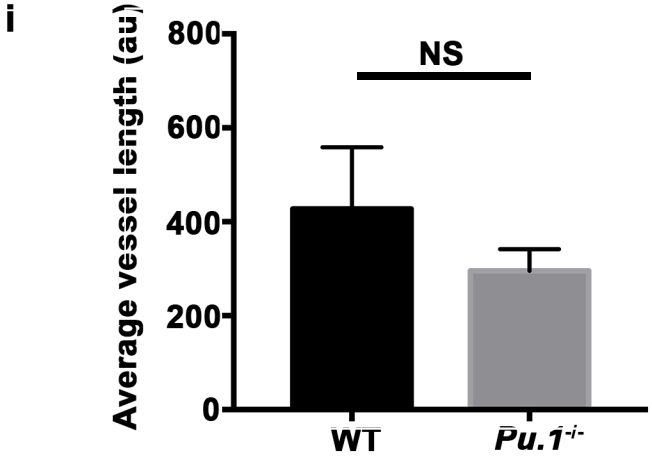

e
Number of endpoints
500
400
300
200
100
0
*
WT
Pu.1-/-

Figure 4.3


f
WT
Pu.1-/-
LYVE1
E19.5
Dorsal
Ventral
Dorsal
Ventral


g
Number of junctions
500
400
300
200
100
0
***
WT
Pu.1-/-


h
Total vessel length (au)
40000
30000
20000
10000
0
NS
WT
Pu.1-/-


i
Average vessel length (au)
800
600
400
200
0
NS
WT
Pu.1-/-

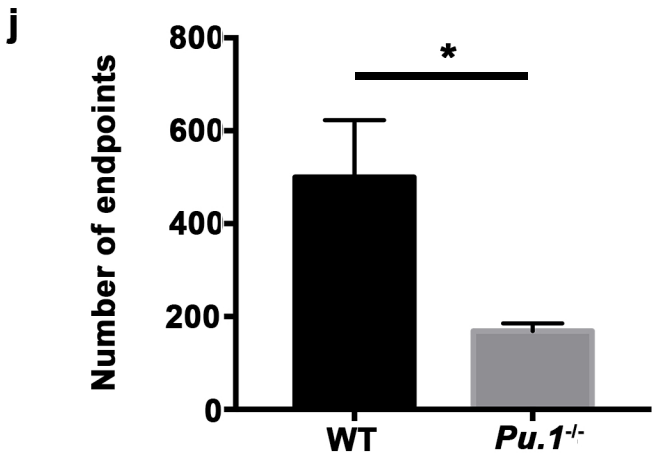

j
Number of endpoints
800
600
400
200
0
*
WT
Pu.1-/-

Figure 4.3 *Pu.1*$^{-/-}$ mice have abnormal lymphatic vessel patterning

(a) Confocal imaging of the dorsal and ventral aspects of E16.5 whole-mount hearts immunofluorescence-stained for lymphatic vessels (LYVE1), demonstrating abnormal lymphatic vascular morphology, branching and migration. Images representative of n=6 per group. Scale bar 200 μm. Respective red inset boxes are shown beneath at higher magnification (Scale bar 100 μm). (b) Quantification of the number of lymphatic vessel junctions on the dorsal aspect of hearts of *Pu.1*$^{-/-}$ and littermate WT controls at E16.5. n=6 per group. (c) Quantification of the total lymphatic vessel length on the dorsal aspect of hearts of *Pu.1*$^{-/-}$ and littermate WT controls at E16.5, n=6 per group. (d) Quantification of average lymphatic vessel length on the dorsal aspect of hearts of *Pu.1*$^{-/-}$ and littermate WT controls at E16.5, n=6 per group. (e) Quantification of total number of lymphatic vessel endpoints on the dorsal aspect of hearts of *Pu.1*$^{-/-}$ and littermate WT controls at E16.5, n=6 per group. (f) Confocal imaging of the dorsal and ventral aspects of E18.5 whole-mount hearts immunofluorescence-stained for lymphatic vessels (LYVE1), demonstrating abnormal lymphatic vascular morphology and branching. Images representative of n=5-6 per group. Scale bar 200 μm. Respective red inset boxes are shown beneath at higher magnification (Scale bar 100 μm). (g) Quantification of the number of lymphatic vessel junctions on the dorsal aspect of hearts of *Pu.1*$^{-/-}$ and littermate WT controls at E18.5, n=5-6 per group. (h) Quantification of total lymphatic vessel length on the dorsal aspect of hearts of *Pu.1*$^{-/-}$ and littermate WT controls at E18.5. n=5-6 per group. (i) Quantification of average lymphatic vessel length on the dorsal aspect of hearts of *Pu.1*$^{-/-}$ and littermate WT controls at E18.5, n=6 per group. (j) Quantification of total number of lymphatic vessel endpoints on the dorsal aspect of hearts of *Pu.1*$^{-/-}$ and littermate WT controls at E18.5, n=6 per group. NS not significant, * $p<0.05$, ** $p<0.01$, *** $p<0.001$. Abbreviations: AU arbitrary units

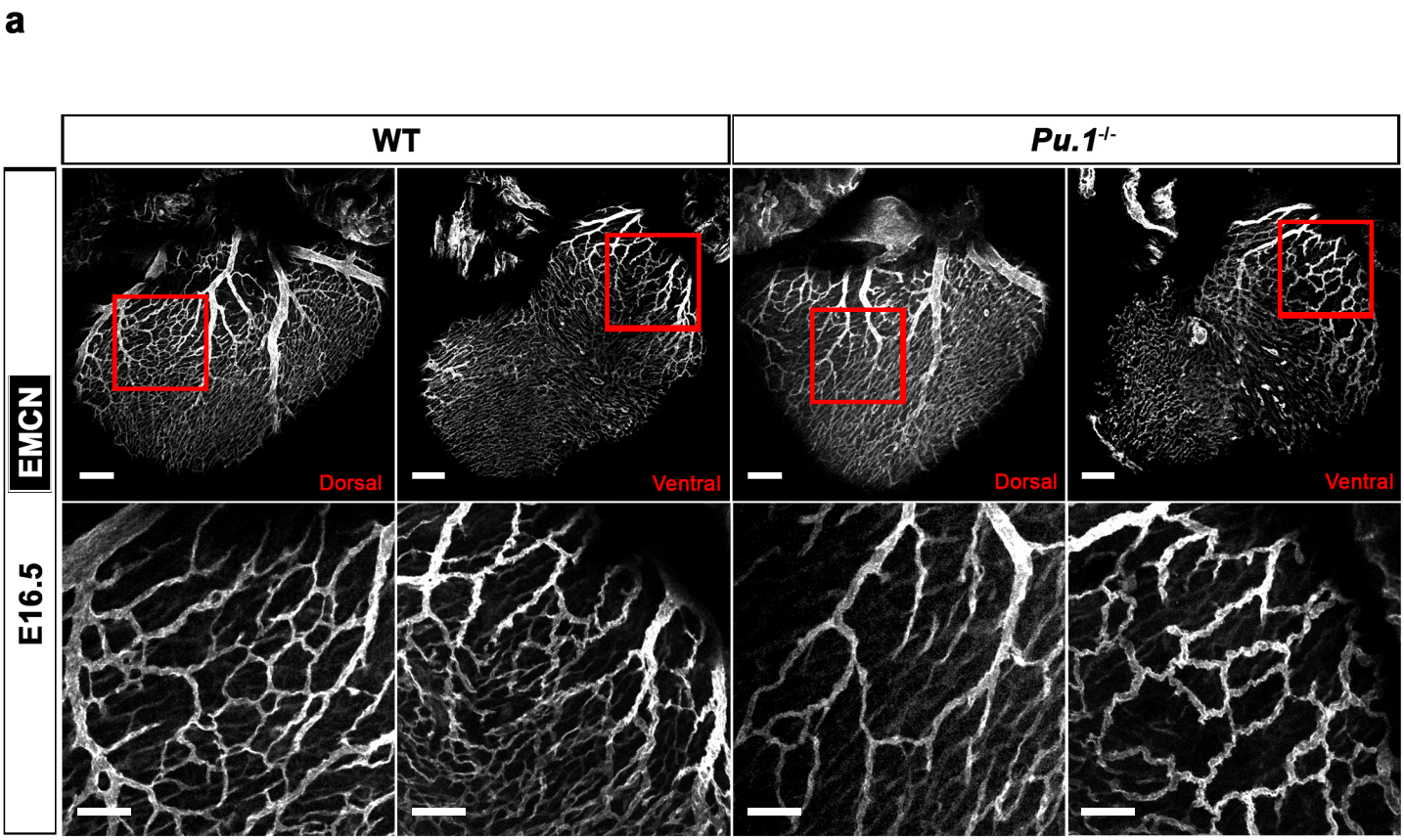
4.2.3 *Pu.1*$^{-/-}$ mice have abnormal coronary blood vessel patterning

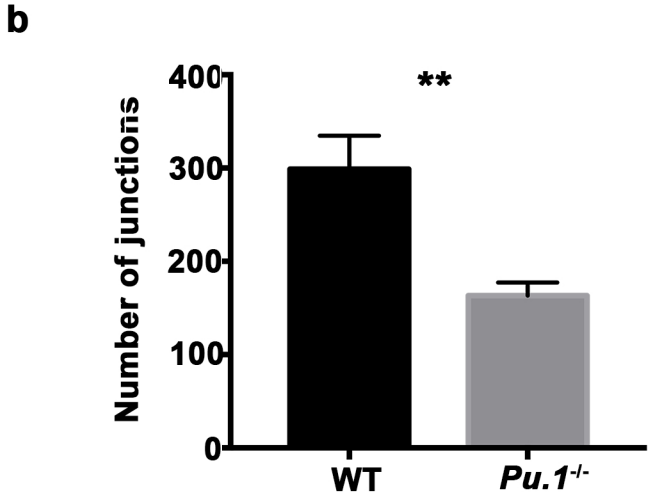
Leid *et al* have recently reported abnormal coronary blood vessel patterning in the setting of constitutive (*Csf1r*$^{op/op}$) and inducible (DTA$^{LysM\text{-}Cre}$) macrophage knockdown in the embryonic mouse heart.(84) I hypothesised that the remodelling of coronary blood vessels might be similarly dysregulated in the *Pu.1*$^{-/-}$ mouse line. After establishing timed matings, embryos were harvested at E16.5 or E19.5, hearts were isolated by microdissection, and tail clips were harvested to identify *Pu.1*$^{-/-}$ embryos and WT littermate controls. Hearts were fixed and stained for the endothelial marker Endomucin (EMCN). Whole-mount hearts were then imaged by confocal microscopy with Z-stack reconstruction. Coronary vessel morphology and branching was quantified using the AngioTool™ plugin for ImageJ.(180)

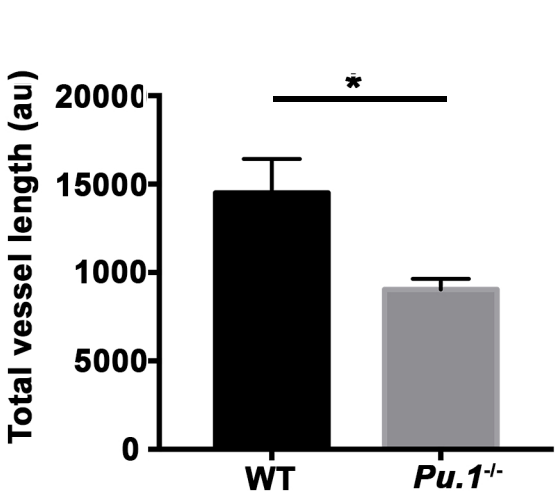
At E16.5, coronary vessel morphology was abnormal on both the dorsal and ventral surfaces of the *Pu.1*$^{-/-}$ heart (Figure 4.4a). The vessels were enlarged in calibre, showed evidence of reduced branching, and reduced distal migration towards the apex of the heart compared to WT (Figure 4.4a). The coronary vasculature was analysed on the dorsal surface of the heart, and revealed that *Pu.1*$^{-/-}$ mice had evidence of a reduced number of coronary vessel junctions (163 ± 14 vs 299 ± 36, n=6 per group, *p=0.0056*, Figure 4.4b) and a significant reduction in total vessel length (9043 ± 601 vs 14511 ± 1907, n=6 per group, *p=0.021*; Figure 4.4c) compared to WT. *Pu.1*$^{-/-}$ mice also showed a trend (not statistically significant) towards reduced average vessel length (146 ± 30 vs 225 ± 29, n=6 per group*, p=0.087*; Figure 4.4d), and a trend towards reduced number of vessel endpoints (312 ± 42 vs 256 ± 25, n=6 per group*, p=0.271*; Figure 4.4e). Taken together, these data suggest that macrophages play a significant role to mediate branching and patterning of the coronary vasculature.

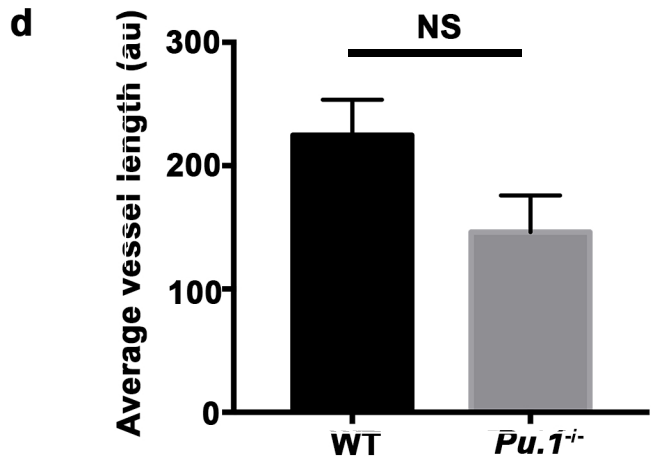
At E19.5, coronary vessel morphology appeared to have normalised in *Pu.1*$^{-/-}$ hearts (Figure 4.4f). The number of junctions in the *Pu.1*$^{-/-}$ mice was comparable to WT (292 ± 58 vs 316 ± 49, n=5-6 per group, *p=0.7634*, Figure 4.4g). There was also no difference in total vessel length (23037 ± 4118 vs 22282 ± 3190, n=5-6 per group, *p=0.8917*, Figure 4.4h). Unexpectedly, however, average vessel length in *Pu.1*$^{-/-}$ mice was increased (191.8 ± 11 vs 137.2 ± 16, n=5-6 per group, *p=0.02*, Figure 4.4i). Finally, compared with WT, there was no difference in the number of endpoints in the coronary vessels of E19.5 *Pu.1*$^{-/-}$ mice (450.2 ± 71 vs 571 ± 65.3, n=5-6 per group, *p=0.2489*, Figure 4.4j). These data suggest that while much of the dysregulation of coronary patterning seen at E16.5 is transient, there is a persistent defect in average vessel length which remains at E19.5.

Figure 4.4


a
WT
Pu.1-/-
EMCN
E16.5
Dorsal
Ventral
Dorsal
Ventral


b
Number of junctions
400
300
200
100
0
**
WT
Pu.1-/-


c
Total vessel length (au)
20000
15000
1000
5000
0
*
WT
Pu.1-/-


d
Average vessel length (au)
300
200
100
0
NS
WT
Pu.1-/-

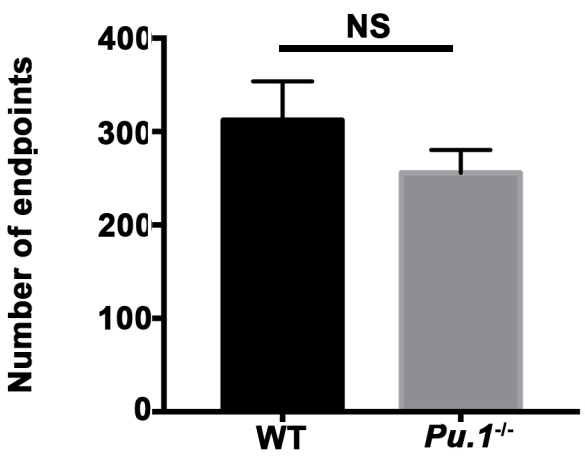
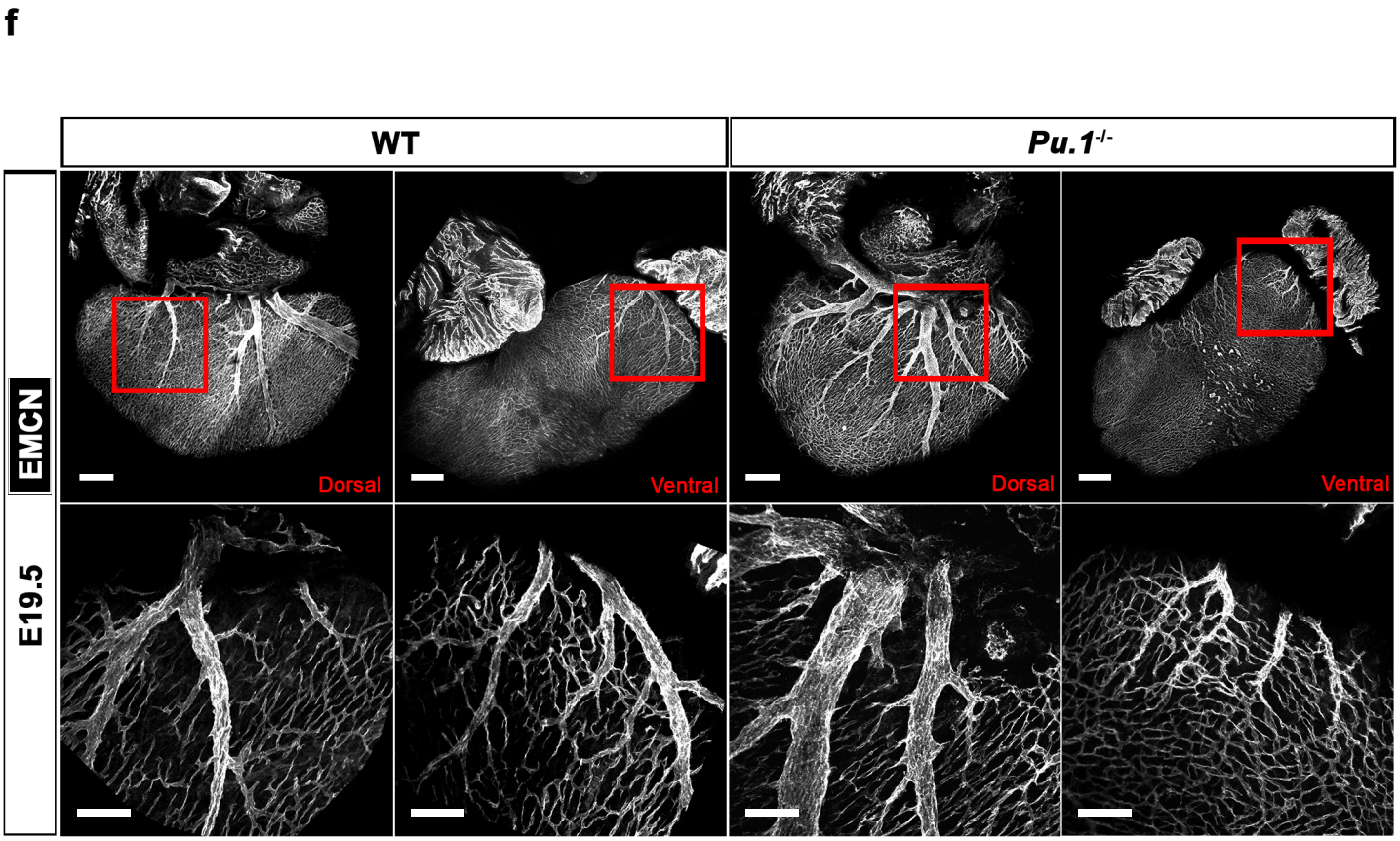
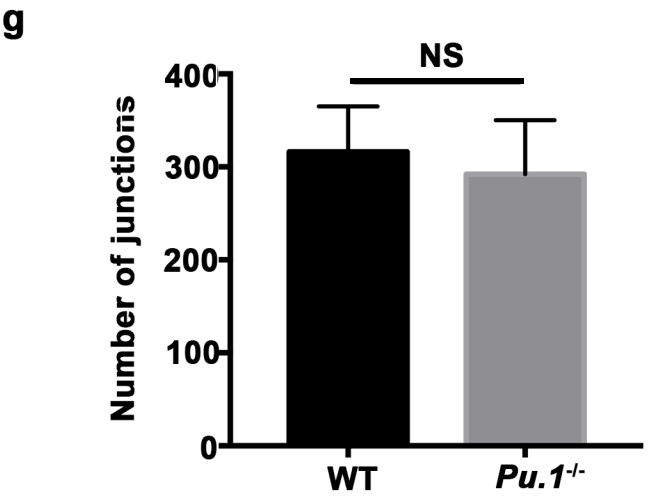
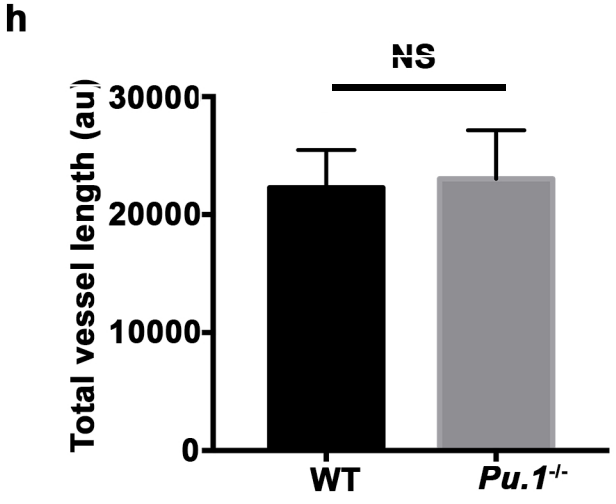
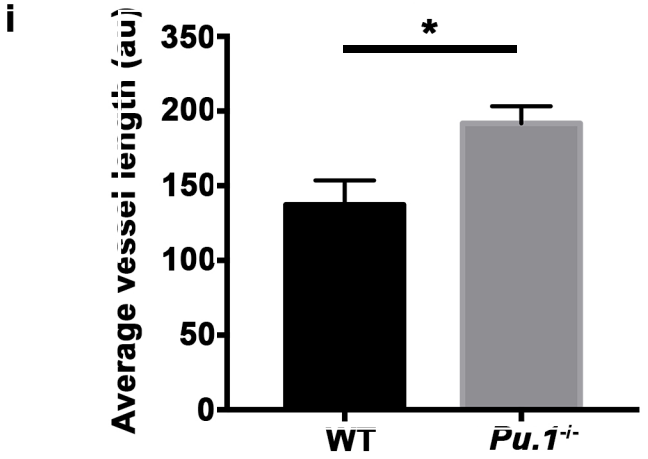

e
Number of endpoints
400
300
200
100
0
NS
WT
Pu.1-/-

Figure 4.4


f
WT
Pu.1-/-
EMCN
E19.5
Dorsal
Ventral
Dorsal
Ventral


g
NS
Number of junctions
400
300
200
100
0
WT
Pu.1-/-


h
NS
Total vessel length (au)
30000
20000
10000
0
WT
Pu.1-/-


i
*
Average vessel length (au)
350
200
150
100
50
0
WT
Pu.1-/-

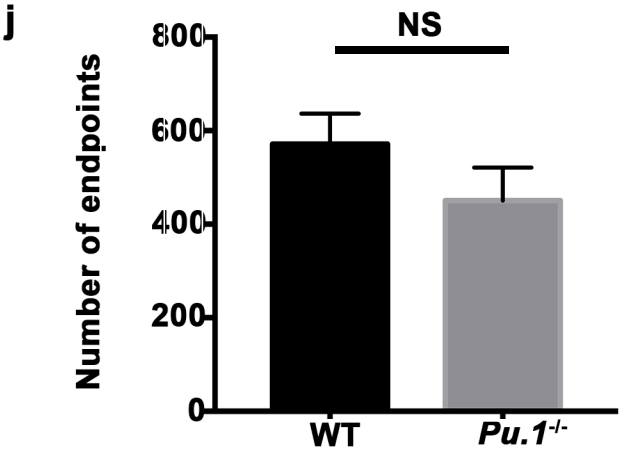

j
NS
Number of endpoints
800
600
400
200
0
WT
Pu.1-/-

Figure 4.4 *Pu.1*$^{-/-}$ mice have abnormal coronary blood vessel patterning
(a) Confocal imaging of the dorsal and ventral aspects of E16.5 whole-mount hearts immunofluorescence-stained for coronary vessels (EMCN), demonstrating abnormal coronary vascular morphology and branching. Images representative of n=6 per group. Scale bar 200 μm. Respective red inset boxes are shown beneath at higher magnification (Scale bar 100 μm). (b) Quantification of the number of coronary vessel junctions on the dorsal aspect of hearts of *Pu.1*$^{-/-}$ and littermate WT controls at E16.5. n=6 per group. (c) Quantification of the total coronary vessel length on the dorsal aspect of hearts of *Pu.1*$^{-/-}$ and littermate WT controls at E16.5, n=6 per group. (d) Quantification of average coronary vessel length on the dorsal aspect of hearts of *Pu.1*$^{-/-}$ and littermate WT controls at E16.5, n=6 per group. (e) Quantification of total number of coronary vessel endpoints on the dorsal aspect of hearts of *Pu.1*$^{-/-}$ and littermate WT controls at E16.5, n=6 per group. (f) Confocal imaging of the dorsal and ventral aspects of E18.5 whole-mount hearts immunofluorescence-stained for coronary vessels (EMCN), demonstrating abnormal coronaryvascular morphology and branching. Images representative of n=5-6 per group. Scale bar 200 μm. Respective red inset boxes are shown beneath at higher magnification (Scale bar 100 μm). (g) Quantification of the number of coronary vessel junctions on the dorsal aspect of hearts of *Pu.1*$^{-/-}$ and littermate WT controls at E18.5, n=5-6 per group. (h) Quantification of total coronary vessel length on the dorsal aspect of hearts of *Pu.1*$^{-/-}$ and littermate WT controls at E18.5. n=5-6 per group. (i) Quantification of average coronary vessel length on the dorsal aspect of hearts of *Pu.1*$^{-/-}$ and littermate WT controls at E18.5, n=6 per group. (j) Quantification of total number of coronary vessel endpoints on the dorsal aspect of hearts of *Pu.1*$^{-/-}$ and littermate WT controls at E18.5, n=6 per group. NS not significant, * $p<0.05$, ** $p<0.01$, *** $p<0.001$. Abbreviations: AU arbitrary units

4.2.4 Lymphatic endothelial cell proliferation is not affected in the *Pu.1*$^{-/-}$ mouse

Having established that an absence of macrophages in *Pu.1*$^{-/-}$ mice is associated with abnormal lymphatic vascular patterning, I sought to investigate the possible mechanism by which macrophages might modulate lymphatic development. In the skin, Gordon *et al* previously reported that macrophage deficiency is associated with hyperproliferation of LECs, leading to abnormal lymphatic vascular calibre.(175) I hypothesised that cardiac lymphatic proliferation might be similarly disrupted in the heart of the *Pu.1*$^{-/-}$ mouse.

After establishing timed matings, embryos were harvested at E16.5, hearts were isolated by microdissection, and tail clips were taken to distinguish *Pu.1*$^{-/-}$ embryos from WT littermate controls. Hearts were fixed and stained by immunofluorescence for the LEC transcription factor PROX1 and the proliferation marker phosphohistone H3 (PHH3), which specifically identifies cells undergoing mitosis. Whole-mount hearts were then imaged by confocal microscopy with Z-stack reconstruction.

At E16.5, proliferating (PHH3+ PROX1+) LECs were visualised on the dorsal surface of the WT heart (Figure 4.5). Compared to the WT, however, no difference in the number of proliferating LECs was observed in the *Pu.1*$^{-/-}$ hearts (Figure 4.5). These findings suggest that LEC proliferation cannot account for the defects in lymphatic vascular calibre and branching in the *Pu.1*$^{-/-}$ mouse.

Figure 4.5

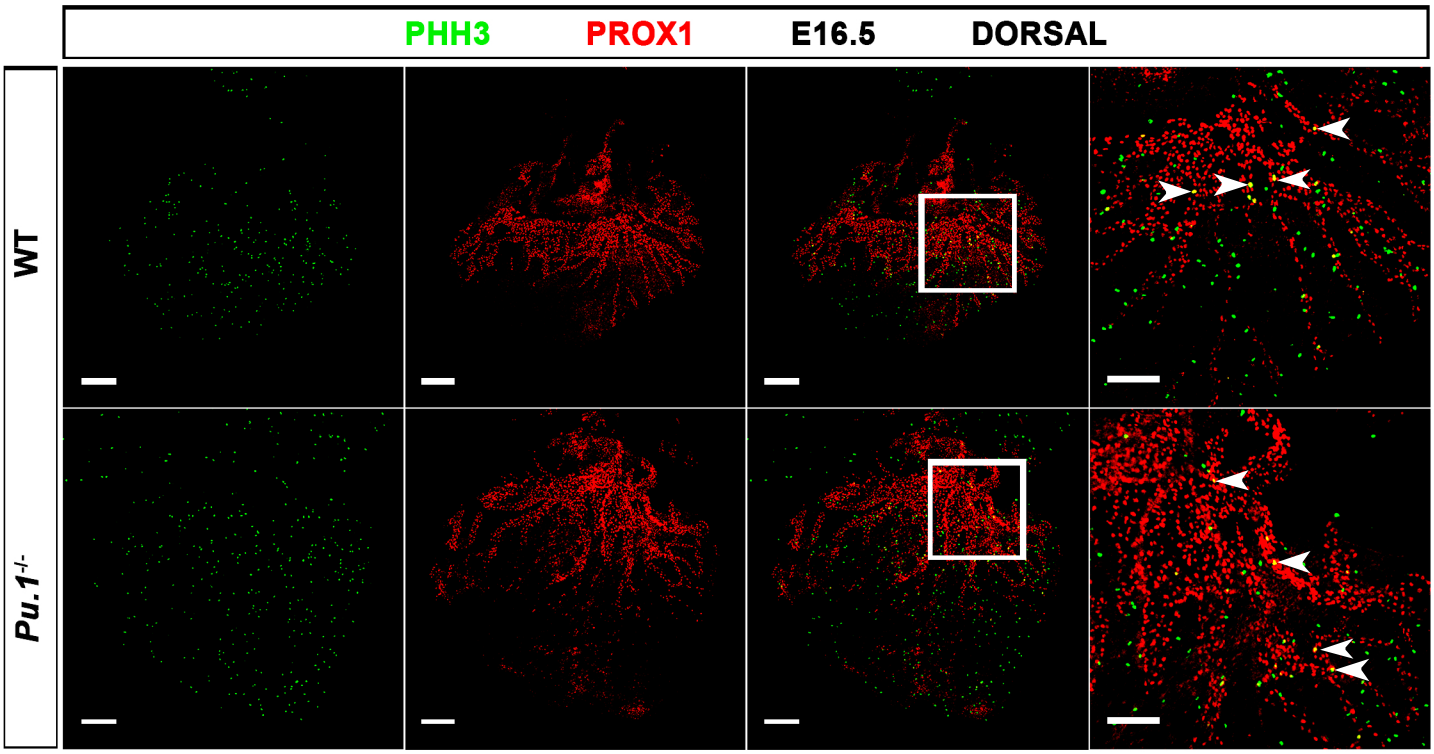


Figure 4.5 Lymphatic endothelial cell proliferation is not affected in the *Pu.1*$^{-/-}$ mouse
(a) Confocal imaging of the dorsal aspect of whole mount E16.5 hearts from *Pu.1*$^{-/-}$ and littermate WT mice, immunofluorescence stained for the proliferation marker PHH3 and the LEC transcription factor PROX1. Actively proliferating LECs are indicated by PHH3+ PROX1+ cells (arrowheads). No difference in LEC proliferation between was observed between *Pu.1*$^{-/-}$ and littermate WT mice. Images representative of n=3 per time point. Scale bar 200 μm. Respective white inset boxes are shown beneath at higher magnification (Scale bar 100 μm).

4.2.5 Macrophages are not a source of VEGFc in the developing heart

In the context of acute inflammation and cancer, macrophages trigger lymphangiogenesis by secretion of VEGFC.(97, 181) VEGFC is also known to play a role in the embryonic heart in angiogenesis and formation of the coronary stems.(118, 182) I hypothesised that macrophages may control lymphatic vascular growth in the embryonic heart by secretion of VEGFC.

Timed matings were established using CX3CR1-GFP mice and embryos were harvested at E16.5. Hearts were isolated by microdissection, fixed, embedded and sectioned in a long axis orientation. Hearts were stained using antibodies raised to GFP, VEGFC, and the nuclear stain 4',6-diamidino-2-phenylindole (DAPI). Imaging was performed by confocal microscopy.

At E16.5, CX3CR1-GFP+ macrophages were clearly visualised in the region of the aortic root (Figure 4.6a). While strong VEGFC expression was observed in the region of the coronary stems, this signal did not colocalise with CX3CR1-GFP macrophages, suggesting that they are not a key source of VEGFC. CX3CR1-GFP+ macrophages were also observed in the epicardium, but again did not express VEGFC (Figure 4.6b). Taken together, these data suggest that VEGFC secretion is not a key mechanism by which macrophages modulate lymphatic vessel patterning during heart development.

Figure 4.6

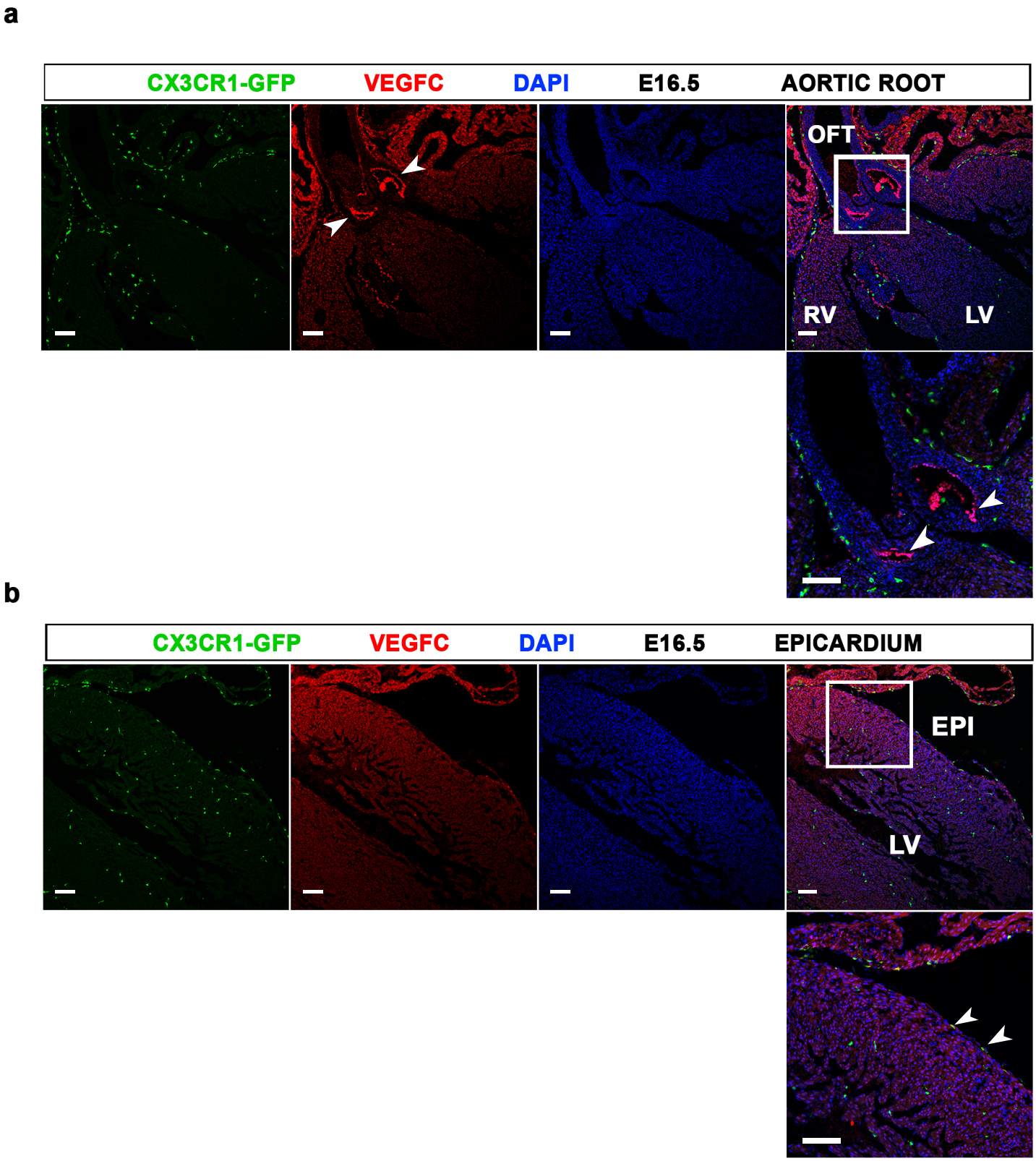


Figure 4.6 Embryonic heart macrophages are not a source of VEGFC
(a) Confocal imaging of immunofluorescence-stained heart cryosections from CX3CR1-GFP mice at E14.5 demonstrating macrophages (CX3CR1-GFP+ cells) concentrated along the aorta and in the epicardium. A region of high VEGFC expression is seen close to the forming coronary stems (arrowheads), but no colocalisation of CX3CR1-GFP+ and VEGFC is seen, suggesting that macrophages are not the major source of VEGFC. (b) Confocal imaging of immunofluorescence-stained heart cryosections from CX3CR1-GFP mice at E14.5 demonstrating macrophages (CX3CR1-GFP+ cells) along the epicardium and within the myocardium. Macrophages (arrowheads) do not express VEGFC. Inset, high-magnification image. Scale bar 100 μm. Images representative of n=3. Abbreviations: EPI epicardium, OFT outflow tract, LV left ventricle, RV right ventricle

4.3 Discussion

4.3.1 Macrophages in lymphatic development

The data presented in this chapter are consistent with a key role for macrophages in regulation of lymphatic patterning in the heart. In the *Pu.1*$^{-/-}$ mouse model at E16.5, cardiac lymphatic vessels were abnormal in calibre, branching and migration. These abnormalities persisted until at least E19.5, which was the latest time point studied. Several studies have investigated the effects of genetic or inducible macrophage ablation on development of the lymphatic vasculature in different model systems. The phenotype associated with macrophage knock-down and the potential mechanisms underlying these, in relation to the findings outline in this chapter, are discussed in turn.

Gordon *et al* analysed the role of macrophages in the development of the dermal lymphatic vasculature.(175) Using the CSF1R-EGFP macrophage reporter mouse line, it was shown that GFP^{+} LYVE1^{+} macrophages are closely associated with the growing dermal lymphatic system at E14.5. In two genetic models of macrophage deficiency (*Pu.1*$^{-/-}$ and *Csf1r*$^{-/-}$ mice), the authors found that size of dermal lymphatic vessels was altered, with an increase in vessel calibre, but the number of branch points was unafffected.(175) In the absence of macrophages there was evidence of hyperproliferation of dermal LECs (defined by increased LEC staining for the mitotic marker phosphohistone H3), which suggested that under normal circumstances macrophages act to restrain LEC proliferation. This effect was organ specific, and hypoplastic jugular lymph sacs were noted in the *Pu.1*$^{-/-}$ mouse. Furthermore, *in vitro*, it was shown that macrophages stimulate rather than restrain LEC proliferation. The authors directly excluded a role for WNT7B and ANGPT2 as macrophage-derived soluble signalling mediators, and showed overall tissue upregulation of a number of

candidate soluble lymphangiogenic factors (e.g. VEGFC, VEGFD, MMP2) in the skin of *Pu.1*$^{-/-}$ mice, suggesting that a lack of these macrophage-derived factors from macrophages was not the causative mechanism.(175)

These findings are similar, but have important differences, to the analysis of the lymphatic vessels in the heart of the *Pu.1*$^{-/-}$ mouse. In the heart, as in the skin, the size of cardiac lymphatic vessels was dysregulated, with enlargement of vessel calibre. In contrast to the skin lymphatics, however, the cardiac lymphatics of the *Pu.1*$^{-/-}$ mouse showed evidence of reduced branching and a reduced number of endpoints at both E16.5 and E19.5. Furthermore, while Gordon *et al* found evidence of LEC hyperproliferation in the *Pu.1*$^{-/-}$, this was not observed in the the heart. This suggests that macrophages have a common role across different tissues to pattern lymphatic vessel calibre, but that there may be multiple mechanisms underlying macrophage control of LECs, depending on the organ or stage of development.

Distinct lymphatic branching phenotypes have been observed in the absence of macrophages in different tissues.(183, 184) Ablation of macrophages (in *Csf1r*$^{-/-}$ mice, or by administration of CSF1R-blocking antibody) led to *enhanced* branch formation of lymphatic vessels on the pleural surface of the diaphragm, without a change in the vessel diameter. This finding suggested that macrophages may normally act to inhibit branch formation in the developing lymphatic system. This phenotype was specific to the diaphragm, and no effect on branching was detected in the mesentery or tail dermis. *In vitro* culture of LECs with conditioned medium from P7 macrophages also inhibited LEC sprouting, but the identity of the soluble mediator responsible was not reported.(183) In contrast, Kubota *et al* studied the role of macrophages in post-natal lymphangiogenesis in the mouse trachea and ear.(184) In the trachea, LYVE1+ macrophages were found to be concentrated in regions of vascularisation. In the *Csf1*$^{op/op}$ mouse model, *reduced* lymphatic branching in the ear

and trachea was observed in the absence of macrophages. Although not highlighted or quantified by the authors, the images also suggest dysregulated (enlarged) vessel calibre in the ear of *Csf1*$^{op/op}$ mice. Cardiac lymphatic development was reported to be grossly normal in *Csf1*$^{op/op}$ mice at E17.0. The ear and trachea branching phenotype was confirmed by treatment in two inducible models of macrophage knockdown (anti-CSF1R antibodies and Ki20227, a small molecule tyrosine kinase inhibitor specific for CSF1R).

In the heart, reduced lymphatic branching was observed in the *Pu.1*$^{-/-}$ heart, similar to findings in the trachea and ear in the *Csf1*$^{op/op}$ mouse model. However, the divergence of branching phenotypes across models of macrophage deficiency suggests that macrophages may have complex and divergent roles in regulation of LEC branching, depending on the tissue or stage of development. This complexity is underpinned by identification of multiple different signalling pathways controlling lymphatic migration and and patterning, several of which are known to be macrophage-derived.

James *et al* reported a role for transforming growth factor beta (TGFβ) signalling in development of the dermal lymphatic vasculature.(185) In mouse models with LEC-specific knockouts of TGFβ receptors, the authors observed reduced lymphatic network branching, reduced LEC proliferation and reduced tip cell formation – a phenotype similar to that reported by Gordon *et al* in the *Pu.1*$^{-/-}$ mouse.(175) In an endothelial-specific knockout of *Tgfbr1* or *Tgfbr2*, the authors observed hyperplastic lymphatic vessels and suggested that TGFβ has a dual role in lymphatic development, whereby it regulates both LEC sprouting and network complexity through negatively regulatiion of proliferation. Tissue macrophages were proposed as a potential source of TGFβ ligands but this was not explored in the study directly.(185)

The release of matrix metalloproteinases is another potential mechanism for macrophage control of LECs, which act by remodelling the ECM. Macrophages are known to synthesise matrix metalloproteinases both in development and in tissue repair.(186) Detry *et al* demonstrated a key role for matrix metalloproteinase 2 (MMP2) in lymphangiogenesis, which acts as an interstitial collagenase to facilitate migration of LECs through the ECM.(187) In the zebrafish, *mmp2* knockdown led to impaired lymphatic vessel formation and in mice, *Mmp2*$^{-}$ knockout led to reduced dermal tail lymphatic complexity. *In vitro*, the authors demonstrated MMP2-mediated effects on migration and branching morphogenesis. It was proposed that the ECM is a critical regulator of LEC migration and branching, and MMP2-based remodelling of the matrix a key control mechanism by which lymphangiogenesis is controlled.

4.3.2 Macrophages in vascular development

The data presented in this Chapter suggest that macrophages in the embryonic heart have a functional role in mediating patterning of the coronary blood vasculature. In the *Pu.1*$^{-/-}$ mouse model at E16.5, coronary vessels were enlarged in calibre, with reduced branching and reduced total vessel length. By E19.5, vessel calibre and branching had normalised, but vessel length was persistently dysregulated, with longer average vessel length in the *Pu.1*$^{-/-}$. These findings might suggest different roles for macrophages at distinct stages of development: at E16.5, macrophages promote branching and migration of vascular endothelial cells, leading to evidence of reduced branching and vessel length. At E19.5, however, macrophages may act to restrain further vascular growth, explaining the finding of increased average vessel length in the in the *Pu.1*$^{-/-}$ heart.

The roles of macrophages in the development of vasculature appear to be species, tissue and stage-specific, with a number of differing mechanisms reported to mediate the interaction between macrophages and endothelial cells, including both soluble mediators and physical contacts. This complexity is illustrated by the role of macrophages in the development of the eye vasculature. After birth, macrophages are required both for controlled regression of hyaloid vasculature, a temporary embryonic vascular plexus, and for development of the permanent retinal vessels. To induce regression of hyaloid vessels, macrophages secrete soluble WNT7B, which acts as a 'death signal' to induce apoptosis of endothelial cells and pericytes.(174) In the retina, macrophages suppress branching by secretion of WNT5A and WNT11, acting via a non-canonical FLT1 pathway.(184, 188) Recruitment of macrophages to retinal vessel branchpoints and leading edges requires NOTCH1, and myeloid-specific *Notch1* knockdown was shown to result in a failure of localisation and disrupted anastomosis between sprouting tip cells.(189)

In the cerebral vasculature, macrophages appear to mediate vascular patterning by physical association with tip cells.(133) Macrophages have been identified to localise at the junctions of cerebral vessels and physically interact with endothelial tip cells, forming a bridge between neighbouring sprouting tip cells prior to fusion, to increase vascular complexity. In the *Pu.1*$^{-/-}$ mouse brain, it was found that there were normal numbers of vascular sprouts but fewer interconnections between vessels, consistent with the data presented in this chapter demonstrating decreased branching in the *Pu.1*$^{-/-}$ mouse heart at E16.5.

Leid *et al* have recently reported abnormal coronary vascular patterning in the heart using the *Csf1*$^{op/op}$ and *LysM*-Cre;R26-DTA mouse models.(84) The authors reported an increased density of PECAM+ vasculature in mutant hearts at E17.5, increased vascular branching, and dysregulation of vessel calibre. An increased percentage of

medium sized vessels (in the size range 9-12um) was observed, with a corresponding reduction of large and small calibre vessels. Transcriptional analysis of CCR2- macrophages, which were shown to localise with coronary vessels, expressed IGF1, a known macrophage-derived mitogen. *In vitro*, CCR2- macrophages stimulated endothelial tube formation and migration of cultured coronary endothelial cells, an effect which could be blocked by blockade of the IGF1 receptor.(84) However, the mechanism by which loss of macrophage IGF1 might lead to hyper-branching was not explored.

These findings of increased vessel branching are in direct contrast to the data showing reduced vascular branching in the *Pu.1*$^{-/-}$ heart, as presented in this chapter. Although this might reflect a difference in the models used (*Pu.1*$^{-/-}$ heart compared to *Csf1*$^{op/op}$), it seems more likely to reflect methodology. In this thesis, the superficial, epicardial layer of vessels as visualised by whole mount imaging were quantified, whereas Leid *et al* quantified vessels in cardiac sections. The apparently divergent findings might therefore be reconciled if macrophages primarily act to promote branching in the superficial epicardial layer. In their absence, the smaller vessels may undergo compensatory hyperbranching, as visualised by Leid *et al*, but not identified in whole mount imaging as shown in this chapter.

In summary, the data in this chapter suggest a role for embryonic macrophages in patterning of the lymphatic and coronary vasculature in the developing heart. There are several limitations, however. The experiments described have been conduced exclusively in the *Pu.1*$^{-/-}$ model of macrophage deficiency, and need to be validated in a second, ideally inducible, model of macrophage knock-down. Secondly, although LEC hyperproliferation and macrophage-derived VEGFC have been excluded as potential mechanisms for macrophage patterning of the lymphatic vasculature, a definite mechanism remains unclear. Finally, the functional

consequences of aberrant patterning of the coronary and lymphatic vasculature remain unknown. These limitations are directing the focus of ongoing experiments, as outlined in the Chapter 7.3.

4.4 Conclusions

The experiments presented in this Chapter identify and characterise a phenotype of abnormal lymphatic and coronary vascular development in the *Pu.1*$^{-/-}$ mouse heart. The findings demonstrate that macrophages normally play a role in regulating lymphatic and coronary vascular vessel calibre, morphology, branching and migration during development of the heart. These effects are complex and developmental-stage dependent. While coronary vascular defects in the *Pu.1*$^{-/-}$ mouse heart are largely compensated for by the end of gestation, lymphatic vascular defects persist, leading to possible functional effects on the heart postnatally. Production of the lymphangiogenic factor VEGFC, and regulation of lymphatic endothelial cell proliferation, were explored and excluded as significant mechanisms by which macrophages regulate lymphatic endothelial growth in the developing heart.

Chapter 5: Macrophages in repair and regeneration after MI

…in fast bondage he bound Prometheus, the devious planner, whipping the painful bindings over a column at midpoint, and against him sent a long-winged eagle to feed on his liver, which was immortal; but whatever this long-winged bird ate during the day grew during the night again to perfection.

Theogony, lines 521-5

5.1 Background

5.1.1 Tissue repair by scar formation and regeneration

The ability of an organism to undertake tissue repair following injury is critically important to its survival.(190) In adult mammals, wound repair occurs by formation of a disorganised, collagenous scar.(191) Formation of scar serves the immediate purpose of stabilising the wound and sealing the injury from the external environment. In the longer term, however, scar may compromise organ integrity or function. This is exemplified by wound healing in the heart after MI, where scar deposition prevents myocardial rupture but leads to downstream arrhythmia, contractile dysfunction and heart failure.(5) In contrast, wound healing in many lower vertebrates such as teleost fish and amphibians occurs by regeneration, without permanent scar.(191)

Regenerative skin wound healing has also been observed in the fetus of mammals, including mice, rats, pigs, monkeys and humans,(192) and also extends into the neonatal period for some tissues, for example the finger digit, hair cells of the cochlea, olfactory bulb and heart.(21, 193-195) The finding that regeneration can occur transiently in mammals suggests that the mode of tissue repair is not hard-wired, and that a combination of species-, organ-, and age-related effects influence healing. Understanding the mechanisms by which injured tissue can be directed to heal by regeneration rather than scar formation would have major therapeutic potential across a number of diseases such as heart failure, stroke, spinal cord injury, pulmonary fibrosis, and skin wound healing.(196)

5.1.2 Macrophages in tissue repair

Historical studies in skin wounding models provided key insights into the general mechanisms of tissue repair, many of which translate to the heart post-MI.(197) Importantly, wound healing is temporally regulated and occurs in distinct but overlapping phases, consisting of an early inflammatory phase, a proliferative phase, and a prolonged maturation and remodelling phase.(198) The inflammatory phase is characterised by coagulation, inflammatory signalling and infiltration of myeloid immune cells, predominantly neutrophils and monocyte-macrophages.(198) The subsequent proliferative phase is defined by recruitment and activation of fibroblasts, leading to formation, deposition and stabilisation of scar tissue and new ECM.(198)

Macrophages infiltrate the injury site in large numbers during the inflammatory phase, and remain during the early proliferative phase of wound healing.(199) Landmark historical studies demonstrated that macrophages are critical for effective adult wound healing.(200-202) Knockdown of macrophages (using anti-macrophage serum in guinea pigs, and more recently diphtheria toxin-knockdown approaches in mice) led to delayed clearance of neutrophils, impaired neovascularisation, reduced myofibroblast differentiation, decreased collagen synthesis and delayed wound healing.(200, 201) Depletion of macrophages during either the inflammatory phase or the proliferative phase of skin healing (up to day 9 after wounding) resulted in reduced granulation tissue formation and delayed wound healing.(202) An important exception to this may be the neonate: skin wounds in the neonatal *Pu.1*$^{-/-}$ mouse were found to heal almost perfectly without scar formation, despite a total absence of macrophages.(203)

Macrophages have multiple roles within the healing wound.(199) Recruited macrophages initially adopt a pro-inflammatory ‘M1’ profile, associated with

production of inflammatory cytokines interleukin-1, interleukin-6 and TNFα.(204) The transition to the proliferative phase is associated with a shift in macrophage phenotype to a reparative ‘M2’ phenotype, defined by production of anti-inflammatory mediators such as IL-1R antagonist, decoy IL-1 receptor type II and IL-10.(199) The mechanisms behind this phenotypic switch are poorly defined, but involve phagocytosis of necrotic debris and neutrophils.(205) In addition to inflammatory cytokine signalling and phagocytosis, macrophages direct wound healing through release of soluble growth factors which modulate re-epithelialization, angiogenesis and recruitment and activation of fibroblasts.(204) Key macrophage-derived growth factors include transforming growth factor (TGF)-β ligands, insulin-like growth factor 1 (IGF1), platelet-derived growth factor (PDGF), IL-13, and prostaglandin F(2α).(206-208) Macrophages also produce a number of biologically active matricellular proteins such as fibronectin, and secrete matrix metalloproteases which remodel the ECM structure.(209, 210) Macrophages are also influenced by fibroblast-derived signals within the wound site, for example osteopontin. This extracellular protein and secreted cytokine, derived largely from fibroblasts, influences macrophage activity through modulation of recruitment and cytokine secretion, inhibiting anti-inflammatory IL-10 production.(211, 212)

5.1.3 Macrophages in tissue regeneration

Macrophages have also been implicated in wound repair by regeneration, such that targeting of macrophages in a range of regenerative models has resulted in failure of regeneration.(213) For example, following limb amputation in the Salamander, clodronate-depletion of macrophages within the first four days of injury resulted in a failure of limb regrowth.(214) This was associated with alterations to the cytokine profile and ECM, suggesting that macrophages play a key role in providing both environmental and matrix cues which direct regeneration.

Macrophages are also required for regeneration in mammals.(213) Following skeletal muscle injury, knock-down of monocytes using CD11b-DTR mice led to muscle scarring, and depletion of macrophages at later stages resulted in smaller diameter muscle fibres.(215) Functionally, macrophages in regenerating skeletal muscle have been demonstrated to promote growth of muscle fibres and restrict endothelial to mesenchymal transition (which leads to fibrosis), instead directing progenitors towards vasculogenesis.(216) In hair cell regeneration, plucking of hairs has been shown to lead to recruitment of inflammatory macrophages, which produce TNFα and activate hair stem cells.(217) Finally, in the liver, macrophage phagocytosis of hepatocyte debris led to secretion of WNT3A, in turn specifying progenitor differentiation towards production of new hepatocytes and resulting in liver regeneration.(218)

Macrophages have recently been shown to be required for regeneration of the neonatal mouse heart following MI.(101) Using clodronate-loaded liposomes to ablate macrophages, Aurora *et al* demonstrated that a lack of macrophages led to a failure of regeneration and formation of a fibrotic scar. This study revealed reduced angiogenesis in macrophage-ablated hearts, and a microarray experiment in which macrophages were profiled at day 3 post-MI from the P1 and P14 mouse heart revealed that P1 macrophages preferentially express known pro-angiogenic genes.(101) Collectively this suggested that macrophages provide angiogenic cues which facilitate regeneration, although these were not fully defined.(101)

5.1.4 Macrophages as determinants of wound healing

The precise factors which determine whether tissue repair occurs by regeneration or scar formation are largely unknown. It is clear, however, that macrophage function

can impact on the outcome of wound healing. Failure of macrophages to transition from an M1 to an M2 phenotype has been demonstrated to lead to persistent inflammation with delayed healing. For example, macrophage iron overload, as occurs in leg ulcers caused by venous stasis, impairs M1 to M2 transition and may underlie poor wound healing in this condition.(219) Similarly, diabetes mellitus has also been demonstrated to inhibit M1 to M2 transition, leading to impaired healing of skin wounds in mice and humans.(220) In the heart post-MI, selective depletion of M2 macrophages resulted in a failure of wound healing, scar deposition and increased ventricular rupture.(221) However, removal of macrophages from the wound site is also required for effective healing, and accelerated clearance of macrophages via the lymphatic system has recently been demonstrated to improve cardiac function and repair.(97)

Whether macrophages play unique roles in tissue regeneration, or provide similar cues which are interpreted differently by downstream cell types, is unknown. Given the central role of macrophages in both regeneration and scar formation, I hypothesised they might act to regulate or direct the mode of tissue repair. Addressing this question is difficult as wound healing by regeneration and scar formation does not commonly occur in the same organ, however, the neonatal and adult MI models allows comparison of macrophage function during regeneration (neonatal mouse at postnatal day 1, P1) and scar formation (neonatal mouse at postnatal day 7, P7, and adult) and were in the studies described in this chapter.

5.1.5 Aims

This chapter addresses the following aims:

1. To quantify the immune response to MI in the regenerative (neonatal P1) and scar-forming (neonatal P7, adult) models of myocardial infarction.

2. To analyse the spatial distribution of macrophages in the regenerating and scar-forming heart.
3. To perform transcriptional analysis by RNA sequencing (RNA-seq) to understand the differences in the macrophage gene expression and function in healing by regeneration and scar formation.
4. To understand key differential signalling pathways in macrophages which may impact on the mode of tissue repair.

5.2 Results

5.2.1 The P1 neonatal mouse heart regenerates after myocardial infarction

The neonatal mouse heart has been reported to heal by regeneration after either resection of the apex or ligation of the left anterior descending (LAD) coronary artery.(21, 22) A 'temporal window' for heart regeneration is open at P1, but has closed by P7, at which point wound healing occurs by scar formation and fibrosis, analogous to the adult mouse or human heart. Both neonatal (P1 and P7) and adult models of MI are established in the Riley Laboratory.(108) The surgical methodology for these models is outlined in detail in Chapter 2. Although the models are similar, neonatal surgery (at P1 or P7) requires induction of cardiorespiratory arrest in order to perform the procedure, while the adult surgery is performed on isoflurane-maintenance anaesthesia and positive pressure ventilation.

Myocardial infarction was induced in the P1, P7 and adult heart by surgical ligation of the LAD coronary artery (Figure 5.1a). The LAD is visible in the P1 and P7 mouse (Figure 5.1a, arrowheads), aiding accurate suture placement. In the adult mouse, however, the LAD lies beneath the epicardial surface and furthermore, has variable course and branching.(222) As such, coronary ligation was performed by encircling the LV wall in the region in which the LAD is expected to pass, with blanching downstream of the suture site used to confirm interruption of LAD blood flow. For both neonatal and adult samples, correct placement of the suture was confirmed at organ harvest. At day 4 post-MI MI, ventricular injury caused by ischaemic necrosis downstream of the suture was evident in the P1, P7 and adult mouse models (Figure 5.1b).

To confirm that P1 and P7/adult mice heal by regeneration and scar formation respectively, hearts from P1, P7 and adult mice were harvested at day 21 post-MI. Following dissection, hearts were fixed, dehydrated, embedded in paraffin, sectioned, and stained with Masson's trichrome to demonstrate collagen (blue) and normal myocardium (red). The myocardium of P1 hearts appeared normal with minimal residual fibrosis (Figure 5.1c). In contrast, both P7 and adult hearts had evidence of loss of myocardium, dense scar deposition and formation of ventricular thrombus (Figure 5.1c).

Figure 5.1

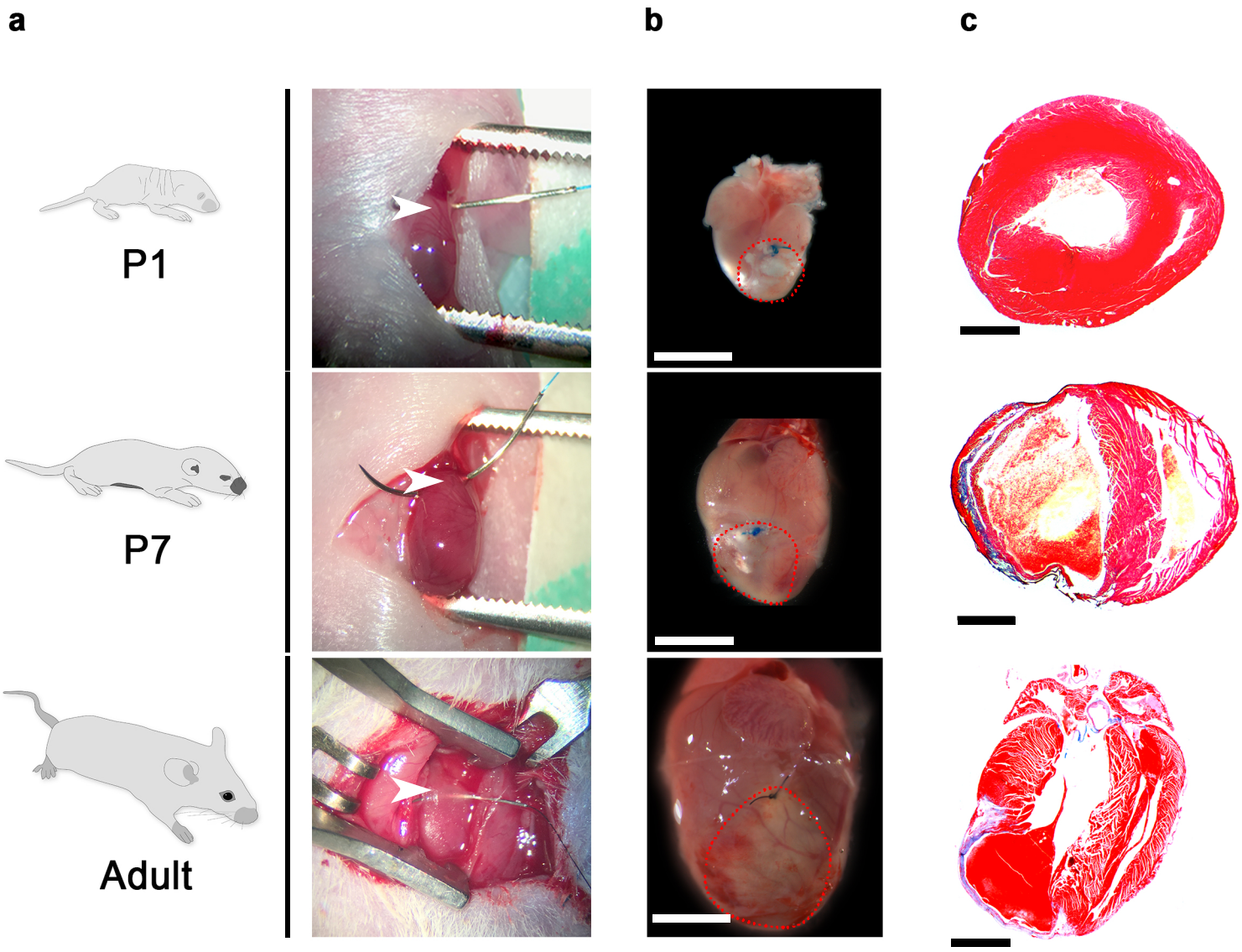


Figure 5.1 The P1 neonatal mouse heart regenerates after myocardial infarction
(a) Surgeon's view of mouse myocardial infarction (MI) procedure in the postnatal day 1 (P1) neonatal mouse, the postnatal day 7 (P7) neonatal mouse, and the adult mouse heart. The position of the left anterior descending coronary artery is highlighted (arrowhead). (b) Macroscopic view of the P1, P7 and adult mouse heart at day 4 following MI surgery, demonstrating tissue injury (highlighted in red) downstream of coronary artery ligation. Scale bar, 2mm. (c) Masson's trichrome-stained sections from the P1, P7 and adult mouse heart at day 21 post-MI, demonstrating regeneration in the P1, in comparison to extensive myocardial loss and scar formation in the P7 and adult heart. Scale bar, 2mm.

5.2.2 Analysis of the immune response to MI in the neonatal and adult heart

The immune response has been proposed as a key regulator of tissue repair, but there are few direct comparisons of the immune response in regenerative and scar forming models. In the heart, the neonatal and adult immune responses have not been directly compared, although minor differences have been reported between P1 and P7.(101) In general, the neonatal immune system is known to be functionally distinct to that of the adult, which may be a consequence of the requirement to tolerate non-shared maternal antigens or the stress and remodelling of development *in utero*.(223)

The immune response to MI was quantified by flow cytometry, utilising a previously validated gating strategy (Figure 5.2a).(224) Leucocytes from the myeloid lineage are the major cellular components of the inflammatory response to MI and were the focus of this experiment.(225) By flow cytometry, the proportion of leucocytes ($CD45^{+}$), myeloid cells (CD45+ CD11b+) neutrophils (CD45+ CD11b+ Ly6G+), macrophages (CD45+ CD11b+ Ly6G- F4/80+) and monocytes (CD45+ CD11b+ Ly6G- F4/80- $Ly6C^{hi/lo}$) were quantified in the heart at baseline and following MI. Macrophage polarisation was assessed by expression of CD206, the mannose receptor, a classical M2 marker.(50) Key time points for study (baseline, day 1, day 4 and day 7) were selected on the basis of previous literature on the adult mouse immune response to MI.(226)

To perform immune cell quantification, animals were culled by a Schedule 1 method at specific time points following MI. Hearts were rapidly removed by blunt dissection, remaining blood was rinsed away in ice-cold PBS, and hearts were digested to a

single-cell suspension. Digestion was stopped at 1 hour by addition of ice-cold HBSS and samples were filtered through a 70um microfilter to remove any remaining tissue debris. Samples were spun down to pellet the cell fraction, and HBSS/collagenase was removed by aspiration. After lysis of red cells, samples were resuspended in 2%FBS/PBS, and stained using antibodies to CD45, CD11b, Ly6G, F4/80, Ly6C and CD206 (see Materials & Methods). Immune cells were quantified by flow cytometry and expressed as a proportion of total live singlet cells in the heart.

The proportions of leucocytes and myeloid cells (with the exception of Ly6C^{hi} monocytes), relative to the neonatal response, were significantly elevated in adult hearts post-MI across early time points (days 1 and 4): CD45+ leucocytes at day 1 (adult 29.41 ± 4.136 n=7 vs P7 15.33 ± 2.656 n=6 vs P1 20.08 ± 3.464 n=4, *p=0.0343*, Figure 5.2b,i); CD45+ leucocytes at day 4 (adult 25.78 ± 2.545 n=5 vs P7 11.25 ± 0.852 n=3 vs P1 9.95 ± 1.827 n=6, *p=0.*0003, Figure 5.2b,i); CD45+ CD11b+ myeloid cells at day 4 (adult 20.82 ± 2.44 n=5 vs P7 7.87 ± 0.5522 n=3 vs P1 7.105 ± 1.493 n=6, *p=0.0004*, Figure 5.2b,ii); CD45+ CD11b+ Ly6G+ neutrophils at day 1 (adult 20.88 ± 3.848 n=6 vs P7 8.294 ± 2.841 n=5 vs P1 8.833 ± 2.4 n=4, *p=0.0280*, Figure 5.2b,iv); CD45+ CD11b+ Ly6G+ neutrophils at day 4 (adult 4.363 ± 1.165 n=4 vs P7 1.33 ± 0.2146 n=3 vs P1 0.7483 ± 0.1915 n=6, *p=0.0051*, Figure 5.2b,iv); CD45+ CD11b+ Ly6G- F4/80+ macrophages at day 4 (adult 12.86 ± 2.021 n=5 vs P7 6.205 ± 0.4463 n=4 vs P1 5.623 ± 1.142 n=6, *p=0.0062*, Figure 5.2b,v).

Neonatal MI led to a pronounced early monocyte infiltration, but this rapidly resolved to approach baseline levels by day 4 (Figure 5.2b, vii). In contrast, at day 4, the adult mouse continued to have a sustained Ly6C^{hi} and Ly6C^{lo} monocyte response (CD45+ CD11b+ Ly6G- F4/80- Ly6C^{hi} monocytes at day 4, adult 1.21 ± 0.232 n=5 vs P7 0.177 ± 0.0219 n=3 vs P1 0.3463 ± 0.156 n=6, *p=0.006*, Figure 5.2b,vii); CD45+

CD11b+ Ly6G- F4/80- Ly6C^{lo} monocytes at day 4 (adult 1.023 ± 0.3013 n=4 vs P7 0.3533 ± 0.0353 n=3 vs P1 0.3075 ± 0.0865 n=6, *p=0.0293*, Figure 5.2b,viii). Next, M2 macrophages were quantified as a proportion of all F4/80+ macrophages in the heart by analysing the expression of the M2 polarisation marker CD206.(227) This revealed significantly greater increases in CD206+ macrophages in adult hearts as compared to either the P1 or P7 setting at day 4 and 7 post MI: CD206+ macrophages at day 4 (expressed as a percentage of all F4/80+ macrophages: adult 73.8 ± 4.229 n=5 vs P7 64.73 ± 1.481 n=3 vs P1 58.93 ± 2.904 n=6, *p=0.0240*); CD206+ macrophages at day 7 (adult 80.32 ± 2.397 n=5 vs P7 63.5 ± 2.338 n=4 vs P1 54.1 ± 3.449 n=3, *p=0.0002*). Collectively these data suggest that the cellular immune response to MI in neonates (P1 and P7) is significantly dampened compared to adult, and that the monocytes have distinct kinetics in response to injury according to developmental stage. However, the lack of a significant difference in the P1 and P7 cellular immune response suggests that neonatal 'immune dampening' may be permissive, but is not sufficient to induce regeneration following MI.

Figure 5.2

a

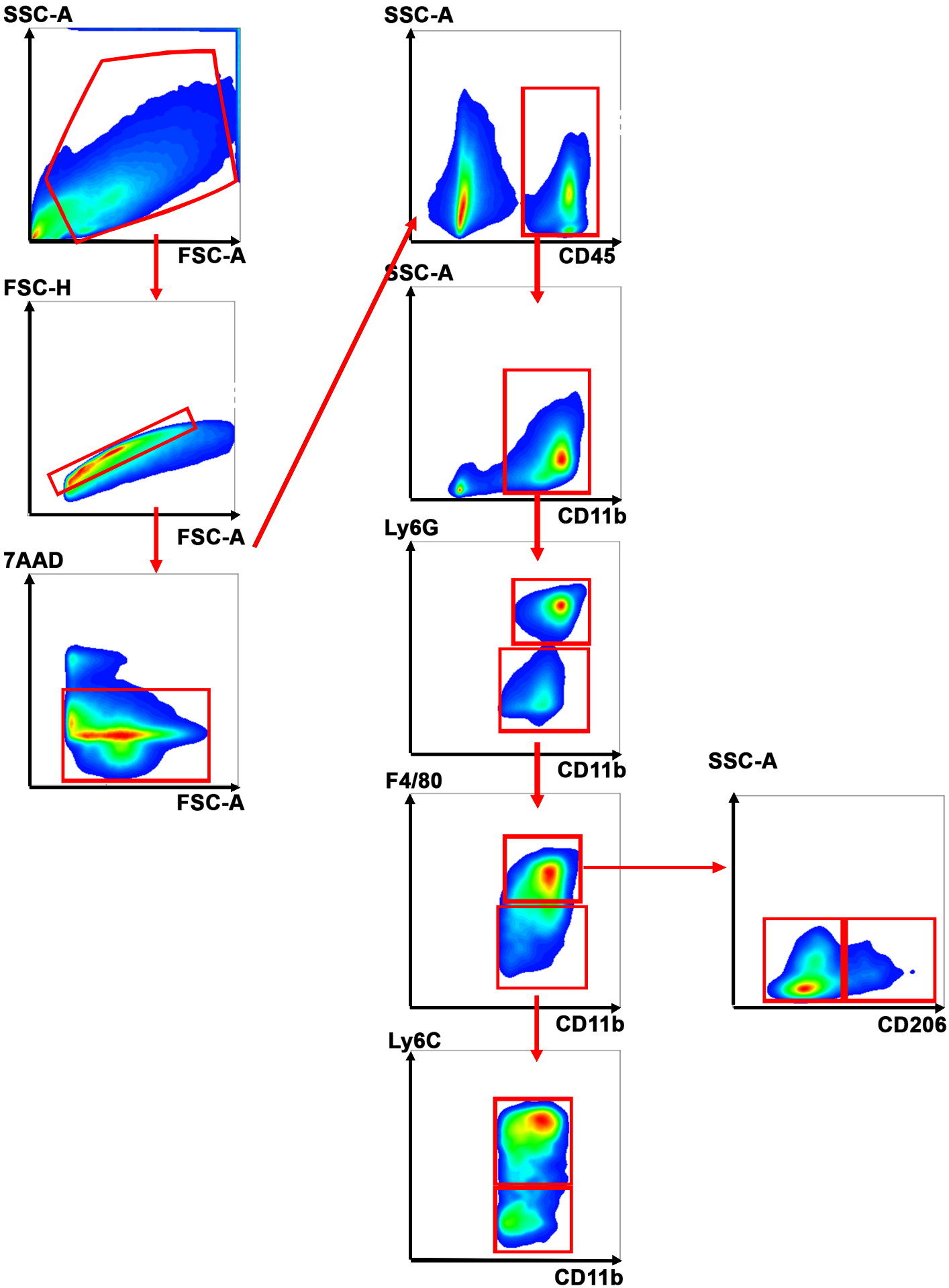

SSC-A
FSC-A
FSC-H
FSC-A
7AAD
FSC-A
SSC-A
CD45
SSC-A
CD11b
Ly6G
CD11b
F4/80
CD11b
Ly6C
CD11b
SSC-A
CD206

Figure 5.2

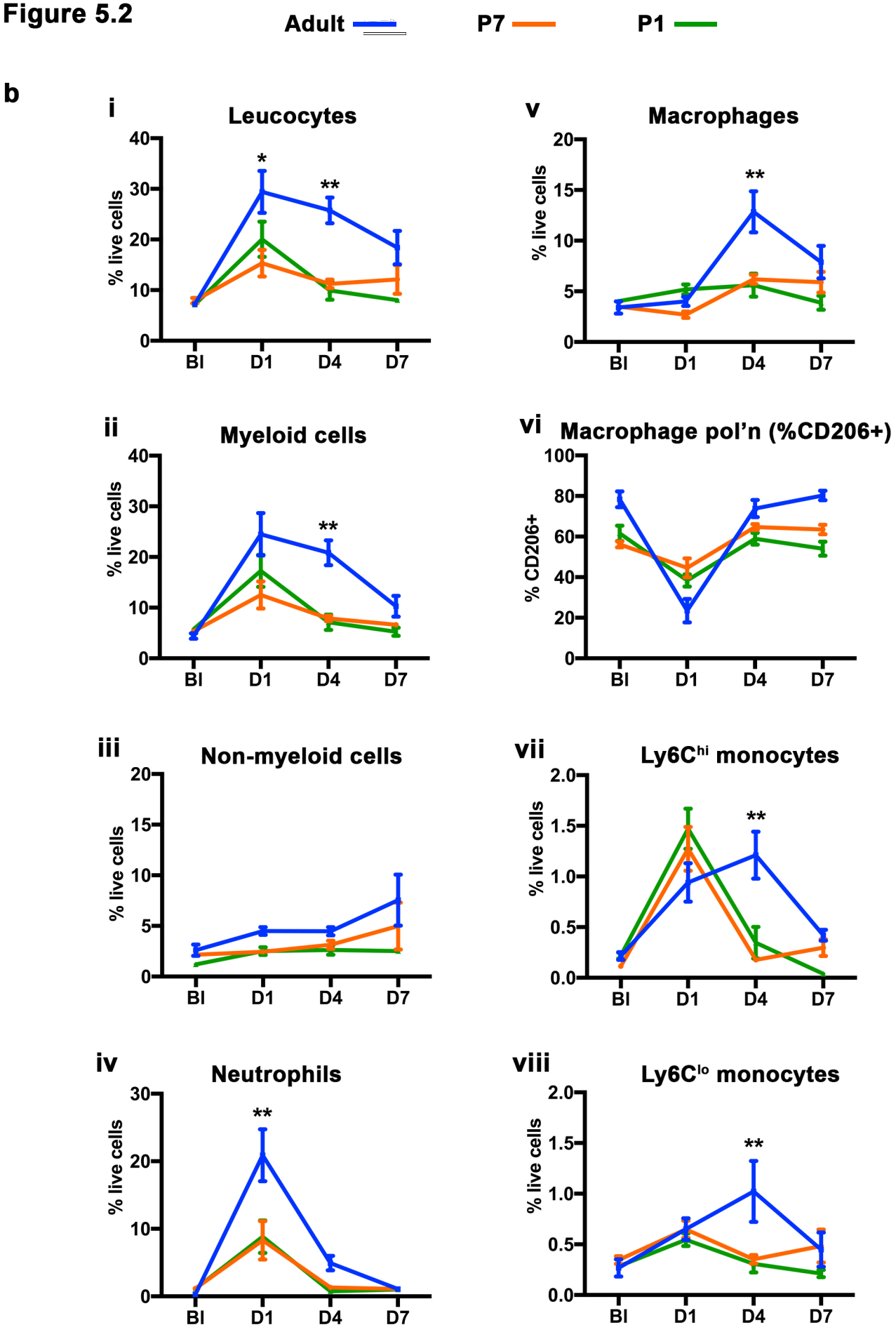

Adult
P7
P1
b
i
Leucocytes
% live cells
40
30
20
10
0
*
**
Bl
D1
D4
D7
v
Macrophages
% live cells
20
15
10
5
0
**
Bl
D1
D4
D7
ii
Myeloid cells
% live cells
40
30
20
10
0
**
Bl
D1
D4
D7
vi
Macrophage pol'n (%CD206+)
% CD206+
100
80
60
40
20
0
Bl
D1
D4
D7
iii
Non-myeloid cells
% live cells
20
15
10
5
0
Bl
D1
D4
D7
vii
Ly6Chi monocytes
% live cells
2.0
1.5
1.0
0.5
0.0
**
Bl
D1
D4
D7
iv
Neutrophils
% live cells
30
20
10
0
**
Bl
D1
D4
D7
viii
Ly6Clo monocytes
% live cells
2.0
1.5
1.0
0.5
0.0
**
Bl
D1
D4
D7

Figure 5.2 Analysis of the immune response to MI in the neonatal and adult mouse
(a) FACS gating strategy to identify myeloid leucocytes. After gating out debris, and gating for singlets and live cells (7AAD negative) (left hand panel), the following cell populations were identified as shown: CD45+ leucocytes, CD45+ CD11b+ myeloid cells, CD45+ CD11b+ Ly6G+ neutrophils, CD45+ CD11b+ Ly6G- F4/80+ macrophages, and CD45+ CD11b+ Ly6G- F4/80- Ly6Chi/lo monocytes. Macrophage polarisation was measured as a proportion of macrophages expressing the M2 surface marker CD206. (b) Flow cytometric quantification of (i) leucocytes, (ii) myeloid cells (iii) non-myeloid cells, (iv) neutrophils, (v) macrophages, (vi) macrophage polarisation, (vii) $Ly6C^{hi}$ monocytes and (viii) $Ly6C^{lo}$ monocytes in the adult (blue), P7 (orange) and P1 (green) heart at Baseline (BI), Day (D1), Day 4 (D4) and Day 7 (D7) following MI. Cell numbers are expressed as a proportion of total live singlet cells, or as a proportion of all F4/80+ macrophages (macrophage polarisation). n=3-8 per time point. Data represent the mean +/- S.E.M. * $p<0.05$, ** $p<0.01$.

5.2.3 Macrophages infiltrate the infarct zone in the neonatal and adult heart following MI

The spatial localisation of macrophages in the neonatal and adult heart following MI has not been directly compared. In heart development, macrophages are recruited to functional niches such as the epicardium, where they play specific roles in remodelling the vascular and lymphatic endothelium (see chapters 3 & 4). In MI, macrophages are known to localise predominantly to the infarct zone.(228)

To examine the distribution of macrophages following MI, hearts were dissected from P1, P7 and adult mice at day 4, fixed, embedded and sectioned in the short axis below the level of the suture. Macrophages were identified by immunofluorescence staining for the macrophage marker CD68 and nuclei were stained for DAPI. Imaging was performed by confocal microscopy

At day 4 post-MI, CD68+ macrophages were visualised in a densely concentrated zone within the anterior left ventricle of the P1, P7 and adult mouse heart, corresponding to the expected infarct zone region (Figure 5.3). In keeping with the results of flow cytometric quantitation of immune cell numbers, there appeared to be fewer macrophages in the neonatal mouse heart compared to the adult (Figure 5.3). Interestingly, a few macrophages were observed in the epicardial region (Figure 5.3). This experiment suggests that MI in the P1, P7 and adult mouse results in recruitment of macrophages to the site of the infarct.

Figure 5.3

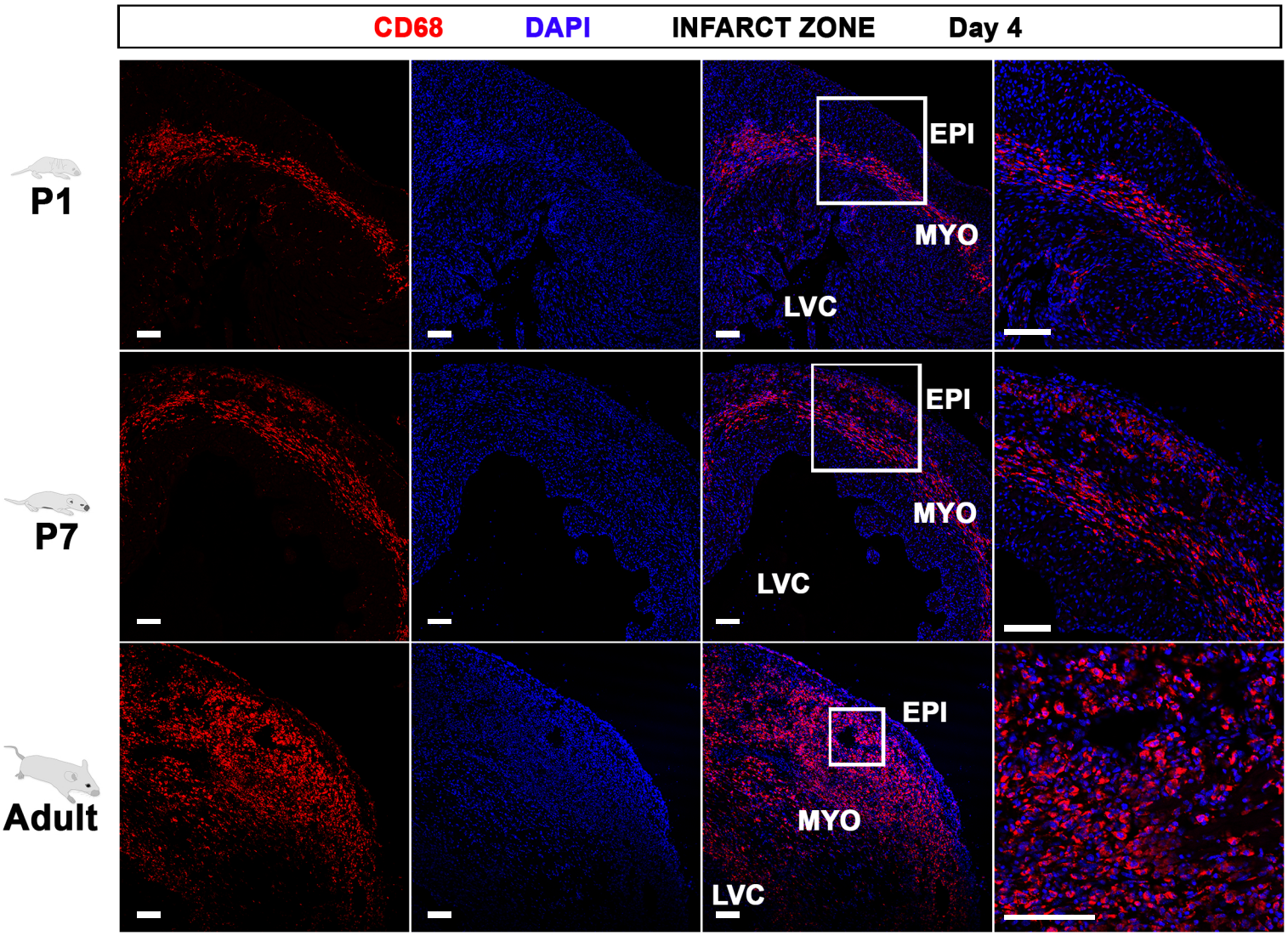


Figure 5.3 Macrophages infiltrate the infarct zone of the neonatal and adult mouse heart
Confocal imaging of immunofluorescence-stained heart cryosections demonstrating localisation of macrophages (CD68+ cells, red) to the infarct zone in the anterior ventricular wall in the P1 (upper), P7 (middle) and adult mouse (lower) at day 4 post-MI. Images representative of n = 3 per group. Respective white boxes enlarged in right hand panel. Scale bar, 100 μm. Abbreviations: EPI epcardium, LVC left ventricular cavity, MYO myocardium.

5.2.4 RNA sequencing of cardiac macrophages

To analyse the possible differences in macrophage function during the context of myocardial repair by regeneration compared to scar formation, transcriptional analysis of the P1, P7 and adult macrophages by RNA sequencing was performed. Analysses were carried out at baseline (prior to MI) and at key time points as determined by previous analysis of the immune response post MI – at day 1 (adult samples only), day 4, and day 7 post-MI (Figure 5.4a) – to inform on the temporal responses of macrophages during injury and repair.

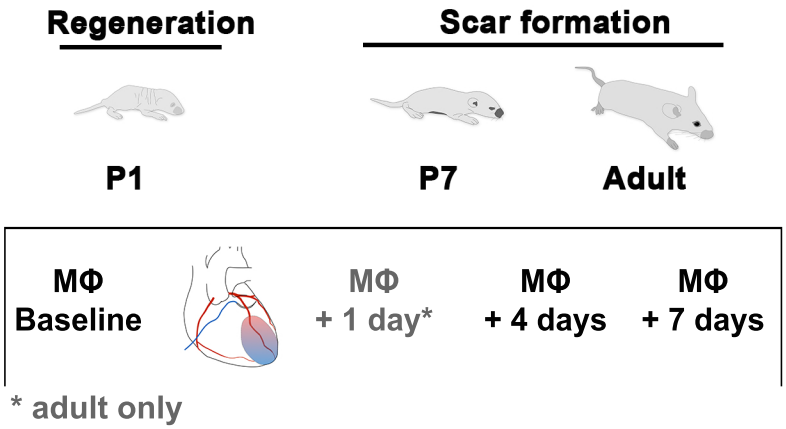
The pipeline for RNA sequencing is outlined in Figure 5.4b and below. Firstly, 10,000 CD45+ CD11b+ Ly6G- F4/80+ macrophages were FAC-sorted from the neonatal and adult heart at baseline and post-MI at the time points indicated, and collected into 20 µl 2%FBS/PBS. Sorted cells were snap frozen in liquid nitrogen to induce lysis, and RNA was then extracted by spin-column nucleic acid purification using the Ambion RNAqueous®-Micro Total RNA Isolation Kit, according to the manufacturer's protocol. Briefly, following cell lysis RNA was bound to a silica gel membrane within a spin column. RNA was washed and then eluted before DNase treatment to remove any traces of contaminating DNA.

Next, RNA quality and quantity was analysed using an RNA pico chip (Agilent Technologies) using an Agilent 2100 BioAnalyzer. The read-out for RNA quality was the RNA Integrity Number (RIN), a proprietary composite score of several factors in the electrophoretic trace including total RNA ratio, height of the 28S peak and the fast area ratio. Only samples of high quality (RIN ≥ 7.0) were taken forward. Next, cDNA was synthesised and amplified from 100pg-300pg of input RNA using SMART-seqTMv4ultra low input kit for RNA (Clontech laboratories). This uses SMART®

(Switching Mechanism at 5' End of RNA Template) technology, which incorporates switching activity of reverse transcriptases to enrich for full-length cDNAs and to add defined PCR adapters directly to both ends of the first-strand cDNA. This ensures the final cDNA libraries contain the 5' end of the mRNA and maintain a true representation of mRNA transcripts; these factors are critical for transcriptome sequencing and gene expression analysis. After cDNA synthesis, cDNA was quality control (QC) checked using a BioAnalyzer, and underwent 'tagmentation' to produce a sequencing library (Nextera XT DNA library preparation kit). Nextera XT uses an engineered transposase to simultaneously tag and fragment (tagment) the cDNA, adding dual indexes to barcode the sample prior to pooling. Each sample then underwent normalisation and pooling for sequencing. The final cDNA concentration in the pooled library was quantified by qPCR relative to cDNA standards (Kapa Biosystems). Samples were then run on the desktop Illumina NextSeq platform, with a total number of ~ 400 million reads per cartridge. After sequencing, support with QC, mapping and downstream bioinformatic data was provided by Madeleine Lemieux, Bioinfo, Canada. Genes with $\log_2$ fold change > 2 and a false discovery rate of < 0.05 were deemed to be significantly differentially expressed.

Figure 5.4

a



b

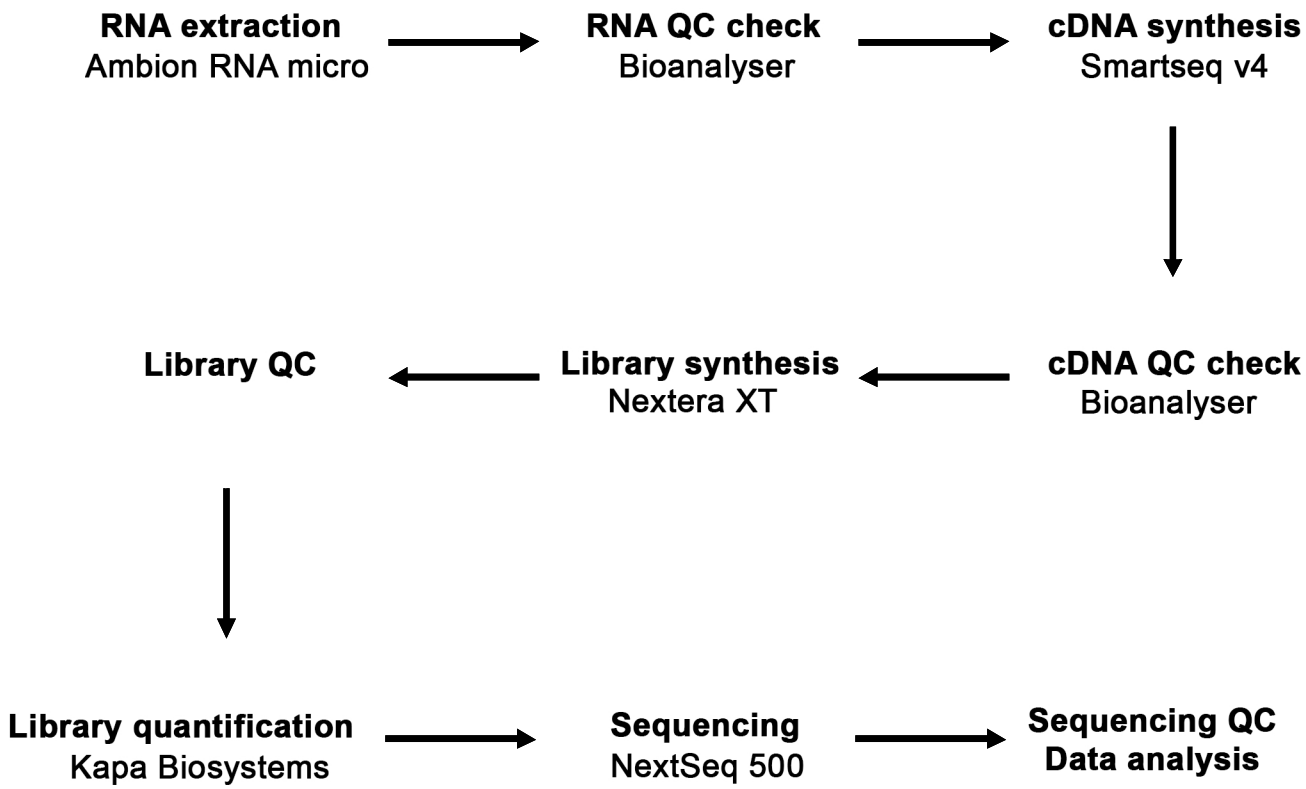


Figure 5.4 RNA sequencing of cardiac macrophages (a) Experimental design: macrophages (Mφ) from the P1 neonate, which heals by regeneration, were compared with macrophages from the P7 neonate and adult mouse, which heal by scar formation. To interrogate the response through the time course of injury and repair, macrophages were extracted at baseline, day 1 post-MI (adult only), day 4 post-MI and day 7 post-MI. (b) Experimental pipeline for RNA sequencing. RNA was extracted from FAC-sorted macrophages by spin-column nucleic acid purification (Ambion RNA micro) and subjected to a quality control (QC) check and quantification using a Bioanalyser. cDNA was then synthesised using Clontech Smartseq v4. cDNA is then QC checked before undergoing library synthesis, which involves concurrent amplification and tagging the cDNA (tagmenting) with dual indexes added to barcode each sample. Samples are then adjusted and pooled. The library is then quantified and adjusted before seqencing on a benchtop Illumina NextSeq 500. The final stage is downstream QC and data analsysis.

5.2.5 Macrophages in the P1, P7 and adult heart are transcriptionally distinct at baseline and following MI

To analyse the overall transcriptional differences between samples, principal component analysis (PCA) was performed. PCA is a mathematical algorithm which identifies variables, the principal components, which are linear combinations of the original variables, and is used to demonstrate the variation in the dataset while reducing its overall dimensionality.(229)

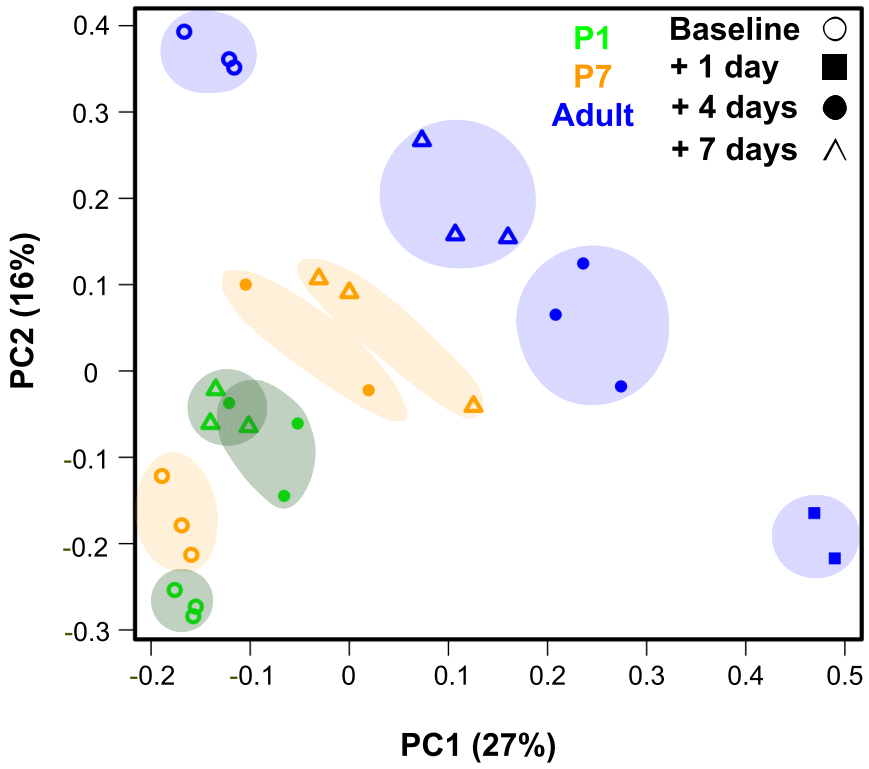
By PCA, P1, P7 and adult macrophages were clearly separated both at baseline and at each specified time point post injury (Fig. 5.5a). In addition to clustering of biological replicates at baseline, we observed clearly divergent transcriptional responses to injury in the P1, P7 and adult samples. The first principal component, accounting for 27% of the variation in the dataset, was found to separate the P1 baseline samples from the adult at day 1 post-MI. The second principal component, accounting for 16% of the variability, separated P1 macrophages from adult macrophages at baseline. Biological replicates were observed to cluster closely together by PCA, confirming the validity of the observed transcriptional differences. Furthermore, P1 and P7 were separated at baseline, and P7 responses at day 4 and 7 were observed to lie mid-way between adult and P1 clusters.

Differential expression analysis was then performed to compare transcriptional activity between baseline and day 4 post-MI (Fig. 5.5b,i) as well as between day 4 and day 7 (Fig. 5.5b,ii). A comparison of baseline and day 4 post-MI revealed 1500 differentially expressed transcripts in the adult. In contrast, 398 and 470 genes were differentially expressed as compared to baseline in the P1 and P7 models, respectively. Of the transcripts upregulated in the adult at day 4 only 39 were

conserved across P1 and P7 samples at this time point. Between day 4 and day 7, 437 genes were differentially expressed in the adult, 419 genes in the P1 mouse, and 217 genes in the P7 mouse. Surprisingly, only 43 genes were conserved across all three stages. Taken together, these data reveal that the neonatal macrophage response is markedly less complex compared to the adult, with fewer differentially expressed genes. The lack of conserved gene expression suggests distinct gene regulatory programmes may underlie macrophage function during neonate (P1 and P7) versus adult cardiac injury. Both P1 and P7 models were characterised by relatively fewer differentially expressed genes after injury, in keeping with the concept of an immature response.

Figure 5.5

a



b

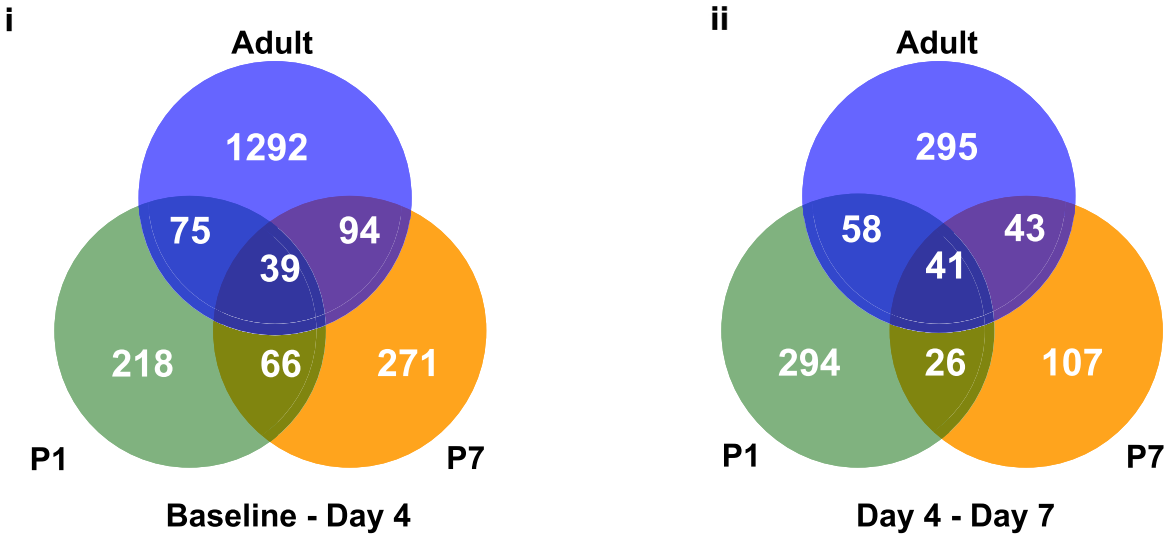


Figure 5.5 Macrophages in the P1, P7 and adult heart are transcriptionally distinct at baseline and following MI (a) Principal Component Analysis showing differential gene expression between macrophages from the P1 (green), P7 (orange) and adult (blue) mouse heart at baseline and indicated time points (day 1, 4 and 7) following MI. Biological replicates are highlighted. (b) Venn diagrams demonstrating the number of differentially expressed genes in macrophages from P1 (green), P7 (orange) and adult (blue) hearts between baseline and day 4 (i), and day 4 and day 7 (ii). Common genes are shown in overlapping segments.

5.2.6 Myocardial repair by regeneration and scar formation is associated with differential macrophage gene expression

To understand the key differences in the macrophage transcriptome, which might underlie cardiac regeneration compared to scar formation, a semi-hierarchical clustering analysis was performed to group genes according to whether their expression differed by healing phenotype. Candidate pro-regenerative genes were identified at day 4 and day 7 post-MI, as those genes which were upregulated in P1, but not in P7/adult. Conversely, candidate scar-forming genes were identified at day 4 and day 7 post-MI as those which were upregulated in P7/adult, but not in P1. Lists of genes identified in this manner were subjected to Gene Ontology analysis to identify candidate pathways.

At day 4, 30 differentially expressed transcripts were identified in P7/adult macrophages, and 9 differentially upregulated genes were identified in P1 macrophages (Figure 5.6a). P7/adult macrophages upregulated mediators of inflammation (*Il6*), metabolism (*Arg*), fibrosis (*Loxl2*) and cytokines *(Ccl7, Ccl8*). P1 samples showed upregulated of histidine decarboxylase (*Hdc*), an enzyme which converts L-histidine to histamine, which has previously been linked to newt limb regeneration.(230) P7/adult genes differentially upregulated at day 7 were associated with gene ontology (GO) terms reflecting biological processes such as positive regulation of apoptotic cell clearance, opsonisation, detection of molecule of bacterial origin and inflammatory response (Figure 5.6b,i). In contrast, significant GO terms associated with the P1 gene set included histamine biosynthetic process, peptidoglycan metabolic process and positive regulation of epithelial cell proliferation in wound healing (Figure 5.6b,ii).

At day 7, P7/adult macrophages upregulated canonical mediators of fibrosis, including *Ctgf*, *Tgfb3*, and *Serpine1*, which are known encode soluble factors associated with fibrosis (Figure 5.6c).(231) In contrast, P1 macrophages uniquely upregulated a subset of genes which may be linked to heart regeneration (Figure 5.6c). P7/adult genes differentially upregulated at day 7 were associated with gene ontology (GO) terms reflecting biological processes such as ECM organisation and response to stress (Figure 5.6d,i). In contrast, GO terms associated with P1 upregulated genes included leukocyte activation and immune system process (Figure 5.6d,ii).

Collectively, these data show that macrophage gene expression is differentially regulated in regenerative and scar-forming environment. Furthermore, these analyses suggest possible gene transcripts and biological pathways which might underlie divergent healing responses.

Figure 5.6

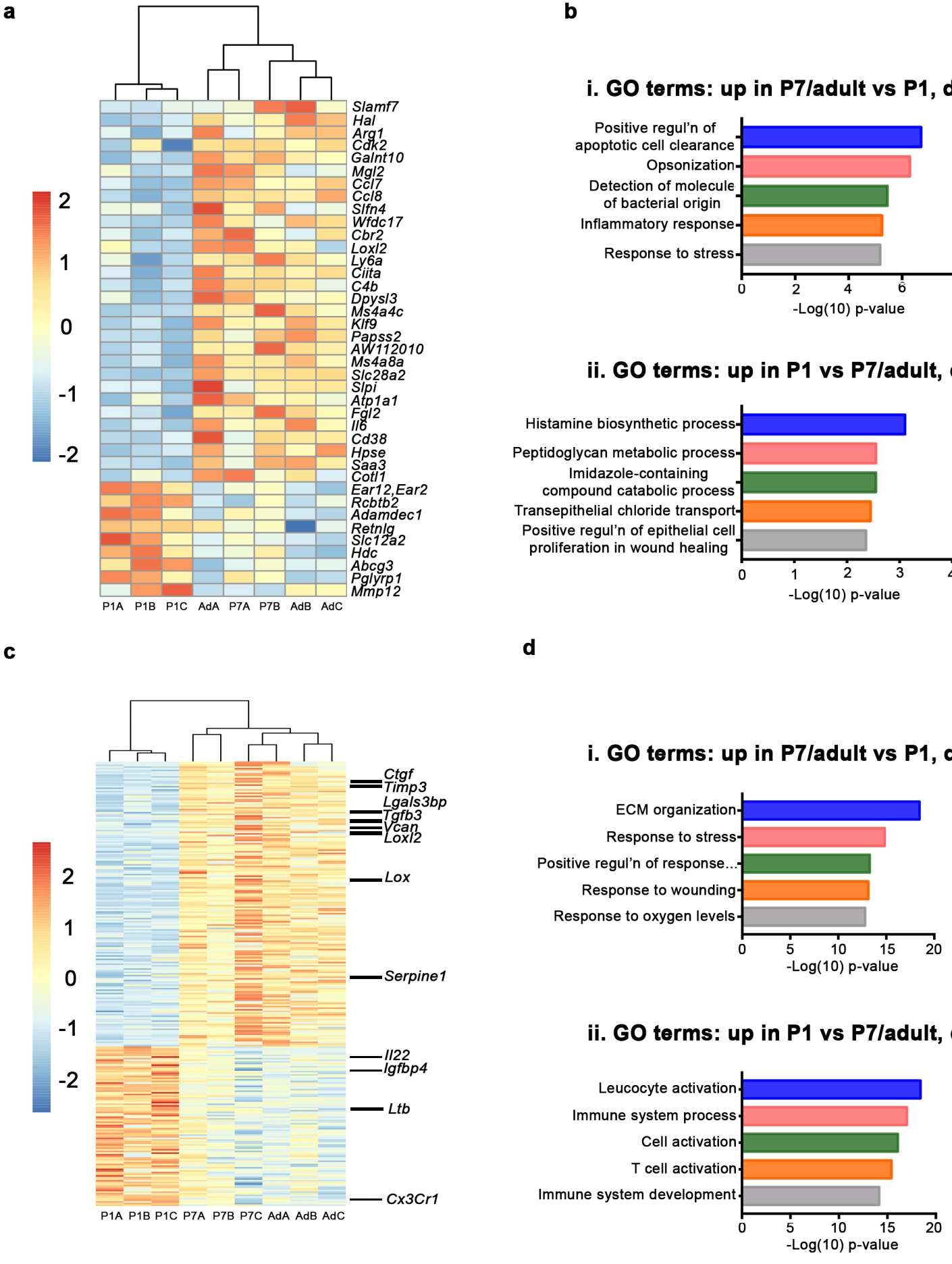

a
Slamf7
Hal
Arg1
Cdk2
Galnt10
Mgl2
Ccl7
Ccl8
Slfn4
Wfdc17
Cbr2
Loxl2
Ly6a
Ciita
C4b
Dpysl3
Ms4a4c
Klf9
Papss2
AW112010
Ms4a8a
Slc28a2
Slpi
Atp1a1
Fgl2
Il6
Cd38
Hpse
Saa3
Cotl1
Ear12,Ear2
Rcbtb2
Adamdec1
Retnlg
Slc12a2
Hdc
Abcg3
Pglyrp1
Mmp12
2
1
0
-1
-2
P1A P1B P1C AdA P7A P7B AdB AdC
b
i. GO terms: up in P7/adult vs P1, day 4
Positive regul'n of apoptotic cell clearance
Opsonization
Detection of molecule of bacterial origin
Inflammatory response
Response to stress
0 2 4 6 8
-Log(10) p-value
ii. GO terms: up in P1 vs P7/adult, day 4
Histamine biosynthetic process
Peptidoglycan metabolic process
Imidazole-containing compound catabolic process
Transepithelial chloride transport
Positive regul'n of epithelial cell proliferation in wound healing
0 1 2 3 4
-Log(10) p-value
c
Ctgf
Timp3
Lgals3bp
Tgfb3
Vcan
Loxl2
Lox
Serpine1
Il22
Igfbp4
Ltb
Cx3Cr1
2
1
0
-1
-2
P1A P1B P1C P7A P7B P7C AdA AdB AdC
d
i. GO terms: up in P7/adult vs P1, day 7
ECM organization
Response to stress
Positive regul'n of response...
Response to wounding
Response to oxygen levels
0 5 10 15 20
-Log(10) p-value
ii. GO terms: up in P1 vs P7/adult, day 7
Leucocyte activation
Immune system process
Cell activation
T cell activation
Immune system development
0 5 10 15 20
-Log(10) p-value

Figure 5.6 Myocardial repair by regeneration and scar formation is associated with differential macrophage gene expression (a) Heatmap showing semi-hierarchical clustering of differentially expressed transcripts between regenerative (P1) and scar-forming (P7 and adult, Ad) mouse models at day 4 post-MI. Red - high expression. Yellow - medium expression. Blue - low expression. Gene names are shown. (b) Gene ontology (GO) terms associated with differentially expressed genes in the P7 and adult mouse (vs P1) at day 4 post-MI (i), and GO terms associated with differentially expressed genes in the P1 mouse (vs P7/adult) at day 4 post-MI (ii). (c) Heatmap showing semi-hierarchical clustering of differentially expressed transcripts between regenerative (P1) and scar-forming (P7 and adult, Ad) mouse models at day 7 post-MI. Red - high expression. Yellow - medium expression. Blue - low expression. Selected genes are highlighted. (d) GO terms associated with differentially expressed genes in the P7 and adult mouse (vs P1) at day 7 post-MI (i), and GO terms associated with differentially expressed genes in the P1 mouse (vs P7/adult) at day 7 post-MI (ii).

5.2.7 Macrophage gene expression is dynamically regulated after MI

MI results in a dynamic environment of injury and repair, in which macrophages undergo a shift from a pro-inflammatory to a reparative phenotype.(232) To identify key macrophage genes underlying inflammation and repair in the adult mammalian mouse heart, unbiased clustering was performed to identify significant distinct temporal profiles across time, using the previously reported Short Time-series Expression Miner (STEM) clustering algorithm, with baseline used as a pseudo-time point zero.(233) The STEM algorithm first identifies a number of candidate temporal profiles independently of the input data, based on the number of time points and thresholds for a gene expression value to be defined as remaining stable, increasing or decreasing between each time point. Each gene in the dataset is then assigned to the model profile to which its time series most closely matches, according to a minimum correlation coefficient. The number of genes *expected* to be assigned to any given profile is then estimated by randomly permutating the original time point values, renormalising the gene's expression values, and then assigning genes to their most closely matching model profile, and repeating across a large number of permutations.(233) Statistical significance is defined as a function of the observed versus expected number of genes. Enriched gene ontology (GO) terms for each temporal profile were identified through STEM.

From adult mouse macrophages, with four time points, STEM clustering identified five statistically significant profiles (Figure 5.7a). These clusters had distinct expression profiles peaking at different phases of myocardial injury and repair (Figure 5.7a). At 24 hours, macrophages activated a cluster of 1086 genes associated with metabolism, the cellular stress response, and the inflammatory response (Figure 5.7a,i, e.g. *Il1b, Il6, Nos2*). At day 4, a cluster of 822 genes was

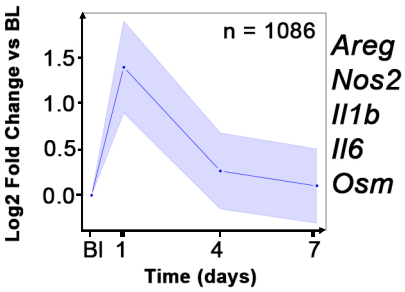
upregulated, linked to the GO term for the cell cycle, suggesting that macrophages in the infarcted heart may undergo a proliferative wave after infiltration (Figure 5.7a,ii, e.g. *Apoe, Trem2*). At day 7 a cluster of 1264 genes was upregulated, comprising soluble mediators and growth factors, associated with the GO terms for proteinaceous ECM (Figure 5.7a,iii, e.g. *Mmp16*). Two clusters identified macrophage genes which were downregulated through the time course post-MI (Figure 5.7a,iv, e.g. *Irf4*, linked to the GO terms for regulation of response to stimulus and cell adhesion, and Figure 5.7b,v, e.g. *Alox8*, linked to the GO terms for response to interferon-beta). Example genes with defined roles in sterile inflammation and repair from each cluster are shown.

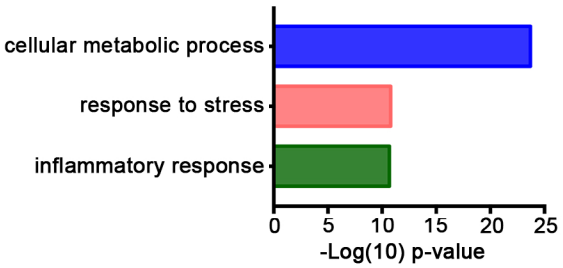
Ablation of macrophages in the P1 heart has been reported to block regeneration, suggesting they are a source of pro-regenerative signalling factors.(101) Temporal clustering of genes was performed on P1 macrophages to identify potential pro-regenerative soluble mediators in the wound healing phase (day 4 – 7). This identified six significant gene clusters with distinct temporal profiles (Figure 5.7b). This approach identified multiple soluble factors with reported mitogenic, pro-survival and angiogenic functions which were upregulated or transiently upregulated following MI (Figure 5.7b,i-v). These included factors from the WNT, BMP and C-X-C motif ligand families, such as *Wnt5a*, previously implicated as a key mediator of intestinal regeneration(234), and *Bmp2*, previously demonstrated to drive neonatal digit regeneration after amputation.(235) GO terms associated with upregulated P1 macrophage gene sets included regulation of epithelial cell proliferation and positive regulation of endothelial cell proliferation (Figure 5.7b, i), also suggesting a pro-regenerative and pro-angiogenic role. Furthermore, genes downregulated by P1 macrophages during regeneration were also identified (Figure 5.7b,vi), which linked to the GO term for complement activation.

Figure 5.7

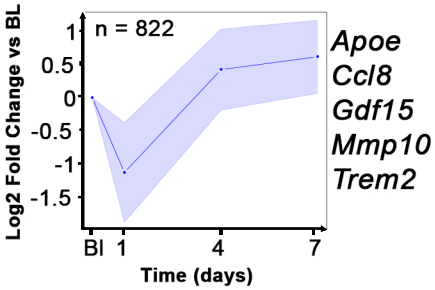
a

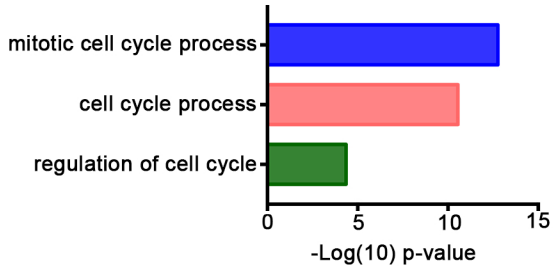
i



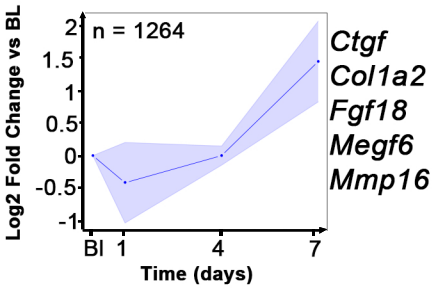


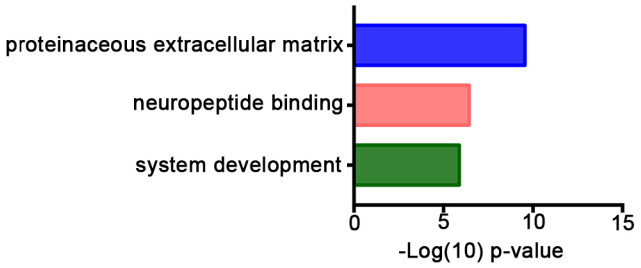
ii



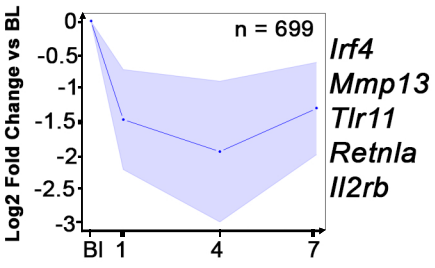


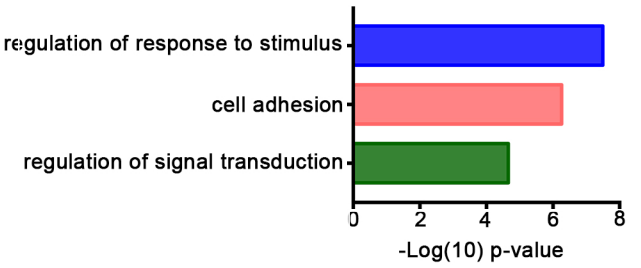
iii



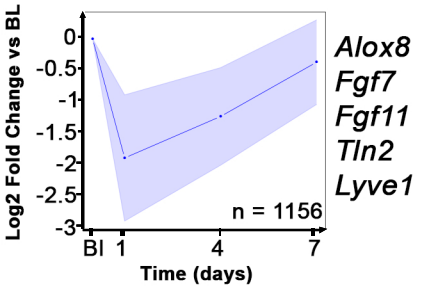


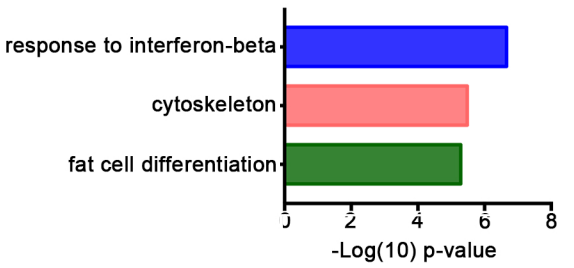
iv





v





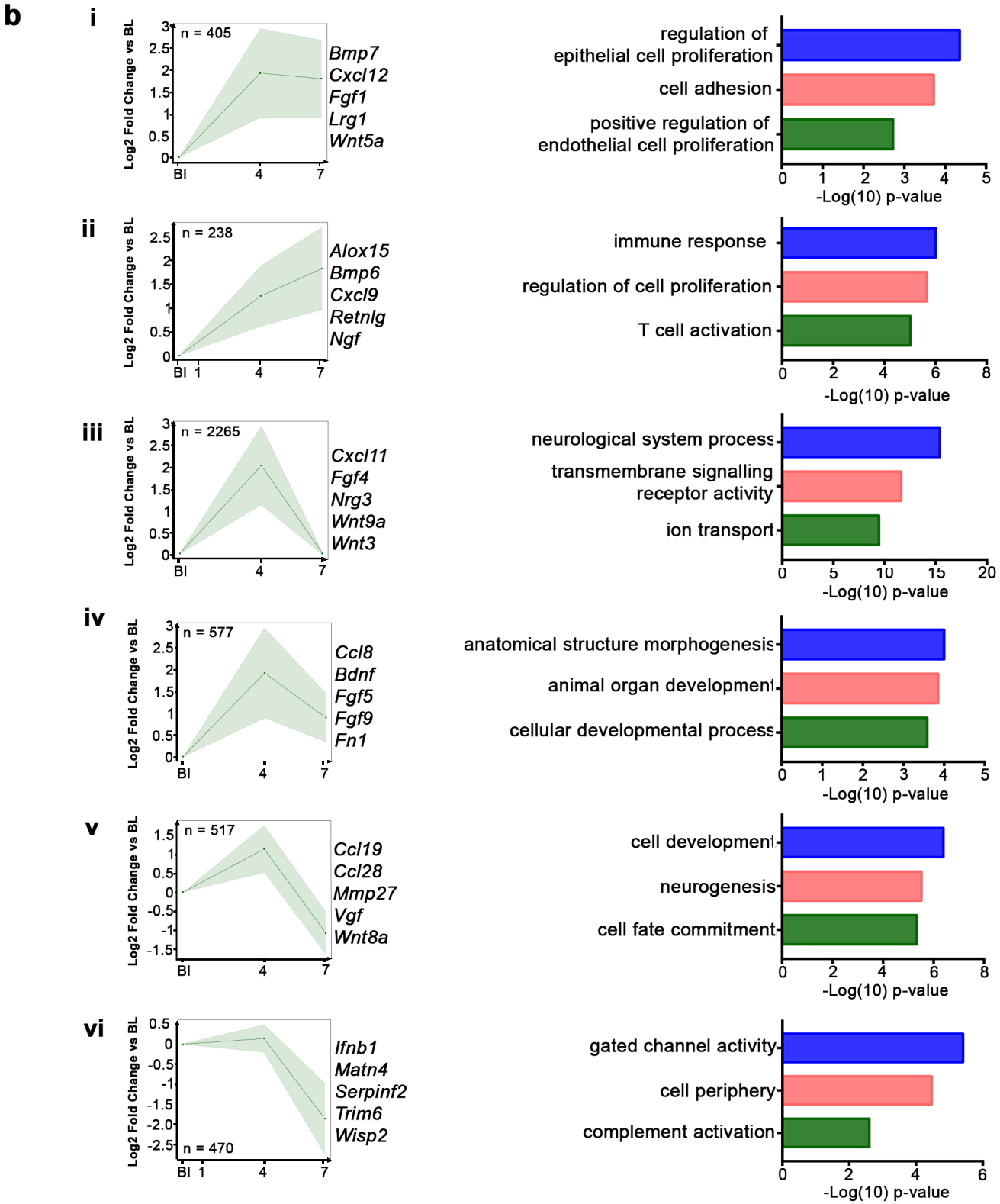


Figure 5.7 Macrophage gene expression is dynamically regulated after MI
(a) Unbiased temporal clustering demonstrating dynamically regulated gene sets in macrophages across the phases of scar-based wound healing in the adult mouse heart post-MI. Significant profiles from the inflammatory (i), transition (ii) and reparative (iii) phases of wound repair are shown. Further gene sets which are downregulated after MI (iv, v) are also shown. n = number of genes within set. Selected genes highlighted. Enriched gene ontology (GO) terms for each gene set are shown to the right (b) Unbiased temporal clustering demonstrating dynamically regulated gene sets in macrophages across the time period of regenerative healing in the P1 neonatal mouse heart post-MI. Significant profiles of gene sets upregulated (i,ii) or transiently upregulated (iii, iv, v) in regeneration are shown. A gene set which is downregulated in regenerative repair is shown in vi. n = number of genes within set. Selected genes are highlighted. Enriched gene ontology (GO) terms for each gene set are shown to the right

5.2.8 Macrophages in the scar-forming heart upregulate extracellular matrix pathways

I hypothesised that genes and pathways which move divergently over time between regenerative (P1) and scar-forming (P7) stages might be most relevant to differential tissue repair. To identify these, all temporal profiles from P1 macrophages were plotted against all temporal profiles in the P7 macrophages (Figure 5.8a). Genes found in divergently moving profiles, i.e. initially upward in P1 and downward in P7, or vice versa, were then identified. This approach showed that genes differentially upregulated in the P7 mouse were primarily associated with the GO term of ECM organization (Figure 5.8b,), while genes differentially upregulated in the P1 mouse were associated with GO terms for nucleosome assembly and positive regulation of IFN-gamma production (Figure 5.8b,ii). This analysis further supports the concept that distinct macrophage programmes may contribute to divergent modes of tissue healing.

Expression of ECM and ECM-related genes in P1 and P7 macrophages were then directly compared (Figure 5.8c) These genes were identified as those expressed by adult macrophages in the proliferative phase of healing (temporal profile Figure 5.7a, iii) which also linked to the GO term Proteinaceous Extracellular Matrix. This analysis showed that scar-formation in the P7 is associated with differential upregulation of multiple ECM genes including *Col8a1*, *Col5a2*, *Col6a2*, *Fbn1, Postn,* and *Bgn*, as well as upregulation of the major fibrillar collagen mRNA isoforms *Col1a1, Col1a2, Col3a1*.

Figure 5.8

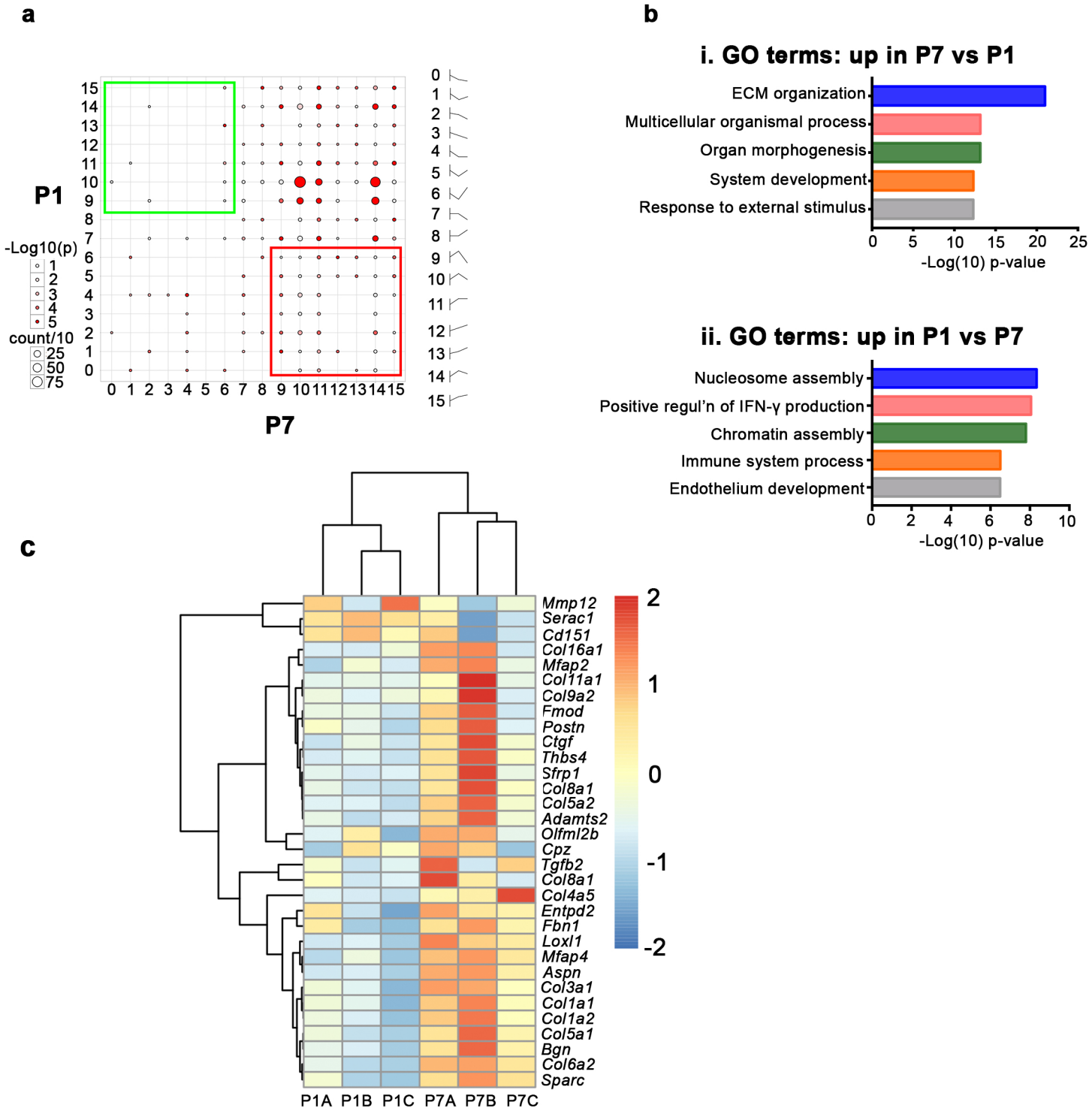


Figure 5.8 Macrophages in the scar-forming heart upregulate extracellular matrix pathways
(a) Heatmap showing size of gene overlap (circle size) and statistical significance (colour) between all macrophage temporal profiles in the P1-regenerating and P7-scar forming mouse heart. Profile shape is shown in the legend. Discordantly moving genes are highlighted in green (initially upwardly expressed in P1, downwardly expressed in P7) and red (initially upwardly expressed in P7, downwardly expressed in P1). (b) GO terms associated with divergently upregulated genes over time in macrophages in the P7 mouse heart (vs P1; i) and in the P1 mouse heart (vs P7; ii). (c) Heatmap showing expression of ECM components in the regenerating P1 and scar-forming P7 mouse at day 7. ECM genes for comparison were identified from as those expressed by adult mouse macrophages during the reparative phase of post-MI (temporal profile Fig 5.7a,iii) which also linked to the Gene Ontology term Proteinaceous Extracellular Matrix.

5.3 Discussion

5.3.1 The neonatal and adult immune response to injury

The data presented in this chapter demonstrate that the immune response to MI in the neonate is quantitatively distinct to the adult. Specifically, MI in the P1/P7 was associated with significantly fewer CD45+ leucocytes, CD45+ CD11b+ myeloid cells, CD45+ CD11b+ Ly6G+ neutrophils, CD45+ CD11b+ Ly6G- F4/80+ macrophages and distinct CD45+ CD11b+ Ly6G- F4/80- Ly6C+ monocyte kinetics compared to the adult. These findings are in keeping with previous studies which have suggested a dampened immune response in the neonatal period, which is also associated with susceptibility to infectious organisms.(236)

Several studies have demonstrated that the immune response to skin wounding in the fetus is distinct to the adult response, with fetal skin wounds leading to minimal inflammatory cell infiltration.(237-239) Driving inflammation in fetal rabbit wound by inoculating wound site with bacteria results leads to increased numbers of macrophages, neutrophils, and downstream healing by collagen deposition and scar formation.(240) Conversely, Smad3-null mice, which are unable to transduce signals from TGF-β, show reduced numbers of monocytes and accelerated wound re-epithelialisation.(241) These data suggest that a relative ‘lack’ of immune response, may be important or permissive to scarless wound healing.

While neonates have long been thought of as immunodeficient, in keeping with an immature immune response, recent data suggest that the immune system may be actively suppressed. In the neonatal intestine, there is active suppression of CD4+ lymphocytes is mediated by T-regulatory cells.(242) Furthermore, a recently identified population of CD71+ erythryoid lineage cells in the neonatal mouse spleen

(and human umbilical cord) have immunosuppressive properties and limit inflammation during commensal colonisation after birth.(243)

The neonatal and adult immune response to MI has not previously been compared. However, in a previous analysis of the immune response to MI in P1 and P14 mice, Aurora *et al* reported differences in these two neonatal models. Specifically, in P1 mice there was a marginal increase in mononuclear phagocytes (CD11b+ Ly6G-) and macrophages at day 7, increased numbers of $Ly6C^{hi}$ monocytes at baseline and day 1, and reduced numbers of $Ly6C^{lo}$ monocytes at P1. In contrast, the data presented in this chapter – which demonstrates no quantitatively significant difference between P1 and P7 cellular immune response – suggest that neonatal 'immune dampening' may be permissive but is not sufficient to induce regeneration following MI.

5.3.2 Macrophages roles in regenerative versus scar-based healing

In this chapter, RNA sequencing of macrophages was undertaken to explore the functional roles of macrophages following MI. The analyses of RNA sequencing presented indicate that macrophages have distinct transcriptional profiles at baseline and after MI in the P1, P7 and and adult heart. Despite the apparent similarity in terms of wound healing by scar formation in both the P7 neonate and adult, the macrophage transcriptional profile was distinct, with the P7 macrophage transcriptome being an intermediate state between P1 and adult by principal component analysis. The differences in macrophage transcriptome were primarily explored with reference to the wound healing phenotype: regeneration and scar formation. By identifying significant differences in macrophage gene expression from the P1 heart in comparison to the P7/adult, distinct gene sets and biological

pathways were identified which might underlie, or contribute to, the observed difference in wound healing.

P1 macrophages at day 7 were found to differentially upregulate several mediators which have previously been implicated in regeneration or healing. These included *Il22*, which has recently been associated with regeneration of intestinal epithelium(244) and pancreatic beta-cells.(245) *Igfbp4* has previously reported as a cardiogenic growth factor which promotes cardiomyocyte differentiation during development.(246) *Ltb* has been associated with mucosal wound healing via IL-23.(247) In contrast, P7 macrophages at day 7 upregulated canonical mediators of fibrosis, including *Lox* and *Loxl2*, which have previously been reported to be associated with cross-linking and stabilisation of collagen fibrils in scar deposition.(248)

Pathway analysis of divergent temporal profiles highlighted a potential role for IFN-gamma in P1 macrophages. Interestingly, IFN-gamma has previously been shown to be required for effective muscle regeneration by activating proliferation of muscle fibres.(249) In P7 macrophages, pathway analysis identified ECM components associated with scar formation. These findings demonstrate differential macrophage function during healing by heart regeneration and scar formation, and support the concept that macrophages may be a determinant of the mode of tissue repair.

5.3.3 Dynamics of macrophage function after myocardial infarction

The data presented in this chapter show the results of unbiased temporal clustering of the macrophage transcriptome at key time points following MI. This approach uncovered co-regulated macrophage gene sets which are differentially expressed over time, which correspond to key phases of wound healing. In the adult mouse

heart following MI, at 24 hours macrophages expressed genes primarily associated with cell stress and inflammatory cytokine signalling. At day 4, macrophages activated pathways required for activation of the cell cycle and proliferation, suggesting they may proliferate in the heart following infiltration. At day 7, genes associated with the formation and remodelling of ECM were activated. These data support the concept of multiple roles which are temporally regulated through the course of MI healing.

Only a small number of previous studies have performed unbiased analyses of the macrophage transcriptome in the context of sterile inflammation.(232, 250) In skeletal muscle injury, microarray profiling of $Ly6C^{+}$ $CX3CR1^{lo}$ and $Ly6C^{-}$ $CX3CR1^{hi}$ macrophage subsets was recently reported.(232) Consistent with the data presented in this chapter, the macrophage transcriptome was found to be highly dynamic, with time following injury being the major determinant of macrophage transcriptional response. In support of a role for macrophages in organisation of the ECM, as described in this chapter, the $Ly6C^{-}$ macrophage subset was found to be characterised by production of matrix molecules.(232)

One limitation of the bulk-RNA sequencing approach used in this chapter is that it does not provide information on the heterogeneity of macrophages at a given time point. For example, it has been demonstrated that macrophages derived from the embryonic yolk sac respond differently to monocyte-derived macrophages(102), which cannot be explored. In addition, it is unclear to what extent a given macrophage progresses through multiple different transcriptional states, or whether early macrophages are replaced by subsequent macrophages which progresses directly to reparative stages.

5.4 Conclusions

The experiments presented in this chapter analyse the numbers and roles of macrophages in the neonatal and adult heart following experimental MI. There are several key findings. First, that there are quantitative differences in the immune response to MI between the neonate and adult. Second, as defined by RNA sequencing, the macrophage transcriptome is distinct in the P1 neonate, P7 neonate and adult both at baseline, and during wound repair following MI. Third, candidate mediators of divergent healing are identified, with critical differences relating to production of regenerative cues in the P1 and profibrotic mediators in the P7/adult.

Chapter 6: Macrophages in scar formation following myocardial infarction

To be alive at all is to have scars

John Steinbeck, The Winter of our Discontent

6.1 Background

The transcriptional analyses presented in Chapter 5 indicate that a key difference between macrophages in the regenerating (P1) and scar-forming (P7/adult) heart is in regulation of pathways related to the ECM. In the context of scar formation, macrophages were found to upregulate canonical soluble mediators of tissue fibrosis and ECM components, suggesting both an indirect and cell-autonomous contribution to fibrosis. The experiments presented in this chapter were designed to validate this finding and interrogate the roles of macrophages in scar formation following MI.

6.1.1 Mechanisms of scar formation following MI

Formation of scar involves the production, extracellular deposition, and remodelling of collagen.(251) Collagen fibrils consist of a long, triple-stranded helix in which 3 α-chains wind around each other to form a superhelix. In vertebrates at least 28 collagen subtypes have been identified, encoded by 42 genes, however the primary 'fibrillar' collagens which contribute to scar are collagen type I and collagen type III.(251) Assembly of collagen scar involves intracellular synthesis of collagen pro-α chains, which undergo a sequence of post-translational modifications including hydroxylation and glycosylation. Pro-collagen fibrils are assembled into triple helices and then secreted into the extracellular space. This process is catalysed by prolyl-4-hydroxylase, an enzyme which adds proline onto pro-collagen α-monomers to produce stable protocollagen molecules.(251)

Following MI, collagen mRNA synthesis begins rapidly. In the rat, type III pro-collagen mRNA has been shown to be upregulated by day 2 post-MI.(252) Type I pro-collagen mRNA was upregulated by day 4, and remained elevated at 90-days post-MI. Ongoing remodelling of scar continues over several weeks, such that by 6

weeks post-MI, the majority of LV scar is composed of type I collagen.(253) Properties of the scar are influenced by the precise collagen type and content, fibre diameter, orientation and degree of cross-linking. Failure to upregulate and deposit collagen effectively jeopardises the structural integrity of the heart following MI. In a mouse model of procollagen-α2 deficiency (analogous to human osteogenesis imperfecta), healing following MI is impaired with increased incidence of ventricular rupture.(254)

The cellular source of collagen protein in the post-MI heart is the myofibroblast. Myofibroblasts predominate in the proliferative phase of healing, and are defined at the cellular level by expression of α-smooth muscle actin and production of collagen proteins.(255) Myofibroblasts were first identified in skin wound granulation tissue, as spindle-shaped cells containing ultrastructurally prominent microfilment bundles.(256) Multiple sources of myofibroblasts have been described in the literature, with reported contributions from resident cardiac fibroblasts, epithelium (via epithelial-to-mesenchymal transition), endothelial cells (via endothelial to mesenchymal transition), pericytes, smooth muscle cells, mesenchymal stem cells and fibrocytes (fibroblast progenitor cells derived from bone marrow).(257) Recently, the majority of myofibroblasts have been reported to arise from resident (Tcf21+) cardiac fibroblasts.(258)

6.1.2 Linking inflammation to scar formation

Inflammation is intricately linked to fibrosis, and strategies targeting the immune response lead to changes in scar formation.(221, 259-261) This link between inflammation and fibrosis is mediated, at least in part, by macrophage-myofibroblast communication. The infiltration of macrophages (particularly those derived from $CX3CR1^{+}$ monocytes) triggers recruitment of fibroblasts to wound site.(262) In

addition, macrophage-derived cytokines such TNF-α, IL-1 and IGF-1 drives proliferation and activation of fibroblasts into collagen-producing myofibroblasts.(263) In addition, arginase expression by macrophages supports scar formation by production of glutamate and L-proline, both of which are required for collagen synthesis.(264) Macrophages also direct collagen stabilisation: in injured skin, interleukin-4 receptor α (IL-4Rα)-activation in macrophages leads to upregulation of Relm-α, resulting in lysyl hydroxylase 2-mediated collagen cross-linking and stabilisation by fibroblasts.(265) Knockdown of macrophages in injured skin and myocardium results in alterations to myofibroblast function: ablation of macrophages in excisional skin wounds resulted in reduced transcription of *Col1a2*.(266) Similarly, targeted ablation of M2 macrophages in the post-MI heart using *Trib1*$^{-/-}$ mice led to impaired fibroblast activation due to reduced levels of Il-1α and osteopontin, failure of collagen fibril formation and an increased incidence of ventricular rupture.(221)

6.1.3 Aims

This chapter addresses the following aims:

1. To validate differential expression of pro-fibrotic signals by macrophages in the regenerating versus scar-forming heart.
2. To investigate a potential role for macrophages in cell-autonomous contribution to scar by production of collagen proteins.
3. To investigate the role of macrophage ontogeny as a determinant of scar formation in the heart post-MI.

6.2 Results

6.2.1 Scar formation in the late neonatal mouse MI model

The mechanisms by which scar formation occurs in the neonatal mouse model have not been studied. To investigate deposition of collagen scar in the P1 and P7 mouse, samples were harvested at day 7 post-MI. Hearts were removed by blunt dissection and then either processed for RNA extraction, cDNA synthesis and qPCR analysis of fibrillar collagen expression, or fixed in PFA, embedded and cryosectioned for immunofluorescence staining. Sections were immunofluorescence stained for collagen I, and CD68 to visualise macrophages. Imaging was performed by confocal microscopy.

At day 7 post-MI, organised fibrils of collagen I were laid down in the infarct region in the P7 mouse (Figure 6.1a). In contrast, day 7 in the P1 mouse, collagen I was present in the injury site but remained sporadic and disorganised (Figure 6.1a). As expected, deposition of collagen fibrils in the P7 mouse was associated with upregulation of RNA encoding the fibrillar collagens *Col1a1*, *Col1a2* and *Col3a1* at day 7 post-MI (Figure 6.1b). During scarring in the P7 heart, CD68+ macrophages were frequently observed in close proximity to deposited collagen I fibres (Figure 6.1c), suggesting a functional interaction.

Figure 6.1

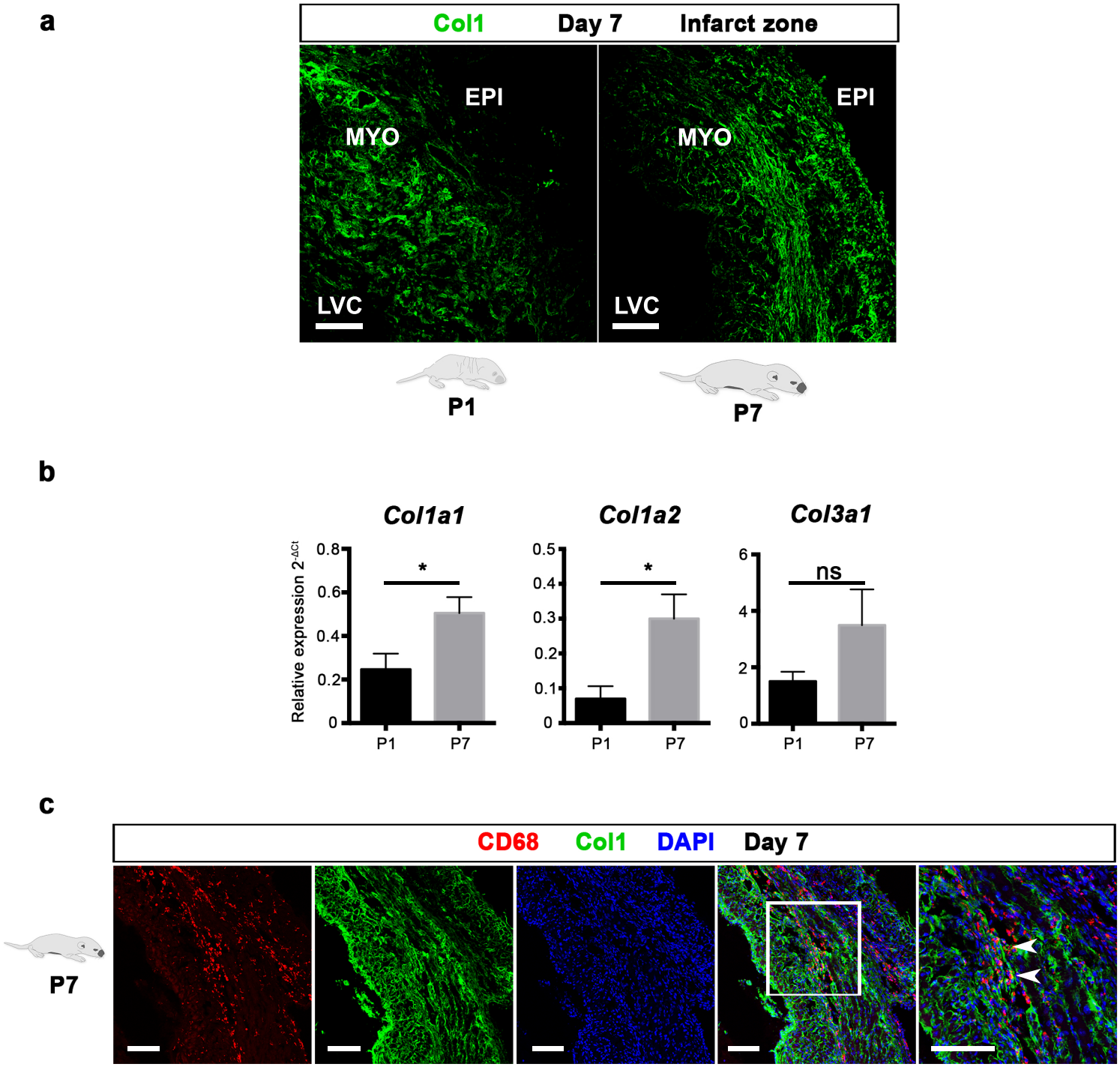


Figure 6.1 Organised fibrillar collagen deposition characterises scar formation in the P7 neonatal mouse (a) Confocal imaging of immunofluorescence-stained heart cryosections at day 7 post-MI from P1 and P7 mice, demonstrating disorganised expression of collagen I (green) across the injury site in the anterior left ventricular wall in the P1 mouse, in contrast to organised, fibrillar collagen I deposition in the P7 mouse (representative of n = 3 per group, scale bar = 100 μm). (b) qPCR showing upregulation of fibrillar collagen genes Col1a1, Col1a2, Col3a1 in whole heart samples from the P7 mouse compared to the P1 at day 7 post-MI. (c) Confocal imaging of immunofluorescence-stained heart cryosections at day 7 post-MI from P7 mice, showing CD68+ macrophages (red) in close colocalisation with collagen I (Col1, green) fibrils in the process of scar formation (representative of n = 3, scale bar = 100 μm). Abbreviations: Epi epcardium, Myo myocardium, LVC left ventricular cavity

6.2.2 Macrophages differentially express pro-fibrotic mediators in the regenerating and scar-forming heart

Transcriptional profiling of macrophages suggested that a key difference between macrophages in the scar forming P7/adult heart in comparison to the P1 regenerative setting is the expression of canonical profibrotic mediators such as *Lox, Loxl2, Tgfb3, Serpine1* and *Ctgf*. These soluble factors are known to drive fibroblast activation to myofibroblasts and promote scar formation.

To investigate expression of CTGF in the P1 and P7 mouse, samples were harvested at day 7 post-MI, corresponding to upregulation of fibrotic mediators in the RNAseq dataset. Hearts were removed by blunt dissection, fixed in PFA, embedded in OCT and cryosectioned. Heart sections were immunofluorescence stained for CD68 to visualise macrophages, and for CTGF. Imaging was performed by confocal microscopy.

In the P7 mouse, at day 7 post-MI CD68+ macrophages in the infarct zone frequently stained positive for CTGF (Figure 6.2a). In contrast, in the P1 mouse at day 7 post-MI, CD68+ macrophages in the infarct zone did not express CTGF (Figure 6.2a). This finding suggests that macrophages differentially express pro-fibrotic mediators in the context of regeneration and scar formation. Given the known roles of CTGF in driving fibrosis, activation of a CTGF+ pro-fibrotic macrophage phenotype may direct the mode of tissue repair away from regeneration towards scar formation.

Figure 6.2

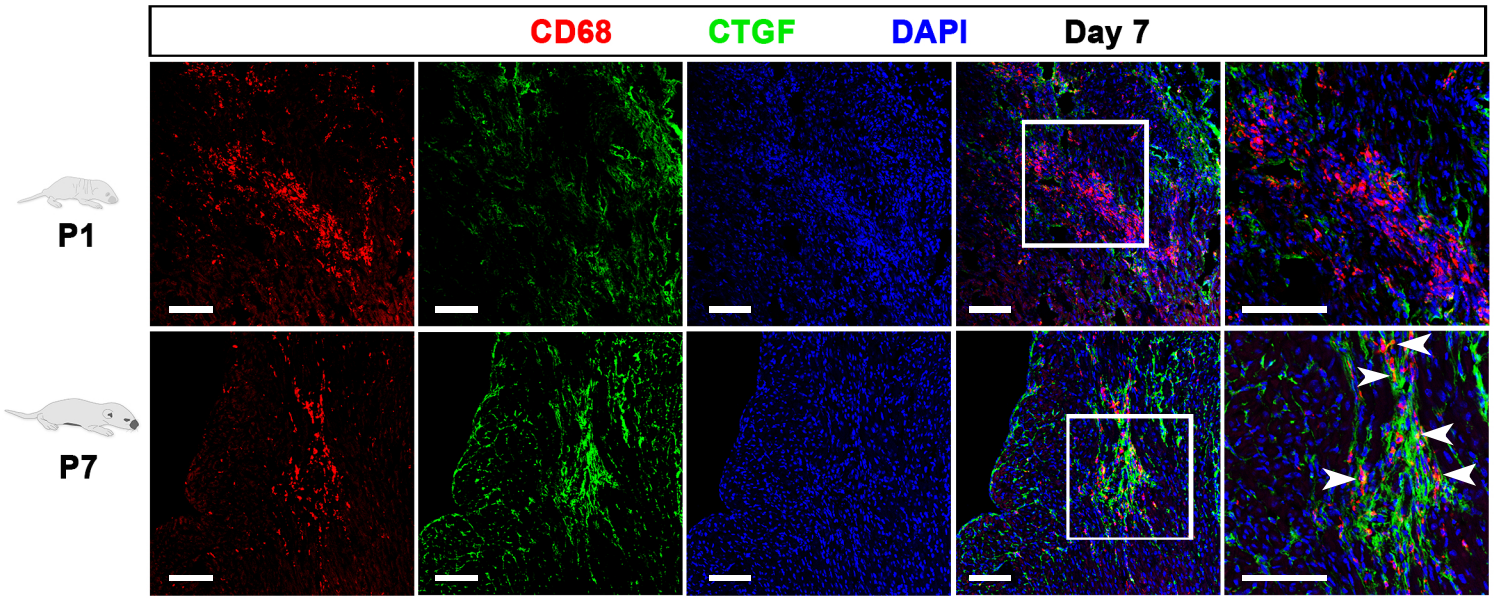


Figure 6.2 Macrophages differentially express CTGF in the P1 and P7 hearts following MI
Confocal imaging of immunofluorescence-stained heart cryosections at day 7 post-MI from P1 and P7 mice, showing CD68+ macrophages (red) and Connective Tissue Growth Factor (CTGF; green), a soluble pro-fibrotic mediator driving activation of myofibroblasts. As suggested by transcriptional profiling of macrophages in regeneration and scar formation, CTGF is expressed widely by macrophages in the infarct zone of the P7 scar-forming heart, but minimally by macrophages in the P1 (representative of n = 3 per group, scale bar = 100 μm).

6.2.3 Macrophages express collagen proteins

Transcriptional analysis of macrophages demonstrated dynamic upregulation of genes encoding fibrillar collagens *Col1a1*, *Col1a2* and *Col1a3* at day 7 post-MI in the scar-forming P7 heart (Figure 6.1a). Macrophages have not previously been reported to express collagens in the heart post-MI, a role thought to be exclusively undertaken by myofibroblasts.

To investigate whether macrophages expressed collagen in the heart, the *Col1a2*-CreERT mouse line was crossed with female R26R-EYFP reporter mice. Subsequent *Col1a2*-CreERT; R26R-EYFP offspring underwent MI surgery at P7 (Figure 6.1b). To activate Cre recombinase, mice were injected with tamoxifen at day 5 post-MI (an early profibrotic time point) and harvested at day 7. Hearts were removed by dissection, fixed, embedded in OCT and sectioned. Macrophages were identified by staining for CD68, and potential expression of EYFP was enhanced by antibody staining for GFP.

At day 7 post-MI, EYFP+ cells were seen throughout the infarct zone. Of these, a small number also stained positive for CD68+, suggesting that a subset of *Col1a2*-CreERT;R26-EYFP+ cells were macrophages (Figure 6.3c). This finding suggests that CD68+ macrophages can produce collagen autonomously, and may therefore contribute to P7 scar formation by production of collagens in addition to release of soluble pro-fibrotic signalling cues.

Figure 6.3

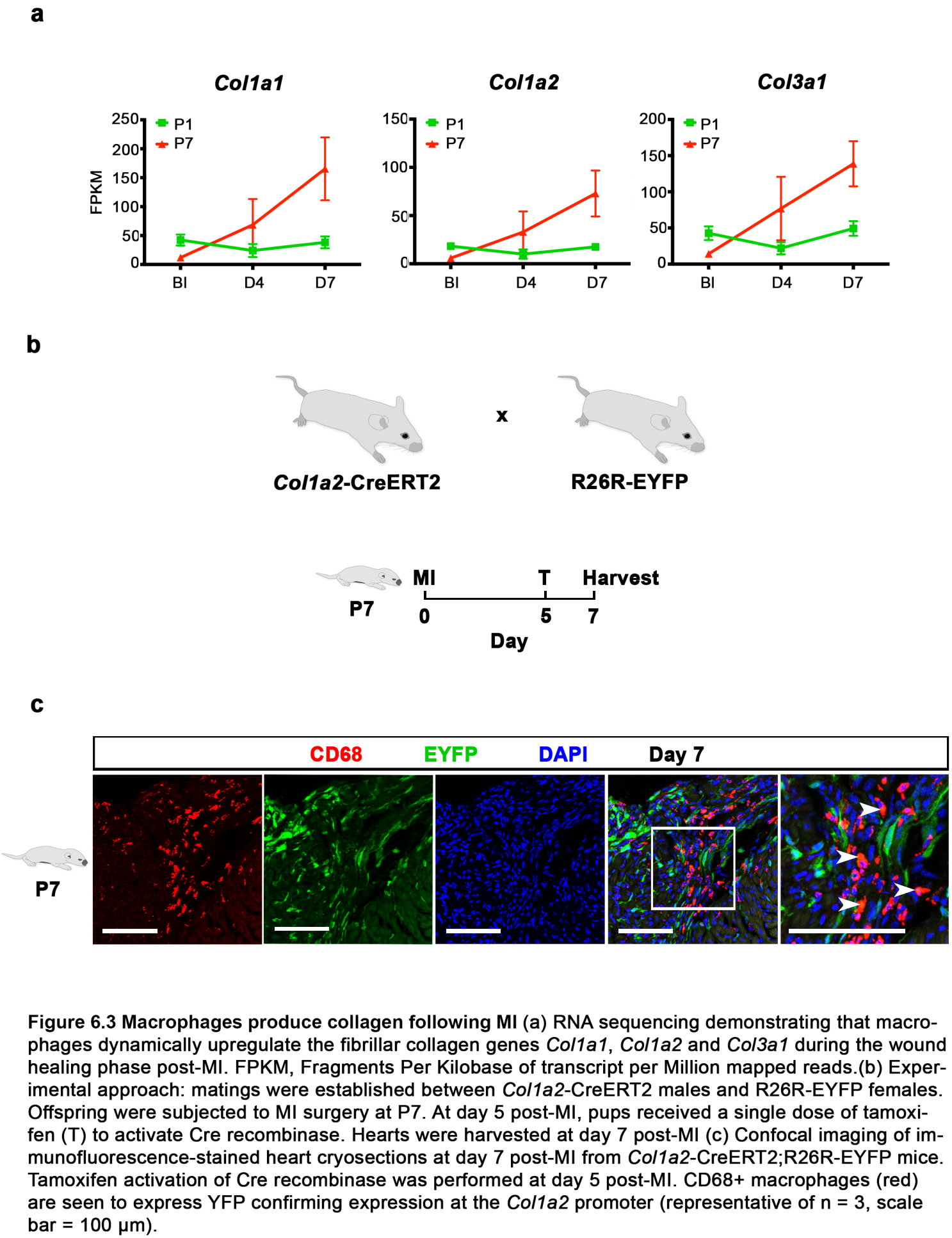


Figure 6.3 Macrophages produce collagen following MI (a) RNA sequencing demonstrating that macrophages dynamically upregulate the fibrillar collagen genes *Col1a1*, *Col1a2* and *Col3a1* during the wound healing phase post-MI. FPKM, Fragments Per Kilobase of transcript per Million mapped reads.(b) Experimental approach: matings were established between *Col1a2*-CreERT2 males and R26R-EYFP females. Offspring were subjected to MI surgery at P7. At day 5 post-MI, pups received a single dose of tamoxifen (T) to activate Cre recombinase. Hearts were harvested at day 7 post-MI (c) Confocal imaging of immunofluorescence-stained heart cryosections at day 7 post-MI from *Col1a2*-CreERT2;R26R-EYFP mice. Tamoxifen activation of Cre recombinase was performed at day 5 post-MI. CD68+ macrophages (red) are seen to express YFP confirming expression at the *Col1a2* promoter (representative of n = 3, scale bar = 100 μm).

6.2.4 Adult splenic monocytes are sufficient to impede regeneration in the P1 neonatal mouse model

Compared to the adult, the neonatal mouse heart has previously been shown to preserve embryonic tissue-resident macrophages, which promote angiogenesis, in comparison to the adult.(102) This is in keeping with the data presented in Chapter 5, in which the neonatal mouse heart has a relatively dampened immune response to MI. I hypothesised that exogenous addition of adult splenic monocytes would be sufficient to drive inflammation and fibrosis in the P1 injured heart, despite an otherwise regenerative environment. To test this, adoptive transfer of adult splenic monocytes from a CD68-GFP donor into a P1 neonate undergoing MI surgery was performed (Figure 6.4a). Monocytes were isolated using the EasySep^{TM} Mouse Monocyte Enrichment Kit. Adoptive transfer of 50 x 10^3 CD68-GFP+ adult splenic monocytes was performed by intracardiac injection at the time of surgery. P1 hearts were harvested at either day 3, to visualise GFP+ cells in the heart, confirming successful adoptive transfer or day 21, to quantify scar size by histology. Samples were stained by Masson's trichrome with the area of scar then quantified as a proportion of the LV area at at least two levels below the suture.

At day 3 post-MI, donor GFP+ macrophages could be visualised in the infarct zone of the P1 recipient (Figure 6.2b). At 21 days post-MI, P1 hearts which had received adoptively transferred monocytes had significantly larger areas of scar deposition than control (Figure.6.2c & d, scar percentage 3.989 ± 0.743% vs 0.807 ± 0.246%, n = 5 in PBS group, n = 6 in monocyte group, *p=0.0046*), at a time point when P1 hearts have ordinarily regenerated completely.(21) This experiment demonstrated that adult splenic monocytes giving rise to CD68+ macrophages drive irreversible scarring and pro-fibrotic healing, irrespective of the local environment.

Figure 6.4

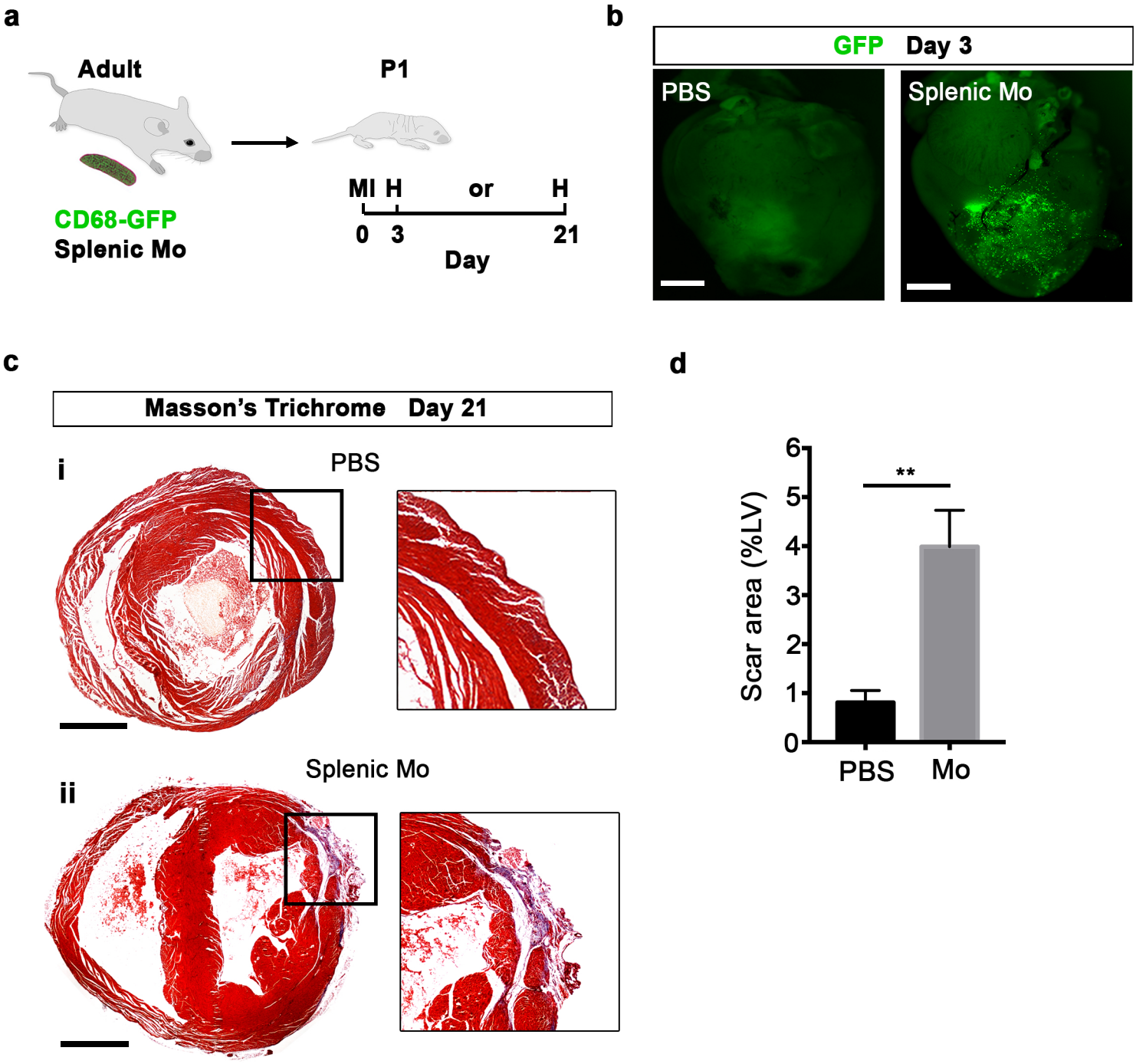


Figure 6.4 Adoptive transfer of adult splenic monocytes to the P1 neonate is sufficient to impede heart regeneration (a) Experimental design for adoptive transfer: monocytes were isolated by magnetic column purification from the spleens of CD68-GFP+ donors. At the time of P1 MI surgery, 50 ± 10 x 10^3 monocytes/PBS, or PBS alone, were transferred to the P1 by intracardiac injection. P1 neonates were then harvested at either day 3 (for imaging) or day 21 (for histology) (b) Fluorescence imaging for GFP demonstrating that at day 3 post-MI, adoptively transferred GFP+ monocytes are visualised in the anterior wall of the recipient P1 (representative of n = 3 per group). Scale bar = 1mm. (c) Masson's trichrome staining of heart sections showing that at day 21 post-MI, P1 neonates which received PBS vehicle showed histological evidence of regeneration (i), while P1 neonates which received adult monocytes had residual scar formation (ii). Scale bar = 1mm. (d) Adoptive transfer of adult monocytes led to a significant increase in scar size at 21 days, as measured as a percentage of the left ventricular area (scar percentage 3.99 ± 0.74% vs 0.81 ± 0.25%, n = 5 in PBS group, n = 6 in monocyte group, $p<0.01$). Abbreviations: Mo monocytes

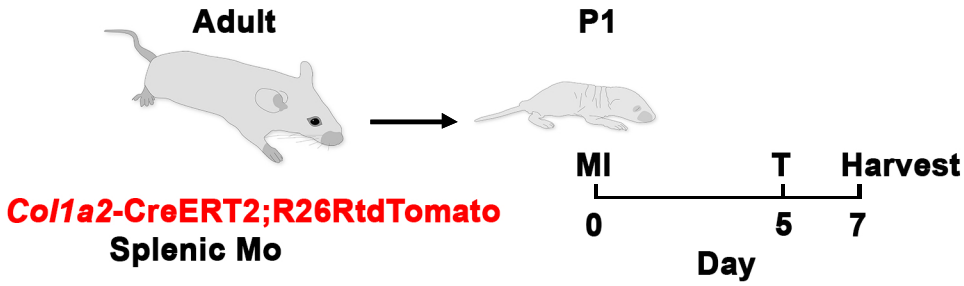
6.2.5 Adult splenic monocyte-derived macrophages produce collagen in the neonatal environment

Next, the mechanism by which adult monocytes drive fibrosis following adoptive transfer into the P1 heart was investigated. I hypothesised that this pro-fibrotic effect may occur in part by cell-autonomous deposition of collagen. To test this, monocytes were isolated from the spleens of adult *Col1a2*-CreERT; R26R-tdTomato reporter mice, and adoptively transferred into P1 recipients undergoing MI. At day 5 post-MI, Cre recombinase was activated by a single dose of tamoxifen (Figure 6.5a), leading to expression of TdTomato in any cells with transcription driven by the *Col1a2* promoter. Pups were culled at day 7 post-MI and hearts were removed by dissection, fixed in PFA, embedded in OCT, sectioned and immunofluorescence stained for F4/80. Imaging was performed by confocal microscopy.

At day 7 post-MI, F4/80+ macrophages could be visualised in the infarct zone of the heart (Figure 6.5b). Furthermore, a small subset of cells also stained positive for TdTomato, confirming that adoptively transferred monocytes had activated the TdTomato reporter and were thus expressing *Col1a2*-CreERT2 (Figure 6.5b). This finding suggests that adult mouse monocytes, which give rise to differentiated macrophages post-MI, can contribute collagen to the scar and that cell-autonomous production of collagen is a component of the pro-fibrotic adult monocyte response. Moreover, the adult donor monocytes appeared to be programmed towards a fibrotic state, irrespective of encountering a pro-regenerative (P1) environment in the host.

Figure 6.5

a



b

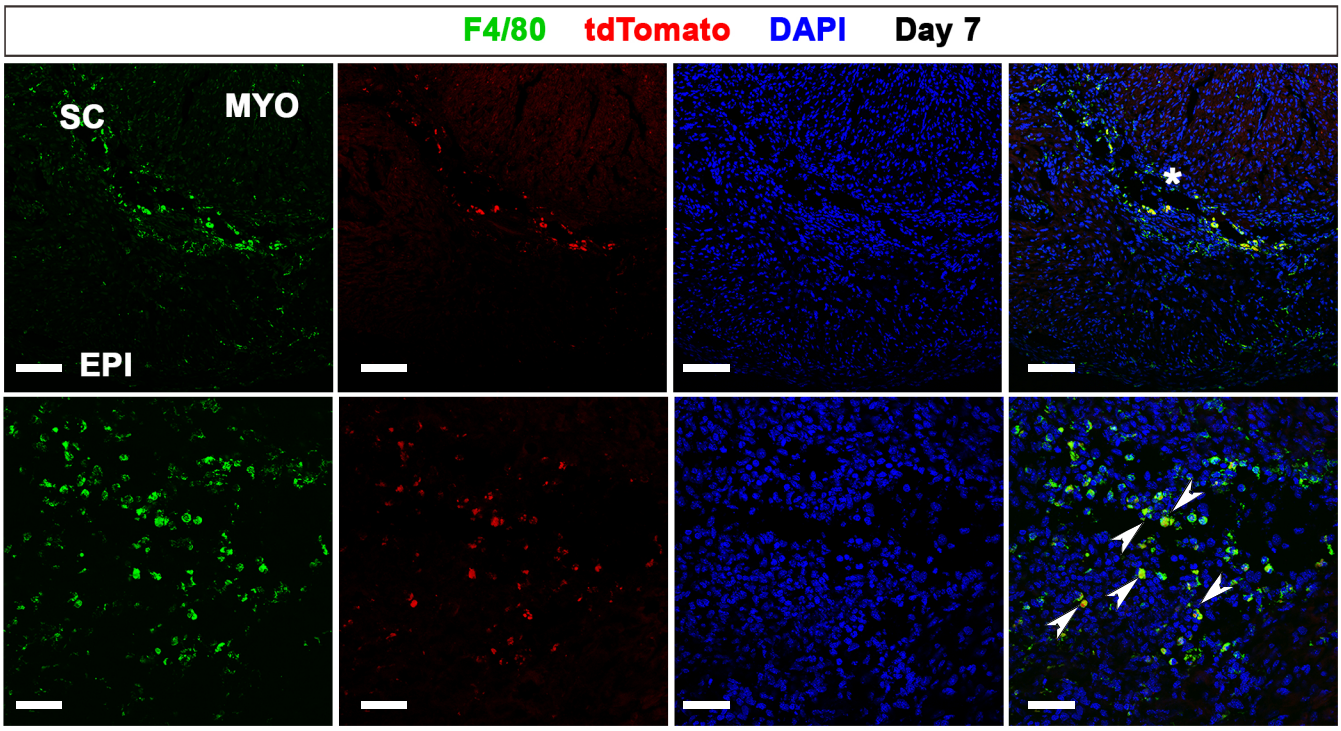


Figure 6.5 Adult splenic-derived macrophages express COL1A2 in the P1 neonatal envinronment to drive scar formation (a) To investigate whether monocytes contribute collagen scar to inhibit fibrosis in the P1 regenerating heart, splenic monocytes were transferred from adult Col1a2-CreERT2;R26RtdTomato mice to P1 recipients undergoing MI. At day 5, the pups were injected with tamoxifen to activate Cre recombinase, and then sacrificed at day 7. (b) Confocal imaging of immunofluorescence-stained heart cryosections to show F4/80+ macrophages (green), tdTomato (red) and DAPI (blue). A subset of F4/80+ macrophages in the infarct zone (white asterisk) were co-labelled by tdTomato, indicating that they had arisen from donor monocytes and had activated the *Col1a2*CreERT2. At higher magnification F4/80+/tdTomato+ cells were observed within the injury site (white arrowheads). ep- epicardium, my- myocardium, sc- scar; scale bar top left panel= 100 μm; bottom left panel 50 μm. Representative of n=3. Abbreviations: EPI epicardium, MYO myocardium, SC scar

6.3 Discussion

6.3.1 Macrophage expression of pro-fibrotic mediators

The data presented in this chapter demonstrate that pro-fibrotic signals are differentially expressed by macrophages in the context of regeneration and scar-formation, as suggested by the transcriptional analysis presented in Chapter 5. By immunofluorescence staining, the canonical fibrotic mediator CTGF was found to be widely expressed by macrophages in the infarct zone of the P7 neonatal mouse at day 7, but minimally by macrophages in the P1 heart. In future, other differentially expressed pro-fibrotic mediators in P7/adult macrophages including *Lox*, *Loxl1* and *Tgfb3* should be validated.

The mechanisms controlling activation of the pro-fibrotic macrophage phenotype *in vivo* are not well defined. Ingestion of apoptotic neutrophils, efferocytosis, is known to induce an M2 IL-10^{hi} macrophage state characterised by expression of Arginase, which supports collagen synthesis.(267) However, no difference in neutrophil number were observed in the heart of the P1 neonate compared to the P7 neonate (chapter 5), suggesting that neutrophil burden is not the key driver of fibrosis in P7 macrophages. It is possible that there is a greater apoptotic cardiomyocyte burden in the P7/adult heart, or that as yet unknown environmental cues are responsible for triggering a pro-fibrotic phenotype in macrophages in the scar-forming heart.

6.3.2 Macrophages as collagen-producing cells

In this chapter data are presented to demonstrate that macrophages have the capacity not just to influence scar formation by indirect activation of myofibroblast function, but to contribute to fibrosis by direction production of collagen protein (COL1A2). The role of collagen production has historically been ascribed to the

myofibroblast, but increasing evidence suggests that there is functional overlap between the haematopoetic system and fibroblasts, with evidence of a functional continuum between the two.(268-270) In Drosophila, hemocytes (phagocytic cells of the immune system, analagous to macrophages) have been shown to deposit collagen IV in the contexts of renal tubule formation and regulation of the ovarian germline stem cell niche, through control of BMP signalling.(271, 272) Elimination of hemocytes, or specific blockade of hemocyte collagen IV production, led to abnormal adult niches with excess stem cells.(272) In mice, myofibroblasts have been found to undertake the classical macrophage role of phagocytosis to support clearance of apoptotic neutrophils following MI.(273)

In vertebrates, a myofibroblast-like cell of haematopoietic origin has been identified and described as a ‘fibrocyte’.(274) This term was first used in 1994 to describe a monocyte-derived cell expressing haematopoetic markers (e.g. CD45, CD11b, CD34) , which has the capacity to produce ECM proteins such as collagen I and III.(274, 275) Fibrocytes were subsequently shown to arise from a bone marrow precursor which was present in the CD14+ portion of human peripheral blood mononuclear cells. These cells were found to contribute to skin wound healing and pathological fibrosis. In the mouse heart following ischaemic reperfusion, cells expressing a combination of blood (CD45) and mesenchymal markers (collagen I, α-SMA) were found to be present in the heart.(276) These cells were LacZ positive in bone marrow chimeric mice made from a congenic line expressing LacZ, confirming that they had arisen from a bone marrow progenitor. Expression of macrophage markers such as CD68+ or F4/80+ is largely unknown, however, and it is therefore possible that the CD68+ cells found to express collagen in the heart are fibrocytes.

Several previous studies have reported that *bona fide* macrophages are capable of producing collagen proteins. First, *in vitro* cultured macrophages derived from primary mouse peritoneal macrophages have been shown to produce collagen I.(277) Human macrophages (derived from primary monocytes or the THP-1 cell line) have also been reported to produce type VI and type VIII collagen *in vitro*, as well as within atherosclerotic plaques.(278, 279) Tumour-associated macrophages have been reported to produce collagen, which contributes to the fibrotic capsule surrounding a tumour.(280) However, prior to this study there were no reports documenting collagen production by macrophages in the context of heart injury and repair.

The expression of adhesion G protein-coupled receptors such as F4/80 on myeloid cells provides a potential mechanism by which macrophages may interact with, and directly modulate, the ECM. Adhesion-GPCRs are large surface membrane proteins comprised of multiple EGF modules, with dual adhesion and signalling roles.(281) EMR2, for example, is expressed on neutrophils and other myeloid cells, and has been shown to bind the glycosaminoglycan chondroitin sulphate, a common ECM component.(282) Similarly, the adhesion-GPCR GPR56, expressed on natural killer cells, binds tissue transglutaminase (TG2), a ubiquitous cross-linking enzyme, leading to suppression of tumour growth and metastasis.(283) The upstream ECM ligands and downstream signalling cascades for the many adhesion-GPCRs are undefined but are an important research target to fully define the interaction between the ECM and cells of the immune system.

6.3.3 Monocytes as a determinant of wound healing

In this chapter experimental data are presented which demonstrate that adoptive transfer of adult splenic monocytes was sufficient to impede regeneration, and led to

scar formation in the P1 heart. In part, this occurred by direct expression of collagen protein by the donor monocytes. These data, therefore, support the concept that activation of inflammation, in this case by adoptively transferring adult monocytes into the P1 neonate, drives fibrotic pathways which contribute to a failure of tissue regeneration.

One possible mechanism for fibrosis following adoptive transfer relates to the lineage origins of monocytes. As described in detail in Chapter 3, macrophages are derived from at least two origins, including tissue-resident cells from the embryonic YS and monocytes which arise from the HSC.(53) Monocyte reservoirs in the spleen and bone marrow contribute the majority of macrophages in the adult heart following MI.(60, 91) Importantly, these different lineages appear to have long-lasting effects on the macrophage response in the setting of injury. Lavine *et al* demonstrated that the neonatal heart selectively expands the number of embryonic YS-derived MHC-II^{low}CCR2^{-} macrophages, without recruitment of additional CCR2+ monocytes.(102) In contrast, the adult heart selectively recruited monocytes and MHC-II^{high}CCR2+ monocyte-derived macrophages. *In vitro*, MHC-II^{low}CCR2^{-} macrophages were angiogenic and pro-proliferative. Furthermore, in the adult, blockade of CCR2^{+} monocytes was sufficient to preserve MHC-II^{low}CCR2− and MHC-II^{high}CCR2− subsets and improve heart repair.(102) In the adult mouse heart, tissue resident macrophages die locally in the early phase post-MI and are replaced by infitriltrating monocyte-derived populations, and this loss of the tissue-resident population relative to the neonate may be significant.(60) In the brain, differences in phagocytic activity and cytokine production have been observed between microglia and infiltrating monocyte-derived macrophages in experimental models of ischaemic stroke and autoimmune demyelination.(284, 285) To confirm that lineage origin is the driver of fibrosis in the adoptive-transfer P1 model, a further control experiment with adoptive transfer of tissue-resident macrophages into the P1 heart would be required – the

hypothesis being that fibrosis would not occur. This was not performed as resident macrophages could not be extracted using the EasySep™ Monocyte Isolation Kit. Furthermore, the markers of tissue-resident macrophage populations are not well-defined or distinct from infiltrating populations to be able to selectively sort this population after MI.

6.4 Conclusions

The experiments presented in this chapter first confirm differential expression of the pro-fibrotic mediator CTGF by macrophages in the P7 scar-forming heart following injury, in comparison to macrophages in the P1 regenerating heart. Second, macrophages have been shown to be capable of producing the fibrillar collagen protein COL1A2, suggesting that they may contribute to fibrosis by cell autonomous production of scar. Third, monocytes transplanted into the P1 environment are sufficient to impede regeneration, which in part, is mediated by expression of COL1A2 protein by adoptively transferred monocyte-macrophages. Adult macrophages are hard-wired as pro-fibrotic independent of local environment and can directly contribute collagen during scarring of the injured heart in contrast to the prevailing view that collagen deposition is carried out exclusively by myofibroblasts post-MI.

Chapter 7: General discussion

7.1 Discussion of findings

The overall findings of this thesis are discussed with reference to the aims as outlined in Chapter 1. These were:

1) To characterise the spatiotemporal infiltration of macrophages in cardiac development

2) To determine whether embryonic macrophages function as lymphatic progenitor cells within the embryonic heart

3) To investigate potential roles for macrophages in remodelling of coronary or lymphatic vessels in cardiac development

4) To compare macrophage pathways during cardiac repair by regeneration compared to scar formation

5) To validate functional roles for macrophages in directing repair by regeneration or scar formation

The extent to which these aims were achieved and the limitations of the findings are discussed in turn in this chapter. The implications of the findings to the wider field are outlined, and ongoing and future experimental work derived from this thesis is described.

7.1.1 Spatiotemporal infiltration of macrophages in cardiac development

The experimental results presented in Chapter 3 provide a detailed characterisation of the spatiotemporal dynamics of macrophage infiltration into the embryonic heart. Macrophage identity was definitively confirmed by dual labelling using the CX3CR1-GFP reporter mouse line in combination with antibody staining for the canonical macrophage markers F4/80 or CD68. Macrophages were found to be present in the developing heart at E12.5, prior to connection of the coronary artery stems and before the onset of the blood circulation. The number of macrophages in the embryonic heart expanded significantly between E12.5 and E14.5, and again by E16.5. By whole mount immunofluorescence imaging, macrophage spatial distribution was shown to vary through this period: At E12.5, macrophages were concentrated around the outflow tract, the sinus venosus, and in the epicardium. By E14.5, macrophages were distributed across the heart and were frequently found to colocalise with the developing vascular and lymphatic endothelial networks. A subset of macrophages defined by expression of LYVE1+ were shown to localise to the epicardium at E14.5 and physically interact with lymphatic endothelium, particularly at branch points and leading edges. Macrophages in the embryonic heart were derived from both embryonic YS and HSC sources, with the LYVE1+ macrophage subset found to arise entirely from the YS.

These findings raise the question of how macrophages are recruited to the embryonic heart, prior to the onset of the circulation. The observation that macrophages are initially concentrated in the epicardium at E12.5 (Chapter 3) suggests that it may provide early chemoattractive signals. In support of this concept, Stevens *et al* have recently reported that epicardial activation is required for recruitment of YS-derived macrophages to the heart.(85) After ablation of epicardial cells at E11.5 (using *Wt1*-CreERT2; R26-DTA mice) there was a significant reduction

of epicardial macrophage numbers at E13.5.(85) Interestingly, macrophages are also commonly seen in the reactivated epicardium following MI in adult mice (Cahill, unpublished data), again supporting the idea that epicardial activation provides chemoattractive cues to macrophages.

There are several candidate signalling mechanisms which might mediate macrophage recruitment to the epicardium. Macrophages express CX3CR1, the receptor for the chemokine fractalkine (also known as CX3CL1), which is a potent attractant for monocyte-macrophages.(70) CX3CL1 mediates recruitment of CCR2-negative monocyte-macrophage populations and may be upregulated by activated epicardium. Alternatively, activated epicardial-derived cells are known to secrete monocyte chemoattractant protein 1 (MCP1, also known as chemokine C-C motif ligand 2, CCL2).(286) A MCP1-based mechanism is less likely, however, as its cognate receptor CCR2 is not expressed on YS-derived macrophages.(84) After recruitment, adhesion of macrophages to the epicardium may be mediated by the Vascular cell adhesion molecule 1 (VCAM1)-Very Late Antigen-4 (VLA4) system. The activated epicardium expresses the cell adhesion molecule VCAM1, and genetic knockout of *Vcam1* leads to a failure of epicardial and coronary development.(287) VLA4 is widely expressed on leucocytes and its interaction with VCAM mediates recruitment of monocytes at sites of inflammation.(288) To investigate this further, the epicardium could be immunofluorescence stained for CXCL1, MCP1 and VCAM1.

7.1.2 Embryonic macrophages as lymphatic progenitor cells

Previous work in the Riley laboratory has demonstrated that the cardiac lymphatic endothelium derives not only from venous endothelium, as historically thought, but also from a non-venous progenitor cell of uncertain identity.(123) Specifically, Klotz *et al* found that a proportion of LECs were not labelled by *Tie2*-Cre lineage tracing, which would be expected to label all venous endothelium and its derivatives.(123) However, a small number of LECs were labelled by the inducible *Csf1r*-Mer-Cre-Mer mouse line, after induction of *Cre* recombinase at E7.5, implicating a CSF1R+ progenitor at the YS stage.(123) Klotz *et al* found that non-venous cardiac LECs were also labelled by lineage tracing with the *Vav*-Cre mouse line, suggesting a haematopoietic origin.(289) Recent studies have characterised YS-stage CSF1R+ cells as EMPs, a primitive haematopoietic progenitor which gives rise to tissue-resident macrophages.(56) Following the observation that macrophages are found in extremely close proximity to developing LECs, and the close lineage relationship between EMPs and macrophages, I investigated whether macrophages might act as LEC progenitors.

To further investigate the identity of the LEC progenitor, lineage tracing was performed using the *Csf1r*-MerCreMer, *Cx3cr1*-CreERT2 and *Flt3*-CreERT2 mouse lines.(56, 106, 144) These experiments confirmed that CSF1R+ lineage definitively contributes to cardiac LECs, however, unexpectedly, there was minimal contribution from CSF1R+ progenitors when labelled at E8.5-E10.5, which would be expected to label EMPs derived from the YS and haemogenic endothelium.(56) Instead, the CSF1R+ lineage contribution was greatest after labelling at E12.5, by which point haematopoietic progenitors are focused in the fetal liver. If the E12.5 CSF1R+ population was derived from EMPs only, labelling at E8.5-E10.5 should show equivalent incorporation to cardiac LECs at E16.5. The finding of a major difference

between labelling at E12.5 and earlier time points suggests that while there is a minor YS-derived contribution to LECs, the majority of LEC progenitors are not classical EMPs. Lineage tracing in the *Cx3cr1*-CreERT2 mouse line demonstrated conclusively that that the LEC progenitor is not a classical CX3CR1+ macrophage, and the hypothesis that macrophages act as progenitors for cardiac LECs was therefore rejected. Furthermore, lineage tracing using the *Flt3*-CreERT2 mouse line, which labels all derivatives of definitive haematopoiesis, demonstrated that the LEC progenitor was not downstream of the HSC. To investigate the divergent findings of *Csf1r* and *Cx3cr1* lineage tracing, the expression of these myeloid markers by cells in the embryonic heart was investigated by flow cytometry. Surprisingly, there was extensive divergence in expression of these markers. While CX3CR1-GFP+ cells were classical macrophages expressing F4/80, CSF1R+ cells were F4/80- and expressed higher levels of KIT, a marker associated with an endothelial fate.(290, 291)

A number of questions remain. First, the precise identity or origin of the CSF1R+ progenitor which contributes to cardiac LECs could not be positively identified. Based on the data in Chapter 3, this cell is now known not to be a CX3CR1+ macrophage and is not a classical CSF1R+ EMP derived from the YS. Furthermore, it is not downstream of FLT3+ definitive haematopoiesis, which begins in the AGM at E10.5 and continues in the fetal liver. Future investigation of this progenitor population might therefore focus on CSF1R+ FLT3- progenitors present at the fetal liver stage E12.5. Interestingly, a population of cells expressing the Stem Cell Leukaemia gene enhancer transgene (SCL-PLAP+) in the fetal liver at E12.5 has recently been found to differentiate into LYVE1+ LECs following adoptive transfer into newborns or conditioned adult recipients.(292) The origin of this SCL-PLAP+ progenitor population, prior to the fetal liver stage, has not been identified.

7.1.3 Functional roles for macrophages in remodelling of coronary or lymphatic vessels in cardiac development

Chapter 4 addressed the hypothesis that macrophages play a functional role in remodelling coronary and lymphatic vessels in the developing heart. Experiments were conducted using a previously validated genetic mouse model of macrophage deficiency, the *Pu.1*$^{-/-}$ mouse.(80) First, macrophages were shown to be absent from the embryonic heart of the *Pu.1*$^{-/-}$ mouse by flow cytometry. Next, by whole-mount confocal imaging of immunofluorescence-stained hearts, quantitatively significant abnormalities of both the coronary vasculature and lymphatics were identified, in comparison to wild-type littermate controls. Specifically, *Pu.1*$^{-/-}$ mice showed evidence of significantly reduced coronary and lymphatic vascular branching, and aberrant vessel length at E16.5. Loss of macrophages was also associated with markedly altered lymphatic vessel calibre and reduced distal migration at E16.5. While coronary abnormalities appeared to be transient, and had largely resolved by E19.5, lymphatic vessel patterning remained abnormal throughout development. These data suggest a key role for macrophages in patterning the growing coronary and lymphatic endothelium during heart development.

These findings contribute to a growing literature on the roles of macrophages in patterning the developing vasculature. In the heart, Leid *et al* have recently reported that YS-derived macrophages 'prune' the branches of the developing coronary vasculature in the mouse heart.(84) Genetic ablation of macrophages (in the *Csf1*$^{op/op}$ mouse and *LysM*-Cre;R26R-DTA) led to increased vascular branching at E17.5. The finding of hyperbranching, in comparison with reduced coronary branching as identified in this thesis in the *Pu.1*$^{-/-}$ mouse, might be explained by the use of the different models: in the *Csf1*$^{op/op}$ mouse not all macrophage populations are lost.(293) Alternatively, the methodology used to study and quantify coronary vessels might

explain the difference: in this thesis, coronary vessels were identified by whole-mount staining for the vascular marker Endomucin. In contrast, Leid *et al* utilised immunohistochemistry for PECAM, with quantification of vessels in cross section.(84) The finding of hypo-branching of coronary and lymphatic vessels outlined in this thesis is currently undergoing validation in a second model of macrophage ablation, using the *Cx3cr1*-CreERT2;R26R-DTA line (see below).

There are two key limitations to the findings presented in Chapter 4. First, the functional significance of macrophage-mediated endothelial remodelling has not been demonstrated. Reduced coronary branching is likely to lead to reduced vessel density and this in turn may result in impaired coronary blood flow and tissue perfusion. Reduced lymphatic branching may limit lymph drainage from the extracellular space, leading to myocardial oedema. Both may impair cardiac performance. In support of this, myocardial oedema induced by elevation of coronary sinus pressure has previously been demonstrated to acutely reduce cardiac output in dogs, and in the chronic setting, drive cardiac fibrosis.(294) After MI, formation of new lymphatic vessels by lymphangiogenesis is required for resolution of inflammation.(97) Stimulation of lymphangiogenesis by treatment with VEGFC, leading to increased lymphatic branching and density, resulted in enhanced clearance of oedema and macrophages, with improved healing and LV function.(97, 295) While the long-term effects of dysregulated vascular patterning cannot be investigated in the *Pu.1*$^{-/-}$ mouse model, which dies in the neonatal period, this may be possible in an inducible knockdown model such as *Cx3cr1*-CreERT2;R26R-DTA, in which macrophages can be transiently ablated.

Second, it remains unclear how epicardial macrophages selectively associate and interact with the nascent coronary and lymphatic vasculature. One possibility is that LYVE1, which was shown to be expressed on both lymphatic endothelium and

epicardial (lymphatic-associated) macrophages, mediates the association between the two. LYVE1 is a receptor for the large ubiquitous glycosaminoglycan polymer hyaluronan (HA).(296) Recently, expression of LYVE1 on LECs has been shown to mediate uptake of HA-bearing dendritic cells by lymphatic vessels at sites of inflammation.(297) Expression of LYVE1 on macrophages (as observed in the epicardial subset) and LECs would allow these cells to colocalise via a bridging HA polymer, i.e. LYVE1-HA-LYVE1. Against this hypothesis, however, is the finding that no abnormalities of lymphatic vessel formation were observed in the skin and intestinal mucosa of *Lyve1*$^{-/-}$ mice, suggesting it is dispensable for lymphatic vessel patterning.(298) It remains to be determined whether there are lymphatic defects in the developing hearts of *Lyve1*$^{-/-}$ mice, however. Macrophage association with lymphatic endothelium may also be mediated by VLA-4 and VLA-5, which would be another possible candidate mechanism.(299)

How macrophages modulate vessel branching and calibre is also unknown. In the skin of *Pu.1*$^{-/-}$ mice, Gordon *et al* identified LEC hyperproliferation and suggested that macrophages provide cues to restrain LEC cell division.(175) This mechanism was excluded in the heart, however. In the context of inflammation, lymphangiogenic sprouting is stimulated by macrophage-derived VEGFC.(97) However, no evidence of macrophage-derived VEGFC was identified in the developing heart. An alternative possibility is that macrophages secrete another soluble mediator of lymphatic sprouting, such as TGF-β, or remodel the ECM (for example by production of MMP2) to facilitate migration of endothelial network. In support of this, perturbation of the TGF-β pathway and the MMP system have previously been demonstrated to result in abnormalities of lymphatic calibre and branching, although this was not studied in the context of the cardiac lymphatics, which is now a focus of further investigation.(185, 187)

7.1.4 Comparison of macrophage pathways during healing by regeneration compared to scar formation

Chapter 5 addressed the question of whether macrophages undertake distinct roles during myocardial healing by regenerative repair versus scar formation. Mammalian heart regeneration has recently been described in the neonatal mouse, restricted to a temporally limited period of 1-2 days following birth.(21) Outside this regenerative window, neonatal and adult mice heal by scar formation, comparable to adult humans following MI. The neonatal mouse model of cardiac regeneration permits analysis of divergent modes of tissue repair following MI, in the same species. Macrophages have long been implicated as cellular mediators of wound healing, but how they influence divergent modes of tissue repair has not previously been studied.

The data presented in Chapter 5 show that the macrophage response to MI differs quantitatively and functionally in the neonate and adult. As quantified by flow cytometry, both neonatal models (P1 and P7) show evidence of a dampened immune cell response to MI compared to the adult, suggesting immaturity or active suppression of immune cell infiltration. To understand the functional roles of macrophages, unbiased transcriptional analysis of FAC-sorted macrophages was performed using RNA sequencing. These data demonstrated that the gene expression profiles of macrophages from the P1, P7 and adult hearts are distinct at baseline and serial time points after injury. Comparison of differentially expressed genes in regeneration and scar formation revealed that macrophages activate distinct pathways in divergent tissue repair: in regeneration, releasing soluble mediators with reported roles in healing, and in scar formation, activating pro-fibrotic pathways and producing extracellular matrix components. Analysis of gene sets by unbiased temporal clustering provided insight into macrophage roles during the

different phases of injury and repair, and potential candidate soluble mediators implicated in activation of cardiomyocyte proliferation in regeneration.

There are limitations to the experimental approach and subsequent findings. First, mouse models of MI have intrinsic problems: the procedure is an invasive surgical intervention and induction of MI requires coronary ligation, unlike human MI, where coronary occlusion is caused by thrombus following plaque rupture. The surgical procedure entails induction of cardiorespiratory arrest by cooling in the neonate, which might conceivably affect the downstream injury, inflammatory or healing response. This is controlled for, to the extent that the surgical approach is identical in P1 and P7 models, however, due to variability in the course and branching of the LAD, there may be variability in the size of the infarct. Although this was minimised by only using mice with confirmed correct suture placement at tissue harvest, the variability might be further reduced by subjecting each animal to magnetic resonance imaging (MRI) to quantify the MI, although this is currently limited by logistics and cost. Second, given that macrophages were bulk sorted, differences between different macrophage populations (e.g. tissue resident vs monocyte-derived) could not be assessed. This will be the focus of future experimental work as outlined below. Despite these caveats, the data presented in Chapter 5 provide novel insights into divergent macrophage functions in the context of heart regeneration and scar formation, meeting the aim as outlined.

7.1.5 Functional roles for macrophages during regenerative and scar-forming healing

Transcriptional analysis of macrophages outlined in Chapter 5 identified that macrophages differentially activate pro-fibrotic pathways to direct scar formation in the non-regenerating heart. Differentially upregulated genes from macrophages in

the P7/adult heart included *Tgfb3* and *Ctgf*, which have known roles to activate myofibroblasts. The functional effects of candidate pro-regenerative and pro-fibrotic factors is currently being assessed *in vitro* (see below, chapter 7.3.4). In addition, macrophages in the scar-forming heart upregulated matricellular proteins and collagens, suggesting a possible role in direct formation of ECM and scar respectively. These pathways were further investigated and validated in Chapter 6.

First, by immunofluorescence staining of heart cryosections from the P1 and P7 heart, it was demonstrated that macrophages express CTGF in the scar-forming heart, but not during regeneration. Second, to investigate a cell-autonomous role for macrophages in production of collagen, samples were analysed from *Col1a2*-Cre; R26R-EYFP mice subjected to MI at P7. This experiment confirmed that a subset of CD68+ macrophages expressed EYFP, suggesting transcriptional activity driven by the *Col1a2* promoter.

Next, the hypothesis that adult monocytes would be sufficient to drive fibrosis in the regenerative environment was examined. Adult spleen-derived monocytes were adoptively transferred into P1 recipients undergoing MI surgery. Compared to vehicle control, transfer of monocytes led to a statistically significant increase in scar deposition and a failure of heart regeneration. Adoptive transfer of monocytes from the spleen of adult *Col1a2*-Cre; R26R-tdTomato mice demonstrated that these cells activate expression of TdTomato (suggesting transcription of COL1A2) following adoptive transfer to deposit scar. Taken together, these findings suggest that adult monocytes are intrinsically biased towards activation of pro-fibrotic pathways, despite transfer to the P1 regenerative environment, and are a capable of driving scar formation in part by production of collagen.

There are several limitations to the findings presented in this chapter. First, while a subset of *Col1a2*-Cre;R26R-EYFP cells were observed to express the macrophage marker CD68, the expression of myofibroblast markers (e.g. α-SMA) was not assessed. It is not clear whether the CD68+ EYFP+ cells retain a 'pure' macrophage identity, or have undergone partial transdifferentiation to adopt a myofibroblast fate. Transdifferentiation of macrophages into fibroblasts has previously been reported *in vitro* and in the context of *Schistosoma mansoni* infection.(300, 301) Second, it was not possible to confirm that macrophage expression of EYFP led to downstream extracellular deposition of collagen within the scar. This would require a transgenic mouse expressing a collagen-reporter fusion protein (rather than activation of a separate reporter protein at the R26 locus, as in the *Col1a2*-CreERT2; R26R-EYFP) which does not exist in the mouse. Third, the relative contribution of macrophage-derived collagen, compared to that produced by myofibroblasts, was not assessed but will be undertaken as a future requirement. Finally, as discussed in Chapter 6, to confirm that adult monocytes, rather than macrophage excess in general, drives fibrosis in the P1 heart, an additional control group receiving tissue-resident macrophages would be required.

7.2 Conclusions

The work presented in this thesis has provided novel insights into the functions of macrophages in the heart during development, repair and regeneration. Detailed analysis of the embryonic heart has demonstrated infiltration of macrophages from the yolk-sac and monocytes, and organised colocalisation with coronary and lymphatic vessels in the epicardium. The concept of macrophages acting as lymphatic progenitor cells has been refuted. Instead, by analysis of the *Pu.1*$^{-/-}$ mouse model, a role for macrophages in regulating branching and patterning of the coronary and lymphatic vasculature has been identified.

Transcriptional analysis of macrophages in regeneration and scar formation demonstrated that macrophages activate distinct pathways which are likely to contribute to these divergent modes of heart repair. Activation of a broad pro-fibrotic macrophage program including production of soluble pro-fibrotic mediators and ECM components was restricted to the P7 and adult mouse heart, suggesting a specific functional role in scar formation. Furthermore, a novel role for macrophages in production of collagen protein was identified, which appeared to be intrinsically programmed and activated by adult splenic monocytes even within the regenerative environment.

7.3 Future work

The aims of future work are

1) To confirm the *Pu.1*$^{-/-}$ coronary vascular and lymphatic phenotype in an inducible model of macrophage ablation

2) To investigate the mechanisms by which macrophages remodel the developing coronary and lymphatic vessels

3) To define the intrinsic factors (e.g. epigenetic landscape) which determine differences in macrophage response to injury

4) To validate the functional effects of macrophage-derived soluble factors

5) To investigate the nature of macrophage heterogeneity in development, injury and repair

These questions and potential experimental approaches are discussed in turn.

7.3.1 Confirmation of the *Pu.1*$^{-/-}$ coronary vascular and lymphatic phenotype in an inducible model of macrophage ablation

I have established that genetic ablation of macrophages in the *Pu.1*$^{-/-}$ mouse model results in abnormal patterning of coronary vasculature and lymphatic vessels. However, this model has intrinsic limitations, including loss of other immune cells (e.g. B cells). Although the number of other affected immune cells in the heart is very small, suggesting they are are unlikely to participate in the observed phenotype, it is important to validate the *Pu.1*$^{-/-}$ phenotype in a second model of macrophage-specific ablation. To achieve this, we will cross mice from the *Cx3cr1*-CreERT2 line, which expresses Cre recombinase selectively in macrophages, with mice from the R26-DTA line, which expresses the diphtheria A toxin gene at the Rosa-26 locus after Cre-mediated excision of a STOP sequence. Induction of Cre recombinase by tamoxifen dosing at E12.5 will thus permit selection ablation of macrophages. Embryos will then be harvested, genotyped, and stained by whole mount immunofluorescence imaging for abnormalities in the coronary vasculature and lymphatic vessels.

7.3.2 Mechanisms of macrophage patterning of the developing coronary and lymphatic vessels

The mechanisms by which macrophages remodel the coronary and lymphatic endothelial network remain unclear. This could be further investigated by *in vitro* or *in vivo* approaches. The Riley laboratory is establishing a system for culture of LECs derived from human induced pluripotent stem cells, and for the induction of lymphangiogenesis via Matrigel. An effect on lymphatic branching or outgrowth might be investigated by addition of macrophages, or macrophage-conditioned media, to the LEC culture. An effect mediated by macrophage-conditioned media would suggest a mechanism mediated by a soluble factor, which could be isolated by use

of selective blocking antibodies or chemical inhibitors. Using a similar approach, macrophages have previously been shown to enhance endothelial tube formation, via secretion of IL-1 α.(302) An alternative strategy would be to isolate LYVE1+ and LYVE1- CX3CR1-GFP+ macrophages from the embryonic heart, and analyse differentially expressed genes or pathways which are enriched in the LYVE1+ population.

7.3.3 Intrinsic factors controlling the macrophage response to injury

The data presented within this thesis demonstrate that macrophages activate different pathways to influence tissue repair by regeneration and scar formation. Furthermore, activation of profibrotic pathways appears to be an intrinsic property of splenic monocytes. In comparison, tissue-resident macrophages appear have recently been reported to retain pro-angiogenic and regenerative roles.(102) The mechanisms by which these pathways are differentially controlled is largely unknown.

To investigate this further, the transcriptome and epigenetic landscape of macrophages of different origins will be analysed in parallel. YS-derived macrophages will be irreversibly labelled in *Cx3cr1*-CreER;R26R-tdTomato embryos at E8.5, prior to the onset of definitive haematopoiesis. These mice will then be aged to adulthood, and will undergo MI surgery at 8 weeks of age. CD45+ CD11b+ LyG6-F4/80+ macrophages will be isolated by flow cytometry, and separated into those labelled by TdTomato, derived from the YS, and those unlabelled, which will predominantly comprise monocyte-derived macrophages. RNAseq and ATACseq will then be performed to understand how differences in epigenetic landscape may control gene expression around candidate angiogenic (e.g. *Vegfa)* and fibrotic (e.g. *Tgfb1*, *Col1a1*) genes in different macrophage populations.

7.3.4 Functional effects of macrophage-derived soluble factors

Heart regeneration is fundamentally reliant on cardiomyocyte cell-cycle re-entry.(12) The mechanisms by which this process is achieved in regenerative organisms such as the neonatal mouse and zebrafish are partly understood and involve a complex interplay of soluble ligand stimulation, matrix signals, and intracellular permissive cell cycle control.(12) Macrophage-derived soluble ligands have been proposed to provide a key trigger to initiate cell cycle reactivation and cardiomyocyte proliferation in neonatal (P1) cardiomyocytes, but the identity of these factors and their relative effects is unknown. In wound healing by scar formation, macrophage-derived factors are known to drive recruitment, activation and proliferation of fibroblasts.

The RNAseq data presented in Chapter 5 contain potential candidate factors which may differentially promote P1 cardiomyocyte proliferation, or fibroblast activation, after injury. By collaboration with Professor Mauro Giacca in Trieste, we will analyse the ability of approximately 80 candidate macrophage-derived soluble factors to stimulate P1 cardiomyocyte proliferation, or fibroblast proliferation, in a high-throughput *in vitro* assay. Proliferating cardiomyocytes are identified by detection of increasing cardiomyocyte number over time. If macrophage-derived soluble factors are able to stimulate cardiomyocyte proliferation, their effects on adult cardiomyocytes will also be assessed. Understanding how neonatal and adult cardiomyocytes respond to growth signals may provide insights to novel therapeutic pathways. In addition, identification of factors which selectively activate cardiomyocytes, or fibroblasts, could be therapeutically exploited to control cardiomyocyte proliferation and scar formation after MI.

7.3.5 Macrophage heterogeneity in development, injury and repair

As discussed in the Introduction, the concept of macrophage 'polarisation', as discovered *in vitro*, has somewhat constrained understanding of the complexity and plasticity of macrophage responses *in vivo*. The next stage towards understanding macrophage heterogeneity is undertaking single cell sequencing of macrophages from the heart *in vivo*. This has now been performed by two major studies, yielding significant insights into macrophage function. The first, performed by Hulsmans *et al*, demonstrated that cardiac tissue-resident macrophages express the gap junction Cx43.(86) This led to the insight that macrophages physically couple to cells of the cardiac conduction system, and that ablation of macrophages results in conduction abnormalities.(86) Second, Mass *et al* conducted single cell sequencing of CD45+ cells from the E9.0 embryo, revealing that EMPs differentiate into tissue-resident macrophages via an intermediate 'pre-macrophage' stage defined by upregulation of *Cx3cr1*.(303) This study also identified a new tissue-resident macrophage specific reporter, *Tnfrsf11a*-Cre, allowing tracking of EMP-derived macrophages independently of HSC-derived macrophages.(303)

Single cell sequencing of macrophages from the adult mouse heart following MI would provide major insights into the heterogeneity of macrophage response. It seems likely that macrophages within different spatial regions of the heart play distinct roles following injury, for example, in the infarct zone compared to the remote zone, or in the epicardium. Single cell sequencing followed by *in situ* or immunofluorescence validation would provide valuable insights into these different populations. Furthermore, single cell approaches might also assist in identification of pathways mediating the differentiation of infiltrating monocytes into macrophages, and the degree to which different macrophage subpopulations undertake discrete functional tasks.

7.4 Appendices

7.4.1 Timing & venue of research

The research presented in this thesis was performed from October 2014 to September 2017 in the Departments of Physiology, Anatomy and Genetics (DPAG) and Cardiovascular Medicine (CV MED) at the University of Oxford. The supervisors were Professor Paul Riley (DPAG) and Professor Robin Choudhury (CV MED).

7.4.2 Funding

The DPhil project was funded by the Wellcome Trust PhD Programme in Basic Science for Clinicians.

7.4.3 Publications

Manuscripts in preparation/submission:

Cahill TJ*, Simões FC*, Kenyon A, Gavriouchkina D, Lemieux ME, Barnette DN, Rohling M, Weinberger M, Masmanian E, Williams R, Greaves DR, Choudhury RP, Sauka-Spengler T, Riley PR. Macrophages directly contribute collagen to scar formation during zebrafish heart regeneration and mouse heart repair. *Submitted*

* joint first authorship

Cahill TJ, Sun X, Vieira J, Lord AM, Jacobsen SE, Choudhury RP, Riley PR. Macrophages pattern the developing cardiac lymphatic system. *In preparation.*

Manuscripts published:

Cahill TJ, Choudhury RP, Riley PR. Heart regeneration and repair after myocardial infarction: translational opportunities for novel therapeutics. *Nature Reviews Drug Discovery.* 2017. DOI: 10.1038/nrd.2017.106

7.4.4 Presentations at scientific meetings

Molecular Mechanisms of Heart Development, Keystone, USA.
Oral presentation. Cahill TJ *et al.* Macrophages activate distinct programs of regeneration and scar formation to direct repair following myocardial infarction. 27 March 2017

Development & Cell Biology Open Day, Oxford, UK.
Oral presentation. Cahill TJ. Macrophage roles in cardiac injury, repair and regeneration. 9 June 2016.

Programming the Failing Heart to a Regenerative State: Fondation Leducq Network Meetings. Oral presentations. Cahill TJ. Macrophages in cardiac repair and regeneration. Trieste, Italy, 20-21 June 2015; Maui, USA ,17-19 January 2016; Oxford, UK, 21-22 June 2016; Boulder, USA, 24-26 March 2017; Utrecht, Holland, 20-22 August 2017.

References

1. Braunwald E. Heart Failure. JACC: Heart Failure. 2013;1(1):1-20.

2. Roger VL. Epidemiology of heart failure. Circulation Research. 2013;113(6):646-59.

3. Cahill TJ, Ashrafian H, Watkins H. Genetic cardiomyopathies causing heart failure. Circulation Research. 2013;113(6):660-75.

4. Braunwald E. The war against heart failure: the Lancet lecture. The Lancet. 2015;385(9970):812-24.

5. Frangogiannis NG. The inflammatory response in myocardial injury, repair, and remodelling. Nature Reviews Cardiology. 2014;11(5):255-65.

6. Packer M. Pathophysiology of chronic heart failure. The Lancet. 1992;340(8811):88-92.

7. Sutton MG, Sharpe N. Left ventricular remodeling after myocardial infarction. Circulation. 2000;101(25):2981-8.

8. Pfeffer MA, Braunwald E. Ventricular remodeling after myocardial infarction. Experimental observations and clinical implications. Circulation. 1990;81(4):1161-72.

9. Jernberg T, Johanson P, Held C, Svennblad B, Lindbäck J, Wallentin L. Association between adoption of evidence-based treatment and survival for patients with ST-elevation myocardial infarction. Journal of the American Medical Association. 2011;305(16):1677-84.

10. Puymirat E, Simon T, Steg PG, Schiele F, Guéret P, Blanchard D, et al. Association of changes in clinical characteristics and management with improvement in survival among patients with ST-elevation myocardial infarction. Journal of the American Medical Association. 2012;308(10):998-1006.

11. Velagaleti RS, Pencina MJ, Murabito JM, Wang TJ, Parikh NI, Agostino RB, et al. Long-term trends in the incidence of heart failure after myocardial infarction. Circulation. 2008;118(20):2057-62.

12. Cahill TJ, Choudhury RP, Riley PR. Heart regeneration and repair after myocardial infarction – translational opportunities for novel therapeutics. Nature Reviews Drug Discovery. 2017;In press.

13. Dinsmore CE. A history of regeneration research: milestones in the evolution of a science. New York: Cambridge University Press; 1991.

14. Oberpriller JO, Oberpriller JC. Response of the adult newt ventricle to injury. Journal of Experimental Zoology. 1974;187(2):249-53.

15. Poss KD, Wilson LG, Keating MT. Heart regeneration in zebrafish. Science. 2002;298(5601):2188-90.

16. Gonzalez-Rosa JM, Mercader N. Cryoinjury as a myocardial infarction model for the study of cardiac regeneration in the zebrafish. Nature Protocols. 2012;7(4):782-8.

17. Wang J, Panáková D, Kikuchi K, Holdway JE, Gemberling M, Burris JS, et al. The regenerative capacity of zebrafish reverses cardiac failure caused by genetic cardiomyocyte depletion. Development. 2011;138(16):3421-30.

18. Parente V, Balasso S, Pompilio G, Verduci L, Colombo GI, Milano G, et al. Hypoxia/reoxygenation cardiac injury and regeneration in zebrafish adult heart. PLOS ONE. 2013;8(1):e53748.

19. Vivien CJ, Hudson JE, Porrello ER. Evolution, comparative biology and ontogeny of vertebrate heart regeneration. Regenerative Medicine. 2016;1:16012.

20. Witman N, Murtuza B, Davis B, Arner A, Morrison JI. Recapitulation of developmental cardiogenesis governs the morphological and functional regeneration of adult newt hearts following injury. Developmental Biology. 2011;354(1):67-76.

21. Porrello ER, Mahmoud AI, Simpson E, Hill JA, Richardson JA, Olson EN, et al. Transient Regenerative Potential of the Neonatal Mouse Heart. Science. 2011;331(6020):1078-80.

22. Porrello ER, Mahmoud AI, Simpson E, Johnson BA, Grinsfelder D, Canseco D, et al. Regulation of neonatal and adult mammalian heart regeneration by the miR-15 family. Proceedings of the National Academy of Sciences. 2013;110(1):187-92.

23. Kikuchi K, Holdway JE, Werdich AA, Anderson RM, Fang Y, Egnaczyk GF, et al. Primary contribution to zebrafish heart regeneration by gata4+ cardiomyocytes. Nature. 2010;464(7288):601-5.

24. Jopling C, Sleep E, Raya M, Marti M, Raya A, Belmonte JCI. Zebrafish heart regeneration occurs by cardiomyocyte dedifferentiation and proliferation. Nature. 2010;464(7288):606-9.

25. Senyo SE, Steinhauser ML, Pizzimenti CL, Yang VK, Cai L, Wang M, et al. Mammalian heart renewal by pre-existing cardiomyocytes. Nature. 2013;493(7432):433-6.

26. Murry CE, Soonpaa MH, Reinecke H, Nakajima H, Nakajima HO, Rubart M, et al. Haematopoietic stem cells do not transdifferentiate into cardiac myocytes in myocardial infarcts. Nature. 2004;428(6983):664-8.

27. Balsam LB, Wagers AJ, Christensen JL, Kofidis T, Weissman IL, Robbins RC. Haematopoietic stem cells adopt mature haematopoietic fates in ischaemic myocardium. Nature. 2004;428(6983):668-73.

28. Ahuja P, Sdek P, MacLellan WR. Cardiac Myocyte Cell Cycle Control in Development, Disease, and Regeneration. Physiological Reviews. 2007;87(2):521.

29. Bergmann O, Bhardwaj RD, Bernard S, Zdunek S, Barnabé-Heider F, Walsh S, et al. Evidence for Cardiomyocyte Renewal in Humans. Science. 2009;324(5923):98.

30. Gemberling M, Karra R, Dickson AL, Poss KD. Nrg1 is an injury-induced cardiomyocyte mitogen for the endogenous heart regeneration program in zebrafish. eLife. 2015;4:e05871.

31. Schindler YL, Garske KM, Wang J, Firulli BA, Firulli AB, Poss KD, et al. Hand2 elevates cardiomyocyte production during zebrafish heart development and regeneration. Development. 2014;141(16):3112.

32. Heallen T, Zhang M, Wang J, Bonilla-Claudio M, Klysik E, Johnson RL, et al. Hippo Pathway Inhibits Wnt Signaling to Restrain Cardiomyocyte Proliferation and Heart Size. Science. 2011;332(6028):458.

33. Xin M, Kim Y, Sutherland LB, Murakami M, Qi X, McAnally J, et al. Hippo pathway effector Yap promotes cardiac regeneration. Proceedings of the National Academy of Sciences. 2013;110(34):13839-44.

34. Haubner BJ, Schneider J, Schweigmann UU, Schuetz T, Dichtl W, Velik-Salchner C, et al. Functional recovery of a human neonatal heart after severe myocardial infarction. Circulation Research. 2016;118(2):216-21.

35. Fratz S, Hager A, Schreiber C, Schwaiger M, Hess J, Stern HC. Long-term myocardial scarring after operation for anomalous left coronary artery from the pulmonary artery. The Annals of Thoracic Surgery. 2011;92(5):1761-5.

36. Carlson BM. Some principles of regeneration in mammalian systems. The Anatomical Record Part B: The New Anatomist. 2005;287B(1):4-13.

37. Kaufmann SHE. Immunology's foundation: the 100-year anniversary of the Nobel Prize to Paul Ehrlich and Elie Metchnikoff. Nature Immunology. 2008;9(7):705-12.

38. Wynn TA, Chawla A, Pollard JW. Macrophage biology in development, homeostasis and disease. Nature. 2013;496(7446):445-55.

39. Nguyen KD, Qiu Y, Cui X, Goh YPS, Mwangi J, David T, et al. Alternatively activated macrophages produce catecholamines to sustain adaptive thermogenesis. Nature. 2011;480(7375):104-8.

40. Kohyama M, Ise W, Edelson BT, Wilker PR, Hildner K, Mejia C, et al. Role for Spi-C in the development of red pulp macrophages and splenic iron homeostasis. Nature. 2009;457(7227):318-21.

41. Pozzi LA, Maciaszek JW, Rock KL. Both dendritic cells and macrophages can stimulate naive CD8 T cells in vivo to proliferate, develop effector function, and differentiate into memory cells. The Journal of Immunology. 2005;175(4):2071-81.

42. Junt T, Moseman EA, Iannacone M, Massberg S, Lang PA, Boes M, et al. Subcapsular sinus macrophages in lymph nodes clear lymph-borne viruses and present them to antiviral B cells. Nature. 2007;450(7166):110-4.

43. Sica A, Mantovani A. Macrophage plasticity and polarization: in vivo veritas. The Journal of Clinical Investigation. 2012;122(3):787-95.

44. Smith JD, Trogan E, Ginsberg M, Grigaux C, Tian J, Miyata M. Decreased atherosclerosis in mice deficient in both macrophage colony-stimulating factor (op)

and apolipoprotein E. Proceedings of the National Academy of Sciences. 1995;92(18):8264-8.

45. Xu H, Barnes GT, Yang Q, Tan G, Yang D, Chou CJ, et al. Chronic inflammation in fat plays a crucial role in the development of obesity-related insulin resistance. The Journal of Clinical Investigation. 2003;112(12):1821-30.

46. Murray PJ, Wynn TA. Protective and pathogenic functions of macrophage subsets. Nature Reviews Immunology. 2011;11(11):723-37.

47. Nathan CF, Murray HW, Wiebe ME, Rubin BY. Identification of interferon-gamma as the lymphokine that activates human macrophage oxidative metabolism and antimicrobial activity. The Journal of Experimental Medicine. 1983;158(3):670-89.

48. Stein M, Keshav S, Harris N, Gordon S. Interleukin 4 potently enhances murine macrophage mannose receptor activity: a marker of alternative immunologic macrophage activation. The Journal of Experimental Medicine. 1992;176(1):287-92.

49. Mills CD, Kincaid K, Alt JM, Heilman MJ, Hill AM. M-1/M-2 Macrophages and the Th1/Th2 Paradigm. The Journal of Immunology. 2000;164(12):6166-73.

50. Lawrence T, Natoli G. Transcriptional regulation of macrophage polarization: enabling diversity with identity. Nature Reviews Immunology. 2011;11(11):750-61.

51. Nahrendorf M, Swirski FK. Abandoning M1/M2 for a Network Model of Macrophage Function. Circulation Research. 2016;119(3):414-7.

52. van Furth R, Cohn ZA, Hirsch JG, Humphrey JH, Spector WG, Langevoort HL. The mononuclear phagocyte system: a new classification of macrophages, monocytes, and their precursor cells. Bulletin of the World Health Organization. 1972;46(6):845-52.

53. Ginhoux F, Guilliams M. Tissue-resident macrophage ontogeny and homeostasis. Immunity. 2016;44(3):439-49.

54. Fogg DK, Sibon C, Miled C, Jung S, Aucouturier P, Littman DR, et al. A clonogenic bone marrow progenitor specific for macrophages and dendritic cells. Science. 2006;311(5757):83-7.

55. Medvinsky A, Rybtsov S, Taoudi S. Embryonic origin of the adult hematopoietic system: advances and questions. Development. 2011;138(6):1017-31.

56. Gomez Perdiguero E, Klapproth K, Schulz C, Busch K, Azzoni E, Crozet L, et al. Tissue-resident macrophages originate from yolk-sac-derived erythro-myeloid progenitors. Nature. 2015;518(7540):547-51.

57. Schulz C, Perdiguero EG, Chorro L, Szabo-Rogers H, Cagnard N, Kierdorf K, et al. A lineage of myeloid cells independent of Myb and hematopoietic stem cells. Science. 2012;336(6077):86.

58. Hoeffel G, Chen J, Lavin Y, Low D, Almeida Francisca F, See P, et al. C-Myb+ erythro-myeloid progenitor-derived fetal monocytes give rise to adult tissue-resident macrophages. Immunity. 2015;42(4):665-78.

59. Epelman S, Lavine Kory J, Beaudin Anna E, Sojka Dorothy K, Carrero Javier A, Calderon B, et al. Embryonic and adult-derived resident cardiac macrophages are maintained through distinct mechanisms at steady state and during Inflammation. Immunity. 2014;40(1):91-104.

60. Heidt T, Courties G, Dutta P, Sager H, Sebas M, Iwamoto Y, et al. Differential contribution of monocytes to heart macrophages in steady-state and after myocardial infarction. Circulation Research. 2014;115(2):284-95.

61. Molawi K, Wolf Y, Kandalla PK, Favret J, Hagemeyer N, Frenzel K, et al. Progressive replacement of embryo-derived cardiac macrophages with age. The Journal of Experimental Medicine. 2014;211(11):2151-8.

62. Hume DA, Gordon S. Mononuclear phagocyte system of the mouse defined by immunohistochemical localization of antigen F4/80. Identification of resident macrophages in renal medullary and cortical interstitium and the juxtaglomerular complex. The Journal of Experimental Medicine. 1983;157(5):1704–9.

63. Austyn JM, Gordon S. F4/80, a monoclonal antibody directed specifically against the mouse macrophage. European Journal of Immunology. 1981;11(10):805-15.

64. Langenhan T, Aust G, Hamann J. Sticky Signaling—Adhesion Class G Protein–Coupled Receptors Take the Stage. Science Signaling. 2013;6(276):re3.

65. Lin HH, Faunce DE, Stacey M, Terajewicz A, Nakamura T, Zhang-Hoover J, et al. The macrophage F4/80 receptor is required for the induction of antigen-specific efferent regulatory T cells in peripheral tolerance. The Journal of Experimental Medicine. 2005;201(10):1615-25.

66. Holness CL, Simmons DL. Molecular cloning of CD68, a human macrophage marker related to lysosomal glycoproteins. Blood. 1993;81(6):1607-13.

67. Gordon S, Plüddemann A, Martinez Estrada F. Macrophage heterogeneity in tissues: phenotypic diversity and functions. Immunological Reviews. 2014;262(1):36-55.

68. Iqbal AJ, McNeill E, Kapellos TS, Regan-Komito D, Norman S, Burd S, et al. Human CD68 promoter GFP transgenic mice allow analysis of monocyte to macrophage differentiation in vivo. Blood.124(15):e33-44.

69. Imai T, Hieshima K, Haskell C, Baba M, Nagira M, Nishimura M, et al. Identification and molecular characterization of fractalkine receptor CX3CR1, which mediates both leukocyte migration and adhesion. Cell. 1997;91(4):521-30.

70. Jung S, Aliberti J, Graemmel P, Sunshine MJ, Kreutzberg GW, Sher A, et al. Analysis of fractalkine receptor CX3CR1 function by targeted deletion and green fluorescent protein reporter gene insertion. Molecular and Cellular Biology. 2000;20(11):4106-14.

71. Parkhurst CN, Yang G, Ninan I, Savas JN, Yates JR, Lafaille JJ, et al. Microglia promote learning-dependent synapse formation through BDNF. Cell. 2013;155(7):1596-609.

72. Ryan GR, Dai X-M, Dominguez MG, Tong W, Chuan F, Chisholm O, et al. Rescue of the colony-stimulating factor 1 (CSF-1)–nullizygous mouse phenotype with a CSF-1 transgene and identification of sites of local CSF-1 synthesis. Blood. 2001;98(1):74-84.

73. Mossadegh-Keller N, Sarrazin S, Kandalla PK, Espinosa L, Stanley ER, Nutt SL, et al. M-CSF instructs myeloid lineage fate in single haematopoietic stem cells. Nature. 2013;497(7448):239-43.

74. Sherr CJ, Rettenmier CW, Sacca R, Roussel MF, Look AT, Stanley ER. The c-fms proto-oncogene product is related to the receptor for the mononuclear phagocyte growth factor, CSF 1. Cell. 1985;41(3):665-76.

75. Visvader J, Verma IM. Differential transcription of exon 1 of the human c-fms gene in placental trophoblasts and monocytes. Molecular and Cellular Biology. 1989;9(3):1336-41.

76. Nandi S, Gokhan S, Dai X-M, Wei S, Enikolopov G, Lin H, et al. The CSF-1 receptor ligands IL-34 and CSF-1 exhibit distinct developmental brain expression patterns and regulate neural progenitor cell maintenance and maturation. Developmental Biology. 2012;367(2):100-13.

77. Menke J, Iwata Y, Rabacal WA, Basu R, Yeung YG, Humphreys BD, et al. CSF-1 signals directly to renal tubular epithelial cells to mediate repair in mice. The Journal of Clinical Investigation. 2009;119(8):2330-42.

78. Sasmono RT, Oceandy D, Pollard JW, Tong W, Pavli P, Wainwright BJ, et al. A macrophage colony-stimulating factor receptor–green fluorescent protein transgene is expressed throughout the mononuclear phagocyte system of the mouse. Blood. 2003;101(3):1155-63.

79. Olson MC, Scott EW, Hack AA, Su GH, Tenen DG, Singh H, et al. PU.1 is not essential for early myeloid gene expression but is required for terminal myeloid differentiation. Immunity. 1995;3(6):703-14.

80. McKercher SR, Torbett BE, Anderson KL, Henkel GW, Vestal DJ, Baribault H, et al. Targeted disruption of the PU.1 gene results in multiple hematopoietic abnormalities. The EMBO Journal. 1996;15(20):5647-58.

81. Scott EW, Simon MC, Anastasi J, Singh H. Requirement of transcription factor PU.1 in the development of multiple hematopoietic lineages. Science. 1994; 9(265):1573-7.

82. Satoh J-i, Asahina N, Kitano S, Kino Y. A comprehensive profile of ChIP-seq-based PU.1/Spi1 target genes in microglia. Gene Regulation and Systems Biology. 2014;8:127-39.

83. Lichanska AM, Browne CM, Henkel GW, Murphy KM, Ostrowski MC, McKercher SR, et al. Differentiation of the mononuclear phagocyte system during mouse embryogenesis: the role of transcription factor PU.1. Blood. 1999;94(1):127-38.

84. Leid JM, Carrelha J, Boukarabila H, Epelman S, Jacobsen SE, Lavine KJ. Primitive embryonic macrophages are required for coronary development and maturation. Circulation Research. 2016;118(10):1498-511.

85. Stevens SM, von Gise A, VanDusen N, Bin Z, Pu WT. Epicardium is required for cardiac seeding by yolk sac macrophages, precursors of resident macrophages of the adult heart. Developmental Biology. 2016;413(2):153-9.

86. Hulsmans M, Clauss S, Xiao L, Aguirre AD, King KR, Hanley A, et al. Macrophages facilitate electrical conduction in the heart. Cell. 2017;169(3):510-22.e20.

87. Zou N, Ao L, Cleveland JC, Yang X, Su X, Cai G-Y, et al. Critical role of extracellular heat shock cognate protein 70 in the myocardial inflammatory response and cardiac dysfunction after global ischemia-reperfusion. American Journal of Physiology - Heart and Circulatory Physiology. 2008;294(6):H2805-13.

88. Huebener P, Abou-Khamis T, Zymek P, Bujak M, Ying X, Chatila K, et al. CD44 Is critically involved in infarct healing by regulating the inflammatory and fibrotic response. The Journal of Immunology. 2008;180(4):2625-33.

89. Ivey CL, Williams FM, Collins PD, Jose PJ, Williams TJ. Neutrophil chemoattractants generated in two phases during reperfusion of ischemic myocardium in the rabbit. Evidence for a role for C5a and interleukin-8. The Journal of Clinical Investigation. 1995;95(6):2720-8.

90. Dewald O, Zymek P, Winkelmann K, Koerting A, Ren G, Abou-Khamis T, et al. CCL2/Monocyte chemoattractant protein-1 regulates inflammatory responses critical to healing myocardial infarcts. Circulation Research. 2005;96(8):881-9.

91. Nahrendorf M, Swirski FK, Aikawa E, Stangenberg L, Wurdinger T, Figueiredo J-L, et al. The healing myocardium sequentially mobilizes two monocyte subsets with divergent and complementary functions. The Journal of Experimental Medicine. 2007;204(12):3037-47.

92. Hilgendorf I, Gerhardt LMS, Tan TC, Winter C, Holderried TAW, Chousterman BG, et al. Ly-6Chigh monocytes depend on Nr4a1 to balance both inflammatory and reparative phases in the infarcted myocardium. Circulation Research. 2014;114(10):1611-22.

93. Wan E, Yeap XY, Dehn S, Terry R, Novak M, Zhang S, et al. Enhanced efferocytosis of apoptotic cardiomyocytes through myeloid-epithelial-reproductive tyrosine kinase links acute inflammation resolution to cardiac repair after infarction. Circulation Research. 2013;113(8):1004-12.

94. Korf-Klingebiel M, Reboll MR, Klede S, Brod T, Pich A, Polten F, et al. Myeloid-derived growth factor (C19orf10) mediates cardiac repair following myocardial infarction. Nature Medicine. 2015;21(2):140-9.

95. van Amerongen MJ, Harmsen MC, van Rooijen N, Petersen AH, van Luyn MJA. Macrophage depletion impairs wound healing and increases left ventricular remodeling after myocardial injury in mice. The American Journal of Pathology. 2007;170(3):818-29.

96. Leuschner F, Rauch PJ, Ueno T, Gorbatov R, Marinelli B, Lee WW, et al. Rapid monocyte kinetics in acute myocardial infarction are sustained by extramedullary monocytopoiesis. The Journal of Experimental Medicine. 2012;209(1):123-37.

97. Vieira J, Norman S, Cahill TJ, Villa Del Campo C, Rohling M, D.N. B, et al. Immunomodulation via the cardiac lymphatic system to improve heart repair. Manuscript submitted. 2017.

98. Maekawa Y, Anzai T, Yoshikawa T, Asakura Y, Takahashi T, Ishikawa S, et al. Prognostic significance of peripheral monocytosis after reperfused acute myocardial infarction:a possible role for left ventricular remodeling. Journal of the American College of Cardiology. 2002;39(2):241-6.

99. Frangogiannis NG, Dewald O, Xia Y, Ren G, Haudek S, Leucker T, et al. Critical role of monocyte chemoattractant protein-1/CC chemokine ligand 2 in the pathogenesis of ischemic cardiomyopathy. Circulation. 2007;115(5):584-92.

100. Han C, Nie Y, Lian H, Liu R, He F, Huang H, et al. Acute inflammation stimulates a regenerative response in the neonatal mouse heart. Cell Research. 2015;25(10):1137-51.

101. Aurora AB, Porrello ER, Tan W, Mahmoud AI, Hill JA, Bassel-Duby R, et al. Macrophages are required for neonatal heart regeneration. The Journal of Clinical Investigation. 2014;124(3):1382-92.

102. Lavine KJ, Epelman S, Uchida K, Weber KJ, Nichols CG, Schilling JD, et al. Distinct macrophage lineages contribute to disparate patterns of cardiac recovery and remodeling in the neonatal and adult heart. Proceedings of the National Academy of Sciences. 2014;111(45):16029-34.

103. Madisen L, Zwingman TA, Sunkin SM, Oh SW, Zariwala HA, Gu H, et al. A robust and high-throughput Cre reporting and characterization system for the whole mouse brain. Nature Neuroscience. 2010;13(1):133-40.

104. Srinivas S, Watanabe T, Lin C-S, William CM, Tanabe Y, Jessell TM, et al. Cre reporter strains produced by targeted insertion of EYFP and ECFP into the ROSA26 locus. BMC Developmental Biology. 2001;1:4.

105. Qian B-Z, Li J, Zhang H, Kitamura T, Zhang J, Campion LR, et al. CCL2 recruits inflammatory monocytes to facilitate breast tumor metastasis. Nature. 2011;475(7355):222-5.

106. Benz C, Martins VC, Radtke F, Bleul CC. The stream of precursors that colonizes the thymus proceeds selectively through the early T lineage precursor stage of T cell development. The Journal of Experimental Medicine. 2008;205(5):1187-99.

107. Zheng B, Zhang Z, Black CM, de Crombrugghe B, Denton CP. Ligand-dependent genetic recombination in fibroblasts: a potentially powerful technique for investigating gene function in fibrosis. The American Journal of Pathology. 2002;160(5):1609-17.

108. Masters M. Epicardial signalling in mammalian heart regeneration: University of Oxford; 2015.

109. Pinto AR, Chandran A, Rosenthal NA, Godwin JW. Isolation and analysis of single cells from the mouse heart. Journal of Immunological Methods. 2013;393(1–2):74-80.

110. Buckingham M, Meilhac S, Zaffran S. Building the mammalian heart from two sources of myocardial cells. Nature Reviews Genetics. 2005;6(11):826-37.

111. Xin M, Olson EN, Bassel-Duby R. Mending broken hearts: cardiac development as a basis for adult heart regeneration and repair. Nature Reviews Molecular Cell Biology. 2013;14(8):529-41.

112. Srivastava D. Making or breaking the heart: from lineage determination to morphogenesis. Cell. 2006;126(6):1037-48.

113. Hutchins GM, Kessler-Hanna A, Moore GW. Development of the coronary arteries in the embryonic human heart. Circulation. 1988;77(6):1250-7.

114. Red-Horse K, Ueno H, Weissman IL, Krasnow MA. Coronary arteries form by developmental reprogramming of venous cells. Nature. 2010;464(7288):549-53.

115. Tian X, Hu T, Zhang H, He L, Huang X, Liu Q, et al. Subepicardial endothelial cells invade the embryonic ventricle wall to form coronary arteries. Cell Research. 2013;23(9):1075-90.

116. Katz TC, Singh MK, Degenhardt K, Rivera-Feliciano J, Johnson RL, Epstein JA, et al. Distinct compartments of the proepicardial organ give rise to coronary vascular endothelial cells. Developmental Cell. 2012;22(3):639-50.

117. Hirakow R. Development of the cardiac blood vessels in staged human embryos. Acta Anatomica. 1983;115(3):220-30.

118. Chen HI, Poduri A, Numi H, Kivela R, Saharinen P, McKay AS, et al. VEGF-C and aortic cardiomyocytes guide coronary artery stem development. The Journal of Clinical Investigation. 2014;124(11):4899-914.

119. Watanabe T, Koibuchi N, Chin MT. Transcription factor CHF1/Hey2 regulates coronary vascular maturation. Mechanisms of Development. 2010;127(9–12):418-27.

120. Volz KS, Jacobs AH, Chen HI, Poduri A, McKay AS, Riordan DP, et al. Pericytes are progenitors for coronary artery smooth muscle. eLife. 2015;4:e10036.

121. Kampmeier OF. On the lymph flow of the human heart, with reference to the development of the channels and the first appearance, distribution, and physiology of their valves. American Heart Journal. 1928;4(2):210-22.

122. Aspelund A, Robciuc MR, Karaman S, Makinen T, Alitalo K. Lymphatic system in cardiovascular medicine. Circulation Research. 2016;118(3):515-30.

123. Klotz L, Norman S, Vieira JM, Masters M, Rohling M, Dube KN, et al. Cardiac lymphatics are heterogeneous in origin and respond to injury. Nature. 2015;522(7554):62-7.

124. Flaht A, Jankowska-Steifer E, Radomska DM, Madej M, Gula G, Kujawa M, et al. Cellular phenotypes and spatio-temporal patterns of lymphatic vessel development in embryonic mouse hearts. Developmental Dynamics. 2012;241(9):1473-86.

125. Tian X, Hu T, Zhang H, He L, Huang X, Liu Q, et al. De novo formation of a distinct coronary vascular population in neonatal heart. Science. 2014;345(6192):90-4.

126. Sabin FR. On the origin of the lymphatic system from the veins and the development of the lymph hearts and thoracic duct in the pig. American Journal of Anatomy. 1902;1(3):367-89.

127. Stanczuk L, Martinez-Corral I, Ulvmar MH, Zhang Y, Laviña B, Fruttiger M, et al. cKit lineage hemogenic endothelium-derived cells contribute to mesenteric lymphatic vessels. Cell Reports. 2015;10(10):1708-21.

128. Martinez-Corral I, Ulvmar MH, Stanczuk L, Tatin F, Kizhatil K, John SW, et al. Nonvenous origin of dermal lymphatic vasculature. Circulation Research. 2015;116(10):1649-54.

129. Manasek FJ. Myocardial cell death in the embryonic chick ventricle. Journal of Embryology and Experimental Morphology. 1969;21(2):271-84.

130. Pexieder T. Cell death in the morphogenesis and teratogenesis of the heart. Advances in Anatomy, Embryology and Cell Biology. 1975;51(3):3-99.

131. Pexieder T. The tissue dynamics of heart morphogenesis I. The phenomena of cell death. Zeitschrift für Anatomie und Entwicklungsgeschichte. 1972;137(3):270-84.

132. Sorokin SP, McNelly NA, Hoyt RF. Early development of macrophages in intact and organ cultured hearts of rat embryos. The Anatomical Record. 1994;239(3):306-14.

133. Fantin A, Vieira JM, Gestri G, Denti L, Schwarz Q, Prykhozhij S, et al. Tissue macrophages act as cellular chaperones for vascular anastomosis downstream of VEGF-mediated endothelial tip cell induction. Blood. 2010;116(5):829-40.

134. Brachtendorf G, Kuhn A, Samulowitz U, Knorr R, Gustafsson E, Potocnik AJ, et al. Early expression of endomucin on endothelium of the mouse embryo and on putative hematopoietic clusters in the dorsal aorta. Developmental Dynamics. 2001;222(3):410-9.

135. Cavallero S, Shen H, Yi C, Lien C-L, Kumar SR, Sucov HM. CXCL12 signaling is essential for maturation of the ventricular coronary endothelial plexus and establishment of functional coronary circulation. Developmental Cell. 2015;33(4):469-77.

136. Pinto AR, Paolicelli R, Salimova E, Gospocic J, Slonimsky E, Bilbao-Cortes D, et al. An abundant tissue macrophage population in the adult murine heart with a distinct alternatively-activated macrophage profile. PLOS ONE. 2012;7(5):e36814.

137. Boyer SW, Schroeder AV, Smith-Berdan S, Forsberg EC. All hematopoietic cells develop from hematopoietic stem cells through Flk2/Flt3-positive progenitor cells. Cell stem cell. 2011;9(1):64-73.

138. Koni PA, Joshi SK, Temann U-A, Olson D, Burkly L, Flavell RA. Conditional vascular cell adhesion molecule 1 deletion in mice. The Journal of Experimental Medicine. 2001;193(6):741-54.

139. Maruyama K, Ii M, Cursiefen C, Jackson DG, Keino H, Tomita M, et al. Inflammation-induced lymphangiogenesis in the cornea arises from CD11b-positive macrophages. The Journal of Clinical Investigation. 2005;115(9):2363-72.

140. Religa P, Cao R, Bjorndahl M, Zhou Z, Zhu Z, Cao Y. Presence of bone marrow–derived circulating progenitor endothelial cells in the newly formed lymphatic vessels. Blood. 2005;106(13):4184-90.

141. Lee JY, Park C, Cho YP, Lee E, Kim H, Kim P, et al. Podoplanin-expressing cells derived from bone marrow play a crucial role in postnatal lymphatic neovascularization. Circulation. 2010;122(14):1413-25.

142. Zumsteg A, Baeriswyl V, Imaizumi N, Schwendener R, Rüegg C, Christofori G. Myeloid cells contribute to tumor lymphangiogenesis. PLOS ONE. 2009;4(9):e7067.

143. Hall KL, Volk-Draper LD, Flister MJ, Ran S. New model of macrophage acquisition of the lymphatic endothelial phenotype. PLOS ONE. 2012;7(3):e31794.

144. Parkhurst Christopher N, Yang G, Ninan I, Savas Jeffrey N, Yates Iii John R, Lafaille Juan J, et al. Microglia promote learning-dependent synapse formation through Brain-Derived Neurotrophic Factor. Cell. 2013;155(7):1596-609.

145. Kretzschmar K, Watt Fiona M. Lineage Tracing. Cell. 2012;148(1–2):33-45.

146. Kerjaschki D, Huttary N, Raab I, Regele H, Bojarski-Nagy K, Bartel G, et al. Lymphatic endothelial progenitor cells contribute to de novo lymphangiogenesis in human renal transplants. Nature Medicine. 2006;12(2):230-4.

147. Li J, Chen K, Zhu L, Pollard JW. Conditional deletion of the colony stimulating factor-1 receptor (c-fms proto-oncogene) in mice. Genesis. 2006;44(7):328-35.

148. Erblich B, Zhu L, Etgen AM, Dobrenis K, Pollard JW. Absence of colony stimulation factor-1 receptor results in loss of microglia, disrupted brain development and olfactory deficits. PLOS ONE. 2011;6(10):e26317.

149. Chitu V, Stanley ER. Colony-stimulating factor-1 in immunity and inflammation. Current Opinion in Immunology. 2006;18(1):39-48.

150. Pollard JW. Trophic macrophages in development and disease. Nature Reviews Immunology. 2009;9(4):259-70.

151. Yoshida H, Hayashi S-I, Kunisada T, Ogawa M, Nishikawa S, Okamura H, et al. The murine mutation osteopetrosis is in the coding region of the macrophage colony stimulating factor gene. Nature. 1990;345(6274):442-4.

152. Dai X-M, Ryan GR, Hapel AJ, Dominguez MG, Russell RG, Kapp S, et al. Targeted disruption of the mouse colony-stimulating factor 1 receptor gene results in osteopetrosis, mononuclear phagocyte deficiency, increased primitive progenitor cell frequencies, and reproductive defects. Blood. 2002;99(1):111-20.

153. Lin H, Lee E, Hestir K, Leo C, Huang M, Bosch E, et al. Discovery of a cytokine and Its receptor by functional screening of the extracellular proteome. Science. 2008;320(5877):807-11.

154. Burda P, Laslo P, Stopka T. The role of PU.1 and GATA-1 transcription factors during normal and leukemogenic hematopoiesis. Leukemia. 2010;24(7):1249-57.

155. Kim HG, de Guzman CG, Swindle CS, Cotta CV, Gartland L, Scott EW, et al. The ETS family transcription factor PU.1 is necessary for the maintenance of fetal liver hematopoietic stem cells. Blood. 2004;104(13):3894-900.

156. Iwasaki H, Somoza C, Shigematsu H, Duprez EA, Iwasaki-Arai J, Mizuno S-i, et al. Distinctive and indispensable roles of PU.1 in maintenance of hematopoietic stem cells and their differentiation. Blood. 2005;106(5):1590-600.

157. Chow A, Brown BD, Merad M. Studying the mononuclear phagocyte system in the molecular age. Nature Reviews Immunology. 2011;11(11):788-98.

158. van Rooijen N, van Kesteren-Hendrikx E. Clodronate liposomes: perspectives in research and therapeutics. Journal of Liposome Research. 2002;12(1-2):81-94.

159. MacDonald KPA, Palmer JS, Cronau S, Seppanen E, Olver S, Raffelt NC, et al. An antibody against the colony-stimulating factor 1 receptor depletes the resident subset of monocytes and tissue- and tumor-associated macrophages but does not inhibit inflammation. Blood. 2010;116(19):3955-63.

160. Ivanova A, Signore M, Caro N, Greene NDE, Copp AJ, Martinez-Barbera JP. In vivo genetic ablation by Cre-mediated expression of diphtheria toxin fragment A. Genesis 2005;43(3):129-35.

161. Li H, Demetris AJ, McNiff J, Matte-Martone C, Tan HS, Rothstein DM, et al. Profound depletion of host conventional dendritic cells, plasmacytoid dendritic cells and B cells does not prevent GVHD induction. Journal of Immunology. 2012;188(8):3804-11.

162. Birnberg T, Bar-On L, Sapoznikov A, Caton ML, Cervantes-Barragán L, Makia D, et al. Lack of conventional dendritic cells ic compatible with normal development and T cell homeostasis, but causes myeloid proliferative syndrome. Immunity.29(6):986-97.

163. Wiktor-Jedrzejczak W, Bartocci A, Ferrante AW, Ahmed-Ansari A, Sell KW, Pollard JW, et al. Total absence of colony-stimulating factor 1 in the macrophage-deficient osteopetrotic (op/op) mouse. Proceedings of the National Academy of Sciences. 1990;87(12):4828-32.

164. Van Wesenbeeck L, Odgren PR, MacKay CA, D'Angelo M, Safadi FF, Popoff SN, et al. The osteopetrotic mutation toothless (tl) is a loss-of-function frameshift mutation in the rat Csf1 gene: Evidence of a crucial role for CSF-1 in osteoclastogenesis and endochondral ossification. Proceedings of the National Academy of Sciences. 2002;99(22):14303-8.

165. Tondravi MM, McKercher SR, Anderson K, Erdmann JM, Quiroz M, Maki R, et al. Osteopetrosis in mice lacking haematopoietic transcription factor PU.1. Nature. 1997;386(6620):81-4.

166. Edwards JR, Mundy GR. Advances in osteoclast biology: old findings and new insights from mouse models. Nature Reviews Rheumatology. 2011;7(4):235-43.

167. Prinz M, Priller J. Microglia and brain macrophages in the molecular age: from origin to neuropsychiatric disease. Nature Reviews Neuroscience. 2014;15(5):300-12.

168. Michaelson MD, Bieri PL, Mehler MF, Xu H, Arezzo JC, Pollard JW, et al. CSF-1 deficiency in mice results in abnormal brain development. Development. 1996;122(9):2661-72.

169. Cunningham CL, Martínez-Cerdeño V, Noctor SC. Microglia regulate the number of neural precursor cells in the developing cerebral cortex. The Journal of Neuroscience. 2013;33(10):4216-33.

170. Sierra A, Encinas JM, Deudero JJP, Chancey JH, Enikolopov G, Overstreet-Wadiche LS, et al. Microglia shape adult hippocampal neurogenesis through apoptosis-coupled phagocytosis. Cell Stem Cell. 2010;7(4):483-95.

171. Paolicelli RC, Bolasco G, Pagani F, Maggi L, Scianni M, Panzanelli P, et al. Synaptic pruning by microglia is necessary for normal brain development. Science. 2011;333(6048):1456-8.

172. Rademakers R, Baker M, Nicholson AM, Rutherford NJ, Finch N, Soto-Ortolaza A, et al. Mutations in the colony stimulating factor 1 receptor (CSF1R) cause hereditary diffuse leukoencephalopathy with spheroids. Nature genetics. 2012;44(2):200-5.

173. Diez-Roux G, Argilla M, Makarenkova H, Ko K, Lang RA. Macrophages kill capillary cells in G1 phase of the cell cycle during programmed vascular regression. Development. 1999;126(10):2141-7.

174. Lobov IB, Rao S, Carroll TJ, Vallance JE, Ito M, Ondr JK, et al. WNT7b mediates macrophage-induced programmed cell death in patterning of the vasculature. Nature. 2005;437(7057):417-21.

175. Gordon EJ, Rao S, Pollard JW, Nutt SL, Lang RA, Harvey NL. Macrophages define dermal lymphatic vessel calibre during development by regulating lymphatic endothelial cell proliferation. Development. 2010;137(22):3899-910.

176. Chazaud B, Sonnet C, Lafuste P, Bassez G, Rimaniol A-C, Poron F, et al. Satellite cells attract monocytes and use macrophages as a support to escape apoptosis and enhance muscle growth. The Journal of Cell Biology. 2003;163(5):1133-43.

177. Gouon-Evans V, Rothenberg ME, Pollard JW. Postnatal mammary gland development requires macrophages and eosinophils. Development. 2000;127(11):2269-82.

178. Banaei-Bouchareb L, Gouon-Evans V, Samara-Boustani D, Castellotti MC, Czernichow P, Pollard JW, et al. Insulin cell mass is altered in Csf1op/Csf1op macrophage-deficient mice. Journal of Leukocyte Biology. 2004;76(2):359-67.

179. Qiu Y, Nguyen Khoa D, Odegaard Justin I, Cui X, Tian X, Locksley Richard M, et al. Eosinophils and type 2 cytokine signaling in macrophages orchestrate development of functional beige fat. Cell. 2014;157(6):1292-308.

180. Zudaire E, Gambardella L, Kurcz C, Vermeren S. A Computational Tool for Quantitative Analysis of Vascular Networks. PLOS ONE. 2011;6(11):e27385.

181. Schoppmann SF, Birner P, Stöckl J, Kalt R, Ullrich R, Caucig C, et al. Tumor-associated macrophages express lymphatic endothelial growth factors and are related to peritumoral lymphangiogenesis. The American Journal of Pathology. 2002;161(3):947-56.

182. Chen HI, Sharma B, Akerberg BN, Numi HJ, Kivela R, Saharinen P, et al. The sinus venosus contributes to coronary vasculature through VEGFC-stimulated angiogenesis. Development. 2014;141(23):4500-12.

183. Ochsenbein AM, Karaman S, Proulx ST, Goldmann R, Chittazhathu J, Dasargyri A, et al. Regulation of lymphangiogenesis in the diaphragm by macrophages and VEGFR-3 signaling. Angiogenesis. 2016;19(4):513-24.

184. Kubota Y, Takubo K, Shimizu T, Ohno H, Kishi K, Shibuya M, et al. M-CSF inhibition selectively targets pathological angiogenesis and lymphangiogenesis. J Exp Med. 2009;206(5):1089-102.

185. James JM, Nalbandian A, Mukouyama Y-s. TGFβ signaling is required for sprouting lymphangiogenesis during lymphatic network development in the skin. Development. 2013;140(18):3903-14.

186. Bonnans C, Chou J, Werb Z. Remodelling the extracellular matrix in development and disease. Nature reviews Molecular cell biology. 2014;15(12):786-801.

187. Detry B, Erpicum C, Paupert J, Blacher S, Maillard C, Bruyère F, et al. Matrix metalloproteinase-2 governs lymphatic vessel formation as an interstitial collagenase. Blood. 2012;119(21):5048-56.

188. Stefater JA, 3rd, Lewkowich I, Rao S, Mariggi G, Carpenter AC, Burr AR, et al. Regulation of angiogenesis by a non-canonical Wnt-Flt1 pathway in myeloid cells. Nature. 2011;474(7352):511-5.

189. Outtz HH, Tattersall IW, Kofler NM, Steinbach N, Kitajewski J. Notch1 controls macrophage recruitment and Notch signaling is activated at sites of endothelial cell anastomosis during retinal angiogenesis in mice. Blood. 2011;118(12):3436-9.

190. Gurtner GC, Werner S, Barrandon Y, Longaker MT. Wound repair and regeneration. Nature. 2008;453(7193):314-21.

191. Eming SA, Martin P, Tomic-Canic M. Wound repair and regeneration: mechanisms, signaling, and translation. Science Translational Medicine. 2014;6(265):265sr6.

192. Larson BJ, Longaker MT, Lorenz HP. Scarless fetal wound healing: a basic science review. Plastic and Reconstructive surgery. 2010;126(4):1172-80.

193. Han M, Yang X, Lee J, Allan CH, Muneoka K. Development and regeneration of the neonatal digit tip in mice. Developmental Biology. 2008;315(1):125-35.

194. Cox BC, Chai R, Lenoir A, Liu Z, Zhang L, Nguyen D-H, et al. Spontaneous hair cell regeneration in the neonatal mouse cochlea in vivo. Development (Cambridge, England). 2014;141(4):816-29.

195. Graziadei PP, Levine RR, Graziadei GA. Regeneration of olfactory axons and synapse formation in the forebrain after bulbectomy in neonatal mice. Proceedings of the National Academy of Sciences. 1978;75(10):5230-4.

196. Gourdie RG, Dimmeler S, Kohl P. Novel therapeutic strategies targeting fibroblasts and fibrosis in heart disease. Nature Reviews Drug Discovery. 2016;15(9):620-38.

197. Martin P. Wound healing - aiming for perfect skin regeneration. Science. 1997;276(5309):75-81.

198. Eming SA, Krieg T, Davidson JM. Inflammation in Wound Repair: Molecular and Cellular Mechanisms. Journal of Investigative Dermatology. 2007;127(3):514-25.

199. Minutti CM, Knipper JA, Allen JE, Zaiss DMW. Tissue-specific contribution of macrophages to wound healing. Seminars in Cell & Developmental Biology. 2017;61:3-11.

200. Leibovich SJ, Ross R. The role of the macrophage in wound repair. A study with hydrocortisone and antimacrophage serum. The American Journal of Pathology. 1975;78(1):71-100.

201. Goren I, Allmann N, Yogev N, Schürmann C, Linke A, Holdener M, et al. A transgenic mouse model of inducible macrophage depletion: effects of diphtheria toxin-driven lysozyme M-specific cell lineage ablation on wound inflammatory, angiogenic, and contractive processes. The American Journal of Pathology. 2009;175(1):132-47.

202. Lucas T, Waisman A, Ranjan R, Roes J, Krieg T, Müller W, et al. Differential roles of macrophages in diverse phases of skin repair. The Journal of Immunology. 2010;184(7):3964.

203. Martin P, D'Souza D, Martin J, Grose R, Cooper L, Maki R, et al. Wound Healing in the PU.1 Null Mouse—Tissue Repair Is Not Dependent on Inflammatory Cells. Current Biology. 2003;13(13):1122-8.

204. Koh TJ, DiPietro LA. Inflammation and wound healing: The role of the macrophage. Expert Reviews in Molecular Medicine. 2011;13:e23-e.

205. Fadok VA, Bratton DL, Konowal A, Freed PW, Westcott JY, Henson PM. Macrophages that have ingested apoptotic cells in vitro inhibit proinflammatory cytokine production through autocrine/paracrine mechanisms involving TGF-beta, PGE2, and PAF. Journal of Clinical Investigation. 1998;101(4):890-8.

206. Wynn TA, Barron L. Macrophages: master regulators of inflammation and fibrosis. Seminars in Liver Disease. 2010;30(3):245-57.

207. Kaviratne M, Hesse M, Leusink M, Cheever AW, Davies SJ, McKerrow JH, et al. IL-13 activates a mechanism of tissue fibrosis that is completely TGF-β independent. The Journal of Immunology. 2004;173(6):4020.

208. Oga T, Matsuoka T, Yao C, Nonomura K, Kitaoka S, Sakata D, et al. Prostaglandin F2[alpha] receptor signaling facilitates bleomycin-induced pulmonary fibrosis independently of transforming growth factor-[beta]. Nature Medicine. 2009;15(12):1426-30.

209. Gratchev A, Guillot P, Hakiy N, Politz O, Orfanos CE, Schledzewski K, et al. Alternatively activated macrophages differentially express fibronectin and its splice variants and the extracellular matrix protein βIG-H3. Scandinavian Journal of Immunology. 2001;53(4):386-92.

210. Murry CE, Giachelli CM, Schwartz SM, Vracko R. Macrophages express osteopontin during repair of myocardial necrosis. The American Journal of Pathology. 1994;145(6):1450-62.

211. Mori R, Shaw TJ, Martin P. Molecular mechanisms linking wound inflammation and fibrosis: knockdown of osteopontin leads to rapid repair and reduced scarring. The Journal of Experimental Medicine. 2008;205(1):43.

212. Rittling SR. Osteopontin in macrophage function. Expert Reviews in Molecular Medicine. 2011;13:e15.

213. Aurora AB, Olson EN. Immune modulation of stem cells and regeneration. Cell Stem Cell. 2014;15(1):14-25.

214. Godwin JW, Pinto AR, Rosenthal NA. Macrophages are required for adult salamander limb regeneration. Proceedings of the National Academy of Sciences. 2013;110(23):9415-20.

215. Arnold L, Henry A, Poron F, Baba-Amer Y, van Rooijen N, Plonquet A, et al. Inflammatory monocytes recruited after skeletal muscle injury switch into antiinflammatory macrophages to support myogenesis. The Journal of Experimental Medicine. 2007;204(5):1057-69.

216. Zordan P, Rigamonti E, Freudenberg K, Conti V, Azzoni E, Rovere-Querini P, et al. Macrophages commit postnatal endothelium-derived progenitors to angiogenesis and restrict endothelial to mesenchymal transition during muscle regeneration. Cell Death & Disease. 2014;5:e1031.

217. Chen CC, Wang L, Plikus Maksim V, Jiang Ting X, Murray Philip J, Ramos R, et al. Organ-level quorum sensing directs regeneration in hair stem cell populations. Cell. 2015;161(2):277-90.

218. Boulter L, Govaere O, Bird TG, Radulescu S, Ramachandran P, Pellicoro A, et al. Macrophage-derived Wnt opposes Notch signaling to specify hepatic progenitor cell fate in chronic liver disease. Nature Medicine. 2012;18(4):572-9.

219. Sindrilaru A, Peters T, Wieschalka S, Baican C, Baican A, Peter H, et al. An unrestrained proinflammatory M1 macrophage population induced by iron impairs wound healing in humans and mice. The Journal of Clinical Investigation. 2011;121(3):985-97.

220. Mirza RE, Fang MM, Weinheimer-Haus EM, Ennis WJ, Koh TJ. Sustained inflammasome activity in macrophages impairs wound healing in type 2 diabetic humans and mice. Diabetes. 2014;63(3):1103-14.

221. Shiraishi M, Shintani Y, Shintani Y, Ishida H, Saba R, Yamaguchi A, et al. Alternatively activated macrophages determine repair of the infarcted adult murine heart. The Journal of Clinical Investigation. 2016;126(6):2151-66.

222. Ahn D, Cheng L, Moon C, Spurgeon H, Lakatta EG, Talan MI. Induction of myocardial infarcts of a predictable size and location by branch pattern probability-assisted coronary ligation in C57BL/6 mice. American Journal of Physiology - Heart and Circulatory Physiology. 2004;286(3):H1201-7.

223. Simon AK, Hollander GA, McMichael A. Evolution of the immune system in humans from infancy to old age. Proceedings of the Royal Society B: Biological Sciences. 2015;282(1821):20143085.

224. Lorchner H, Poling J, Gajawada P, Hou Y, Polyakova V, Kostin S, et al. Myocardial healing requires Reg3beta-dependent accumulation of macrophages in the ischemic heart. Nature Medicine. 2015;21(4):353-62.

225. Frangogiannis NG. Regulation of the inflammatory response in cardiac repair. Circulation Research. 2012;110(1):159-73.

226. Nahrendorf M, Swirski Fk Fau - Aikawa E, Aikawa E Fau - Stangenberg L, Stangenberg L Fau - Wurdinger T, Wurdinger T Fau - Figueiredo J-L, Figueiredo Jl Fau - Libby P, et al. The healing myocardium sequentially mobilizes two monocyte subsets with divergent and complementary functions. The Journal of Experimental Medicine. 2007;204(12):3037-47.

227. Stein M, Keshav S, Harris N, Gordon S. Interleukin 4 potently enhances murine macrophage mannose receptor activity: a marker of alternative immunologic macrophage activation. J Exp Med. 1992;176(1):287-92.

228. Frantz S, Nahrendorf M. Cardiac macrophages and their role in ischaemic heart disease. Cardiovascular Research. 2014;102(2):240-8.

229. Ringner M. What is principal component analysis? Nature Biotechnology. 2008;26(3):303-4.

230. Deck JD, Shapiro SL. Retardation of the newt limb regeneration with semicarbazide, an inhibitor of histamine formation. The Anatomical Record. 1963;146(3):225-33.

231. Talman V, Ruskoaho H. Cardiac fibrosis in myocardial infarction-from repair and remodeling to regeneration. Cell Tissue Res. 2016;365(3):563-81.

232. Varga T, Mounier R, Horvath A, Cuvellier S, Dumont F, Poliska S, et al. Highly dynamic transcriptional signature of distinct macrophage subsets during sterile inflammation, resolution, and tissue repair. The Journal of Immunology. 2016;196(11):4771.

233. Ernst J, Bar-Joseph Z. STEM: a tool for the analysis of short time series gene expression data. BMC Bioinformatics. 2006;7(1):191.

234. Miyoshi H, Ajima R, Luo CT, Yamaguchi TP, Stappenbeck TS. Wnt5a potentiates TGF-beta signaling to promote colonic crypt regeneration after tissue injury. Science. 2012;338(6103):108-13.

235. Yu L, Han M, Yan M, Lee EC, Lee J, Muneoka K. BMP signaling induces digit regeneration in neonatal mice. Development. 2010;137(4):551-9.

236. Kollmann TR, Crabtree J, Rein-Weston A, Blimkie D, Thommai F, Wang XY, et al. Neonatal innate TLR-mediated responses are distinct from those of adults. The Journal of Immunology. 2009;183(11):7150-60.

237. Whitby DJ, Ferguson MWJ. Immunohistochemical localization of growth factors in fetal wound healing. Developmental Biology. 1991;147(1):207-15.

238. McCallion RL, Ferguson MWJ. Fetal Wound Healing and the Development of Antiscarring Therapies for Adult Wound Healing. In: Clark RAF, editor. The Molecular and Cellular Biology of Wound Repair. Boston, MA: Springer US; 1988. p. 561-600.

239. Cowin AJ, Brosnan MP, Holmes TM, Ferguson MWJ. Endogenous inflammatory response to dermal wound healing in the fetal and adult mouse. Developmental Dynamics. 1998;212(3):385-93.

240. Frantz FW, Bettinger DA, Haynes JH, Johnson DE, Harvey KM, Dalton HP, et al. Biology of fetal repair: The presence of bacteria in fetal wounds induces an adult-like healing response. Journal of Pediatric Surgery. 1993;28(3):428-34.

241. Ashcroft GS, Yang X, Glick AB, Weinstein M, Letterio JJ, Mizel DE, et al. Mice lacking Smad3 show accelerated wound healing and an impaired local inflammatory response. Nature Cell Biology. 1999;1(5):260-6.

242. Torow N, Yu K, Hassani K, Freitag J, Schulz O, Basic M, et al. Active suppression of intestinal CD4(+)TCRαβ(+) T-lymphocyte maturation during the postnatal period. Nature Communications. 2015;6:7725.

243. Elahi S, Ertelt JM, Kinder JM, Jiang TT, Zhang X, Xin L, et al. Immunosuppressive CD71(+) erythroid cells compromise neonatal host defence against infection. Nature. 2013;504(7478):158-62.

244. Lindemans CA, Calafiore M, Mertelsmann AM, O'Connor MH, Dudakov JA, Jenq RR, et al. Interleukin-22 promotes intestinal-stem-cell-mediated epithelial regeneration. Nature. 2015;528(7583):560-4.

245. Hill T, Kis an inhibitor of canonical Wnt signalling required for cardiogenesisrougly O, Nikoopour E, Bellemore S, Lee-Chan E, Fouser LA, et al. The involvement of interleukin-22 in the expression of pancreatic beta cell regenerative Reg genes. Cell Regen (Lond). 2013;2(1):2.

246. Zhu W, Shiojima I, Ito Y, Li Z, Ikeda H, Yoshida M, et al. IGFBP-4 is an inhibitor of canonical Wnt signalling required for cardiogenesis. Nature. 2008;454(7202):345-9.

247. Macho-Fernandez E, Koroleva EP, Spencer CM, Tighe M, Torrado E, Cooper AM, et al. Lymphotoxin beta receptor signaling limits mucosal damage through driving IL-23 production by epithelial cells. Mucosal Immunol. 2015;8(2):403-13.

248. Gonzalez-Santamaria J, Villalba M, Busnadiego O, Lopez-Olaneta MM, Sandoval P, Snabel J, et al. Matrix cross-linking lysyl oxidases are induced in response to myocardial infarction and promote cardiac dysfunction. Cardiovasc Res. 2016;109(1):67-78.

249. Cheng M, Nguyen M-H, Fantuzzi G, Koh TJ. Endogenous interferon-γ is required for efficient skeletal muscle regeneration. American Journal of Physiology - Cell Physiology. 2008;294(5):C1183.

250. Troidl C, Möllmann H, Nef H, Masseli F, Voss S, Szardien S, et al. Classically and alternatively activated macrophages contribute to tissue remodelling after myocardial infarction. Journal of Cellular and Molecular Medicine. 2009;13(9b):3485-96.

251. Myllyharju J, Kivirikko KI. Collagens, modifying enzymes and their mutations in humans, flies and worms. Trends in Genetics. 2004;20(1):33-43.

252. Cleutjens JP, Verluyten MJ, Smiths JF, Daemen MJ. Collagen remodeling after myocardial infarction in the rat heart. The American Journal of Pathology. 1995;147(2):325-38.

253. Whittaker P, Boughner DR, Kloner RA. Analysis of healing after myocardial infarction using polarized light microscopy. The American Journal of Pathology. 1989;134(4):879-93.

254. Hofmann U, Bonz A, Frantz S, Hu K, Waller C, Roemer K, et al. A Collagen α2(I) Mutation Impairs Healing after Experimental Myocardial Infarction. The American Journal of Pathology.180(1):113-22.

255. Willems IE, Havenith MG, De Mey JG, Daemen MJ. The alpha-smooth muscle actin-positive cells in healing human myocardial scars. The American Journal of Pathology. 1994;145(4):868-75.

256. Gabbiani G, Ryan GB, Majno G. Presence of modified fibroblasts in granulation tissue and their possible role in wound contraction. Experientia. 1971;27(5):549-50.

257. Ma Y, de Castro Brás LE, Toba H, Iyer RP, Hall ME, Winniford MD, et al. Myofibroblasts and the extracellular matrix network in post-myocardial infarction cardiac remodeling. Pflugers Archiv. 2014;466(6):1113-27.

258. Kanisicak O, Khalil H, Ivey MJ, Karch J, Maliken BD, Correll RN, et al. Genetic lineage tracing defines myofibroblast origin and function in the injured heart. Nat Commun. 2016;7:12260.

259. Courties G, Heidt T, Sebas M, Iwamoto Y, Jeon D, Truelove J, et al. In vivo silencing of the transcription factor IRF5 reprograms the macrophage phenotype and improves infarct healing. Journal of the American College of Cardiology. 2014;63(15):1556-66.

260. Majmudar MD, Keliher EJ, Heidt T, Leuschner F, Truelove J, Sena BF, et al. Monocyte-directed RNAi targeting CCR2 improves infarct healing in atherosclerosis-prone mice. Circulation. 2013;127(20):2038.

261. Peranteau WH, Zhang L, Muvarak N, Badillo AT, Radu A, Zoltick PW, et al. IL-10 overexpression decreases inflammatory mediators and promotes regenerative healing in an adult model of scar formation. Journal of Investigative Dermatology. 2008;128(7):1852-60.

262. Ishida Y, Gao J-L, Murphy PM. Chemokine receptor CX3CR1 mediates skin wound healing by promoting macrophage and fibroblast accumulation and function. The Journal of Immunology. 2007;180(1):569.

263. Shinde AV, Frangogiannis NG. Fibroblasts in myocardial infarction: a role in inflammation and repair. Journal of Molecular and Cellular Cardiology. 2014;70:74-82.

264. Thompson RW, Pesce JT, Ramalingam T, Wilson MS, White S, Cheever AW, et al. Cationic amino acid transporter-2 regulates immunity by modulating arginase activity. PLoS Pathogens. 2008;4(3):e1000023.

265. Knipper Johanna A, Willenborg S, Brinckmann J, Bloch W, Maaß T, Wagener R, et al. Interleukin-4 receptor α signaling in myeloid cells controls collagen fibril assembly in skin repair. Immunity. 2015;43(4):803-16.

266. Rodero MP, Legrand JMD, Bou-Gharios G, Khosrotehrani K. Wound-associated macrophages control collagen 1α2 transcription during the early stages of skin wound healing. Experimental Dermatology. 2013;22(2):143-5.

267. Filardy AA, Pires DR, Nunes MP, Takiya CM, Freire-de-Lima CG, Ribeiro-Gomes FL, et al. Proinflammatory clearance of apoptotic neutrophils induces an IL-12(low) IL-10(high) regulatory phenotype in macrophages. The Journal of Immunology. 2010;185(4):2044.

268. Furtado MB, Nim HT, Boyd SE, Rosenthal NA. View from the heart: cardiac fibroblasts in development, scarring and regeneration. Development. 2016;143(3):387.

269. Arlein WJ, Shearer JD, Caldwell MD. Continuity between wound macrophage and fibroblast phenotype: analysis of wound fibroblast phagocytosis. American Journal of Physiology - Regulatory, Integrative and Comparative Physiology. 1998;275(4):R1041.

270. Hall SE, Savill JS, Henson PM, Haslett C. Apoptotic neutrophils are phagocytosed by fibroblasts with participation of the fibroblast vitronectin receptor and involvement of a mannose/fucose-specific lectin. The Journal of Immunology. 1994;153(7):3218.

271. Bunt S, Hooley C, Hu N, Scahill C, Weavers H, Skaer H. Hemocyte-Secreted Type IV Collagen Enhances BMP Signaling to Guide Renal Tubule Morphogenesis in Drosophila. Developmental Cell. 2010;19(2):296-306.

272. Van De Bor V, Zimniak G, Papone L, Cerezo D, Malbouyres M, Juan T, et al. Companion Blood Cells Control Ovarian Stem Cell Niche Microenvironment and Homeostasis. Cell Reports.13(3):546-60.

273. Nakaya M, Watari K, Tajima M, Nakaya T, Matsuda S, Ohara H, et al. Cardiac myofibroblast engulfment of dead cells facilitates recovery after myocardial infarction. The Journal of Clinical Investigation. 2017;127(1):383-401.

274. Reilkoff RA, Bucala R, Herzog EL. Fibrocytes: emerging effector cells in chronic inflammation. Nature Reviews Immunology. 2011;11(6):427-35.

275. Bucala R, Spiegel LA, Chesney J, Hogan M, Cerami A. Circulating fibrocytes define a new leukocyte subpopulation that mediates tissue repair. Molecular Medicine. 1994;1(1):71-81.

276. Haudek SB, Xia Y, Huebener P, Lee JM, Carlson S, Crawford JR, et al. Bone marrow-derived fibroblast precursors mediate ischemic cardiomyopathy in mice. Proceedings of the National Academy of Sciences. 2006;103(48):18284-9.

277. Vaage J, Lindblad WJ. Production of collagen type I by mouse peritoneal macrophages. Journal of Leukocyte Biology. 1990;48(3):274-80.

278. Weitkamp B, Cullen P, Plenz G, Robenek H, Rauterberg J. Human macrophages synthesize type VIII collagen in vitro and in the atherosclerotic plaque. The FASEB Journal. 1999;13(11):1445-57.

279. Schnoor M, Cullen P, Lorkowski J, Stolle K, Robenek H, Troyer D, et al. Production of type VI collagen by human macrophages: a new dimension in macrophage functional heterogeneity. The Journal of Immunology. 2008;180(8):5707.

280. Vaage J, Harlos JP. Collagen production by macrophages in tumour encapsulation and dormancy. British Journal of Cancer. 1991;63(5):758-62.

281. Yona S, Lin H-H, Siu WO, Gordon S, Stacey M. Adhesion-GPCRs: emerging roles for novel receptors. Trends in Biochemical Sciences. 2008;33(10):491-500.

282. Stacey M, Chang G-W, Davies JQ, Kwakkenbos MJ, Sanderson RD, Hamann J, et al. The epidermal growth factor–like domains of the human EMR2 receptor mediate cell attachment through chondroitin sulfate glycosaminoglycans. Blood. 2003;102(8):2916.

283. Xu L, Begum S, Hearn JD, Hynes RO. GPR56, an atypical G protein-coupled receptor, binds tissue transglutaminase, TG2, and inhibits melanoma tumor growth and metastasis. Proceedings of the National Academy of Sciences. 2006;103(24):9023.

284. Ritzel RM, Patel AR, Grenier JM, Crapser J, Verma R, Jellison ER, et al. Functional differences between microglia and monocytes after ischemic stroke. Journal of Neuroinflammation. 2015;12(1):106.

285. Yamasaki R, Lu H, Butovsky O, Ohno N, Rietsch AM, Cialic R, et al. Differential roles of microglia and monocytes in the inflamed central nervous system. The Journal of Experimental Medicine. 2014;211(8):1533.

286. Zhou B, Honor LB, He H, Ma Q, Oh J-H, Butterfield C, et al. Adult mouse epicardium modulates myocardial injury by secreting paracrine factors. The Journal of Clinical Investigation. 2011;121(5):1894-904.

287. Kwee L, Baldwin HS, Shen HM, Stewart CL, Buck C, Buck CA, et al. Defective development of the embryonic and extraembryonic circulatory systems in vascular cell adhesion molecule (VCAM-1) deficient mice. Development. 1995;121(2):489-503.

288. Ley K, Laudanna C, Cybulsky MI, Nourshargh S. Getting to the site of inflammation: the leukocyte adhesion cascade updated. Nature Reviews Immunology. 2007;7(9):678-89.

289. Joseph C, Quach Julie M, Walkley Carl R, Lane Steven W, Lo Celso C, Purton Louise E. Deciphering hematopoietic stem cells in their niches: a critical appraisal of genetic models, lineage tracing, and imaging strategies. Cell Stem Cell. 2013;13(5):520-33.

290. Jackson KA, Majka SM, Wang H, Pocius J, Hartley CJ, Majesky MW, et al. Regeneration of ischemic cardiac muscle and vascular endothelium by adult stem cells. Journal of Clinical Investigation. 2001;107(11):1395-402.

291. van Berlo JH, Kanisicak O, Maillet M, Vagnozzi RJ, Karch J, Lin S-CJ, et al. c-kit(+) cells minimally contribute cardiomyocytes to the heart. Nature. 2014;509(7500):337-41.

292. Cañete A, Comaills V, Prados I, Castro AM, Hammad S, Ybot‐Gonzalez P, et al. Characterization of a fetal liver cell population endowed with long‐term multiorgan endothelial reconstitution potential. Stem Cells. 2017;35(2):507-21.

293. Felix R, Cecchini MG, Hofstetter W, Elford PR, Stutzer A, Fleisch H. Rapid publication: Impairment of macrophage colony-stimulating factor production and lack of resident bone marrow macrophages in the osteopetrotic op/op Mouse. Journal of Bone and Mineral Research. 1990;5(7):781-9.

294. Laine GA, Allen SJ. Left ventricular myocardial edema. Lymph flow, interstitial fibrosis, and cardiac function. Circulation Research. 1991;68(6):1713-21.

295. Henri O, Pouehe C, Houssari M, Galas L, Nicol L, Edwards-Levy F, et al. Selective stimulation of cardiac lymphangiogenesis reduces myocardial edema and fibrosis leading to improved cardiac function following myocardial infarction. Circulation. 2016.

296. Banerji S, Ni J, Wang S-X, Clasper S, Su J, Tammi R, et al. LYVE-1, a new homologue of the CD44 glycoprotein, is a lymph-specific receptor for hyaluronan. The Journal of Cell Biology. 1999;144(4):789.

297. Johnson LA, Banerji S, Lawrance W, Gileadi U, Prota G, Holder KA, et al. Dendritic cells enter lymph vessels by hyaluronan-mediated docking to the endothelial receptor LYVE-1. Nature Immunology. 2017;18(7):762-70.

298. Gale NW, Prevo R, Espinosa J, Ferguson DJ, Dominguez MG, Yancopoulos GD, et al. Normal lymphatic development and function in mice deficient for the lymphatic hyaluronan receptor LYVE-1. Molecular and Cellular Biology. 2007;27(2):595-604.

299. Bellingan GJ, Xu P, Cooksley H, Cauldwell H, Shock A, Bottoms S, et al. Adhesion molecule–dependent mechanisms regulate the rate of macrophage clearance during the resolution of peritoneal inflammation. The Journal of Experimental Medicine. 2002;196(11):1515-21.

300. Labat ML, Bringuier AF, Arys-Philippart C, Arys A, Wellens F. Monocytic origin of fibrosis. In vitro transformation of HLA-DR monocytes into neo-fibroblasts:

inhibitory effect of all-trans retinoic acid on this process. Biomedicine & Pharmacotherapy. 1994;48(2):103-11.

301. Bertrand S, Godoy M, Semal P, Van Gansen P. Transdifferentiation of macrophages into fibroblasts as a result of Schistosoma mansoni infection. International Journal of Developmental Biology. 1992;36(1):179-84.

302. Kobayashi S, Okabe M, Kimura I, Kimura M. Interferon-γ-activated macrophages release interleukin-1 α to increase tube formation from endothelial cells of rat aorta. Immunopharmacology. 1995;31(1):93-101.

303. Mass E, Ballesteros I, Farlik M, Halbritter F, Günther P, Crozet L, et al. Specification of tissue-resident macrophages during organogenesis. Science. 2016;353(6304):aaf4238-1.